THE UNIVERSITY OF CALGARY

Shear Strength of Beams by Shear-Friction

by

Liying Peng

A THESIS

SUBMITTED TO THE FACULTY OF GRADUATE STUDIES

IN PARTIAL FULFILLMENT OF THE REQUIREMENTS FOR THE

DEGREE OF MASTER OF SCIENCE IN CIVIL ENGINEERING

DEPARTMENT OF CIVIL ENGINEERING

CALGARY, ALBERTA

January, 1999

© Liying Peng 1999

National Library of Canada
Acquisitions and Bibliographic Services
395 Wellington Street
Ottawa ON K1A 0N4
Canada

Bibliothèque nationale du Canada
Acquisitions et services bibliographiques
395, rue Wellington
Ottawa ON K1A 0N4
Canada

Your file Votre référence

Our file Notre référence

The author has granted a non-exclusive licence allowing the National Library of Canada to reproduce, loan, distribute or sell copies of this thesis in microform, paper or electronic formats.

The author retains ownership of the copyright in this thesis. Neither the thesis nor substantial extracts from it may be printed or otherwise reproduced without the author's permission.

L'auteur a accordé une licence non exclusive permettant à la Bibliothèque nationale du Canada de reproduire, prêter, distribuer ou vendre des copies de cette thèse sous la forme de microfiche/film, de reproduction sur papier ou sur format électronique.

L'auteur conserve la propriété du droit d'auteur qui protège cette thèse. Ni la thèse ni des extraits substantiels de celle-ci ne doivent être imprimés ou autrement reproduits sans son autorisation.

0-612-38638-4

Canada

Abstract

Few problems in concrete research have been studied more extensively than the shear failure of reinforced concrete beams. The mechanisms of shear transfer in reinforced concrete beam are complex. The types of failure are varied. It has proved difficult to develop a consistent and physically meaningful theoretical approach for shear failure.

A rational approach with a clear concept and simple expression, the shear-fiction method, is proposed by Loov. The four basic shear-friction equations dealing with beam shear were established in 1997 (Loov, 1997). In order to apply the four basic shear-friction equations to calculate the shear strength of reinforced concrete beams, two supplementary equation were developed to determine the location of the inclined crack and account for the influence of concrete strength. Eight simply supported beams were tested to examine the effect of large stirrup spacings. In order to verify the shear-friction method, test results of 249 beams from the literature were compared with the predictions made by the shear-friction method and CSA, ACI and Euro code procedures. Based on this research work, it can be seen that the shear-friction method provides a better prediction for reinforced concrete beams, with and without shear reinforcement, than either of the three code procedures.

Acknowledgements

I wish to express my deep gratitude to my supervisor, Dr. Robert E. Loov for his extreme patience, careful guidance and continuing encouragement throughout my studies and this research. His extensive knowledge and constructive criticisms expanded the limits of my own capability. I am very fortunate to have been able to learn from him.

I am greatly thankful to the technicians, Don Anson, Don McCullough and Terry Quinn for their skillful assistance, tireless involvement and great help. This test program would not been completed without them.

My appreciation is also extended to the remaining members of the thesis committee and my fellow graduate students: Peijun Guo, Ahmed El-Metwally and Mahmoud Reda.

The financial support provided by NSERC and the Department of Civil Engineering is gratefully acknowledged.

I am also extremely grateful to my husband for his constant encouragement and support without which I would not have taken up and completed this study.

Table of Contents

Approval Page ii

Abstract iii

Acknowledgements iv

Table of Contents v

1 Introduction 1

1.1 General 1

1.2 Objective and Scope 2

1.3 Organization of Thesis 3

2 Literature Review 4

2.1 General 4

2.2 Review of Shear-Friction equations 4

2.2.1 P.W. Birkeland and H.W. Birkeland, 1966 5

2.2.2 R.F. Mast, 1968 7

2.2.3 J.A. Hofbeck, I.O. Ibrahim and A.H. Mattock, 1969 8

2.2.4 A.H. Mattock and N.M. Hawkins, 1972 9

2.2.5 A.H. Mattock, 1974 11

2.2.6 B.R. Hermansen and J. Cowan, 1974 12

2.2.7 A.H. Mattock, L. Johal and H.C. Chow, 1975 13

2.2.8 C.H. Raths, 1977 14

2.2.9 A.F. Shaikh, 1978 15

2.2.10 R.E. Loov, 1978 16

2.2.11 J. Walraven, J. Frenay and A. Pruijssers, 1987 16
2.2.12 A.H. Mattock, 1988 17
2.2.13 S.T. Mau and T.C. Hsu, 1988 18
2.2.14 S.G. Tsoukantas and T.P. Tassios, 1989 19
2.2.15 R.E. Loov and A.K. Patnaik, 1994 19
2.2.16 Summary 20
2.3 Review of Several Main Recent Codes 21
2.3.1 Shear Cracking 21
2.3.2 Truss Model for Slender Beam 23
2.3.3 ACI Procedure (MPa units) 25
2.3.4 CSA Simplified Method (MPa units) 28
2.3.5 CSA General Method (MPa units) 30
2.3.6 Euro Code (MPa units) 34
3 Development of Basic Shear-Friction Equations 37
3.1 Introduction 37
3.2 Basic Shear-friction Equations on Beam Shear (Loov, 1997) 41
3.2.1 General Equation 41
3.2.2 Development of Force in Reinforcement 43
3.2.3 Simplified Equation 45
3.2.4 Design Equation for Shear Reinforced Beams 45
3.3 Validation of Parabolic Stress Equation 46
3.3.1 Comparison with Other Stress Equations 46
3.3.2 Applied Range of Parabolic Stress Equation 50
3.4 Projection of Diagonal Crack 54

3.4.1 Cracking Load 54
3.4.2 Projection of Crack 56
3.4.3 Approximate Equation for Projection of Crack 58
3.4.4 Design Equation for Reinforced Beam without Shear Reinforcement 64
3.5 Influence of Concrete Strength on k 64
3.5.1 Constant k for Normal Concrete Strength 64
3.5.2 Effect of Concrete Strength on k 66
3.6 New Failure Model Based on Shear-Friction 68
3.6.1 Derivation of General Equation 68
3.6.2 Force in Reinforcement 70
3.6.3 Simplified and design equation 71
4 Test Program and Discussion of Test Results 72
4.1 Introduction 72
4.2 Experimental Program 73
4.2.1 Test Specimens 73
4.2.2 Test Set Up 77
4.2.3 Instrumentation 78
4.2.4 Procedure 80
4.3 Test Results 81
4.3.1 Crack Formation and Pattern 81
4.3.2 Ultimate and Cracking Load 84
4.3.3 Force in Longitudinal Reinforcement 84
4.3.4 Strain in Stirrups 86

4.3.5 Deflection at Midspan 88
4.4 Discussion of Test Results 89
4.4.1 Effect of Stirrup Spacing on Shear Strength 89
4.4.2 Force in Longitudinal Reinforcement 97
4.4.3 Location of Crack 100
4.4.4 Effect of Amount of Shear Reinforcement on Shear Strength . 102
5 Comparison of Different Methods with Test Results in Literature 105
5.1 Introduction 105
5.2 Reinforced Concrete Beams without stirrups 105
5.2.1 Review of Equations of Various Methods 105
5.2.2 Summary of Test Beams 109
5.2.3 Effect of Clear Shear Span Ratio a_{cle}/h 112
5.2.4 Effect of Concrete Strength 119
5.2.5 Effect of Longitudinal reinforcement Ratio 122
5.2.6 Summary for Reinforced Concrete Beam without Stirrups . . . 128
5.3 Reinforced Concrete Beam with Stirrups 129
5.3.1 Review of Equation of Various Methods 129
5.3.2 Summary of Test Beams 131
5.3.3 Effect of clear shear span ratio, a_{cle}/h 136
5.3.4 Effect of Amount of Shear Reinforcement 137
5.3.5 Effect of Concrete Strength 143
5.3.6 Effect of s/d ratio 146
5.3.7 Effect of Section Shape 147
5.3.8 Summary for Reinforced Concrete Beams with Stirrups 151

6 Conclusions and Recommendations **153**

6.1 Conclusions 153

6.1.1 Equations developed 153

6.1.2 Reinforced Concrete Beams without Stirrups 154

6.1.3 Reinforced Concrete Beams with Stirrups 155

6.2 Recommendations for Future Work 156

Bibliography **158**

List of Table

4.1 Details of test beams 76

4.2 Mix proportion by mass 76

4.3 Failure and cracking loads of test beams 85

4.4 Comparison of longitudinal forces based on two failure model with test results 99

5.1 Details of test series without stirrups 110

5.2 Comparison of predictions for test series without stirups 111

5.3 Details of test series with stirrups 132

5.4 Comparison of predictions for test series without stirups 134

List of Figures

2.1 Shear-friction hypothesis (Birkeland, 1966) 6

2.2 Comparison of main shear-friction equations 20

2.3 Internal forces in a cracked beam (MacGgregor, 1992) 22

2.4 Truss analogy (MacGregor, 1992) 24

3.1 Parabolic stress equation and Mohr's circle 38

3.2 Types of shear crack of beams without stirrups 39

3.3 Types of shear crack of beams with stirrups 40

3.4 Free -body diagram (Loov,1998) 42

3.5 Effect of variation in longitudinal force on shear and moment (Loov,1998) 44

3.6 Comparison of different stress equations 47

3.7 Shear and flexural stress of a concrete beam 50

3.8 Normal stress vs. crack angle 52

3.9 Normal stress on inclined crack plane 53

3.10 Approximate stresses on inclined crack plane 55

3.11 Crack location 57

3.12 t/h vs. a_{cle}/h for dirrerent f'_c 60

3.13 t/h vs. a_{cle}/h for different ψ 61

3.14 Crack locations predicted comparing to ones tested (no stirrups) . . . 62

3.15 Crack locations predicted comparing to ones tested (with stirrups) . . 63

3.16 Push-off test results (Loov, 1998) 65

3.17 Factor k using general equation 67

3.18 Factor k using design equation 67
3.19 Free-body diagram for parabolic failure model 69

4.1 Detail of test beams (B-1, 2, 5 and 6) 74
4.2 Detail of test beams (B-3, 4, 7 and 8) 75
4.3 Stress-strain curves for steel 78
4.4 Test set up 79
4.5 Crack patterns of test beams (B-1 - B-4) 82
4.6 Crack patterns of test beams (B-5 - B-8) 83
4.7 Longitudinal force in test beams (B-1& B-5) 86
4.8 Longitudinal forces in test beams (B-2 & B-6) 87
4.9 Longitudinal forces in test beams (B-3 & B-7) 87
4.10 Longitudinal forces in test beams (B-4 & B-8) 88
4.11 Losd vs. stirrupstrains for beam 4 89
4.12 Load vs. stirrup strains for beam 7 90
4.13 Effect of $\rho_v f_{vy}$ on load vs. deflection 91
4.14 strength vs. s/d using CSA-s ($T_{vr}/C_{dr} = 0.01$) (Loov, 1998) 93
4.15 Strength vs. s/d using CSA-s($T_{vr}/C_{dr} = 0.03$) (loov, 1998) 94
4.16 Strength vs. s/d using CSA-s ($T_{vr}/C_{dr} = 0.05$) (loov, 1998) 94
4.17 Strength vs. s/d for beam 1-4 96
4.18 Strength vs. s/d for beam 5-7 97
4.19 Effect of large s/d on strength based on shear-friction method 98
4.20 Effect of crack location for beam 1 101
4.21 Effect of crack loation for beam 7 102

4.22 Comparison of crack locations (B-1 - B-4) 103
4.23 Comparison of crack locations (B-5 - B-8) 104

5.1 Effect of a_{cle}/h on beams without stirrups by SF design Equ. 113
5.2 Effect of a_{cle}/h on beams without stirrups by SF general Equ. 114
5.3 Effect of a_{cle}/h on beams without stirrups by CSA simplified method 115
5.4 Effect of a_{cle}/h on beam without stirrups by CSA general method . . 116
5.5 Effect of a_{cle}/h on beam without stirrups by ACI method (Equ. 2.21) 117
5.6 Effect of a_{cle}/h on beams without stirrups by Euro method 118
5.7 Enhancements of shear strength with increased f'_c using different methods 120
5.8 Effect of f'_c on beams without stirrups by SF design Equ. 122
5.9 Effect of fc on beams without stirrups by CSA simplified method . . 123
5.10 Effect of f'_c on beams without stirrups by CSA general method 123
5.11 Effect of f'_c on beams without stirrups by ACI method (Equ. 2.21) . . 124
5.12 Effect of f'_c on beams without stirrups using Euro method 124
5.13 Effect of ρf_y on beams without stirrups by SF design Equ. 125
5.14 Effect of ρf_y on beams without stirrups by CSA simplified method . . 126
5.15 Effect of ρf_y on beams without stirrups by CSA general method . . . 126
5.16 Effect of ρf_y on beams without stirrups by ACI method (Equ. 2.21) . 127
5.17 Effect of ρf_y on beams without stirrups by Euro method 127
5.18 Effect of a_{cle}/h on beams with stirrups by SF design Equ. 137
5.19 Effect of a_{cle}/h on beams with stirrups by SF general Equ. 138
5.20 Effect of a_{cle}/h on beams with stirrups by ACI & CSA-s method . . . 138

5.21 Effect of a_{cle}/h on beams with stirrups by CSA general method . . . 139
5.22 Effect of a_{cle}/h on beams with stirrups by Euro method 139
5.23 Effect of $\rho_v f_{vy}$ on beams with stirrups by SF design Equ. 140
5.24 Effect of $\rho_v f_{vy}$ on beams with stirrups by ACI & CSA-s method . . . 141
5.25 Effect of $\rho_v f_{vy}$ on beams with stirrups by CSA general method 141
5.26 Effect of $\rho_v f_{vy}$ on beams with stirrups by Euro method 142
5.27 Effect of f'_c on beams with stirrups by SF design Equ. 143
5.28 Effect of f'_c on beams with stirrups by ACI & CSA -s method 144
5.29 Effect of f'_c on beams with stirrups by CSA general method 144
5.30 Effect of f'_c on beams with stirrups by Euro method 145
5.31 Effect of s/d on beams with stirrups by SF design Equ. 147
5.32 Effect of s/d on beams with stirrups using ACI & CSA-s method . . 148
5.33 Effect of s/d on beams with stirrups by CSA general method 148
5.34 Effect of s/d on beams with stirrups by Euro method 149
5.35 Number of stirrups crossing shear crack 149
5.36 Effect of section 150

Notation

a	shear span, distance between concentrated load and center of support plate
a	maximum aggregate size in b equation for the CSA general method
a_{cle}	clear shear span, distance between outer edge of plate for concentrated load and inner edge of plate at support
A	area of critical inclined crack plane
A_s	area of longitudinal reinforcement in tension zone
A_v	area of one stirrup
A_{vmin}	minimum area of shear reinforcement for one stirrup
b_w	width of beam web
c	vertical distance from the extreme compression fiber to the neutral axis
d	distance from the extreme compression fiber to the centroid of the longitudinal tension reinforcement
C_{dr}	factored force in concrete web based on d
d_b	diameter of a reinforcing bar
d_{bv}	diameter of a stirrup
d_s	effective length of stirrup
d_v	distance measured perpendicular to the neutral axis between the results of the tensile and compressive forces due to flexure

E_s	modulus of elasticity for longitudinal reinforcement
f'_c	specified compressive strength of concrete
f_r	modulus of rupture of concrete
f_{vy}	specified yield strength of the stirrups
f_y	specified yield strength of the longitudinal reinforcement or steel crossing interface
f_2	stress in compressive concrete strut
f_{2max}	maximum allowable stress in concrete strut
h	overall height of member
j	lever arm factor
k	factor for relating shear strength and normal stress determined from experiments
k_t	factor k calculated by the shear-friction method and shear resistance measured from test
n	number of stirrups crossing inclined plane
R	normal force on an inclined failure plane
s	spacing of stirrups
S	shear force on an inclined failure plane
s	standard deviation
t	projection of inclined crack

T	tension force in longitudinal reinforcement at a given location
T_{opt}	optimum tension force in longitudinal reinforcement at a given location
T_v	force in one stirrup
T_y	yield force in longitudinal reinforcement
v	average shear stress on an inclined failure plane
v_f	factored shear stress acting on beam
V_c	factored shear resistance attributed to the concrete
V_{cg}	factored shear resistance attributed to the concrete using CSA general method
V_{cr}	cracking load
V_r	factored shear resistance of beam
V_n	nominal shear resistance of beam
V_{rg}	factored shear resistance of beam using CSA general method
V_s	factored shear resistance provided by the shear reinforcement
V_{sf}	shear resistance based on the shear-friction method
V_{sg}	factored shear resistance provided by the shear reinforcement using CSA general method
V_t	shear strength determined by test
V	coefficient of variation
x	mean value

x	distance from center of support plate to the starting point of the shear crack
y_t	vertical distance from top of beam to centroid of normal force on inclined plane
β	factor accounting for the shear resistance of cracked concrete
ε_x	longitudinal strain of flexural tension chord of member
ε_1	principle tensile strain in cracked concrete due to factored loads
θ	angle of inclination of critical shear crack (or compressive concrete strut) to longitudinal axis of a beam
λ	factor to account for low density concrete
μ	coefficient of friction
ρ	ratio of longitudinal reinforcement
ρ_v	ratio of transverse reinforcement
ρ_w	ratio of longitudinal reinforcement in ACI code (A_s/b_wd)
σ	average normal stress on an inclined failure plane
ϕ	strength reduction factor
ϕ_c	resistance factor for concrete
ϕ_s	resistance factor for reinforcement
ψ	ratio of web reinforcement index to concrete strength ($\rho_v f_{vy}/f'_c$)

Chapter 1

Introduction

1.1 General

In the past several decades, a tremendous amount of research has been done to investigate the shear behavior of reinforced concrete beams. The knowledge of shear behavior and its failure mechanism has improved significantly. However, complete understanding of shear behavior in various reinforced concrete beams still seems far off due to its complex nature.

For reinforced concrete beams without shear reinforcement, the provisions for shear design in current codes (such as CSA-A23.3-94, ACI 318-M95 and CEB-FIP MC90) are based on empirical equations, due to the complex mechanism of shear transfer, various failure types and interdependent internal forces in beams. The use of these empirical equations to predict the shear strength is not satisfactory. A rational approach is needed.

For reinforced concrete beams with shear reinforcement, the provisions for shear design in the recent codes mentioned above are based on the truss model. The truss model is an excellent conceptual model for showing the approximate forces that exist in cracked concrete beams. The CSA general method is based on the variable angle truss model and the modified compression field theory. It is a physically meaningful rational approach. It is possible to predict not only the strength but also the load-deformation response of members loaded in shear. However, it is quite complicated

for everyday design. In addition, by checking the value of β in Table 11-1 of CSA-A23.3-94, it was found that the shear resistance contributed by concrete is mostly governed by crack slip (shear friction failure) rather than concrete strut crushing (shear compression failure) (Appendix A). The modified compression field theory therefore predicts that most reinforced concrete beams will fail by shear slip before they fail by shear compression.

The concept of shear-friction has been used to explain the behavior of shear transfer at interfaces since its introduction. Can we use the concept of shear-friction to explain the behavior of shear in reinforced concrete beams?

Four basic shear-friction equations were proposed by Loov (1997) to solve shear problems for reinforced concrete beams. This rational approach has a clear concept and a simple expression.

1.2 Objective and Scope

The main objective of this study was to apply the four basic shear-friction equations to reinforced concrete beams, investigate experimentally the effect of large s/d ratios which are beyond the limits in the Canadian code and compare the shear friction method with the several main recent codes.

Two equations and one new failure model were developed in this thesis. One equation describes the relationship between the factor k and the concrete strength. The other can be used to determine the critical crack location in reinforced concrete beams without stirrups. A new parabolic failure model was derived for beams with a curved failure plane. Eight beams were tested to study the effect of large stirrup

spacings. A comparison of the shear-friction method and three recent codes with the test results of 249 beams from the literature was also done.

1.3 Organization of Thesis

In Chapter 2 of this thesis, the development of the shear-friction concept is reviewed. The shear-friction equations proposed by many researchers are presented. The provisions for the shear design of reinforced concrete beams in the CSA, ACI and Euro codes are also reviewed. In Chapter 3, the basic stress equation (Loov, 1978) is confirmed to be suitable for reinforced concrete beams. Two equations which account for the effect of concrete strength and the critical crack location are derived, and a new failure model — the parabolic crack plane model— is developed to deal with reinforced concrete beams with a curved crack plane. Chapter 4 details the testing program and presents test results. By analyzing the test results, the effect of the s/d ratio and $\rho_v f_{vy}$ index are discussed, and the equation for the critical crack location and the equation for longitudinal force are checked. In Chapter 5, by analyzing 249 reinforced concrete beams from the literature, the effects of the a_{cle}/h ratio, concrete strength, ρf_y index, $\rho_v f_{vy}$ index and s/d ratio are discussed for the shear-friction method and the various code procedures. The conclusions and recommendations for future research are summaried in Chapter 6.

Chapter 2

Literature Review

2.1 General

The concept of shear-friction, which is similar to the treatment of friction in mechanics, was first introduced to explain the behavior of shear transfer at the concrete to steel and concrete to concrete interfaces. Extensive experimental research lead to the development of the shear-friction equation. However, the concept of shear-friction has been still mainly used to deal with the shear transfer at interfaces — concrete connections, corbels, composite beams, etc.

The shear design for reinforced concrete beams without shear reinforcements is still based on empirical equations, and the shear design for reinforced concrete beams with shear reinforcements is based on the truss model in several main codes.

The development of the shear-friction equations and the review of CSA A23.3-94, ACI 318-M95 and Euro codes are presented in this Chapter.

2.2 Review of Shear-Friction equations

The concept of shear friction was first introduced to the U.S.A. from Europe in 1958 and was further developed by H.W. Birkeland and others. The ACI building code at that time allowed design for shear transfer to be based on the shear-friction hypothesis proposed by Birkeland (1966) and Mast (1968). This was allowed due to

its simplicity, even though it is conservative for low clamping stresses and unsafe for high clamping stresses. Many researchers have proposed equations based on their own test results since then. Most of these equations are reviewed here.

2.2.1 P.W. Birkeland and H.W. Birkeland, 1966

In the shear friction concept, shear failure was considered as slip not as a tension crack in the usual sense. In this paper, the shear friction hypothesis was built up and the shear-friction equation was proposed.

Considering the monolithic concrete block shown in Figure 2.1 and assuming a crack (failure plane) along m-m, the external shear loads V tend to produce slip along the plane. The slip is resisted by the friction μP . If the crack m-m is rough, sliding motion along it will cause a separation s of the two parts (see Figure 2.1). If reinforcement is placed across the interface, the separation will develop tension T in the reinforcement. Since the reinforcement is well anchored on both sides of the crack, the tension provides a clamping force on the concrete, resulting in an equal compression across the interface. The roughness is similar to a frictionless series of fine sawtooth ramps, having a slope of $\tan\phi$. $T\tan\phi$ is equal to the friction force μP from the equilibrium requirement in Figure 2.1.

Referring to Figure 2.1b, the ultimate shear capacity V_u across the interface will be reached, yielding the reinforcement. The ultimate shear can be written as:

$$V_u = A_s f_y \tan\phi$$

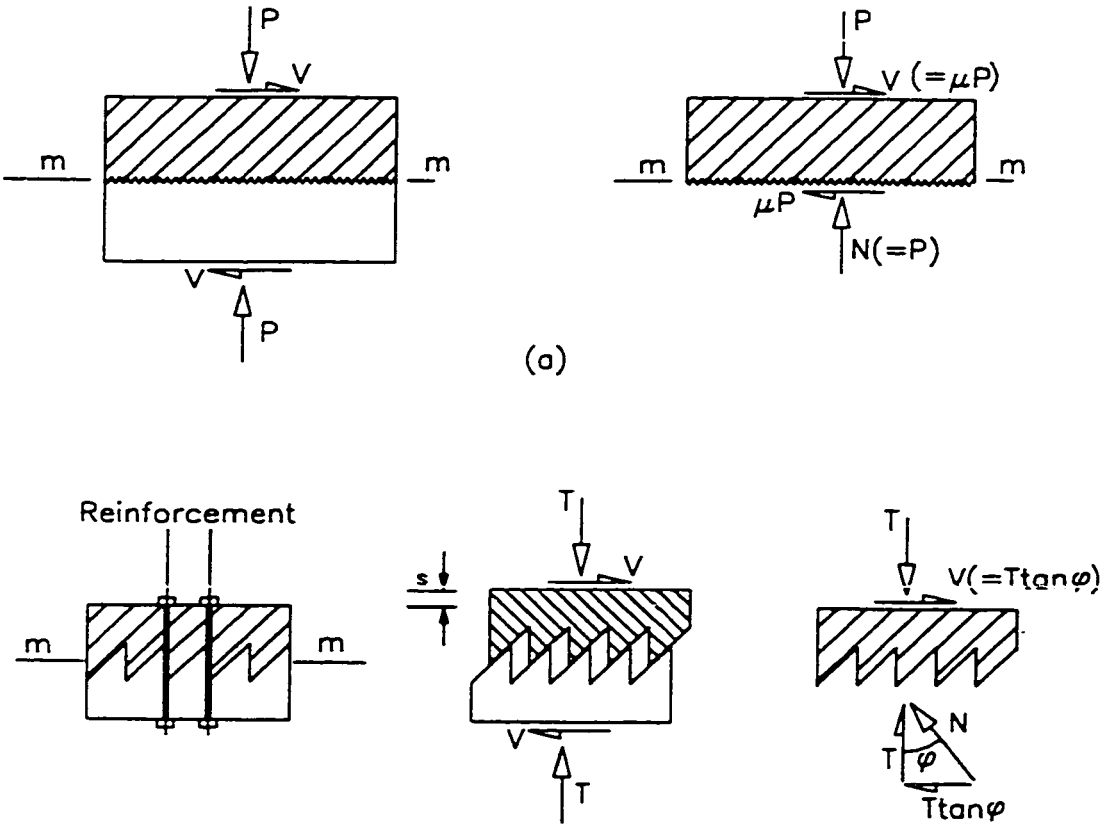

Figure 2.1: Shear-friction hypothesis (Birkeland, 1966)

or expressed as shear stress:

$$v_u = \rho_v f_y \tan\phi \tag{2.1}$$

$\tan\phi = 1.7$ for monolithic concrete

$\tan\phi = 1.4$ for artificially roughened construction joints

$\tan\phi = 0.8$ to 1.0 for ordinary construction joints and for concrete to steel interfaces

Note that:

1) The basic consideration is for an interface (crack) in monolithic concrete, but the concept can be extended to artificially roughened or smooth construction joints and to concrete to steel interface.

2) The shear is developed by friction, not by bond. The reinforcement across the interface is stressed in tension, with dowel action presumed insignificant.

3) Reinforcement must be anchored on both sides of the failure plane sufficiently to develop yield in the steel.

4) The cohesive strength was neglected in shear-friction theory to form a lower bound for test data.

2.2.2 R.F. Mast, 1968

The shear-friction hypothesis was explained in more detail in this paper. The limitations in the application of the shear-friction hypothesis for design were emphasized as following:

1) If any externally applied tension exists across the crack, reinforcement for this

tension must be provided in addition to the reinforcement required by the shear-friction theory.

2) A full tensile anchorage must be provided on both sides of the crack, sufficient to reliably develop the yield strength of the steel, but a finite amount of slip and subsequent separation of the concrete pieces on each side of the crack must take place.

3) The value of the angle of internal friction,ϕ, has been assumed to be independent of concrete strength and stress level.

Mast's shear-friction equation is the same as equation (2.1), but maximum shear stress was set as:

$$v_u = \rho_v f_y \tan\phi \leq 0.15 f_c' \tan\phi \tag{2.2}$$

The value of the friction coefficient $\tan\phi$ was considered more carefully by test results.

$\tan\phi = 1.4$ to 1.7 for a crack in monolithic concrete;

$\tan\phi = 1.4$ for a rough interface between precast and cast- in-place concrete;

$\tan\phi = 1.0$ for concrete cast against steel

$\tan\phi = 0.7$ for concrete against smooth concrete

2.2.3 J.A. Hofbeck, I.O. Ibrahim and A.H. Mattock, 1969

Thirty eight push-off specimens were tested. Fifteen specimens were uncracked at the start of the test and twenty five specimens were cracked along the shear plane before the start of shear test. The ultimate shear transfer strength was studied extensively. Two conclusions relating to shear friction were made, based on their test results for

initially cracked specimens.

The shear-friction equation (2.2) is a conservative estimate of the shear transfer strength of initially cracked specimens with concrete strengths of around 28 MPa and within $\rho_v f_y$ of $0.15 f'_c$. It appears, however, that equation (2.2) would start to become unconservative for concrete strengths of 28 MPa or over, when $\rho_v f_y$ exceeds 4 MPa. This is due to the fact that the shear-friction theory ignores the cohesion effect and compensates by using an apparent angle of internal friction which is much greater than the actual angle of internal friction. That the friction angle used is applicable only to low stress levels is noted by Mast (Mast, 1968). The authors suggested, therefore, that suitable values would be $\tan\phi$ equal to 1.0, and $\rho_v f_y$ not greater than $0.3 f'_c$ or 10.3 MPa (whichever is less).

The dowel action of reinforcing bars crossing the shear plane is substantial in concrete with a pre-existing crack along the shear plane.

Interestingly, for uncracked concrete either cast monolithically or with a rough surface between the precast and cast-in-place concrete, the authors proposed using the Zia failure envelope to derive the relationship between shear transfer strength and reinforcement parameter $\rho_v f_y$ rather than the one based on the shear-friction theory.

2.2.4 A.H. Mattock and N.M. Hawkins, 1972

Ten test series were used in this paper. The authors investigated the effect of the shear plane (initially uncracked and pre-cracked shear plane), the effect of the reinforcement (ρf_y), the effect of concrete strength and the effect of direct stresses acting parallel and transverse to the shear plane (by pull-off and modified push-off test).

For initially cracked concrete with reinforcement normal to the shear plane, the final failure occurs along the existing crack with little or no additional cracks formed across the existing crack except in cases with a high percentage of steel crossing the initial crack. It was hypothesized that the shear resistance was contributed to by the frictional resistance to sliding and the reinforcement dowel effect. The authors thought, at that time, that the concrete strength did not appear to affect the shear transfer strength of an initially cracked under-reinforced specimen. This was consistent with shear strength being primarily developed by friction, since the coefficient of friction was independent of the concrete strength.

The authors proposed a simple design equation for shear transfer across a crack in monolithic concrete as:

in psi units

$$v_u = 200 + 0.8(\rho_v f_y + \sigma_{Nx})$$

in MPa units

$$v_u = 1.38 + 0.8(\rho_v f_y + \sigma_{Nx}) \tag{2.3}$$

in which v_u shall be not more than $0.3f'_c$ and $(\rho_v f_y + \sigma_{Nx})$ be not less than 200 psi (1.38 MPa). σ_{Nx} is the externally applied direct stress acting across the shear plane taken as positive for a compressive stress and negative for a tensile stress. The dowel action and shearing off of surface protrusions were accounted for in the first term. The shear friction resistance with the coefficient of friction (0.8) was accounted for in the second term.

For initially uncracked concrete with reinforcement normal to the shear plane, several short parallel cracks formed in a direction inclined to the shear plane. It was

thought that shear transfer strength is developed by a truss action after diagonal cracking.

2.2.5 A.H. Mattock, 1974

This paper presents an experimental and analytical study of shear transfer across a plane inclined at an arbitrary angle to a parallel or orthogonal array of reinforcement. Twenty three push-off type specimens were tested, having either orthogonal or parallel arrays of reinforcement arranged at various angles to the shear plane.

The mean value of equation (2.3) is:

in psi units

$$v_u = 400 + 0.8(\rho_v f_y + \sigma_{Nx}) \leq 0.3 f'_c$$

in MPa units

$$v_u = 2.76 + 0.8(\rho_v f_y + \sigma_{Nx}) \leq 0.3 f'_c \tag{2.4}$$

$$\rho_v f_y \geq 1.38 \text{ MPa (200 psi)}$$

If θ is the angle of inclination of the rebar to the shear plane, the ultimate shear transfer stress for parallel reinforcement at angle θ to the shear plane can be expressed as:

in psi units

$$v_u = 2.76 \sin 2\theta + \rho_v f_s \left(0.8 \sin^2 \theta - 0.5 \sin 2\theta\right)$$

in MPa units

$$v_u = 400 \sin 2\theta + \rho_v f_s \left(0.8 \sin^2 \theta - 0.5 \sin 2\theta\right) \tag{2.5}$$

where 0.8 is the coefficient of friction $\tan\phi$, so $\phi = 38.7^0$.

The stress in the reinforcement f_s in the above equation is given:

$f_s = 0$ for $0 < \theta < 51.3^0$

$f_s = -1.6 f_y \cos(\theta + 38.7^0)$ for $51.3^0 < \theta < 90^0$

$f_s = f_y$ for $90^0 < \theta < 180^0$

It should be noted that if the bar spacing along the shear plane is constant and θ is varied, calculations indicate that the maximum ultimate shear stress will be developed when θ is 135^0.

2.2.6 B.R. Hermansen and J. Cowan, 1974

In this short paper, the author proposed an ultimate shear stress equation based on data from push-off tests conducted by Anderson, Hofbeck et al and Hermansen, for initially uncracked reinforced concrete specimens which failed in pure shear.

in MPa units

$$v_u = 4.0 + 0.8\rho_v f_y \tag{2.6}$$

This equation is quite similar to equation (2.3). The shear strength is a combination of cohesion and frictional effect.

2.2.7 A.H. Mattock, L. Johal and H.C. Chow, 1975

This paper studied the effect of normal force and moment in the plane on single direction shear transfer strength. Tests are reported on corbel type push-off specimens with tension acting across the shear plane. The authors concluded that:

1) If the moment in the shear plane is less than or equal to the flexural ultimate

moment of the shear plane, the shear transfer strength should not be reduced.

2) Tension across the shear plane results in a reduction in shear transfer strength equal to that which would result from a reduction in the reinforcement parameter $\rho_v f_y$ by an amount equal to the tension stress.

3) It is appropriate to add the normal stress σ_{Nx} to the reinforcement parameter ρf_y when calculating shear transfer strength in both initially cracked and initially uncracked reinforcement.

Another important development is that the authors mentioned an alternate simple expression for shear transfer strength by H.W. Birkeland as:

in psi units

$$v_u = 33.5\sqrt{\rho_v f_y}$$

in MPa units

$$v_u = 2.78\sqrt{\rho_v f_y} \tag{2.7}$$

The parabolic function was introduced for the ultimate shear transfer strength the first time. This equation, however, has not been published, and was only handed out as class notes in 1968. The reasons were that: (1) the coefficient 33.5 has an awkward unit of $\sqrt{\text{psi}}$, (2) the apparent μ will vary with clamping stress from less than 1.0 to infinity, and therefore it has no logical relationship with the fitted curve, and (3) it does not present the designer with the visual impact and simplicity of a concept which is embodied in the linear equation (Birkeland, 1976).

2.2.8 C.H. Raths, 1977

In order to obtain a straight-forward design expression for use in every day design practice, Raths suggested a parabolic shear strength equation for a monolithically cast direct shear interface which is similar to Birkeland's equation (2.7).

$$v_u = C_s(1000\mu)\sqrt{\rho_v f_y} \tag{2.8}$$

in which C_s is a constant used for the effect of concrete density

$C_s = 1.0$ for normal weight concrete

$C_s = 0.85$ for sand light-weight concrete

$C_s = 0.75$ for all-lightweight concrete

and μ is coefficient of friction

$\mu = 1.4$ for monolithically cast

$\mu = 0.6$ for smooth concrete

So that, the equation for monolithically cast concrete can be written as:

in psi units

$$v_u = 37.4C_s\sqrt{\rho_v f_y}$$

in MPa units

$$v_u = 3.11C_s\sqrt{\rho_v f_y}$$

2.2.9 A.F. Shaikh, 1978

The author compared Mattock's equation (2.4), Birkeland's equation (2.7) and Raths's equation (2.8) with test results and proposed the use of Rath's equation in his sug-

gested revisions to shear-friction provisions in PCI. For ultimate shear across any crack plane, the reinforcement normal to the plane can be calculated by:

$$A_v = \frac{V_u}{\phi f_y \mu_e} \tag{2.9}$$

where, V_u is ultimate shear force, ϕ is capacity reduction factor and μ_e is effective coefficient of friction. The effective coefficient of friction is calculated from:

in psi units

$$\mu_e = \frac{1000 C_s^2 \mu}{v_u}$$

in MPa units

$$\mu_e = \frac{6.9 C_s^2 \mu}{v_u}$$

$$\rho_v f_y \geq 120 \text{ psi } (0.83 \text{ MPa})$$

C_s is the same as in Raths's equation.

$\mu = 1.4$ for concrete to concrete, cast monolithically

$\mu = 1.0$ for concrete to hardened concrete, 0.25 in. roughness

$\mu = 0.4$ for concrete to concrete, smooth interface

$\mu = 0.6$ for concrete to steel

The minimum $\rho_v f_y$ results in shear stress equal to the shear resistance due to the cohesion of concrete.

2.2.10 R.E. Loov, 1978

The influence of concrete strength on the shear transfer strength equation was first considered by Loov. He proposed a shear stress equation in the following form:

$$\frac{v_u}{f'_c} = k\sqrt{\frac{\sigma}{f'_c}}$$

It can be rewritten as:

$$v_u = k\sqrt{\sigma f'_c} \tag{2.10}$$

where k is constant and σ is the normal compressive stress across a potential crack plane. In the shear-friction hypothesis, this normal compressive stress is equal to the tensile stress in reinforcement across the crack. The above equation, therefore, can be written as:

$$v_u = k\sqrt{\rho_v f_y f'_c} \tag{2.11}$$

The author considered that the concrete strengths of most test specimens at that time were around 20 to 30 MPa and suggested the value of k is equal to 0.5 for an initially uncracked shear interface. This equation, then, is almost the same as Birkeland's equation (2.7).

2.2.11 J. Walraven, J. Frenay and A. Pruijssers, 1987

In this study, the authors pointed out that the fact that concrete strength did not appear in previous shear-friction equations was due to the concrete strength of the test specimens (from which the equations were derived) varying between 20 and 30 MPa, so that a possible effect of the concrete strength was masked by the natural

scatter of the experimental results.

Based on statistical analysis of 88 push-off tests with a wider range of concrete strength, they came up with a shear transfer strength equation for a pre-cracked shear interface:

in psi units

$$v_u = C_3(0.007\rho_v f_y)^{C_4}$$

in MPa units

$$v_u = C_1(\rho_v f_y)^{C_2} \tag{2.12}$$

where for psi:

$C_3 = 15.7 f_{cc}'^{0.406}$ and $C_4 = 0.0355 f_{cc}'^{0.3}$

where for MPa:

$C_1 = 0.822 f_{cc}'^{0.406}$ and $C_2 = 0.159 f_{cc}'^{0.3}$

where f_{cc}' is concrete compressive strength of 150 mm cubes, and $f_c' = 0.85 f_{cc}'$.

The authors had to make a design chart for design purposes because of its complexity.

2.2.12 A.H. Mattock, 1988

In his discussion on the above paper by J. Walraven, J. Frenay and A. Pruijssers (1987), Mattock mentioned that the effect of concrete strength was accounted for in the equation which was proposed in 1976 in the following form:

in psi units

$$v_u = 4.5 f_c'^{0.545} + 0.8(\rho_v f_y + \sigma_n)$$

$$\leq \ 0.3f_c'$$

in MPa units

$$\begin{aligned} v_u &= 0.467f_c'^{0.545} + 0.8(\rho_v f_y + \sigma_n) \\ &\leq 0.3f_c' \end{aligned} \tag{2.13}$$

Mattock concluded that the resistance to shearing off of the protrusions (the first term in the above equation) should be represented by a term containing the concrete strength, and the frictional resistance (the second term in the above equation) should be independent of the concrete strength.

2.2.13 S.T. Mau and T.C. Hsu, 1988

In their discussion on the paper by J. Walraven, J. Frenay and A. Pruijssers (1987), Mau and Hsu suggested that the non-dimensional web reinforcement index, $\rho_v f_y / f_c'$, was the dominant factor in the determination of the normalized shear strength. Also based on statistical analysis, a shear strength equation was proposed as:

$$\frac{v_u}{f_c'} = 0.66\sqrt{\frac{\rho_v f_y}{f_c'}} < 0.3 \tag{2.14}$$

This equation is very similar to the equation proposed by Loov in 1978. They chose 0.66 (k in Loov's equation (2.10)) for both initially cracked and initially uncracked shear interfaces.

2.2.14 S.G. Tsoukantas and T.P. Tassios, 1989

In this paper, the authors proposed nominal shear stress equations for the connections of a prefabricated linear element.

for smooth interfaces

$$v_u = 0.4\sigma$$

for rough interfaces

$$v_u = 0.5\sqrt[3]{f_c'^2\sigma} \tag{2.15}$$

The effect of concrete strength was taken into account. Different powers were chosen for concrete strength and normal stress at interfaces.

2.2.15 R.E. Loov and A.K. Patnaik, 1994

Based on their test results from 16 beams, the authors incorporated equation (2.11) (Loov, 1978) and proposed a general equation for the design of composite beams in this study.

$$v_n = k\lambda\sqrt{(0.1 + \rho_v f_y) f_c'} \leq 0.25 f_c' \tag{2.16}$$

For composite construction, a factor of 0.5 for k was suggested. For monolithic construction, the value of 0.6 for k was suggested. The factor λ varies for lightweight concrete.

This equation combines the effect of concrete strength and clamping stress. It is equally applicable to lightweight and semi-lightweight concrete. Comparison of the shear strengths calculated from the above equation with a number of test results from push-off test in literature showed very good correlation.

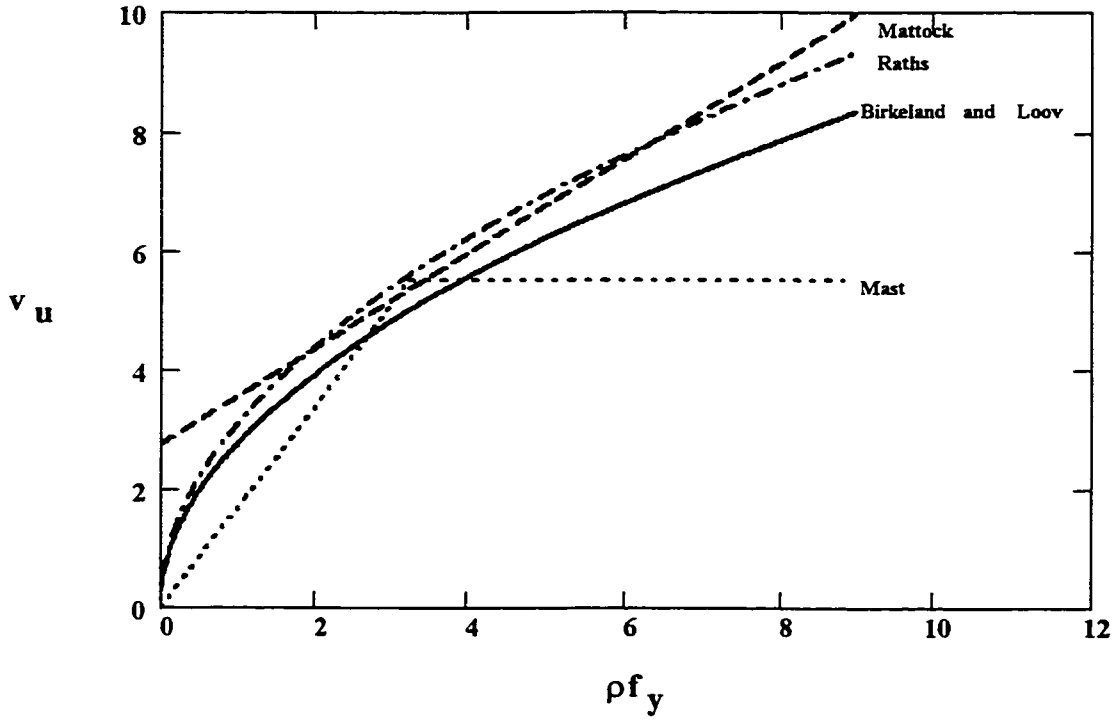

Figure 2.2: Comparison of main shear-friction equations

2.2.16 Summary

Shear friction strength is mainly contributed to by the resistance to shearing off of protrusions on the crack faces, cohesion of concrete (it was neglected by some researchers) and the frictional resistance to sliding.

The concrete strength is a factor in shear friction strength. Increasing concrete strength will increase cohesion of concrete and resistance to shearing off of protrusions on the crack faces. The frictional resistance is independent of the concrete strength if the effect of smoother crack surfaces for high-strength concrete is neglected.

The parabolic shear friction strength equations first came out as an alternate

simple expression of Mattock's equation (2.3). It can be thought that these parabolic equations also accounted for the resistance to shearing off of protrusions on the crack faces and the frictional resistance to sliding, even though these have not been presented as separate terms in their equation. In Figure 2.2, several main shear-friction strength equations are plotted against each other.

2.3 Review of Several Main Recent Codes

In this section, the design provisions in several main recent codes, CSA-A23.3-94, ACI 318M-95 and Euro code, for reinforced concrete beams failing in shear, will be reviewed. Deep beams will not be reviewed, because this thesis' main concern is slender beams. In these codes, for the beams without shear reinforcement, the shear strength is assumed to be equal to the strength corresponding to shear cracking. For the beams with shear reinforcement, the shear strength is calculated based on the truss model. Therefore, it is necessary to review concepts of shear cracking and the truss analogy first.

2.3.1 Shear Cracking

Generally, when a reinforced concrete beam is loaded, flexural cracks initiate and extend vertically up to the neutral axis of the beam. These cracks result in a stress concentration in the compression zone (head of crack). With increased loading, the inclined shear cracks develop in the uncracked region or the flexural cracks extend to be shear cracks. Inclined shear cracks always occur before a shear failure happens. For most beams without shear reinforcement, shear cracking causes immediate shear

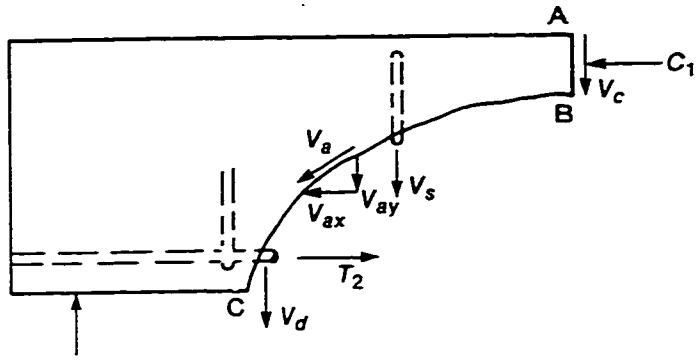

Figure 2.3: Internal forces in a cracked beam (MacGgregor, 1992)

failure. For this reason the shear capacity of a beam is assumed equal to the inclined cracking shear.

As shown in Figure 2.3, up to the inclined cracking load, shear is transferred across the crack in a beam without stirrups by the interlock of the aggregate particles on the two faces of the crack V_a, the dowel action of the longitudinal reinforcement V_d and the uncracked concrete at the top of the beam V_c. It is difficult to determine how much force is transferred by each. MacGregor explained the mechanism of shear transfer in his book reasonably well. Immediately after inclined cracking, as much as 40 to 60% of the total shear may be carried by dowel action and interlock of aggregate together. As the crack widens, the resistance of aggregate interlock decreases, increasing the fraction of the shear resisted by the uncracked concrete and dowel action. The dowel shear leads to a splitting crack in the concrete along the reinforcement. When this crack occurs, dowel action drops to zero. All shear is transferred to the uncracked concrete. This may cause crushing of this region.

(MacGregor, 1992).

It has been thought that the shear cracking load mainly depends on the tensile strength of concrete, longitudinal reinforcement ratio, shear span ratio and size of beam. Some of these have been taken into account in empirical equations in these codes. Some have not been taken into account. Whether these effects have been accounted for properly or not will be shown in Chapter 5.

2.3.2 Truss Model for Slender Beam

The truss analogy is an old concept of concrete structural design. At the beginning of the century, the German engineer Morsch proposed the truss analogy for the design of reinforced concrete beams for shear (Morsch, 1908). A truss mechanism in beams can function only after the formation of diagonal cracks. Referring to Figure 2.4, the equivalent truss of a beam consists of the stirrups (by lumping all stirrups crossing section A-A) acting as tension members and concrete struts (all the diagonal concrete members between cracks cut by section B-B) running parallel to the diagonal cracks. The concrete compression zone and the longitudinal reinforcement form the top and bottom chords of this analogous pin-jointed truss.

If it is assumed that all of the stirrups have yielded by the time the failure load is reached, each of stirrups is carrying a vertical force $A_v f_y$ and all shear is resisted only by stirrups. The forces in the truss can be determined by consideration of equilibrium.

The force in one stirrup is

$$A_v f_y = \frac{V s}{jd} \tan\theta \qquad (2.17)$$

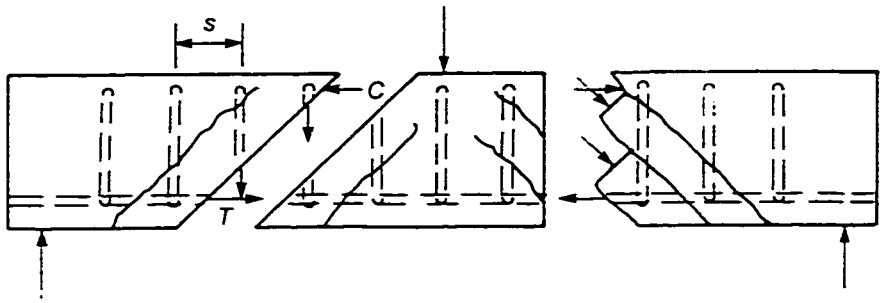

(a) Internal forces in a cracked beam.

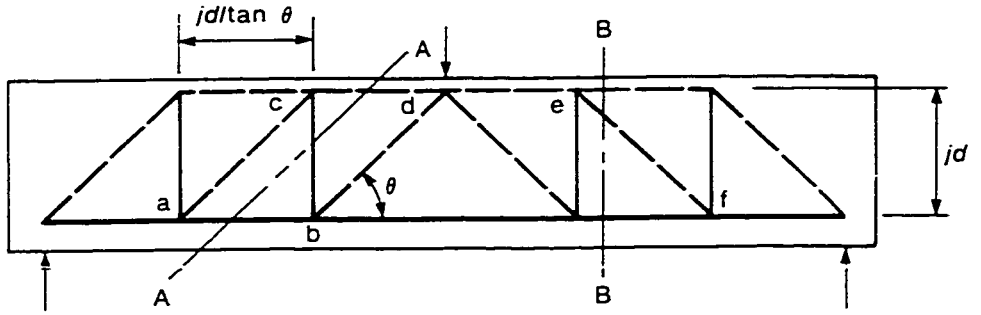

(b) Pin-jointed truss.

Figure 2.4: Truss analogy (MacGregor, 1992)

The average compressive stress in concrete struts is

$$f_{cd} = \frac{V}{b_w jd \cos\theta \sin\theta} \tag{2.18}$$

where A_v is the area of stirrup legs, s is the spacing of stirrups, jd is the distance between the resultants of the internal compressive and tensile forces on a cross section, θ is the angle of the compression struts and b_w is web width of the beam.

In order to avoid crushing of concrete struts and ensure that stirrup stresses reach yield with failure load, the compressive stresses in the concrete struts f_{cd} and the

angle θ need to be limited.

Note that the truss model ignores the shear resisted by concrete. This includes the effect of the interlock of the aggregate particles on the two faces of the crack, the dowel action of the longitudinal reinforcement and the resistance of uncracked concrete at the top of beam.

2.3.3 ACI Procedure (MPa units)

The basic requirement for shear design of slender beams is

$$V_u \leq \phi V_n \tag{2.19}$$

where V_u is the factored shear force, V_n is the nominal ultimate shear capacity of a concrete beam and ϕ is a strength reduction factor equal to 0.85 for shear.

Beams without Shear Reinforcement

The ACI code lumped the contribution of aggregate interlock, dowel action and uncracked concrete together and gives two empirical equations for calculating the shear strength,V_c, of reinforced concrete members subjected to shear and flexure only. The simple one is:

$$V_c = \left(\sqrt{f'_c}/6\right) b_w d \tag{2.20}$$

in which b_w is the web thickness and d is the effective depth of the member. This equation only accounted for the effect of the tensile strength of concrete as $\sqrt{f'_c}$. For this reason, it overestimates the shear capacity of beams with small steel percentages and underestimates the shear strength of beams with large steel percentages.

The more accurate equation is:

$$\begin{aligned} V_c &= \left[\left(\sqrt{f'_c} + 120\rho_w \frac{V_u d}{M_u}\right)/7\right] b_w d \\ &\leq 0.3\sqrt{f'_c} b_w d \end{aligned} \tag{2.21}$$

in which $V_u d/M_u \leq 1$, M_u and V_u are the moment and shear force at section with factored loads, and ρ_w is the longitudinal reinforcement ratio ($A_s/b_w d$). Many researchers, based on their test results, found that the effect of ratio ρ_w and shear span ratio are not properly accounted for in the second equation (2.21).

Beams with Shear Reinforcement

The provision of the ACI code for reinforced concrete beams with web reinforcement is based on a 45^0 truss model. As mentioned before, the truss model ignores tensile stresses in concrete. By referring to equation (2.17), the shear capacity would be zero if beams have no shear reinforcement, which is not true. The ACI code recognized the contribution of concrete, so it is assumed that part of the applied shear is carried by the concrete, V_c, and the rest is carried by the shear reinforcement.

$$V_n = V_c + V_s \tag{2.22}$$

The concrete contribution, V_c, is taken as the shear at the commencement of diagonal cracking and is governed by shear cracking (equation 2.20). The shear force, V_s, resisted by the stirrups is calculated assuming that all stirrups crossing the crack are at yield.

$$V_s = \frac{A_v f_y d}{s} \tag{2.23}$$

This is equivalent to equation (2.17) derived from the truss model if $\theta = 45^0$ and jd is replaced by d. The inclined cracks initially develop primarily at an angle of 35^0 to 45^0, therefore, the design equation based on 45^0 truss model is conservative because more stirrups are encountered across a flat crack.

If the stirrups are inclined at an angle α to the horizontal, the shear resisted by stirrups is:

$$V_s = A_v f_y (\sin\alpha + \cos\alpha)\frac{d}{s} \tag{2.24}$$

The inclined stirrups give larger shear resistance than 90^0 stirrups, but also give larger tension in the longitudinal reinforcement.

Because the shear failure of a beam without stirrups occurs in a brittle manner, the ACI code requires a minimum amount of shear reinforcement wherever $V_u > 0.5V_c$, except in slabs, footings, concrete joint construction and certain shallow and wide beams.

$$A_{v(\min)} = \frac{b_w s}{3f_y} \tag{2.25}$$

To guard against web crushing and to control crack widths, the ACI code limits the maximum amount of shear reinforcement as:

$$V_{s(\max)} = \left(2\sqrt{f'_c}/3\right) b_w d \tag{2.26}$$

To ensure that at least one stirrup crosses an assumed 45^0 inclined crack, the ACI code limits the maximum stirrup spacing as:

When $V_s \leq \left(\sqrt{f'_c}/3\right) b_w d$

$$\begin{aligned} s_{\max} &\leq d/2 \text{ (whichever smaller)} \\ &\leq 600 \text{ mm} \end{aligned}$$

When $V_s > \left(\sqrt{f'_c}/3\right) b_w d$

$$\begin{aligned} s_{\max} &\leq d/4 \text{ (whichever smaller)} \\ &\leq 300 \text{ mm} \end{aligned}$$

2.3.4 CSA Simplified Method (MPa units)

The CSA code incorporates the traditional $V_c + V_s$ shear design approach under the name – Simplified Method. The basic requirement for shear design is:

$$V_r \geq V_f$$

where V_f is factored shear force at section and V_r is the factored resistance of a beam which is:

$$V_r = V_c + V_s \tag{2.27}$$

If a beam has minimum transverse reinforcement or $d \leq 300$ mm, the concrete contribution is given by:

$$V_c = 0.2\lambda\phi_c\sqrt{f'_c}b_w d \tag{2.28}$$

If a beam has less than the minimum transverse reinforcement and $d > 300$ mm,

the concrete contribution is given by:

$$\begin{aligned} V_c &= \left(\frac{260}{1000+d}\right)\lambda\phi_c\sqrt{f'_c}b_w d \\ &\geq 0.1\lambda\phi_c\sqrt{f'_c}b_w d \end{aligned} \tag{2.29}$$

λ = modification factor to account for type of concrete.

ϕ_c = resistance factor for concrete (0.6 for cast in place concrete, 0.65 for precast concrete).

Note that the size effect is accounted for in equation (2.29).

The shear carried by vertical stirrups is:

$$V_s = \frac{\phi_s A_v f_y d}{s} \tag{2.30}$$

ϕ_s = resistance factor for reinforcement (equal to 0.85).

When inclined stirrups are used as shear reinforcement,

$$V_{sg} = \frac{A_v f_y \left(\sin\alpha + \cos\alpha\right) d}{s} \tag{2.31}$$

A minimum area of shear reinforcement shall be provided to avoid sudden shear cracking, when $V_f \geq 0.5V_c$

$$A_{v\,\min} = 0.06\sqrt{f'_c}\frac{b_w s}{f_y} \tag{2.32}$$

except for

(a) slabs and footings;

(b) concrete joint construction;

(c) $h \leq 250$ mm; and

(d) beams cast integrally with slabs where $h \leq 1.5b_w$ and 600 mm.

In order to avoid web crushing and excessive crack widths, the CSA code limits maximum amount of shear reinforcement as:

$$V_{s\max} = 0.8\lambda\phi_c\sqrt{f'_c}b_w d \tag{2.33}$$

The maximum stirrup spacing is limited by:

(a) 600 mm or 0.7d if $V_f/b_w d < 0.1\lambda\phi_c f'_c$

(b) 300 mm or 0.35d if $V_f/b_w d \geq 0.1\lambda\phi_c f'_c$

2.3.5 CSA General Method (MPa units)

The general method for shear design is based on the variable angle truss model and the modified compression field theory. The modified compression field theory is based on a group of assumptions about the behavior of cracked reinforced concrete. One of the important assumption is that the principal stress direction in cracked concrete coincides with the principal strain direction. The basic idea is that using equilibrium equations, compatibility conditions and constitutive laws for the materials, the diagonal compressive average stress in concrete (f_2), the diagonal tensile average stress between cracks in concrete (f_1), the stress in longitudinal bars, the stress in stirrups and the angle of inclination (θ) can be solved. The load-deformation response of reinforced concrete members loaded in shear can be predicted.

Using equilibrium conditions based on the truss model, the compressive and tensile stresses in concrete, and the stresses in longitudinal and shear reinforcement

are related to the applied load.

Using compatibility conditions, the strains in cracked concrete are related to the strains in reinforcement.

Using the stress-strain relationship, the principal tensile stresses (f_1) and compressive stresses (f_2) are related to the principal tensile strains (ε_1) and compressive strains (ε_2). Several key relationships are shown here.

$$f_2 = f_{2\max}\left[2\frac{\varepsilon_2}{\varepsilon_c'} - \left(\frac{\varepsilon_2}{\varepsilon_c'}\right)^2\right] \tag{2.34}$$

where

$$f_{2\max} = \frac{f_c'}{0.8 + 170\varepsilon_1} \leq f_c'$$

If $\varepsilon_1 \leq \varepsilon_{cr}$ then

$$f_1 = E_c\varepsilon_1 \tag{2.35}$$

If $\varepsilon_1 > \varepsilon_{cr}$ then

$$\begin{aligned} f_1 &= \frac{f_{cr}}{1 + \sqrt{500\varepsilon_1}} \\ &\leq \frac{0.18\sqrt{f_c'}\tan\theta}{0.3 + 24w/(a+16)} \end{aligned} \tag{2.36}$$

in which w is crack width, a is the maximum aggregate size, and

$$f_{cr} = 0.33\sqrt{f_c'}$$

In the general method of Clause 11.4, the factored shear strength of a reinforced

concrete section can be expressed as

$$V_{rg} = V_{cg} + V_{sg} \leq 0.25\phi_c f'_c b_w d_v$$

where, d_v is the distance perpendicular to the neutral axis between the resultants of the compressive and tensile force ($d_v \geq 0.9d$).

The concrete contribution, V_{cg}, is given by:

$$V_{cg} = 1.3\beta\sqrt{f'_c} b_w d_v \tag{2.37}$$

The shear resisted by vertical stirrups is

$$V_{sg} = \phi_s \frac{A_v f_y}{s} d_v \cot\theta \tag{2.38}$$

For members with transverse reinforcement inclined at an angle to the longitudinal axis, V_{sg} is:

$$V_{sg} = \phi_s \frac{A_v f_y d_v (\cot\theta + \cot\alpha)\sin\alpha}{s} \tag{2.39}$$

where the factor β reflects the ability of the cracked concrete to transmit tensile stress, and it is calculated from equation (2.36).

$$\begin{aligned} \beta &= \frac{f_1 \cot\theta}{\sqrt{f'_c}} \\ &\leq \frac{0.33\cot\theta}{1+\sqrt{500\varepsilon_1}} \end{aligned} \tag{2.40}$$

$$\leq \frac{0.18\sqrt{f'_c}\tan\theta}{0.3+24w/(a+16)} \tag{2.41}$$

Concrete strut crushing can be avoided by applying the limit of equation (2.40). The crack slipping failure due to wide cracks is limited by equation (2.41).

The value of β and θ is given in Table 11-1 or Figure 11-1 (for members with at least minimum stirrups) and Table 11-2 or Figure 11-2 (for members with less than minimum stirrups) in the code. In these tables and figures, θ_{max} and θ_{min} are limited to ensure stirrups yield at failure and avoid concrete strut crushing. Also note that the size factor is taken into account in Table 11-2 or Figure 11-2.

All values of β in Table 11-1 in the code were checked by Loov (Appendix A). An interesting result was found. All values of β in Table 11-1 with the exception of 3 are based on equation (2.41). This means that most beams that fail by shear will be governed by the crack slip (shear-friction failure) rather than the concrete strut crushing (shear compression failure).

In order to get β and θ, the factored shear stress,v_f, and the maximum longitudinal strain, ε_x, and crack spacing parameter, s_z, needs to be determined first by:

$$v_f = \frac{V_f}{b_w d_v} \tag{2.42}$$

$$\varepsilon_x = \frac{0.5\,(N_f + V_f\cot\theta) + M_f/d_v}{E_s A_s} \tag{2.43}$$

$$s_z = d_v \tag{2.44}$$

= distance between distributed longitudinal reinforcement

Another important feature of a truss is that the distribution of force along the longitudinal steel can be assessed. This is necessary for the curtailment of longitudinal steel.

2.3.6 CEB Code (MPa units)

Shear Cracking

The CEB code also assumes the shear capacity of a beam without shear reinforcement is equal to the shear cracking load because, for most members, it is the cause of immediate failure.

The main factors determining shear cracking loads are the dimensions of the section, the strength of the concrete and the ratio of longitudinal reinforcement based on the web width. The design resistance to shear cracking is given by:

$$V_{RD} = 0.15\,(3d/a)^{\frac{1}{3}}\,\xi\left(\frac{100A_s}{b_w d}f_c'\right)^{\frac{1}{3}} b_w d \tag{2.45}$$

where $\xi = 1 + \sqrt{200/d}$ with d in mm.

The CEB code realized that for very high strength concrete and lightweight aggregate concrete members, the cracks may go through, rather than around, aggregate particles thus reducing the ability of shear transfer. For this reason, the equation (2.47) is only applied to members with normal dense aggregate and with concrete strength up to 50 MPa.

Beam with Shear Reinforcement

The Euro code is also based on a variable truss model, but is simpler than the CSA general method because the contribution of concrete is neglected. The angle θ between the horizontal and the web compression is not fixed to any particular value and only has a lower limit of about $18.4^0(\cot\theta = 3)$ imposed by the difficulty to transfer force across cracks at very low inclinations.

The shear resistance of a beam can be calculated from:

$$V_{RD} = \frac{A_v f_y d_v \cot\theta}{s} \tag{2.46}$$

or

$$V_{RD} = f_c' b_w d_v \frac{\cot\theta}{\sqrt{1+\cot^2\theta}} \tag{2.47}$$

where

$$\cot\theta = \sqrt{\frac{f_c'}{\rho_w f_y} - 1} \tag{2.48}$$

and

$$1 \leq \cot\theta \leq 3 \tag{2.49}$$

The limit of equation (2.49) corresponds to truss angle of 18.4^0 to avoid concrete strut crushing and corresponds to a truss angle of 45^0 to ensure vertical stirrup yielding at failure.

The shear resistance of a beam with inclined shear reinforcement is given by:

$$V = A_v f_y \sin\alpha \frac{d_v \cot\alpha}{s} + f_c' b_w d_v \sin\theta\cos\theta \tag{2.50}$$

or

$$V = A_v f_y \sin\alpha \frac{d_v (\cot\alpha + \cot\theta)}{s} \tag{2.51}$$

where

$$\cot\theta = \sqrt{\left(1 - \frac{\rho_w f_y \sin^2\alpha}{f'_c}\right) / \left(\frac{\rho_w f_y \sin^2\alpha}{f'_c}\right)} \tag{2.52}$$

and

$$(\rho_w f_y)\,\min \geq 0.06\,(f'c)^{\frac{2}{3}}$$

The above equations can be used safely with f'_c up to 80 MPa.

Interestingly, it is pointed out in the Euro code that both simple models, with or without involving a principal tension in the cracked concrete, produce similar results if the web compression is assumed to be at a slightly lower inclination. However, in the modified compression theory, the contribution of the principal tensile stress in the cracked concrete is thought to be important.

Chapter 3

Development of Basic Shear-Friction Equations

3.1 Introduction

Four basic shear-friction equations to predict shear failure in reinforced beam were established by Loov in 1997. These four equations laid a solid foundation for the shear-friction method. Several aspects of this method, however, require further study.

The parabolic stress equation (2.10) (Loov, 1978) is the basis of the four shear-friction equations. Although it is simple and gives a close correlation to a number of test results, the shear stress along the failure plane will tend to infinity with an increase in the normal stress on the failure plane. This is shown in Figure 3.1 by the solid line. This is not a reasonable result. The shear stress must be zero when the normal stress reaches the compressive strength of concrete. This suggests that there may be other stress equations which are more reasonable. For higher normal stresses, an equation producing a result similar to the Mohr's circle for average stresses, represented by the dotted line in Figure 3.1, is needed. Also, this new equation should be as simple as the parabolic one.

By using general shear-friction equations, the shear capacity of every potential inclined failure plane between a support and a load point can be calculated. The plane which has the lowest shear capacity is predicted to be the failure plane. The problem is that for beams without stirrups this plane is always located from the inner edge of the support to the outer edge of the applied load. This does not correspond to

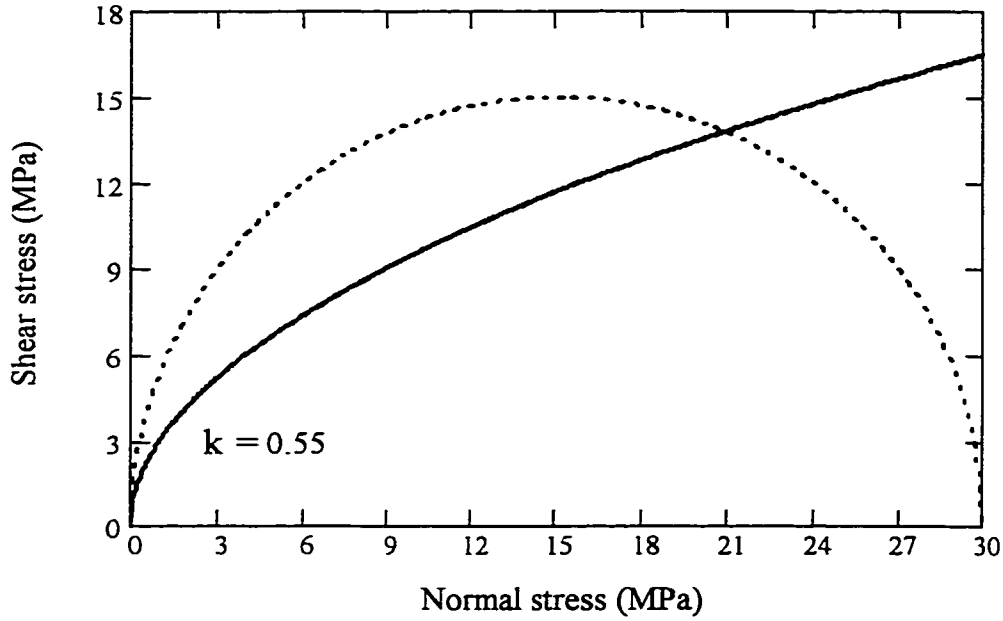

Figure 3.1: Parabolic stress equation and Mohr's circle

test results for beams with a ratio of clear shear span to overall depth of beam more than about 2. Figure 3.2 and 3.3 show typical crack patterns in simply supported reinforced concrete beams failed by shear. The beams with normal concrete strength in Figure 3.2 do not have shear reinforcement (Leonhardt and Walther, 1962). The beams with concrete strengths from 36 MPa to 87 MPa in Figure 3.3 have minimum shear reinforcement (Yoon, Cook and Mitchell, 1996). Therefore we need to find an equation to determine the diagonal crack location with respect to different shear span ratios and different amounts of shear reinforcement.

The factor k was proposed as constant in equation (2.10)(Loov, 1978). It is based on many push-off test results from the literature. The compressive concrete strength in these tests varied from 20MPa to 40MPa. We need to investigate if the

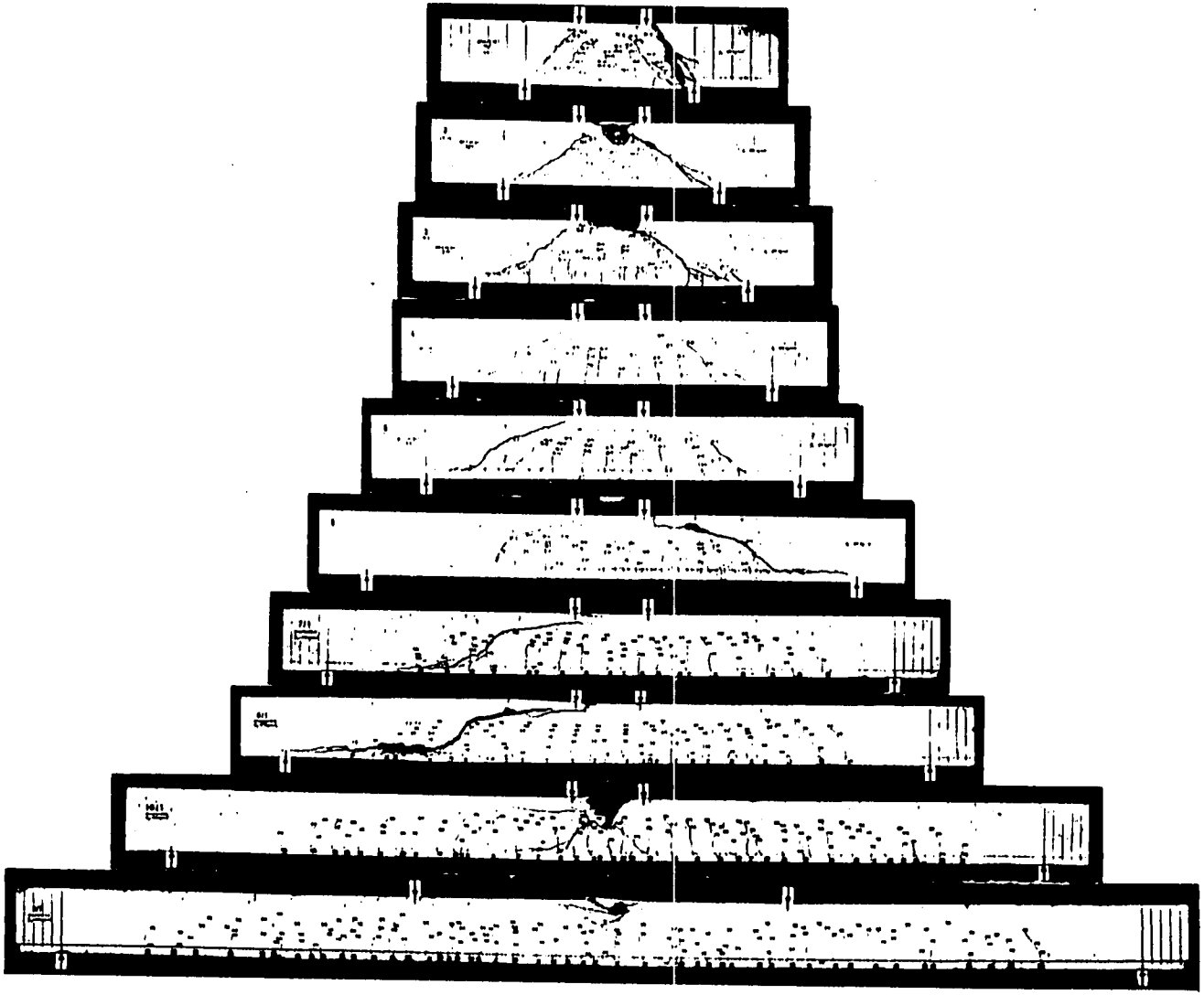

Figure 3.2: Types of shear crack of beams without stirrups

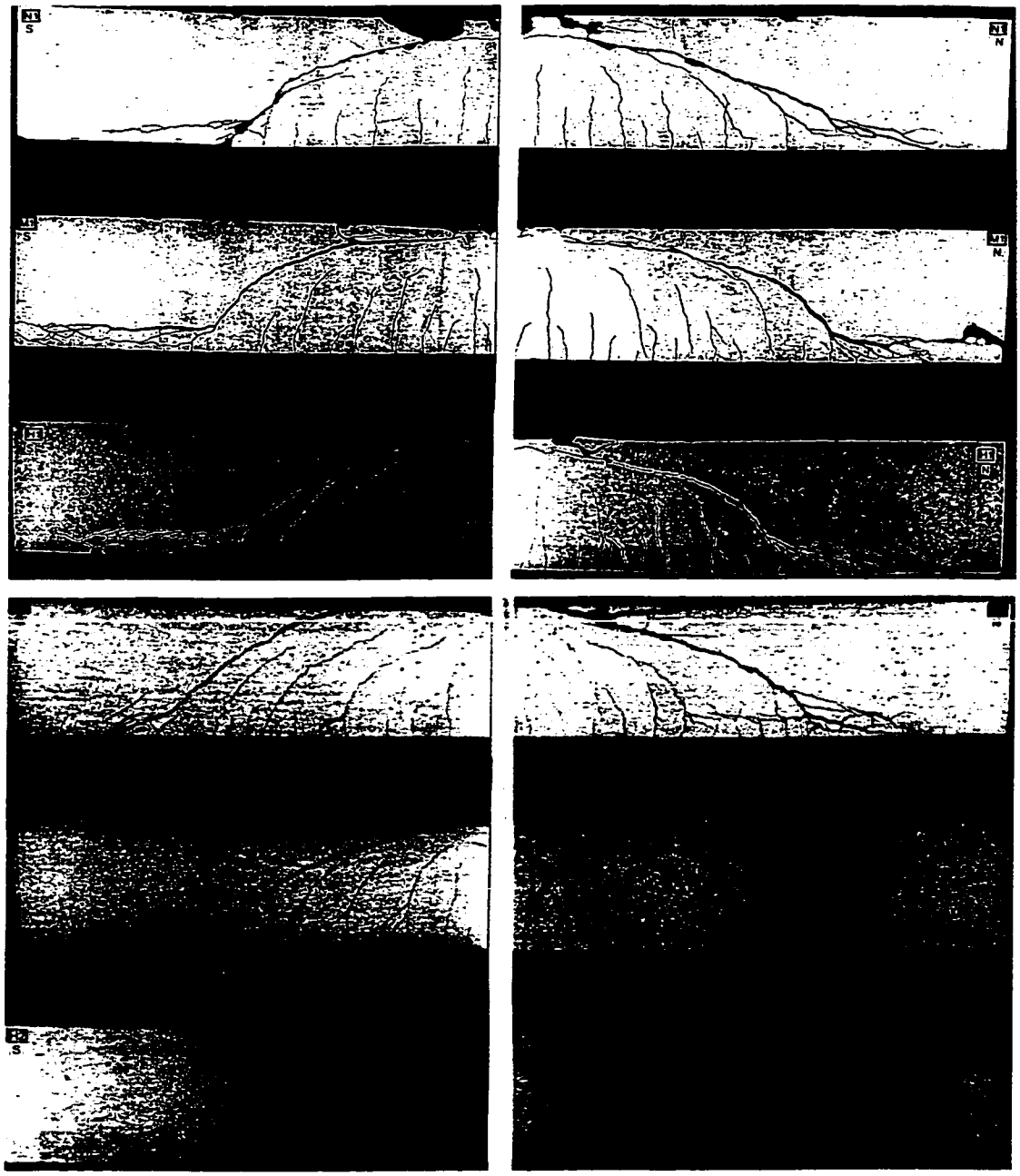

Figure 3.3: Types of shear crack of beams with stirrups

factor k remains constant with an increase in concrete strength.

Basic shear-friction equations are based on the inclined crack plane failure model, but curved failure surfaces are often observed in actual tests, especially in reinforced concrete beam without stirrups or with weak stirrups. These are shown in Figure 3.2 and 3.3, as well as in my tests (Figure 4.5 and 4.6). Is the inclined crack plane failure model close enough to describe what actually happens? A new failure model, the parabolic crack model, is presented in this chapter.

3.2 Basic Shear-friction Equations on Beam Shear (Loov, 1997)

3.2.1 General Equation

Consider a horizontal, simply supported beam loaded by two symmetrical point loads. The beam is assumed to have a constant depth. Figure 3.4 is a free-body diagram of the end of a beam.

The average shear stress (v) and normal stress (σ) on an inclined failure plane are:

$$v = \frac{S}{A} \tag{3.1}$$

$$\sigma = \frac{R}{A} \tag{3.2}$$

where S is the shear force and R is the normal force acting on the inclined plane of area A ($A = b_w h / \sin\theta, b_w$ is the width and h is the overall depth of the beam).

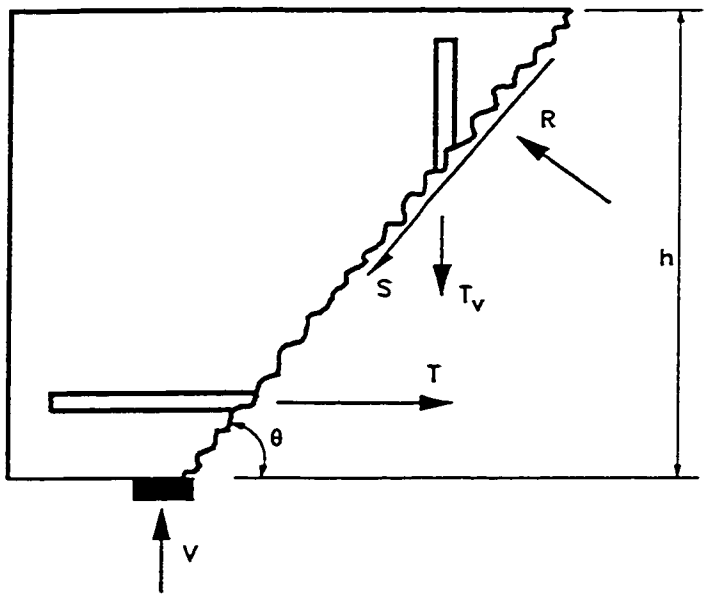

Figure 3.4: Free -body diagram (Loov,1998)

Inserting (3.1) and (3.2) into equation (2.10):

$$v = k\sqrt{\sigma f_c'}$$

We have:

$$S = k\sqrt{Rf_c'A} \tag{3.3}$$

Using force equilibrium we obtain:

$$R = T\sin\theta - (V - \sum T_v)\cos\theta \tag{3.4}$$

$$S = T\cos\theta + (V - \sum T_v)\sin\theta \tag{3.5}$$

where T is the tension force in the longitudinal reinforcement at the crack, T_v is the tension force in each stirrup crossing the crack, θ is the angle between the longitudinal axis and the potential shear failure plane, and V is the vertical force transmitted across the crack.

Introducing (3.4) and (3.5) to equation (3.3) gives a quadratic equation in V_{sf}.

$$V_{sf} = K\left[\sqrt{\frac{2T}{K} + \cot^2\theta} - \cot\theta\right]\left(1 + \cot^2\theta\right) - T\cot\theta + \sum T_v \qquad (3.6)$$

where, $K = 0.5k^2 f'_c b_w h$

The shear capacity of every potential failure plane from the load point to support can be calculated by using this equation. The lowest value is the shear capacity of the beam.

3.2.2 Development of Force in Reinforcement

The maximum force in the reinforcement crossing a crack depends on the anchorage on each side of the crack but can not exceed the yield force.

Figure 3.5 shows the variation of shear-friction strength based on equation (3.6) and the flexure strength for a particular plane in a beam as the tension in the longitudinal reinforcement is increased. The location of the peak can be determined by differentiating V with respect to T and setting this slope equal to zero.

$$\frac{\partial V}{\partial T} = \frac{1 + \cot^2\theta}{\sqrt{T/0.25k^2 f'_c b_w h + \cot^2\theta}} - \cot\theta = 0 \qquad (3.7)$$

$$T_{opt} = 0.25k^2 f'_c b_w h(1 + \sec^2\theta) \qquad (3.8)$$

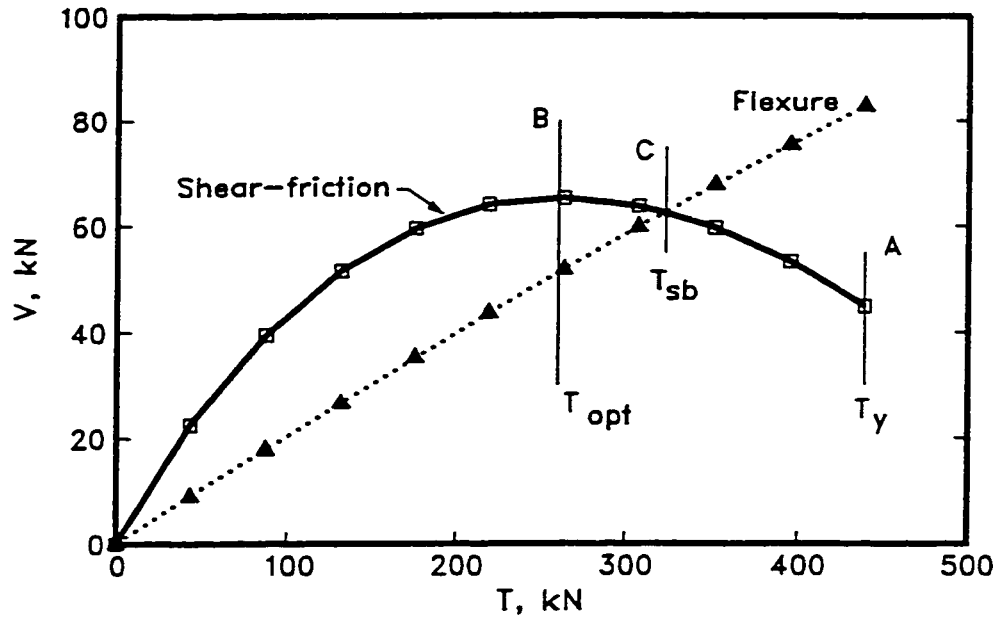

Figure 3.5: Effect of variation in longitudinal force on shear and moment (Loov,1998)

If this force is adequate for moment, then failure due to maximum shear can be expected when this force is reached. If a large longitudinal force is needed to develop the co-requisite moment, then the point of interest is the intersection point. At this point the shear and bending strengths are equal. The shear resistance will be less than the peak value. The use of T_{opt}, however, is appropriate when moment capacity is not reduced.

3.2.3 Simplified Equation

A simplified equation can be obtained by substituting T_{opt} from (3.8) for T in the general equation (3.6).

$$V_{sf} = 0.25k^2 f'_c b_w h \tan\theta + \sum T_v \tag{3.9}$$

This is the upper bound value of the general equation (3.6).

3.2.4 Design Equation for Shear Reinforced Beams

If a failure plane crosses n spaces and intersects $n-1$ stirrups, equation (3.9) can be written as:

$$V_{sf} = 0.25k^2 f'_c b_w h \frac{d_s}{ns} + T_v(n-1) \tag{3.10}$$

The weakest plane through the stirrups will occur when the incremental increase in stirrup force equals the incremental decrease in shear supported by the concrete. Equation (3.10) can be differentiated and set equal to zero if we assume n to be continuous rather than discrete.

$$\frac{\partial V}{\partial n} = -0.25k^2 f'_c b_w h \frac{d_s}{n^2 s} + T_v = 0 \tag{3.11}$$

then:

$$n = \sqrt{\frac{0.25k^2 f'_c b_w h}{T_v} \frac{d_s}{s}} \tag{3.12}$$

Inserting (3.12) into (3.10), the continuous design equation becomes:

$$V_{sf} = k\sqrt{f'_c b_w h T_v \frac{d_s}{s}} - T_v \tag{3.13}$$

This is the lower bound of equation (3.9), since

$$\frac{\partial^2 V}{\partial n^2} = 0.5k^2 f'_c b_w h \frac{d_s}{n^3 s} > 0$$

3.3 Validation of Parabolic Stress Equation

3.3.1 Comparison with Other Stress Equations

As mentioned before, the parabolic stress equation (2.10) is not completely satisfactory because the shear stress will tend to infinity with an increase in normal stress on the crack plane. In response to this problem several more realistic stress equations were proposed, including elliptical, offset circular and general parabolic stress equations. The average normal stress σ vs. the average shear stress v on a failure plane was plotted in Figure 3.6 for each equation illustrating their geometric shapes.

We can see that the shear stresses tend toward zero when the normal stress reaches the concrete stress (σ was assumed to vary from 0 to f'_c). The only question was whether the four basic shear-friction equations could be derived based on the three preceding equations.

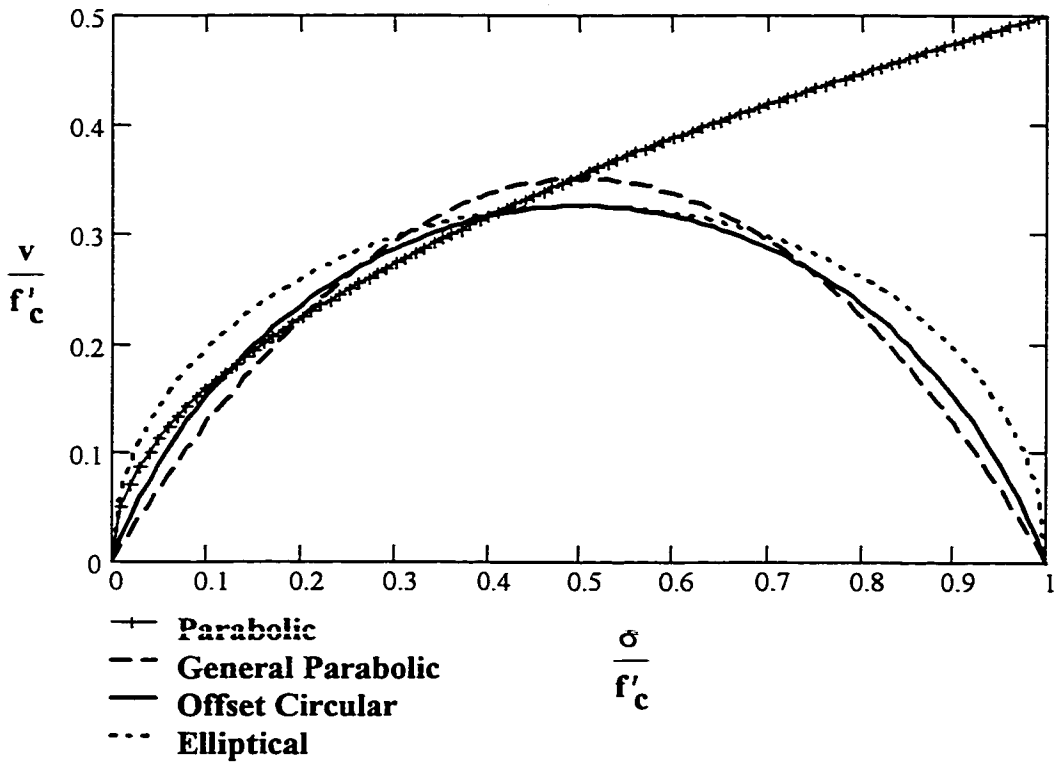

Figure 3.6: Comparison of different stress equations

Elliptical Stress Equation

If we assume the maximum shear stress is $kf_c'/2$ when the normal stress is $0.5f_c'$ the elliptical stress equation can be written as:

$$v = k\sqrt{\sigma(f_c' - \sigma)} \tag{3.14}$$

Similar to section 2, by using the stress equation (3.14) and force equilibrium in Figure 3.4, the general equation based on an elliptical stress equation can be derived

as:

$$V = \frac{k(1+\cot^2\theta)}{2(1+k^2\cot^2\theta)}\left(\sqrt{(kf'_cb_wh\cot\theta)^2+4f'_cb_whT-4T^2}-kf'_cb_wh\cot\theta\right) - \frac{\cot\theta(1-k^2)}{1+k^2\cot^2\theta}\cdot T+\sum T_v \tag{3.15}$$

Also, following the same procedure as in section 2, the force in the longitudinal reinforcement is:

$$T_{opt} = 0.5f'_cb_wh\left(1+\sqrt{\frac{k^2(1-k^2)^2\cos^4\theta-k^2}{(1-k^2)^2\sin^2\theta\cos^2\theta+k^2}+1}\right) \tag{3.16}$$

By substituting T_{opt} for T in (3.15), we would like to get a simplified equation but here, only a very complicated one is obtained. We know, therefore, that elliptical stress equations will be too complicated to use.

Offset Circular Stress Equation

Also by assuming the maximum shear stress is $kf'_c/2$ when the normal stress is $0.5f'_c$ the offset circular stress equation can be mathematically expressed as:

$$v=\sqrt{\sigma(f'_c-\sigma)+\frac{f'^2_c}{16}\left(\frac{1}{k}-k\right)}-\frac{f'_c}{4}\left(\frac{1}{k}-k\right) \tag{3.17}$$

Following the same steps, we have the general equation:

$$V = 0.5f'_cb_wh\sqrt{\left(\cot\theta+\frac{1-k^2}{2k}\right)^2+\frac{4T}{f'_cb_wh}\left(1-\frac{1-k^2}{2k}\cot\theta\right)-\left(\frac{2T}{f'_cb_wh}\right)^2} - 0.5f'_cb_wh\left(\cot\theta+\frac{1-k^2}{2k}\right)+\sum T_v \tag{3.18}$$

By differentiating the above equation with respect to T, the force in reinforcement is given by:

$$T_{opt} = 0.5 f'_c b_w h \left(1 - \frac{1-k^2}{2k} \cot\theta\right) \tag{3.19}$$

Inserting equation (3.19) into the general equation (3.18) gives the following form of simplified equation:

$$V = 0.5 f'_c b_w h \left(\frac{1+k^2}{2k} \csc\theta - \cot\theta + \frac{1+k^2}{2k}\right) + \sum T_v \tag{3.20}$$

Although these three equations are not very complicated, they are still not as simple as (3.6), (3.8), and (3.9) respectively.

General Parabolic Stress Equation

The general parabolic stress equation, represented by the dashed line in Figure 3.6, passes through 0 and 1 when $v/f'_c = 0$. The maximum shear stress is equal to kf'_c at a normal stress of $0.5f'_c$ on the shear failure plane. The stress equation can be written as:

$$v = 4k\sigma \left(1 - \frac{\sigma}{f'_c}\right) \tag{3.21}$$

The general equation was derived as:

$$\begin{aligned} V &= T tan\theta - \frac{f'_c b_w h}{8k}(1 + \cot^2\theta) \\ &\quad \cdot \left((4k\cot\theta + 1) + \sqrt{(4k\cot\theta + 1)^2 - 16k\cot\theta \frac{T}{f'_c b_w h}}\right) + \sum T_v \end{aligned} \tag{3.22}$$

Both the longitudinal force and simplified equations are even more complicated than offset circular ones.

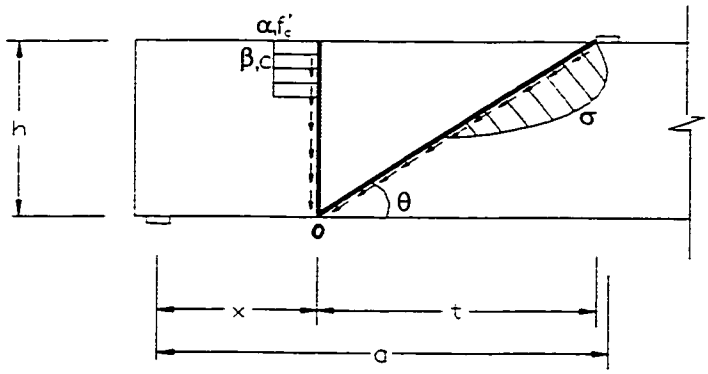

Figure 3.7: Shear and flexural stress of a concrete beam

Therefore, even though these three possible stress equations might give more reseanable predictions than the parabolic one when the normal stress is over half of compressive strength, they are not practical.

3.3.2 Applied Range of Parabolic Stress Equation

Only the parabolic stress equation was found to be simple and practical compared with the other stress equations mentioned above. It also gives a very close correlation to test results if the normal stress on the crack plane is no more than half the compressive strength of concrete. Next, the normal stress on the diagonal crack plane was evaluated to see if it reaches $0.5f'_c$.

To obtain an approximate upper bound to the average normal stress, assume a beam loaded in shear and flexure. We can assume the average normal stress on the inclined plane is σ at the time of failure. This situation is shown in Figure 3.7.

The total normal force on the vertical flexural failure plane can be approximately

calculated by the rectangular stress block.

$$\alpha_1 \phi_c f'_c \beta_1 c b_w$$

According to Clause 10.1.4 and 10.1.7 in the Canadian code and assuming the yield strength of 400 MPa for the longitudinal bars, we have:

$$\left(\frac{c}{d}\right)_{\max} = \frac{700}{700 + f_y} = \frac{7}{11} = 0.636$$

and

$$(\alpha_1 \beta_1) \leq (0.85 - 0.0015 f'_c)\,(0.97 - 0.0025 f'_c)$$

for $f'_c \geq 20$ MPa,

$$(\alpha_1 \beta_1) \leq 0.754$$

For a rectangular section, the upper bound of the average normal stress on the vertical flexural failure plane is:

$$\frac{0.754 \cdot f'_c \cdot 0.636 \cdot d b_w}{b_w h} = 0.48 f'_c \frac{d}{h}$$

The average normal stress will be smaller than the value determined using a uniform distribution. Using moment equilibrium about point 0 in Figure 3.7 we can obtain:

$$0.48 f'_c \frac{d}{h} b_w h \cdot \frac{h}{2} \geq \sigma \frac{b_w h}{\sin\theta} \cdot \frac{1}{2} \frac{h}{\sin\theta} \tag{3.23}$$

in which θ is the angle of the inclined crack. Then equation (3.23) can be rewritten

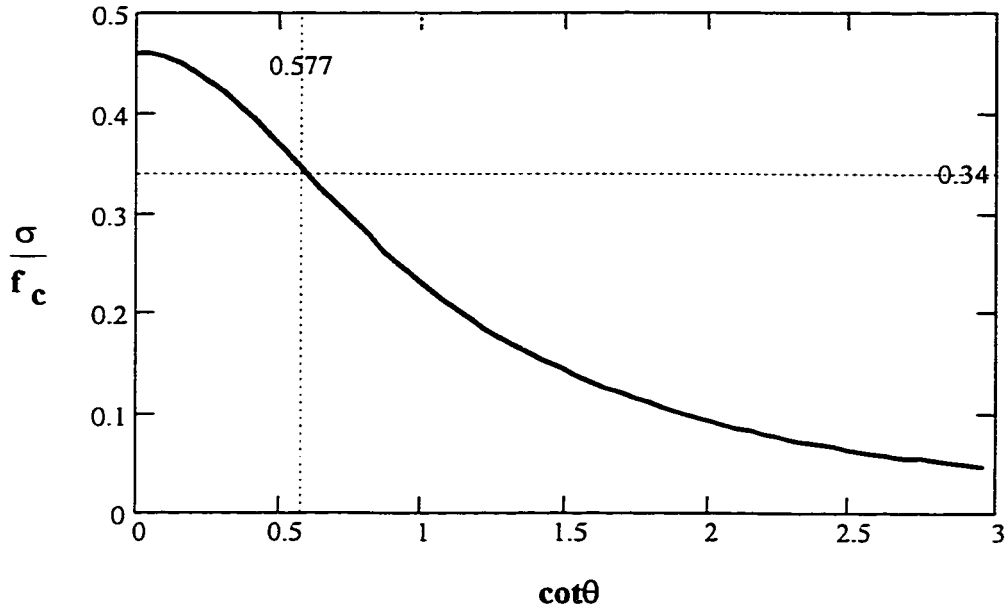

Figure 3.8: Normal stress vs. crack angle

in the following form:

$$\sigma \leq \frac{0.48\, f_c'}{1+\cot^2\theta}\frac{d}{h} \tag{3.24}$$

The average normal stress on the diagonal crack can not be more than the right side of (3.24), because flexure failure will occur rather than shear failure. The ratio σ/f_c' vs. $\cot\theta$ is plotted in Figure 3.8. d/h is generally less than 0.95. The maximum average normal stress corresponds to θ equal to 90^0 (a vertical failure plane).

$$\begin{aligned} \sigma_{\max} &= 0.48 f_c' \frac{d}{h} \\ &\leq 0.48 f_c'(0.95) = 0.46 f_c' \end{aligned} \tag{3.25}$$

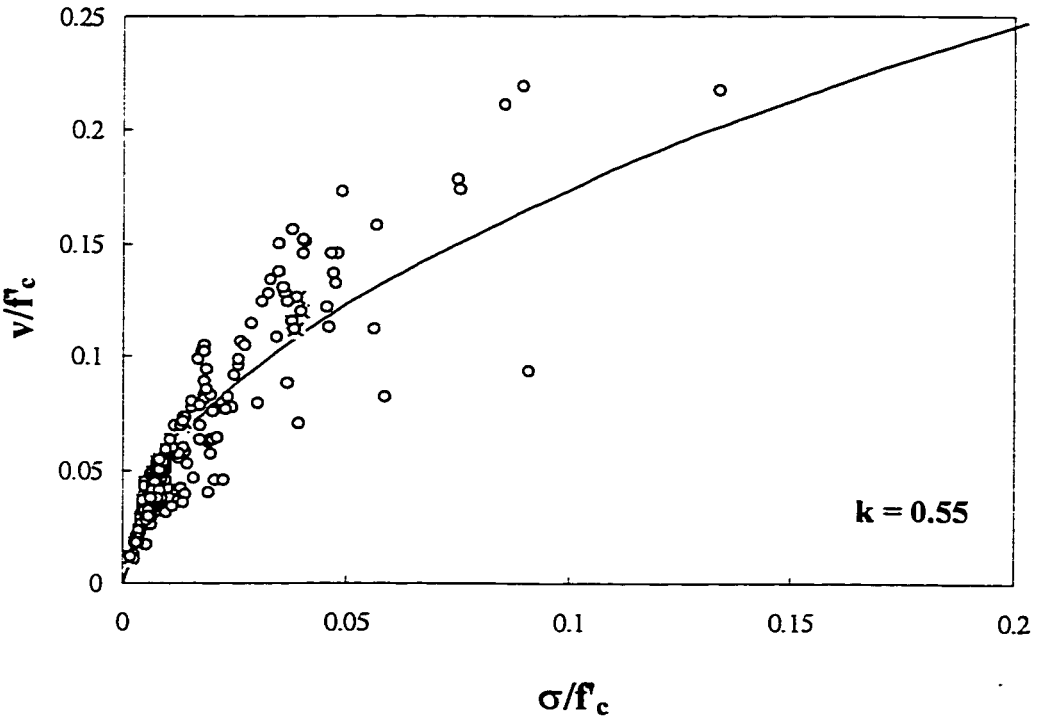

Figure 3.9: Normal stress on inclined crack plane

Generally, the angle of the inclined crack is less than 60^0, thus the maximum average normal stress on the inclined plane is

$$\begin{aligned} \sigma_{\max} &= \frac{0.48\, f_c'}{1+\cot^2 60^0}\frac{d}{h} = 0.36 f_c'\frac{d}{h} \\ &\leq 0.36 f_c'(0.95) = 0.34 f_c' \end{aligned} \tag{3.26}$$

The test results from 211 rectangular reinforced concrete beams with an a_{cle}/h, ratio of clear shear span to overall depth of beams from 0.5 to 5.6; f_c' from 20 to 125 MPa and shear reinforcement index from 0 to 8.3 MPa are plotted in Figure 3.9.

None of their average normal stresses is more than $0.15f'_c$, which confirms the above conclusion. As a result, the parabolic stress equation can be used to solve the shear problem for reinforced concrete beams.

3.4 Projection of Diagonal Crack

3.4.1 Cracking Load

Cracking load is the load at which a critical diagonal crack forms. Basically, the calculation of cracking load is a fracture mechanics problem. Here, we will use a simple method to estimate the diagonal cracking load. Figure 3.10 is a free body diagram of a simply supported, two point loaded, reinforced concrete beam at the time diagonal cracking occurs. M_A is the moment, V_A is shear force and N_A is normal force on the diagonal crack plane A. The x is the distance from the support to the starting point of the diagonal crack, t is the projection of the critical diagonal crack and θ is the angle between the longitudinal axis and the diagonal crack. V_{cr} is the cracking load.

M_A and V_A can be calculated by using equilibrium:

$$N_A = V_{cr}\cos\theta = V_{cr}\frac{t}{\sqrt{t^2+h^2}} \tag{3.27}$$

$$M_A = V_{cr}\left(x+\frac{t}{2}\right) \tag{3.28}$$

The maximum normal stress $\sigma_{\max}$ at the bottom end of the inclined cracking

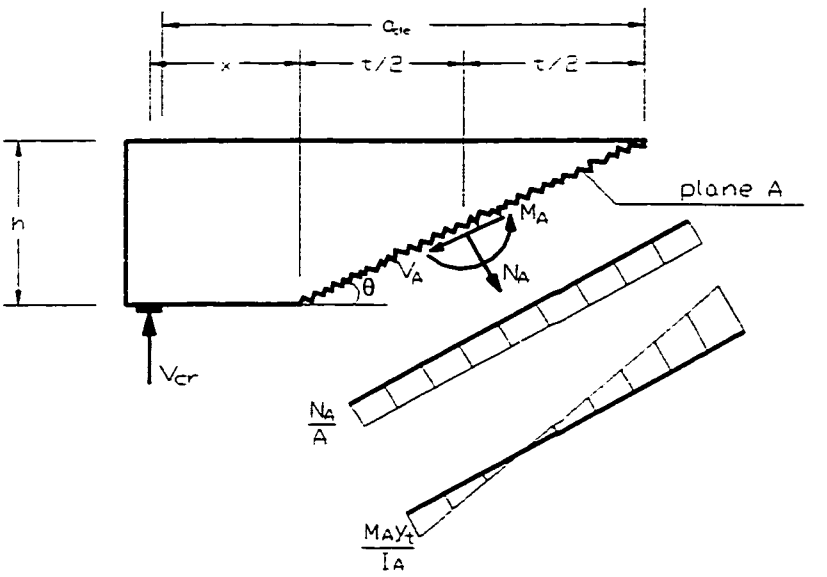

Figure 3.10: Approximate stresses on inclined crack plane

plane can be expressed as:

$$\begin{aligned} \sigma_{\max} &= \frac{N_A}{A} + \frac{M_A \cdot y_t}{I_A} \\ &= \frac{V_{cr} \cdot t}{b_w \cdot (t^2 + h^2)} + \frac{V_{cr}(6x + 3t)}{b_w \cdot (t^2 + h^2)} \\ &= V_{cr} \cdot \frac{6x + 4t}{b_w \cdot (t^2 + h^2)} \end{aligned} \tag{3.29}$$

in which A is the area of the inclined plane , I_A is the moment of inertia of the plane and y_t is the distance from the centroidal axis.

Obviously, $\sigma_{\max}$ cannot be more than the modulus of rupture of concrete f_r, and $x = (a_{cle} + 0.5w_b - t)$ (a_{cle} is clear shear span, w_b is the width of the bearing plane

at support). Then we rewrite (3.29) as:

$$\begin{aligned} V_{cr} &= \frac{b_w . f_r (t^2 + h^2)}{6\,(a_{cle} + 0.5 w_b) - 2t} \\ &\approx \frac{b_w . f_r (t^2 + h^2)}{6 a_{cle} - 2t} \end{aligned} \tag{3.30}$$

3.4.2 Projection of Crack

For a beam with a diagonal crack, the shear capacity can be calculated using the basic shear-friction equation and the cracking load can be calculated using equation (3.30). Then, we can plot the ultimate loads with different shear reinforcements and cracking loads against the distance of the starting point of the crack, x, seen in Figure 3.11. Curve (1) corresponds to the cracking load V_{cr}. Curve (2) corresponds to the strength of the beam without stirrups V_0. Curve (3) corresponds to the strength of the beam with weak stirrups V_w and Curve (4) corresponds to the strength of the beam with strong stirrups V_s.

When the load is increased, diagonal cracks appear in the shear span. Owing primarily to the interlock action of aggregates, shear stresses are transferred along the cracked section. When the development of the diagonal cracks reaches the point where the sliding strength along the crack is exceeded, sliding occurs and the beam fails in shear. In Figure 3.11 it can be seen that when the potential failure plane is located to the left of the intersections a, b and c which correspond to crackinh loads equal to shear strengthes (a for no stirrups, b for weak stirrups and c for strong stirrups respectively) the required shear strength is lower than the cracking load. Hence no shear failure can occur because a critical diagonal crack has not been

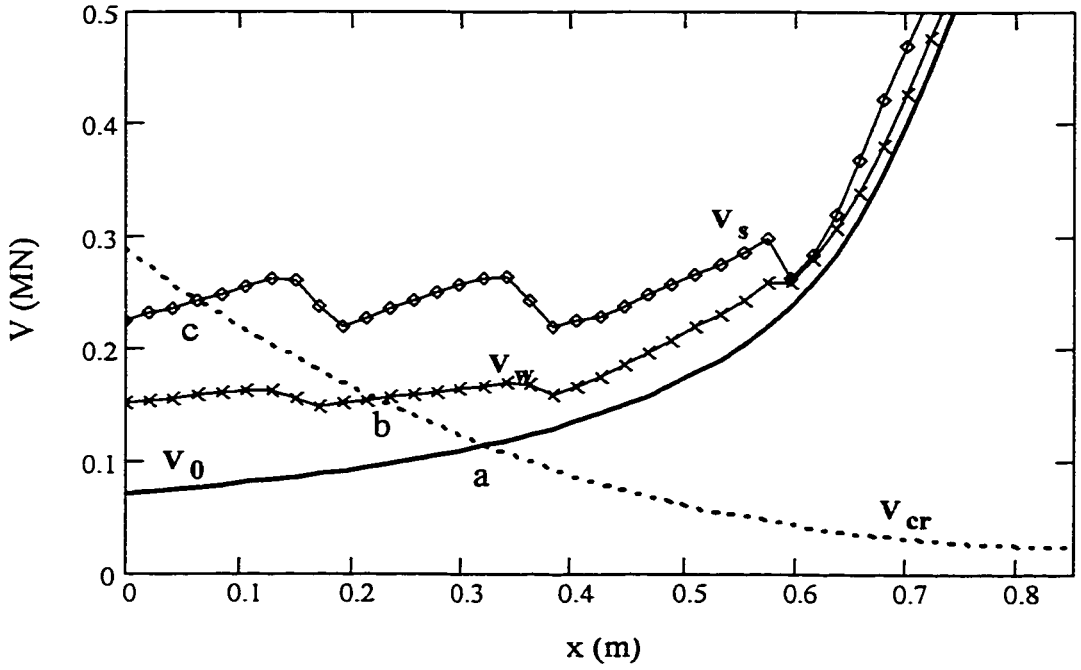

Figure 3.11: Crack location

created at this position (Zhang, 1997).

We only need check the potential failure planes on the right side of a, b and c because shear cracks are not expected on the left side of these points. Obviously, a and b are the starting points of the crack for beams without shear reinforcement and with weak shear reinforcement. That is because the lowest shear capacity always corresponds to the flattest possible failure plane. However, c is not necessarily the starting point of the failure crack if the incremental increase in stirrup force is more than the incremental decrease in shear supported by the concrete.

It was assumed that the beam failed while the critical diagonal crack was occurring, therefore, the projection of the crack can be determined by assuming the shear

capacity of the beam is equal to its cracking load:

$$\begin{aligned} V_{cr} &= V_{sf} \\ \frac{b_w \cdot f_r(t^2+h^2)}{6a_{cle}-2t} &= 0.25k^2 f'_c b_w h \cdot \frac{h}{t} + \rho_v f_{vy} b_w t \end{aligned} \tag{3.31}$$

where ρ_v is the ratio of shear reinforcement and f_{vy} is the yield strength of shear reinforcement. By assuming that the stirrups yield at failure the second portion of the right side of equation (3.31) represents the total tension force in stirrups crossing the crack, $\sum T_v$. The number of stirrups across the shear crack, n, is $(t/s-1)$ if the shear crack starts from a stirrup. The n is t/s if the shear crack starts between stirrups. This will be detailed in Chapter 5. In equation (3.31), $n = t/s$ is used for simplicity, thus

$$\sum T_v = A_v f_{vy} \frac{t}{s} = \rho_v f_{vy} b_w t$$

Now we can rearrange (3.31) as a cubic equation with respect to t/h:

$$\left(\frac{f_r}{f'_c} + 2\frac{\rho_v f_{vy}}{f'_c}\right)\left(\frac{t}{h}\right)^3 - 6\left(\frac{a_{cle}}{h}\right)\left(\frac{\rho_v f_{vy}}{f'_c}\right)\left(\frac{t}{h}\right)^2 + \left(\frac{f_r}{f'_c} + 0.5k^2\right)\left(\frac{t}{h}\right) - 1.5k^2\frac{a_{cle}}{h} = 0 \tag{3.32}$$

The solution for t/h will be too complicated to be used for design purposes. We need a simpler expression for t/h.

3.4.3 Approximate Equation for Projection of Crack

The solution of (3.32) with respect to t/h is a function of a_{cle}/h, $\rho_v f_{vy}/f'_c$, f_r/f'_c and k. After using a computer program to obtain the numerical solution of t/h, it was plotted vs. a_{cle}/h with different f_r/f'_c and k, as seen in Figure 3.12. The k is a

function of f'_c which will be explained later. The rupture strength f_r was calculated using the CEB code which gave closer values to test results than the Canadian code.

$$f_r = 1.4 \cdot \left(\frac{f'_c}{10}\right)^{\frac{2}{3}} \left(\frac{1 + 1.5(\frac{h}{100})^{0.7}}{1.5(\frac{h}{100})^{0.7}}\right) \tag{3.33}$$

Figure 3.12 illustrated that t/h does not change much when f_r/f'_c and k increase compared to a_{cle}/h and $\rho_v f_{vy}/f'_c$in the critical range of a_{cle}/h =1-4. and This means we might ignore them in an approximate equation.

Then, t/h was plotted against a_{cle}/h with different ψ (ψ is $\rho_v f_{vy}/f'_c$) as seen in Figure 3.13. When $\psi \geq 0.03$, t is equal to a_{cle}. t can not be more than a_{cle}.

Instead of the solution of (3.32) a very simple equation has been found which is:

$$\begin{aligned} \frac{t}{h} &\approx (\frac{a_{cle}}{h})^{(0.5+\psi/0.03)} \\ (t &\leq a_{cle}) \end{aligned} \tag{3.34}$$

For no shear reinforcement and minimum shear reinforcement concrete beams, t is a projection of the diagonal crack. For the concrete beams with strong stirrups, t is a range in which shear failure can occur. In Figure 3.13 the symbols represent the approximate equation (3.34) and the lines represent the exact solution from equation (3.32). Note that t calculated by (3.34) would be slightly lower than the exact one from (3.32) shown in Figure 3.13. This allows the use of a simple power.

Figure 3.14 and 3.15 show that equation (3.34) works well when compared with test results. The length t is generally slightly shorter than actual test results, as intended.

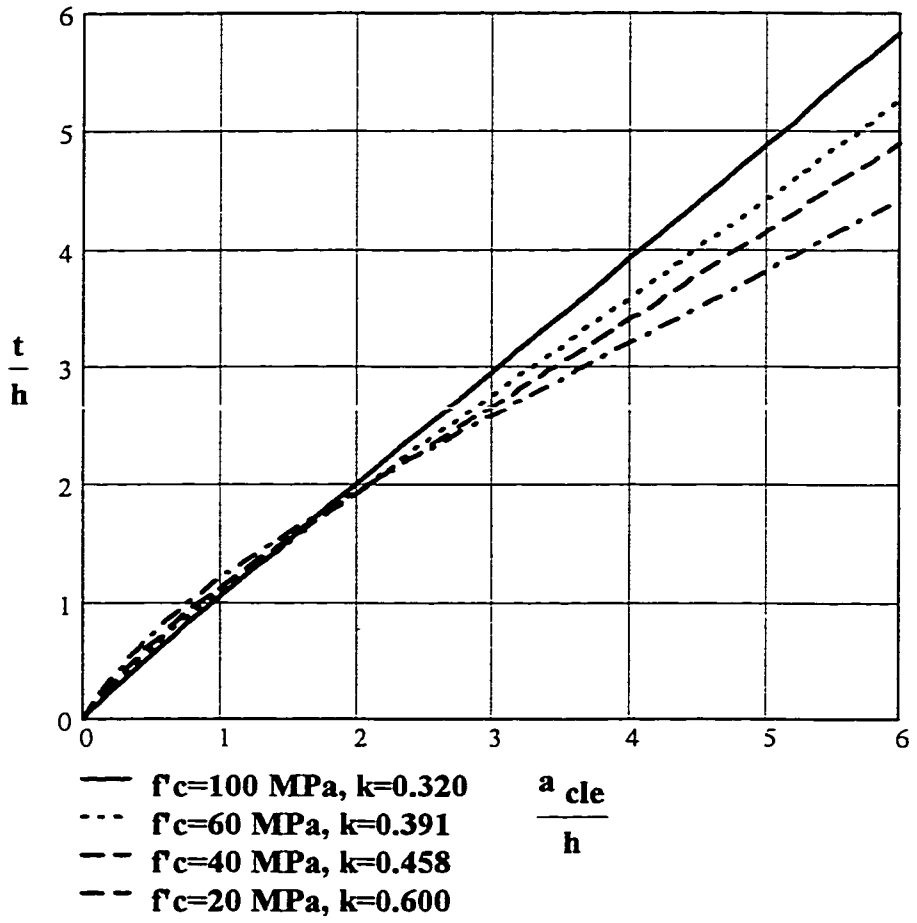

Figure 3.12: t/h vs. a_{cle}/h for dirrerent f'_c

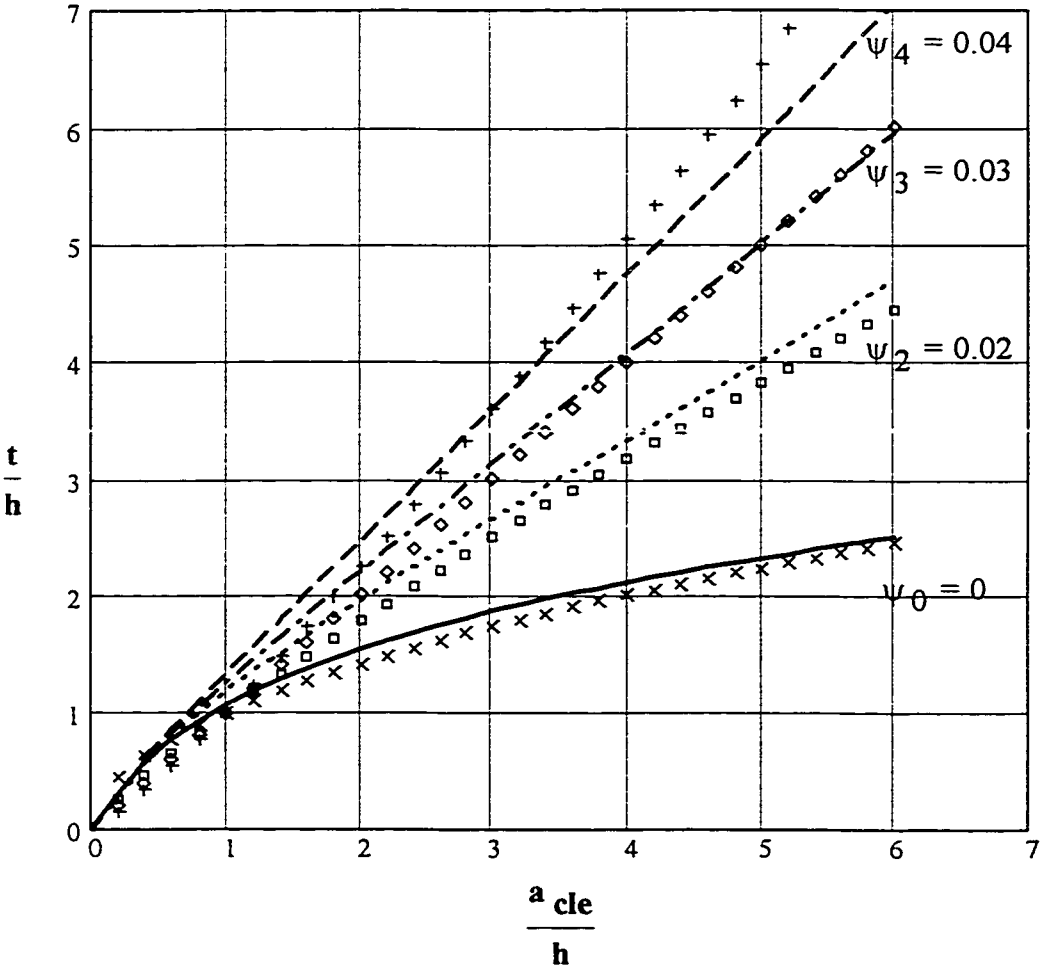

Figure 3.13: t/h vs. a_{cle}/h for different ψ

Figure 3.14: Crack locations predicted comparing to ones tested (no stirrups)

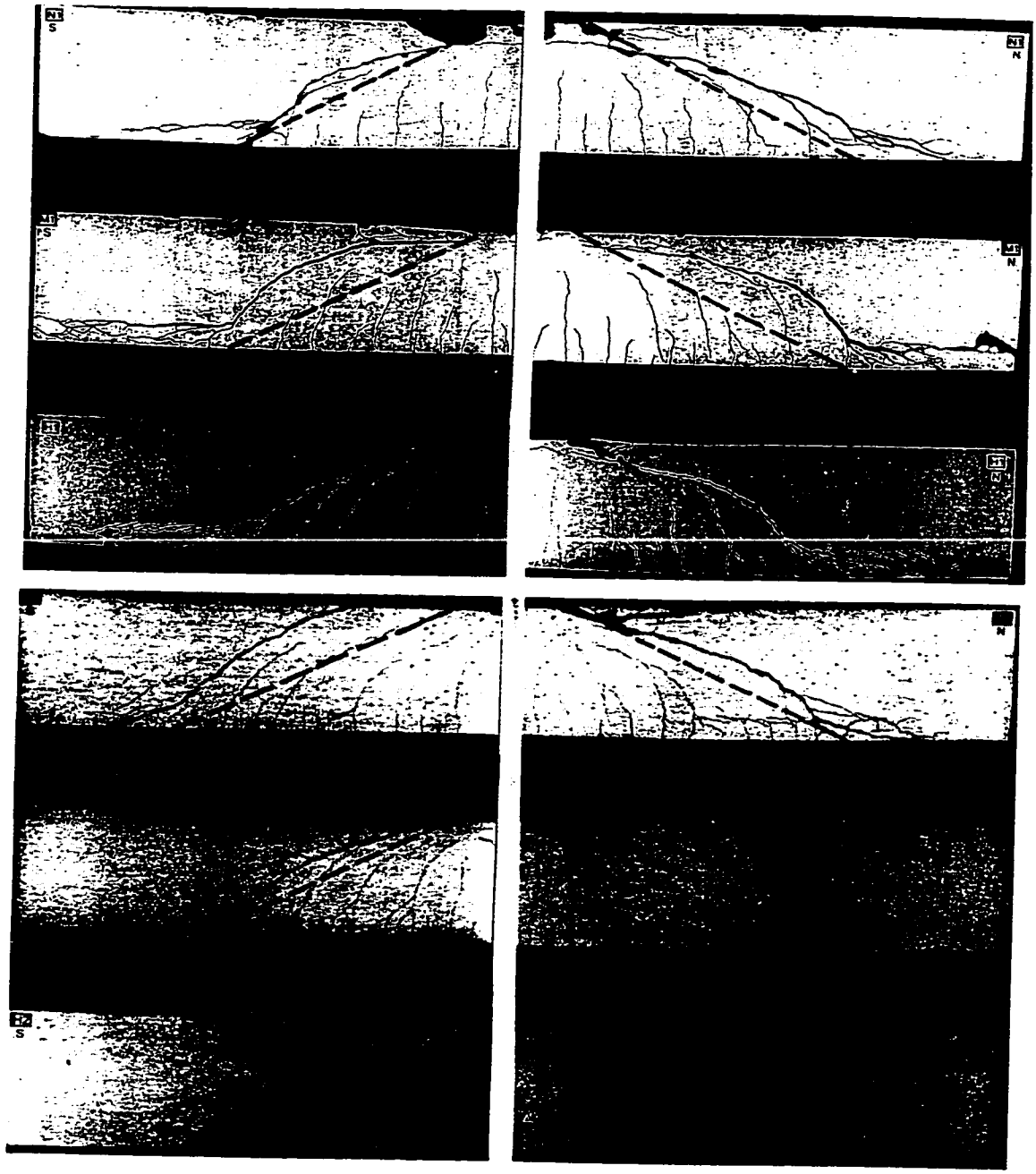

Figure 3.15: Crack locations predicted comparing to ones tested (with stirrups)

3.4.4 Design Equation for Reinforced Beam without Shear Reinforcement

Once the equation for the crack projection had been developed, the design equation for concrete beams without shear reinforcement can be easily derived by inserting (3.34) into (3.9), with $\psi = 0$. Thus:

$$V_{sf} = 0.25k^2 f_c' b_w h \sqrt{\frac{h}{a_{cle}}} \tag{3.35}$$

This equation is simple and works better than the current codes. This will be shown in Chapter 5.

3.5 Influence of Concrete Strength on k

3.5.1 Constant k for Normal Concrete Strength

The parabolic stress equation (2.10) proposed by Loov in 1978 has shown a very good correlation with test results. (see Figure 3.16.) It was used by Patnaik (Patnaik, 1993) in his study of composite beams and has proved to be suitable. The factor k was thought to be constant around 0.55. When we use $k = 0.55$ to calculate high-strength concrete beams, however, the shear capacities calculated by the basic shear-friction equations are higher than test results. Therefore, it appears that the factor k reduces with increased concrete strength.

The equation (11-33) in the Canadian code is:

$$v_r = \lambda \phi_c k \sqrt{\sigma f_c'} + \phi_s \rho_v \cos \alpha_f$$

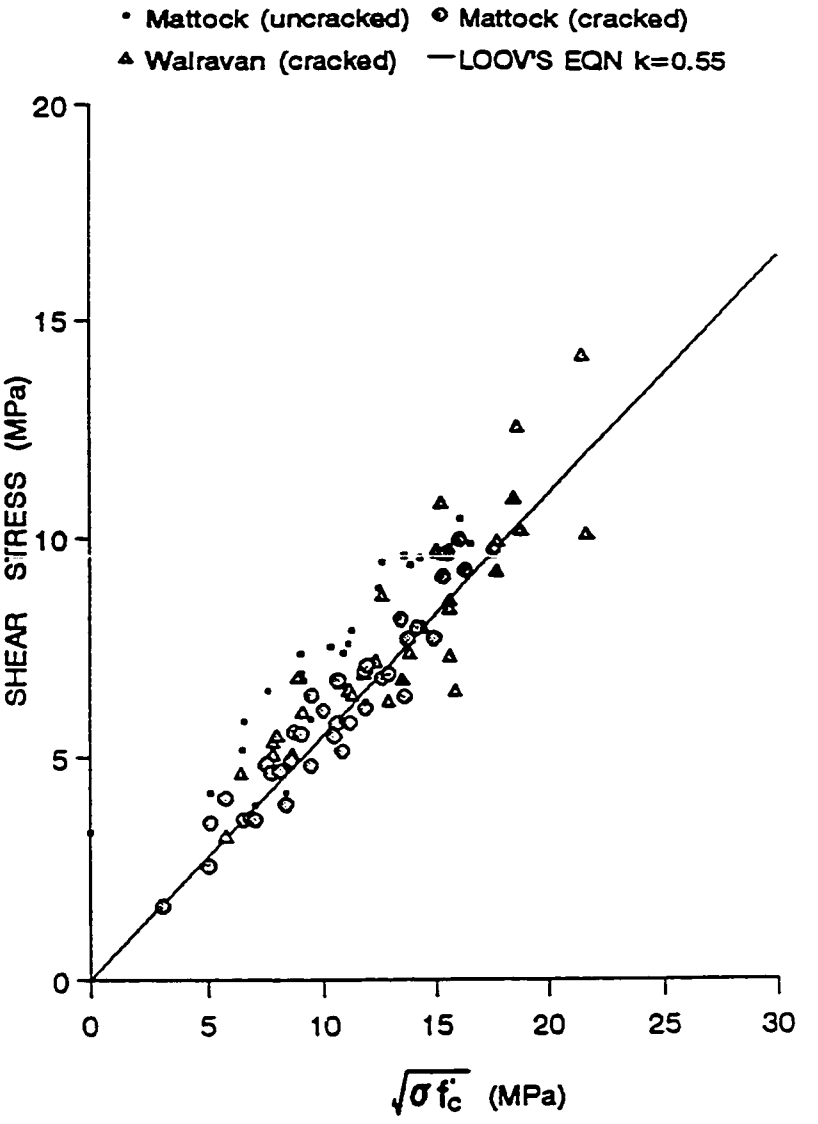

Figure 3.16: Push-off test results (Loov, 1998)

The first term of the equation (11-33) is the same as equation (2.10). The k in (11-33) is 0.5 for concrete placed against hardened concrete and 0.6 for concrete placed monolithically. This implies that k is related to friction on a surface. It is dependent upon how rough the failure surface is. As we know, the failure surfaces of normal strength concrete are normally rougher than those of high strength concrete because shear cracks will go through aggregate for high strength concrete rather than around aggregates, so aggregate interlock on the failure plane decreases with an increase in concrete strength. For this reason, k should change with concrete strength.

3.5.2 Effect of Concrete Strength on k

To investigate k we substitute the shear capacity V_t measured from tests for V_{sf} in the general equation (3.6) and design equation (3.13), then calculate the value of k by using a computer program. This k is called k_t.

The k_t of 185 reinforced concrete beams has been computed and plotted against f'_c as shown in Figures 3.17 and 3.18 in which symbol,+, represents beams without stirrups and symbol,o, represents beams with stirrups. k_{t-g} represents k_t from the general equation in Figure 3.17 and k_{t-d} represents k_t from the design equation in Figure 3.18.

These two figures indicate that k is a variable which is a function of concrete strength. The equation found using statistical regression analysis applying these 185 test results is shown in equations (3.36) and (3.37).

Based on the general equation:

$$k = 2.16 f_c'^{-0.42} \tag{3.36}$$

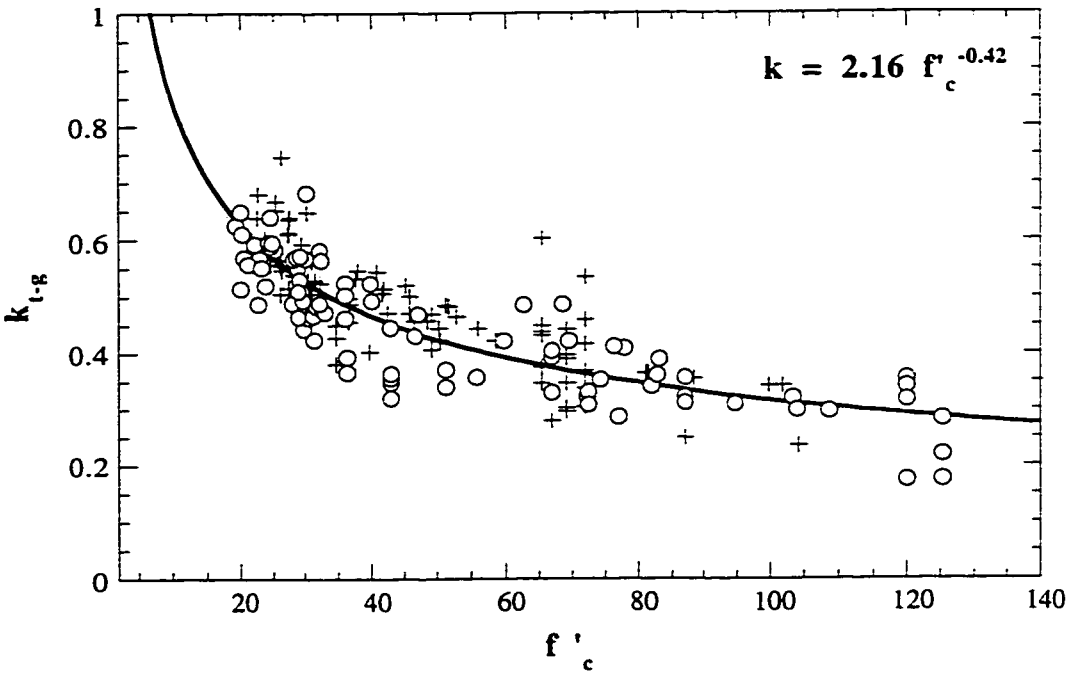

Figure 3.17: Factor k using general equation

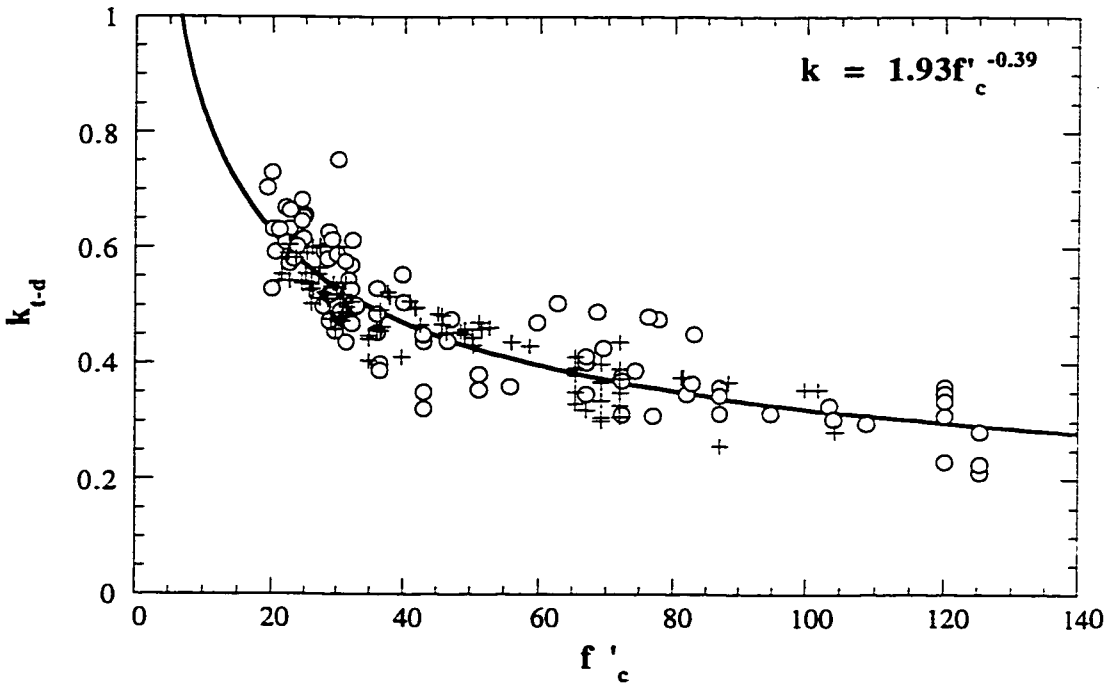

Figure 3.18: Factor k using design equation

Based on the design equation:

$$k = 1.93 f_c'^{-0.39} \tag{3.37}$$

The confidence interval for equation (3.36) is $k \pm 0.0065$ and the confidence intervalfor equation (3.37) is $k \pm 0.0044$ with 95% confident.

The k decreases with an increase of concrete strength. This accords with the smoother surface of the failure plane with a higher concrete strength. Note that the constants in equations (3.36) and (3.37) could slightly vary. They depend on test results chosed and number of tests used.

3.6 New Failure Model Based on Shear-Friction

As mentioned before, many reinforced concrete beams have curved failure surfaces rather than straight failure planes when they are failed in shear. In order to obtain a better prediction, a new failure model - the parabolic crack surface model - is presented here. The exact stress distribution on the failure surface is hard to determine. A uniform distribution of normal stress is still assumed as in the inclined crack plane model. Figure 3.19 is a free body diagram of a failed concrete beam based on this model.

3.6.1 Derivation of General Equation

The parabolic crack surface can be mathematically expressed as:

$$y = \frac{h}{t^2} \cdot x^2 \tag{3.38}$$

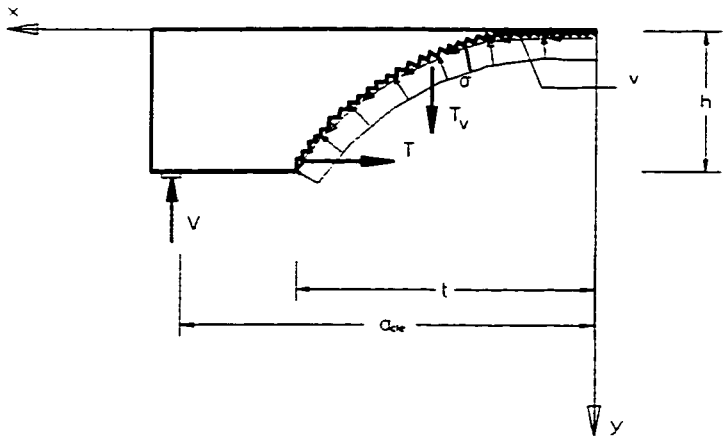

Figure 3.19: Free-body diagram for parabolic failure model

The total horizontal force on this surface due to normal and shear stresses is determined by:

$$F_x = b_w\,(h\sigma + t\,v)$$

The total vertical force on this surface due to normal and shear stresses is also found as:

$$F_y = b_w(hv - t\sigma) \tag{3.39}$$

The force equilibrium from the free body diagram shown in Figure ?? gives:

$$T = b_w(h\sigma + t\,v) \tag{3.40}$$

$$V - \sum T_v = b_w(hv - t\sigma) \tag{3.41}$$

The above equilibrium equations are not sufficient to calculate shear capacity. We must introduce another equation.

Equation (2.10) can be rewritten as: $\sigma = v^2/\left(k^2 f'c\right)$.

Inserting σ into equation (3.40) and expressing it with respect to v yields:

$$v = k^2 f'_c \frac{t}{2h}\left(\sqrt{1+\frac{4h}{k^2 f'_c b_w t^2}\cdot T}-1\right) \tag{3.42}$$

Substituting σ and equation (3.42) into equation (3.41) the general equation of the parabolic crack model can be obtained as below.

$$\begin{aligned} V &= 0.5k^2 f'_c b_w t\left(\sqrt{1+\frac{4h}{k^2 f'_c b_w t^2}\cdot T}-1\right) \\ &\quad -0.25k^2 f'_c b_w \frac{t^3}{h^2}\left(\sqrt{1+\frac{4h}{k^2 f'_c b_w t^2}\cdot T}-1\right)^2 + \sum T_v \end{aligned} \tag{3.43}$$

3.6.2 Force in Reinforcement

As before, the optimum force in the longitudinal reinforcement crossing the crack is determined by differentiating V in (3.43) with respect to T and setting this equal to zero.

$$\frac{\partial V}{\partial T} = \left(\sqrt{1+\frac{4h}{k^2 f'_c b_w t^2}\cdot T}-1\right) - \frac{h^2}{t^2} = 0 \tag{3.44}$$

Solving (3.44) for T, we get following equation:

$$T_{opt} = 0.25k^2 f'_c b_w h\left(\frac{h^2}{t^2}+2\right) \tag{3.45}$$

3.6.3 Simplified equation and design equation

The simplified equation for this new failure model is found by making a substitution of equation (3.45) into (3.43).

$$V = 0.25k^2 f'_c b_w h \tan\theta + \sum T_v \tag{3.46}$$

This is same as equation (3.9), because they are the upper bounds of the general equations.

The design equation is also the same as equation (3.13) due to the fact that the design equation is derived based on the simplified equation.

$$V_{sf} = k\sqrt{f'_c b_w h T_v \frac{d_s}{s}} - T_v \tag{3.47}$$

Equations based on two other failure models, an inclined failure plane with a triangular stress distribution and a parabolic failure surface with a triangular stress distribution, were also derived. It is believed that, for beams with a curved failure surface, the general equation based on a parabolic crack failure model might give a better prediction than the inclined crack model, because the calculations for the tension force in the reinforcement and the tension force in the stirrups are closer to what actually happens.

Chapter 4

Test Program and Discussion of Test Results

4.1 Introduction

There are a number of test data in the literature on reinforced concrete beams with shear reinforcement which have failed by shear, but it is difficult to find data on shear reinforced concrete beam with s/d ratios of more than 0.7. This is because there are some limitations on maximum spacing in various codes. It is necessary to know whether or not these limitations on maximum stirrup spacing are also required for the shear-friction procedure as stated in the Canadian Code. Further information is also required on the force in the longitudinal reinforcement crossing the shear crack. For these two main purposes, eight beams were designed and tested with the same concrete strength of about 30 MPa and the same ratio of longitudinal reinforcement, 2.7%. Each had different stirrup spacing wider than the Canadian code requirement and different diameters of shear reinforcement. In order to assure shear failure, care was taken in the design of the specimens to avoid all other possible modes of failure. The descriptions of the test beams, mix design, materials, instrumentation, test procedure, test results, and discussion of the test results are presented here.

4.2 Experimental Program

4.2.1 Test Specimens

The test beams, as shown in Figure 4.1 and 4.2, consisted of 8 rectangular concrete beams with different amounts of shear reinforcement. All beams had the same cross section, 280 mm width, 320 mm overall depth and 274 mm effective depth. The ratio of the clear shear span a_{cle} to h of each beam was 2.67. The ratio of longitudinal reinforcement, ρ, in each beam was chosen to be 2.7%. Four different s/d ratios were designed, 0.7, 0.9, 1.1 and 1.3. Two different diameters of stirrup were used, 5.7 mm and 11.3 mm. To obtain same effective depth, the covers for beams with 5.7 mm stirrups are 25 mm and the covers for beams with 11.3 mm stirrups are 20 mm. To prevent bond failure the overhangs were designed to be long enough and a large amount of shear reinforcement was used in the overhangs. Another point that needs to be mentioned is that beam No. 8 was designed with a predicted shear capacity only 4.3% more than its flexure capacity to use s/d of 0.7. It was known that there was a chance of flexure failure when it was designed.

To investigate the longitudinal force at the crack, strain gauges were attached to the reinforcement beside the stirrups along the beams, because the potential failure plane would usually start from the point beside a stirrup. The shear capacity is expected to have a large increment immediately after intercepting the stirrup due to the contribution of this stirrup. This can be seen in Figure 3.11. The strain gauges on stirrups were designed to cross shear cracks to assess whether or not No. 10 deformed stirrups had experienced strain hardening and what strain level the 5.7 mm stirrups reached at failure. The details of all test beams are given in Table 4.1.

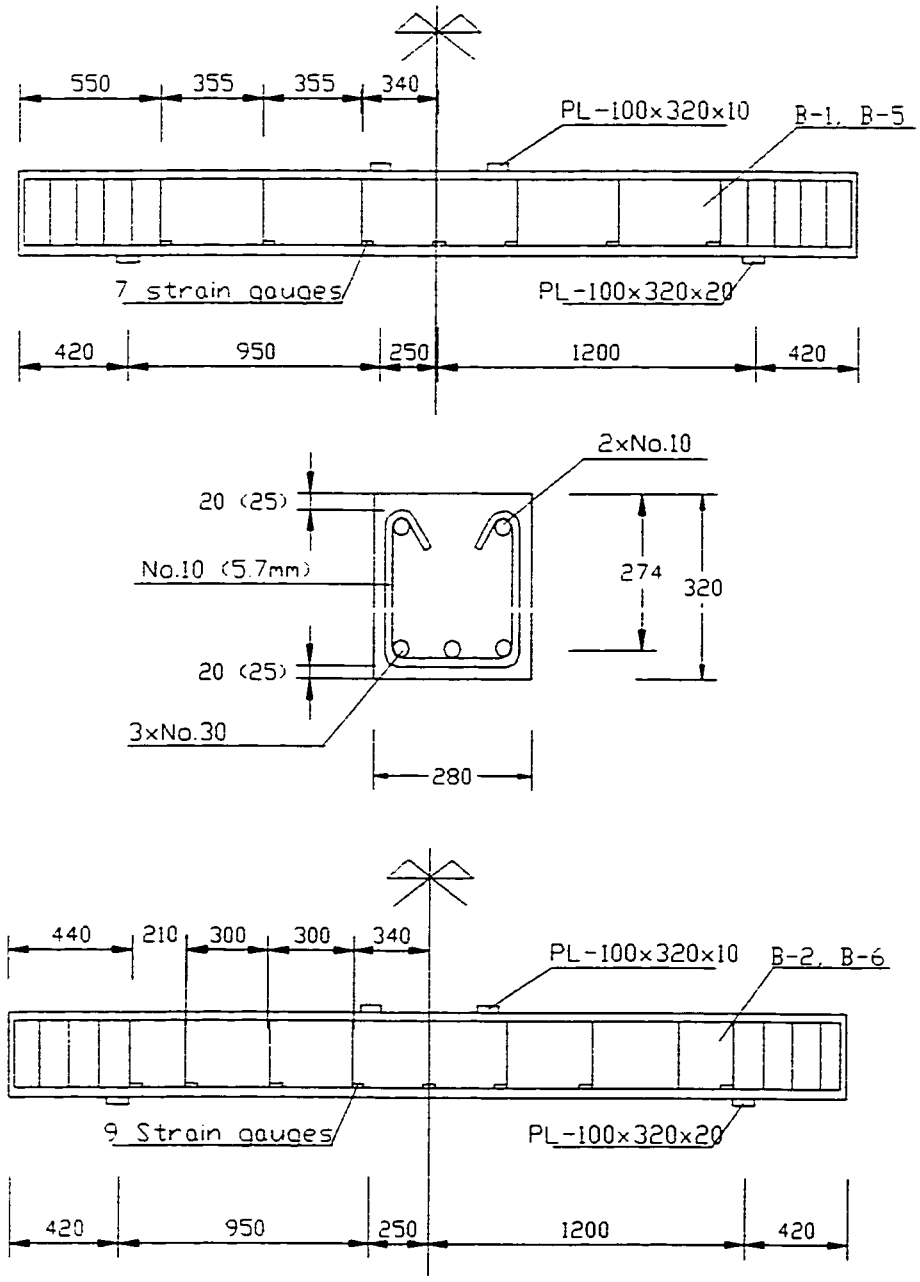

Figure 4.1: Detail of test beams (B-1, 2, 5 and 6)

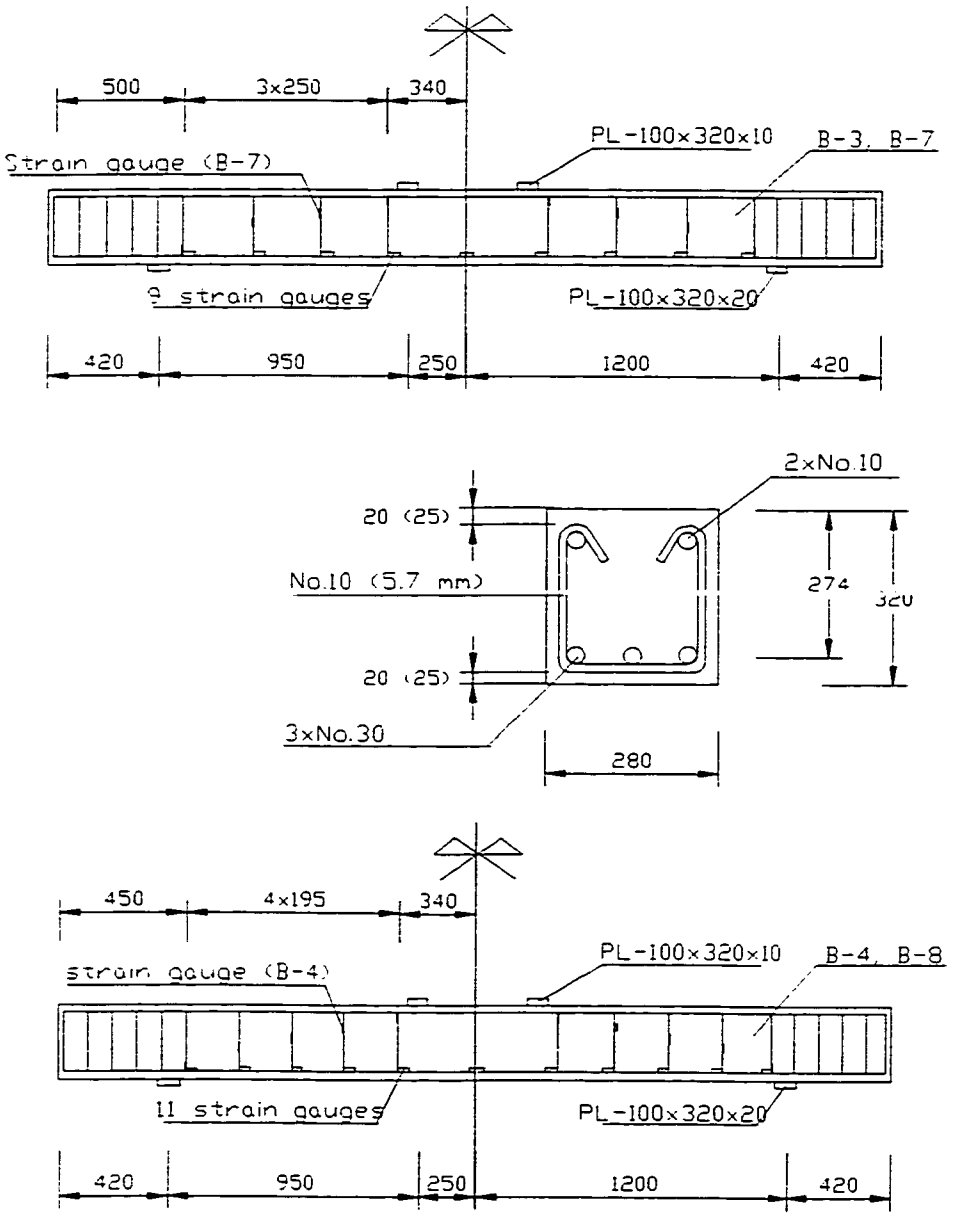

Figure 4.2: Detail of test beams (B-3, 4, 7 and 8)

Table4.1: Details of test beams

Beam	a_{cle}/h	f'_c (MPa)	f_r (MPa)	ρ	A_v (mm^2)	s (mm)	f_y (MPa)	f_{vy} (MPa)
B - 1	2.67	31.3	4.09	0.027	50	355	478	587
B - 2	2.67	31.8	3.83	0.027	50	300	478	587
B - 3	2.67	32.7	3.96	0.027	50	250	478	587
B - 4	2.67	33.0	4.40	0.027	50	195	478	587
B - 5	2.67	32.4	4.35	0.027	200	355	478	456
B - 6	2.67	29.3	4.33	0.027	200	300	478	456
B - 7	2.67	32.2	4.41	0.027	200	250	478	456
B - 8	2.67	33.7	4.04	0.027	200	195	478	456

Table 4.2: Mix proportion by mass

28 Day Target Strength (MPa)	30
Cement, kg	300
Fine Aggregate, kg	870
14 mm Coarse Aggregate, kg	1085
Water, kg	195

Concrete

The design strength of the concrete, f'_c, was 30 MPa. Type 10 portland cement was used in this program. The aggregate consisted of concrete sand and coarse aggregate with a 14 mm maximum nominal size. All these materials were locally supplied. The mix proportion is given in Table 4.2. The strength of the concrete was determined with 200 mm long and 100 mm diameter control cylinders. The concrete cylinders and the corresponding test beams were cured under the same condition — covered by a plastic sheet.

Steel Reinforcement

Three kinds of steel reinforcement were used in this test program: Grade 400 No. 30 bars (d_b = 29.9 mm) with 478 MPa average yield strength, Grade 400 No. 10 bars (d_b = 11.3 mm) with 456 MPa average yield strength and 5.7 mm diameter steel with 587 MPa average yield strength. Their stress-strain curves are shown in Figure 4.3. Curve (1) represents the No.30 longitudinal bar. Curve (2) represents the No.10 stirrup steel. Curve (3) represents the 5.7 mm small stirrup steel. The yield strength of 5.7 mm steel was based on its stress at a strain of 0.35%.

4.2.2 Test Set Up

All beams were simply supported and loaded with two symmetrical point loads acting perpendicular to the axis of the beam. Each beam was supported or loaded by steel plates. The steel plates were 100 mm wide, 20 mm thick and 320 mm long. Mortar was plastered between the steel plates and the test beam at the support to avoid

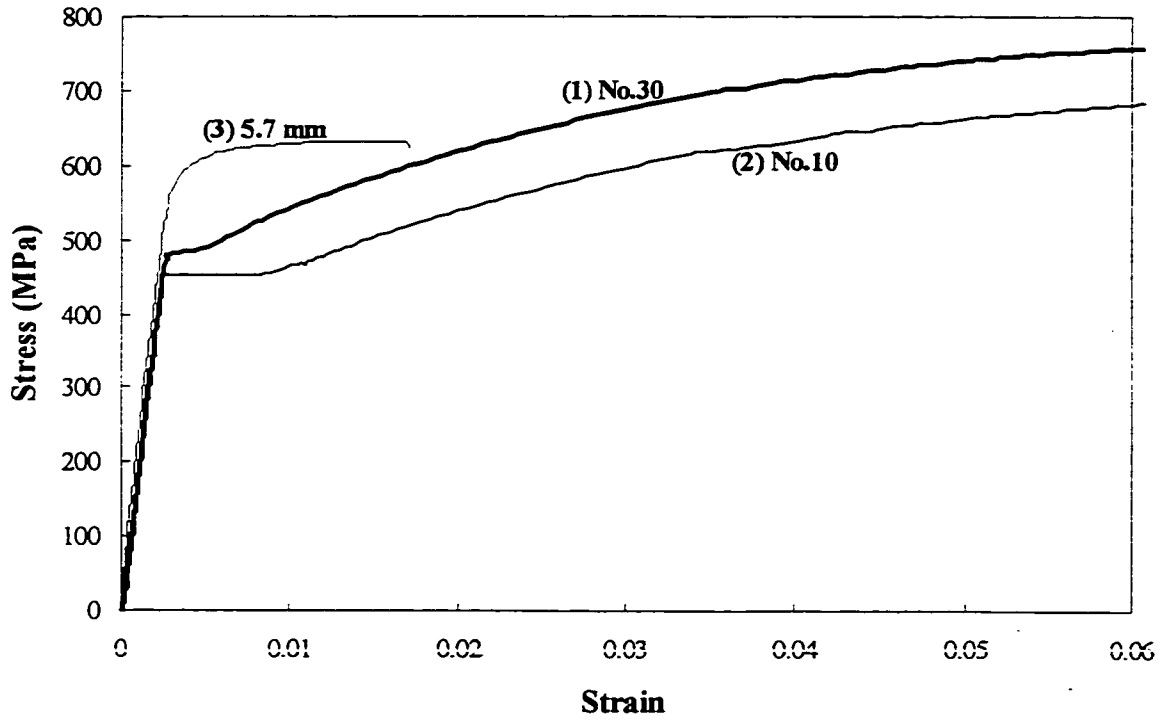

Figure 4.3: Stress-strain curves for steel

torsion due to uneven support on the rough surface of the beams. Fibre boards were placed between the steel plates and the test beam to reduce the horizontal restraining force at the load points after the beams start cracking. Two load cells were set under each steel plate at the support to measure the reaction. Each beam was tested by an Amsler testing machine (type 200 DB 767) shown in Figure 4.4.

4.2.3 Instrumentation

The midspan deflections of the test beams were measured by two displacement transducers. A graph of load against deflection was plotted during the test to help in

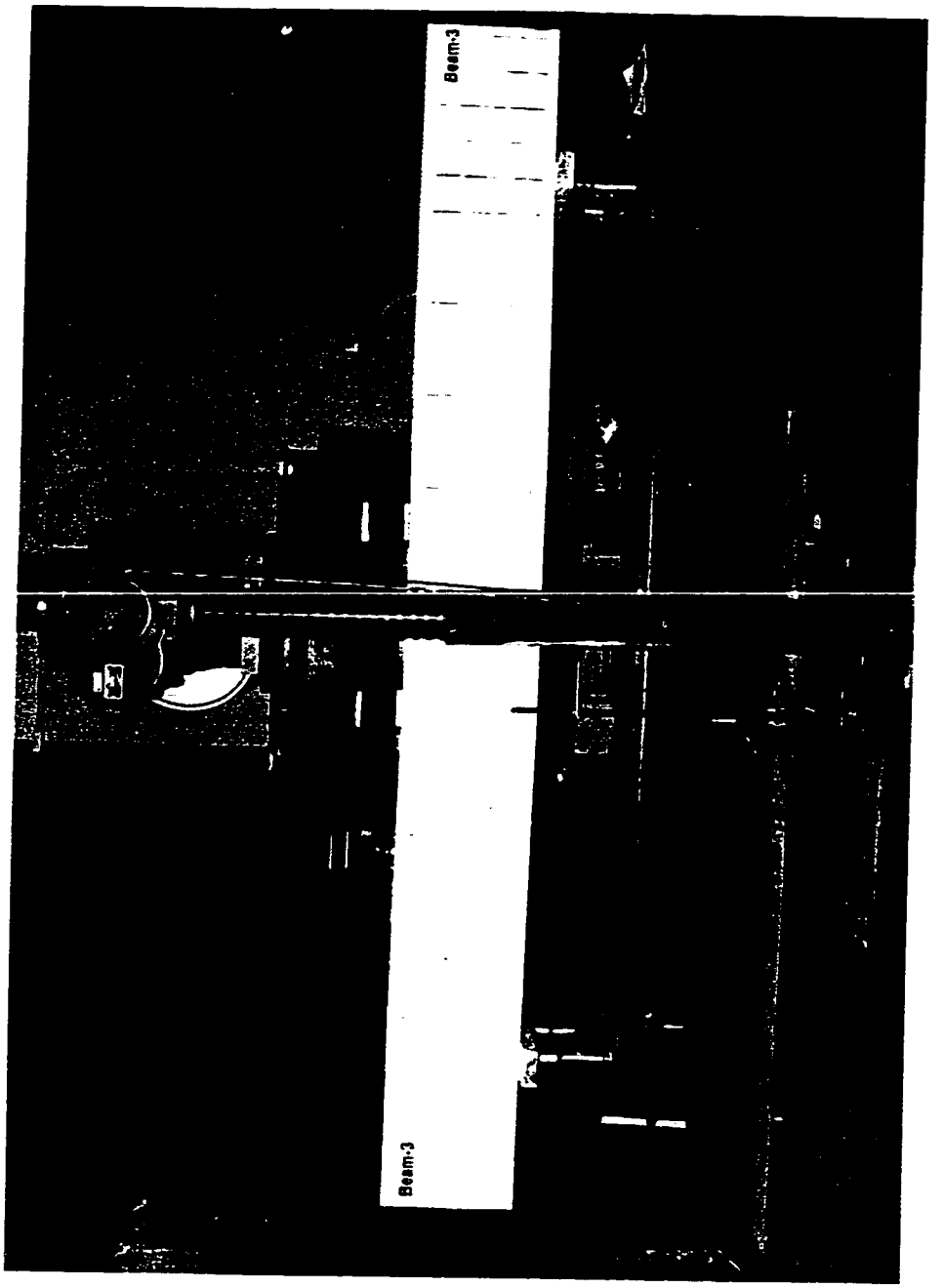

Figure 4.4: Test set up

determining the failure load visually. The applied load was measured by a pendulum dynamometer located in the testing machine and recorded by a Labtech Notebook data acquisition program.

Calibration factors for the load, load cell at the support, displacement transducer and gauge factors for the strains in the reinforcing steel were input into the Labtech Notebook file for each test. The strain gauges used were type EA-06-125BB-120 for No.30 and No.10 bars and type KFC-5-C1-11 for the 5.7 mm stirrups. The strain gauges on the longitudinal bars were located at the neutral axis of the bar to prevent erroneous results due to bending of the bar.

4.2.4 Procedure

Before loading, the readings on all gauges were zeroed. The total load , P_u, estimated by the shear-friction procedure, was applied in increment of 10 kN, so the cracks could be marked and crack widths could be measured. Crack measurements were taken up to 50-60% of the predicted failure load. At each increment, all strain gauge readings were recorded. Following the readings, the beam was inspected and all cracks were marked on each side of the beam. Photographs of each beam were taken at service load and failure load.

The tests of the beams were followed by testing the concrete control cylinders and modulus of rupture test specimens.

4.3 Test Results

4.3.1 Crack Formation and Pattern

During testing, the cracks were marked at service load and the load at which critical shear cracks occurred. The extent of propagation was indicated by a crossed line and the load was written near the line. After the load had dropped, failure cracks were marked and the beams were photographed. Crack patterns at failure for all of the test beams are shown in the photographs of Figure 4.5 and 4.6.

All beams were loaded symmetrically with two equal concentrated loads, which resulted in a region of nearly constant moment in the central part of the beam. In the early stages of loading, the beams were free of cracks. At a load close to 50% - 60% of failure load the first vertical cracks were observed. These cracks always initiated near midspan (in the region of pure moment) and developed vertically up to the neutral axis of the cracked section of the beam. With increasing load more flexural cracks developed in both the center and the shear span regions of the beam. Cracks in the pure moment region were always vertical, but cracks in the shear span curved towards the point of the applied load as can be seen clearly in Figure 4.5 and 4.6.

For the B-1 to B-4 beams with 5.7 mm stirrups, the ultimate shear capacity exceeded the inclined cracking load. This difference became progressively greater from B - 1 to B - 4 as the stirrups spacing was reduced. After the formation of inclined cracks at about mid-depth of the sections, they propagated immediately in two directions: towards the loading point and towards the longitudinal reinforcement.

For the B-5 to B-8 beams with No. 10 stirrups, the behavior was the same as

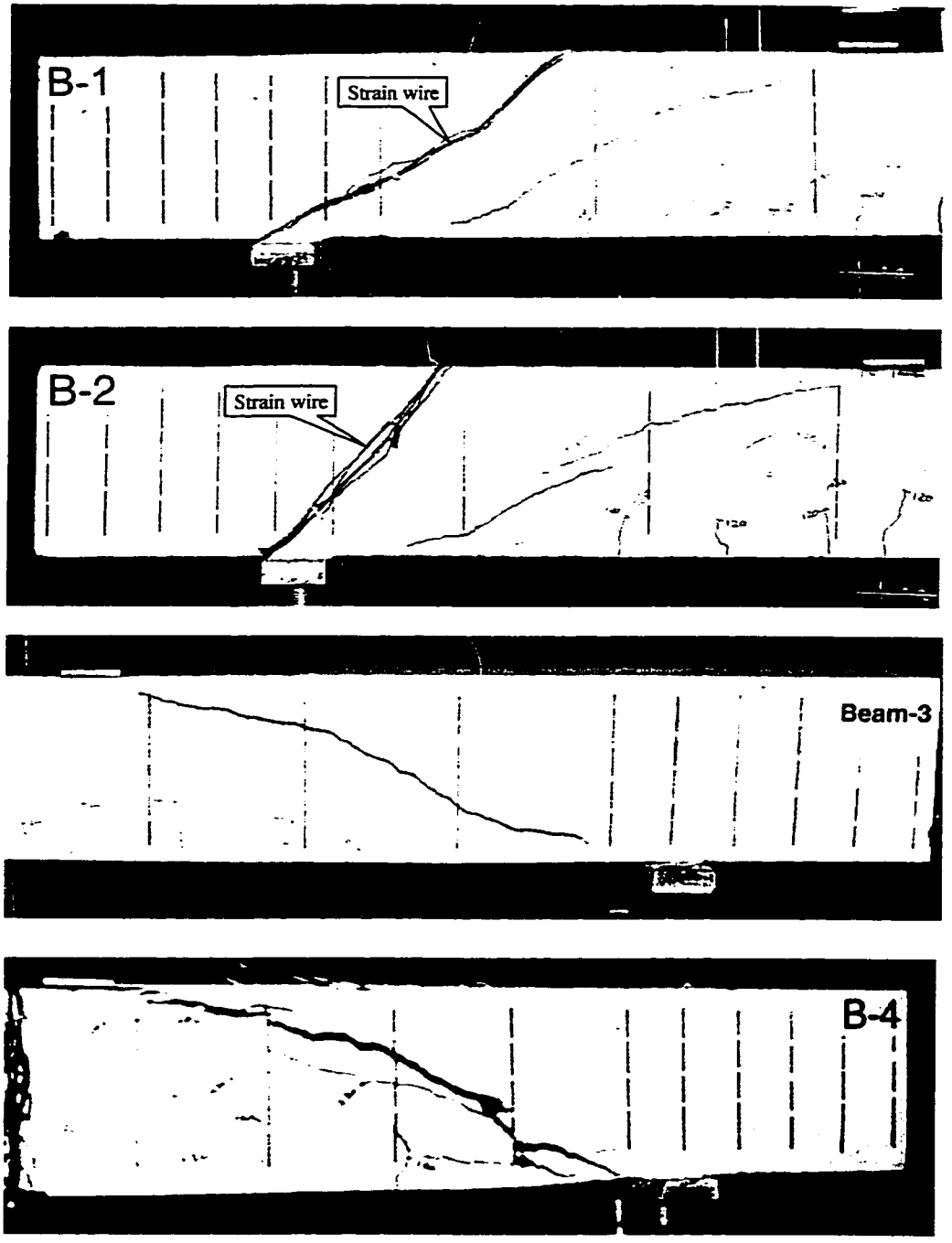

Figure 4.5: Crack patterns of test beams (B-1 - B-4)

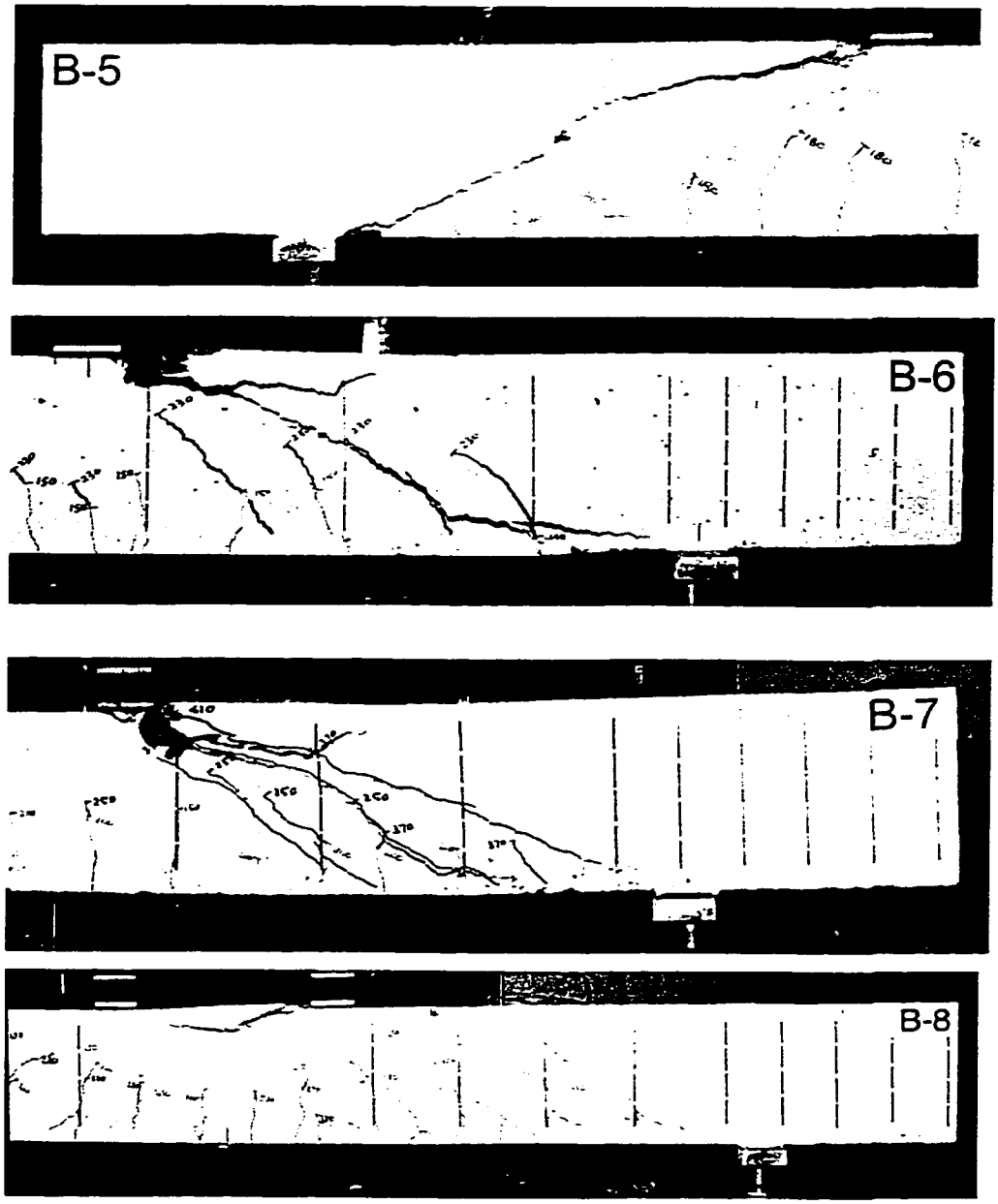

Figure 4.6: Crack patterns of test beams (B-5 - B-8)

B-1 to B-4, up to the inclined cracking load. As the load was increased, additional flexure and inclined cracks formed, and existing cracks lengthened and widened. After yielding of the stirrups, crack widths were very large. The failures of B-5 to B-7 occurred when one of the inclined cracks propagated suddenly into the compression zone near the loading point. The failures were more ductile than those of beams with 5.7 mm stirrups. B-8 failed when the longitudinal reinforcement reached yield strength and the concrete crushed in the compression zone at midspan.

4.3.2 Ultimate and Cracking Load

Table 4.3 shows the ultimate load, V_t, inclined shear cracking load, V_{cr}, and type of failure for various beams. The shear cracking loads shown here are just approximate values, because it is difficult to catch the exact shear cracking load visually during testing. It can be seen that the ratio of crack load to failure load decreases with an increase of the web reinforcement index, $\rho_v f_{vy}$, in Table 4.3. In other words, the brittle failure transferred to ductile failure with an increase of the amount of shear reinforcement.

The ratios of shear capacity measured from tests to the capacity calculated by the shear-friction method using $k = 1.93 f_c'^{-0.39}$, shown in Table 4.3 are mostly over one. The coefficient of variation of the ratios is 0.118.

4.3.3 Force in Longitudinal Reinforcement

The forces in the longitudinal reinforcement of 8 beams at failure load for different locations along the length of the beams was plotted in Figure 4.7, 4.8, 4.9 and 4.10. These forces were calculated from the measurements of the strain gauges on the

longitudinal bars. We can see that all forces have not reached the average yield force of 334 kN except for B-8 at midspan. The force became large from the support to the midspan as expected.

Table 4.3: Failure and cracking loads of test beams

Beam	s/d	$\rho_v f_{vy}$	V_t (MN)	V_{cr} (MN)	V_{cr}/Vt (%)	V_{SFd} (MN)	V_t/V_{SFd}	F. T.
B-1	1.3	0.301	0.114	0.110	96	0.103	1.106	D.S.-s
B-2	1.1	0.356	0.119	0.110	92	0.115	1.036	D.S.-s
B-3	0.9	0.428	0.121	0.115	95	0.129	0.938	D.S.-s
B-4	0.7	0.548	0.143	0.120	84	0.150	0.952	D.S.-g
B-5	1.3	0.921	0.181	0.120	66	0.142	1.278	D.S.-g
B-6	1.1	1.090	0.191	0.115	60	0.160	1.191	D.S.-g
B-7	0.9	1.308	0.187	0.130	70	0.186	1.005	D.S.-g
B-8	0.7		0.224					F
						x =	1.072	
						s =	0.126	
						V =	0.118	

F.T. – Failure Type
D.S.-s – Sudden diagonal shear failure
D.S.-g – Gradual diagonal shear failure
F – Flexural failure
x – Mean value
s – Standard deviation
V – Coefficient of variation

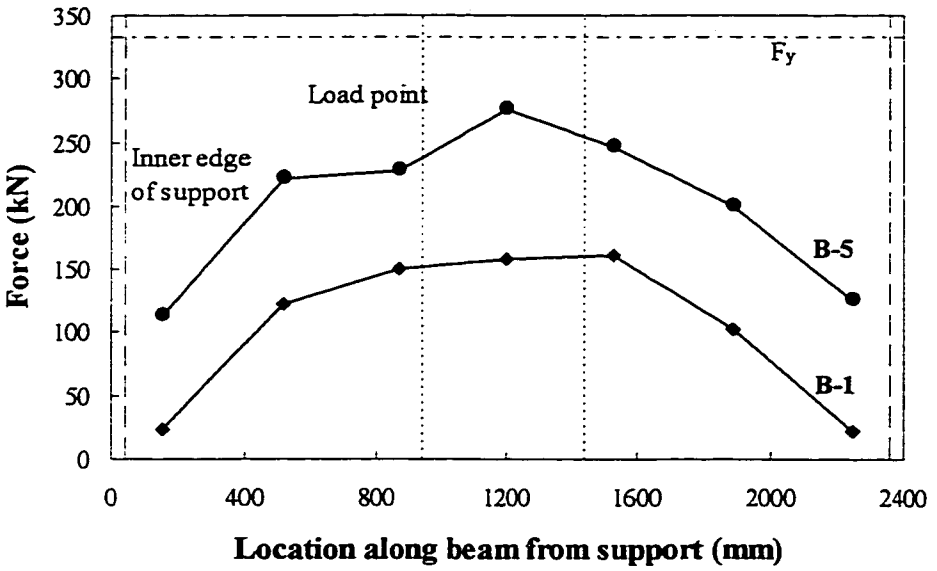

Figure 4.7: Longitudinal force in test beams (B-1& B-5)

4.3.4 Strain in Stirrups

The strain gauges were attached to both legs of the stirrups only in B-4 and B-7. The strain gauges were put on the stirrups near where the critical shear crack was expected. The locations of the critical shear crack were predicted by the shear-friction procedure of the parabolic crack failure model. The factor k used in the equations was based on the test results of the 5 beams tested earlier. Figure 4.11 shows the strain in the three stirrups near the curved crack in B-4 as a function of the load. Figure 4.12 shows the strain in the two stirrups near the curved crack in B-7 as a function of the load.

It is clear the No. 10 stirrups did not experience strain hardening, because the

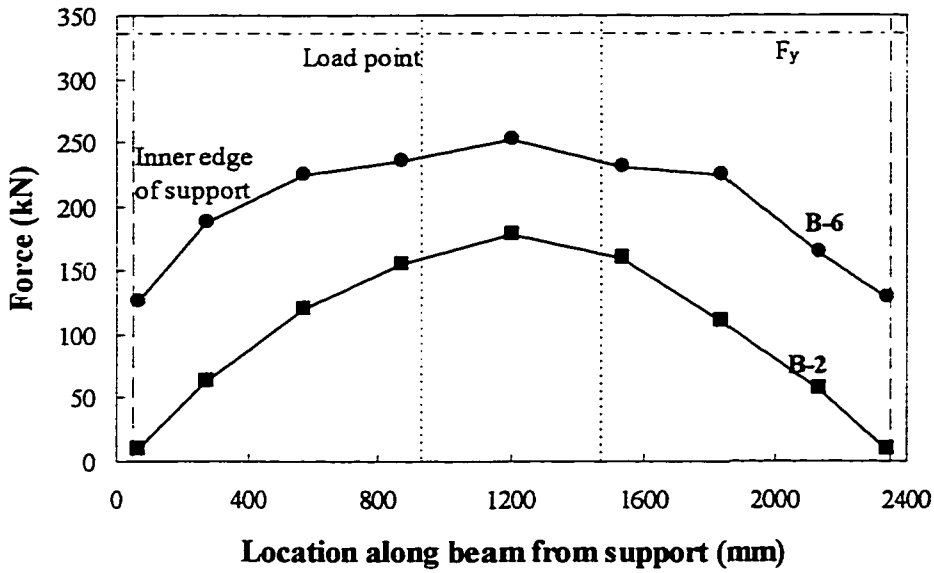

Figure 4.8: Longitudinal forces in test beams (B-2 & B-6)

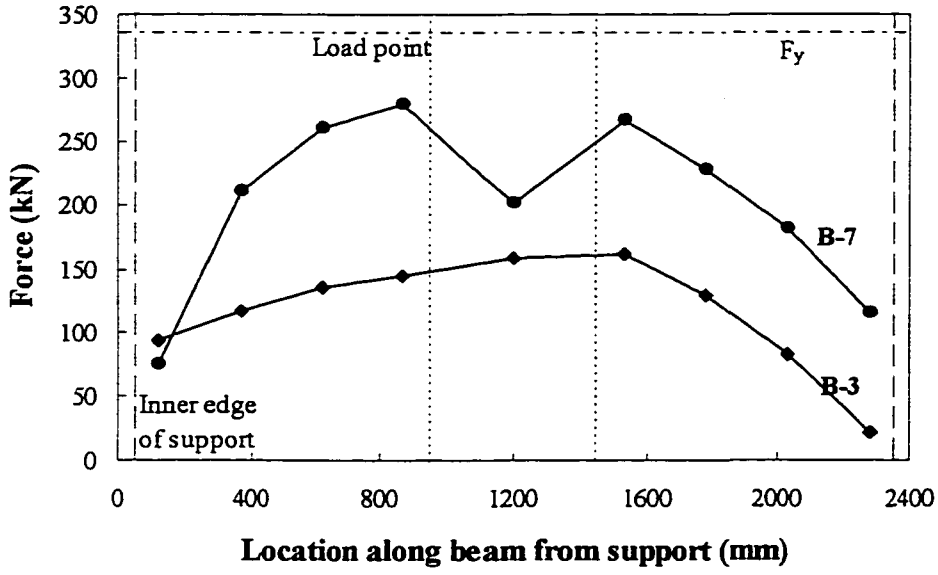

Figure 4.9: Longitudinal forces in test beams (B-3 & B-7)

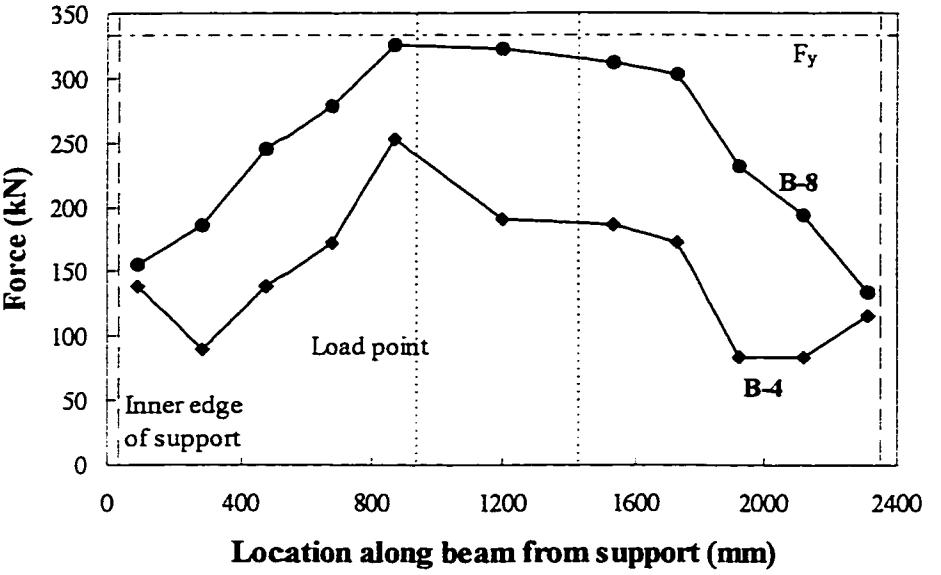

Figure 4.10: Longitudinal forces in test beams (B-4 & B-8)

strain hardening starts after the strain reaches 0.9%. For 5.7 mm stirrups, stirrup No. 2 exceeded the strain of 0.35%, stirrup No. 3 was close to it and stirrup No. 1 was not close to it. The average yield strength for 5.7 mm stirrups chosen to be at a strain of 0.35% seems suitable.

4.3.5 Deflection at Midspan

Deflections at midspan of all beams were measured. The amount of stirrups affected the load-deflection curve. After the inclined shear crack occurred, the deflection at the midspan decreases with an increase of $\rho_v f_{vy}$, as shown in Figure 4.13. Increasing $\rho_v f_{vy}$ increases the stiffness of the beams by resisting the crack widening and controlling propagation of these cracks.

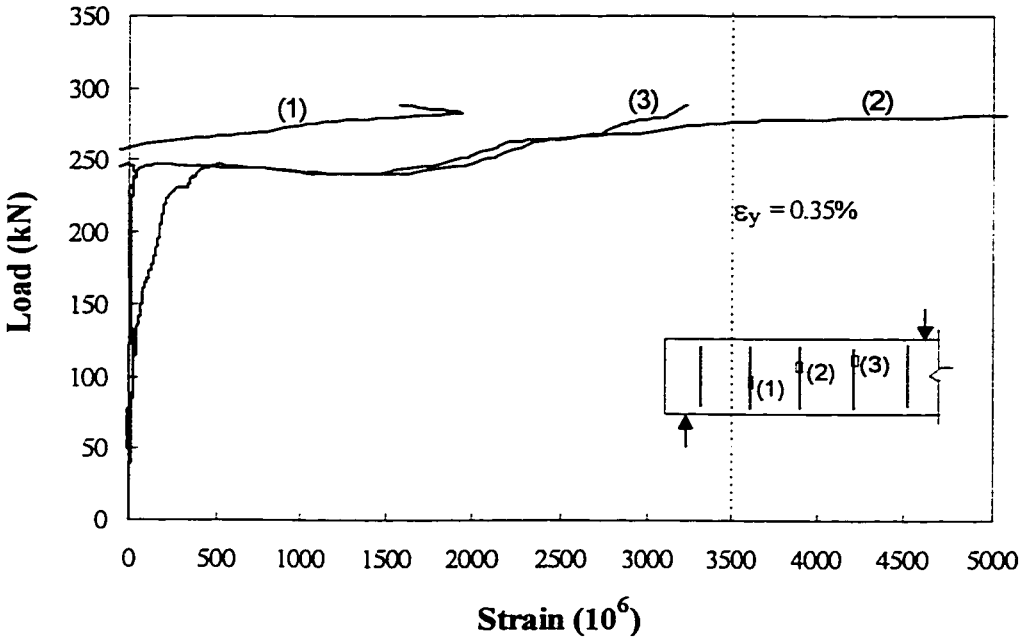

Figure 4.11: Load vs. stirrup strains for beam B-4

4.4 Discussion of Test Results

4.4.1 Effect of Stirrup Spacing on Shear Strength

The current Canadian code gives many limitations on stirrup spacing as supplementary requirements for the Simplified Method and the General Method. It is necessary to investigate whether these limitations on stirrup spacing are also required for the shear-friction method.

Limitations Imposed by Simplified Method (Loov,1998)

CSA–A23.3–94 Equations 11-14, 11-16 and 11-11 can be combined to provide a relationship between the factored shear resistance and the stirrup spacing for a beam

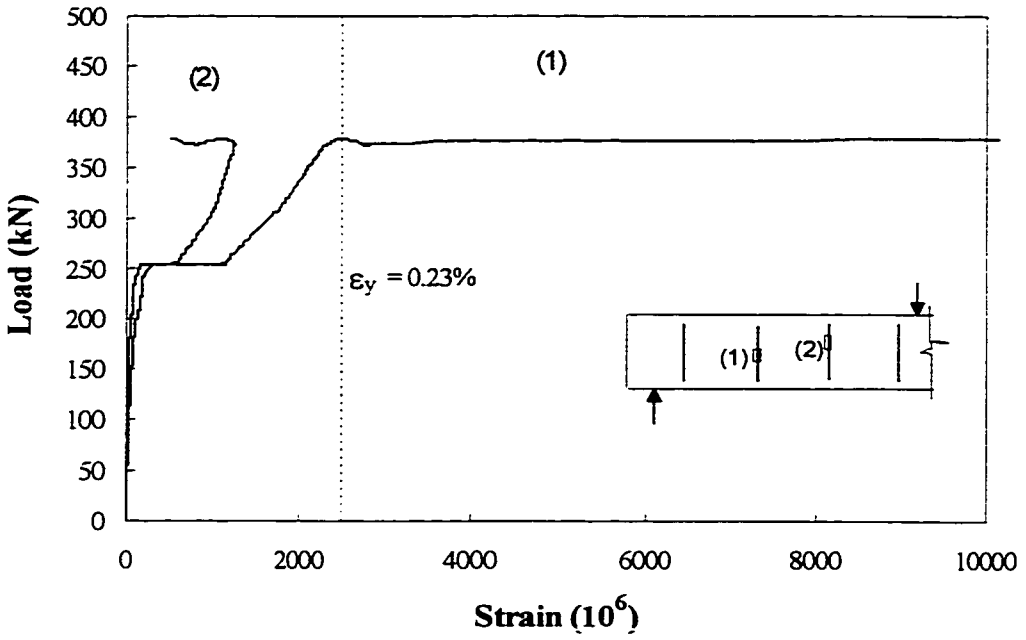

Figure 4.12: Load vs. stirrup strains for beam B-7

of given dimensions and material properties.

$$V_r = 0.2\lambda\phi_c\sqrt{f'_c}b_w d + \phi_s A_v f_{vy}\frac{d}{s} \tag{4.1}$$

Assuming $C_{dr} = \lambda\phi_c f'_c b_w d$ and $T_{vr} = \phi_s A_v f_{vy}$, equation (4.1) can be rewritten as:

$$\frac{V_r}{C_{dr}} = \frac{0.2}{\sqrt{f'_c}} + \frac{T_{vr}}{C_{dr}} \cdot \frac{d}{s} \tag{4.2}$$

Clause 11.2.8.4 requires a minimum steel area given by Equation 11-1.

$$A_v = 0.06\sqrt{f'_c}\frac{b_w s}{f_{vy}} \tag{4.3}$$

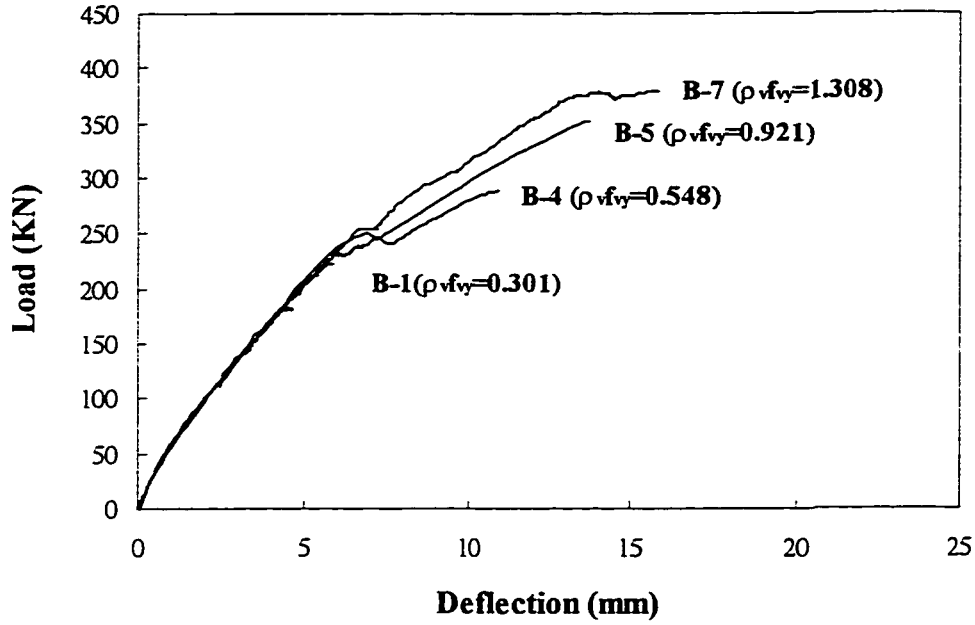

Figure 4.13: Effect of $\rho_v f_{vy}$ on load vs. deflection

This limits the spacing for a given size of stirrup in a particular beam. This maximum stirrup spacing is:

$$\frac{s}{d} = \frac{T_{vr}}{C_{dr}} \cdot \frac{\lambda \phi_c \sqrt{f'_c}}{0.06 \phi_s} \tag{4.4}$$

The restriction with the largest impact is imposed by clause 11.2.11: the spacing of transverse shear reinforcement, s, measured in the longitudinal direction shall not exceed

(a) 600 mm or 0.7d, if $(V_f - \phi_p)/b_w d < 0.1\lambda\phi_c f'_c$; or

(b) 300 mm or 0.35d, if $(V_f - \phi_p)/b_w d \geq 0.1\lambda\phi_c f'_c$

For reinforced beams, these can be expressed as the following non-dimensional

equations.

$$\begin{aligned} \frac{s}{d} &\leq 0.7, \left(\frac{V_r}{C_{dr}} < 0.1\right) \\ \frac{s}{d} &\leq 0.35, \left(\frac{V_r}{C_{dr}} \geq 0.1\right) \end{aligned} \tag{4.5}$$

The maximum permitted shear on a sections is limited by equation 11-5 of the standard which sets a limit on the shear which can be developed by the stirrups. If this is added to the V_c described by equation 11-16 then

$$V_r = 1.0\lambda\phi_c\sqrt{f'_c}\, b_w d \tag{4.6}$$

Expressed in non-dimensional format, (4.6) becomes

$$\frac{V_r}{C_{dr}} \leq \frac{1.0}{\sqrt{f'_c}} \tag{4.7}$$

Clause 11.2.8.1 describes a number of situations which would allow construction without stirrups. Of particular interest is the requirement that minimum stirrups are not required whenever

$$\begin{aligned} V_f &\leq 0.5V_c \\ &= 0.5(0.2)\lambda\phi_c\sqrt{f'_c}\, b_w d \end{aligned} \tag{4.8}$$

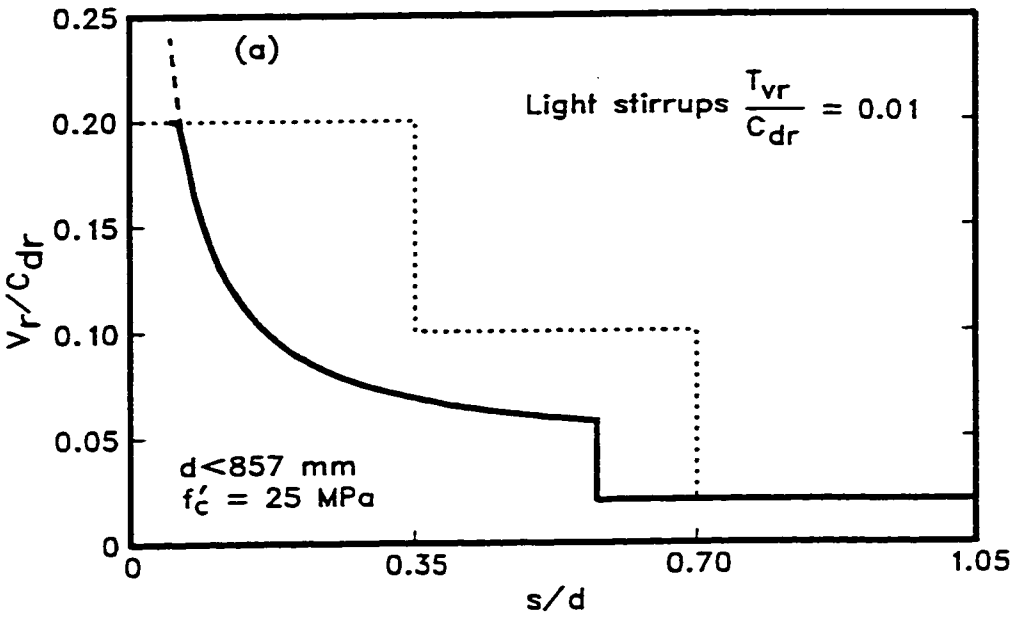

Figure 4.14: strength vs. s/d using CSA-s ($T_{vr}/C_{dr} = 0.01$) (Loov, 1998)

In non-dimensional form, if V_f is set equal to V_r, this is

$$\frac{V_r}{C_{dr}} \leq \frac{0.1}{\sqrt{f'_c}} \tag{4.9}$$

When the supplementary requirements as developed in equations (4.4), (4.5), (4.7) and (4.9) are superimposed on the shear strength equation (4.2), it will often be found that it is these supplementary requirements which govern while the shear strength equation governs for only short intervals. Figure 4.14, 4.15 and 4.16 show the resulting design limits for a concrete strength of 25 MPa.

a) light stirrups, $T_{vr}/C_{dr} = 0.01$

b) moderate stirrups, $T_{vr}/C_{dr} = 0.03$

c) heavy stirrups, $T_{vr}/C_{dr} = 0.05$

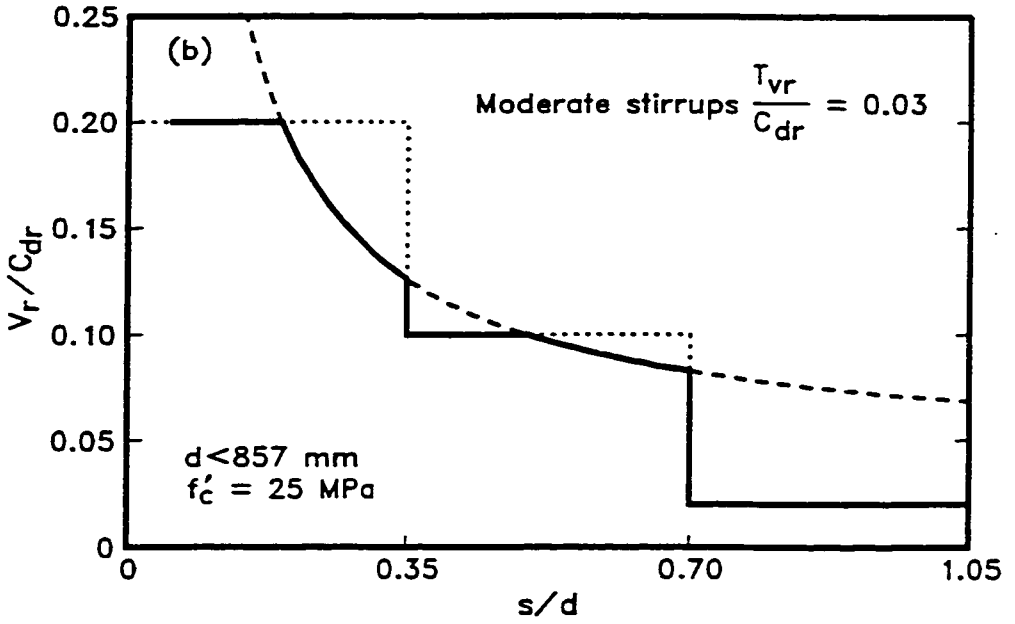

Figure 4.15: Strength vs. s/d using CSA-s($T_{vr}/C_{dr} = 0.03$) (Loov, 1998)

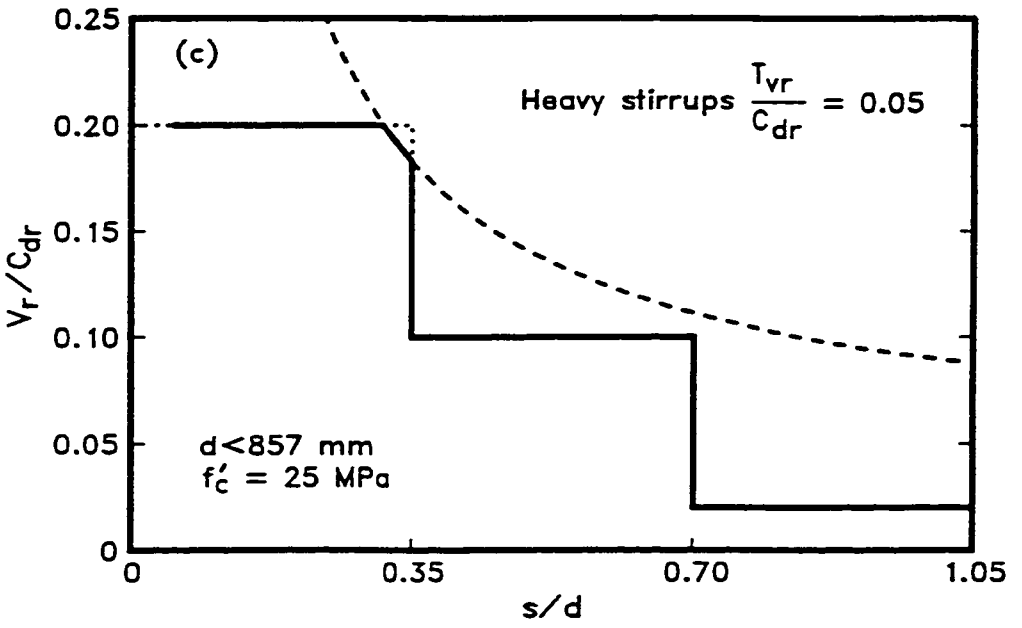

Figure 4.16: Strength vs. s/d using CSA-s ($T_{vr}/C_{dr} = 0.05$) (Loov, 1998)

The solid lines in Figure 4.14, 4.15 and 4.16 form the upper boundary of the permissible values. It is apparent that equations (4.2) and (4.4) generally govern for light stirrups, but that spacing limits of (4.5) and the maximum stress limit of (4.7) become increasingly dominant as the relative stirrup strength is increased. Although the specific values will vary with concrete strength, the general shape of the plot is typical for all strengths. This plot clearly shows the seven surfaces which represent the requirements that have to be met. The discontinuous nature of these limits is evident.

Comparison with Test Results

Two kinds of stirrups were chosen in this test program. One was 5.7 mm stirrup with $f_y = 587$ MPa and $T_v/C_d = 0.0123$. Another was No.10 stirrup with $f_y = 456$ MPa and $T_v/C_d = 0.0376$. Figures 4.17 and 4.18 show the shear stress variations with the ratio of s/d by using CSA–A23.3–94 simplified method, the design equation of shear-friction procedure and test results with two kinds of stirrups respectively. The dotted lines represent the CSA–A23.3–94. The solid lines represent the shear-friction procedure and the symbols represent test results. In Figure 4.17 and 4.18, $\lambda = 1$, $\phi_c = 1$, $\phi_s = 1$, $f'_c = 30$ MPa, $b_w = 280$ mm, $d = 274$ mm, $d_s = 264$ mm for figure 4.11, $d_s = 269$ mm for figure 4.12 and the factor $k = 1.93 f'^{-0.39}_c = 0.53$.

According to CSA–A23.3–94, s/d ratios greater than 0.7 are not permitted with $V/C_d \leq 0.1$. It can be seen in Figure 4.17 and 4.18, however, that the test results are close to or above the solid line based on the shear-friction procedure. If we plot the ratio of the shear capacity measured by test, V_t, to the shear capacity calculated by the shear-friction method, V_{sf}, versus the ratio of s/d in Figure 4.19, it can be seen

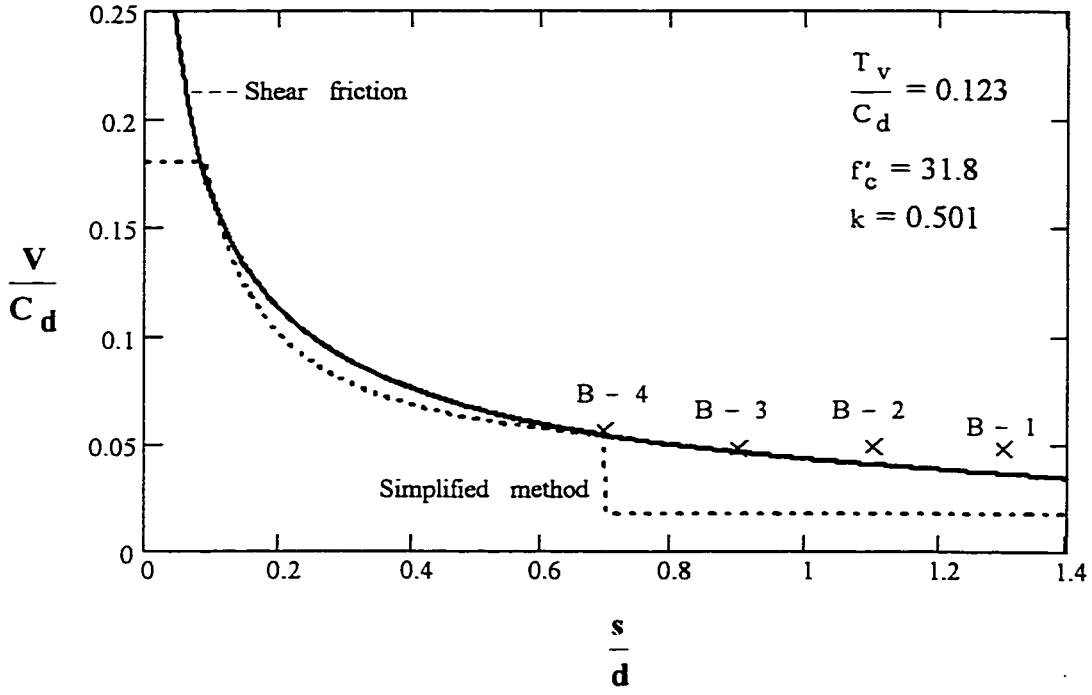

Figure 4.17: Shear strength vs. s/d for beams B-1 to B-4

that the prediction by the shear-friction method tends to be conservative with an increase of the s/d ratio. Therefore, for strength requirement the current limitation of maximum stirrup spacing is not required using the shear-friction procedure. For the requirement to limit shear crack at service load, the maximum spacing might not be required either due to the fact that the shear crack occurred around service load (60% of failure load) to only one beam (B-6) shown in Table 4.3.

For shear reinforced concrete beams with s/d ratio less than 0.7 and $V/C_d \geq 0.1$, the prediction of the shear-friction method also correlates to the test results very well. This will be discussed further in Chapter 5.

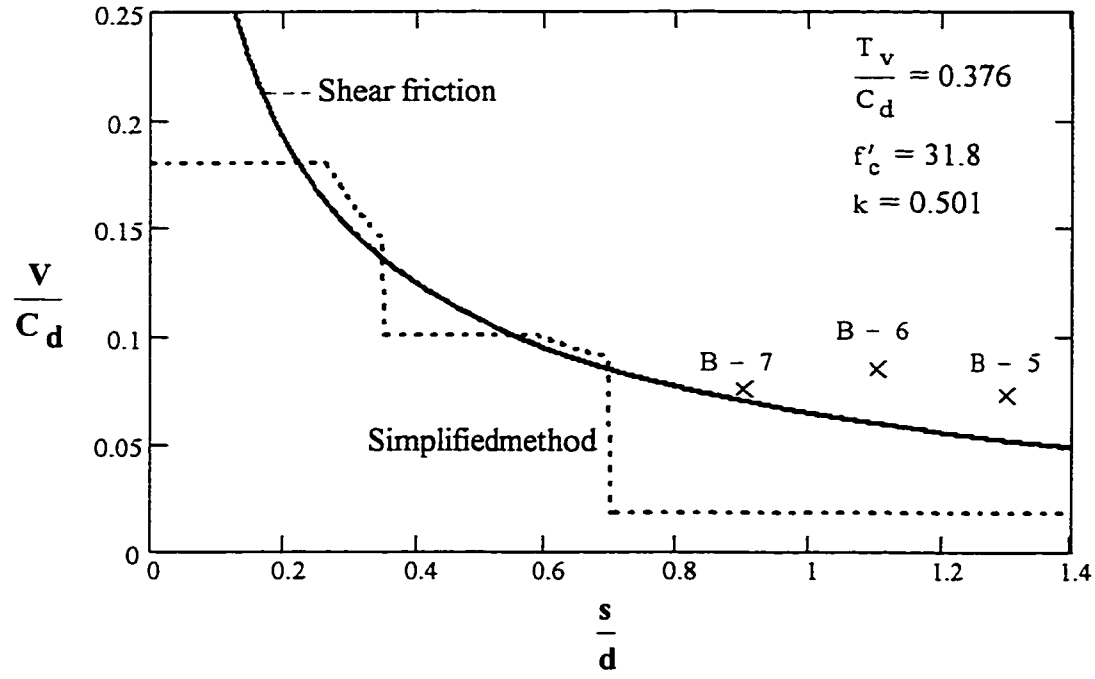

Figure 4.18: Shear strength vs. s/d for beams B-5 to B-7

4.4.2 Force in Longitudinal Reinforcement

As mentioned in Chapter 3, the design equation for the shear-friction method was derived by using the optimum force in the longitudinal reinforcement, T_{opt}, at which the shear reaches a maximum value. It is necessary to investigate if it is suitable to calculate the longitudinal force using this T_{opt}.

To obtain the force, T_t, in the reinforcement crossing the crack from the test, the distance from the intersection of the shear crack and the bar to the load point, t_d, was measured for each beam. Once we know t_d or the intersection point, the longitudinal force can be obtained from the strain test data of the longitudinal bar by using interpolation between the two adjacent gauges.

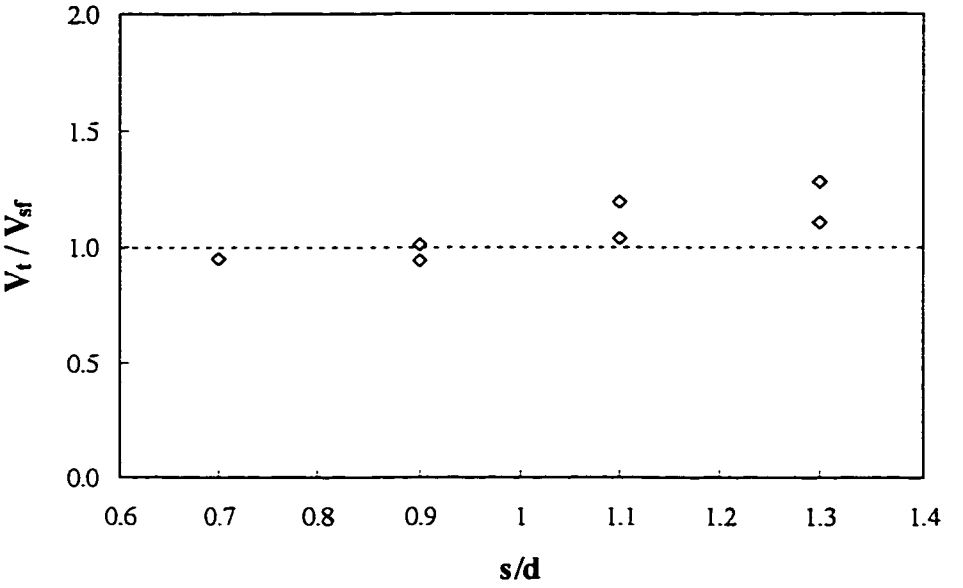

Figure 4.19: Effect of large s/d on strength based on shear-friction method

Based on the inclined crack failure model, the longitudinal force can be calculated by equation:

$$T_{opt} = 0.25k^2 f'_c b_w h(1 + \sec^2\theta) \tag{3.8}$$

In order to examine whether T_{opt} is close to T_{test} or not, the factor k in the above equation is calculated by substituting the shear capacity measured from testing, V_t, into the simplified equation (3.9), and solving for k . This k is called k_t. The $sec^2\theta$ term was $(t_d^2 + d^2)/t_d^2$. Hence,the above equation can be written as:

$$T = 0.25k_t^2 f'_c b_w h \left(2 + \frac{d^2}{t_d^2}\right) \tag{4.10}$$

Similarly, based on the parabolic crack failure model, the longitudinal force can

be calculated by equation:

$$T_{opt} = 0.25k^2 f'_c b_w h \left(2 + \frac{h^2}{t^2}\right) \tag{3.45}$$

in which the factor k is calculated by substituting the shear capacity measured from testing, V_t, into the simplified equation (3.46), and solving k. This k is called k_{pt}. Using t_d instead of t and d instead of h, the above equation (3.45) can be written as:

$$T_p = 0.25k_{pt}^2 f'_c b_w h \left(2 + \frac{d^2}{t_d^2}\right) \tag{4.11}$$

Table 4.4: Comparison of longitudinal forces based on two failure models with test results

Beam	t_d (mm)	k_t	T (kN)	k_{pt}	T_p (kN)	T_t (kN)	T_t/T	T_t/T_p
B - 1	570	0.467	0.340	0.453	0.321	0.218	0.641	0.679
B - 2	640	0.483	0.363	0.470	0.343	0.188	0.518	0.548
B - 3	710	0.476	0.356	0.471	0.349	0.304	0.854	0.871
B - 4	720	0.472	0.353	0.523	0.434	0.343	0.972	0.790
B - 5	725	0.560	0.488	0.561	0.489	0.393	0.805	0.804
B - 6	640	0.573	0.470	0.590	0.491	0.492	1.047	1.002
B - 7	665	0.488	0.371	0.541	0.458	0.446	1.202	0.974
						x =	0.863	0.810
						s =	0.235	0.160
						V =	0.273	0.198

T and T_p in Table 4.4 were calculated by equation (4.10) and (4.11). The result of this table shows that the parabolic crack failure model gave a better prediction than the inclined crack failure model as expected. The longitudinal force calculated by the inclined crack model, however, is quite close to test results.

4.4.3 Location of Crack

It will be helpful for engineers to know the location of the critical crack along a beam's length for shear design. A number of test data in the literature confirmed that the critical section is not necessarily near the support. One of the advantages of the shear-friction method is that the location of the failure plane can be predicted.

As mentioned before, equation (3.34) for the projection of the crack gives the range in which shear failure would occur for reinforced concrete beams with stirrups and the simplified equation (3.9) predicts the plane of the lowest shear capacity in this range. Therefore, the location of the critical shear crack can be determined. The shear capacity calculated by the simplified equation (3.9) of B-2 and B-7 against the starting point of the potential failure plane, x (from 0 to a_{cle}), is plotted in Figure 4.20 and Figure 4.21, in which x_c represents the starting point of the failure plane predicted by equations (3.34) and (3.9), x_1 represents the starting point of the failure plane predicted by only equation (3.9) and V_t represents the failure load of the beams.

It can be seen in Figure 4.20 (for B-1) that if we only used the simplified equation (3.9) to calculate shear capacity, the failure plane corresponding to the lowest shear capacity would start from x_1 and the failure load predicted would be 0.104 MN instead of V_t which is 0.114 MN. By using both equation (3.34) and (3.9), the failure plane will start from around x_c and the shear capacity at this plane is 0.111 which

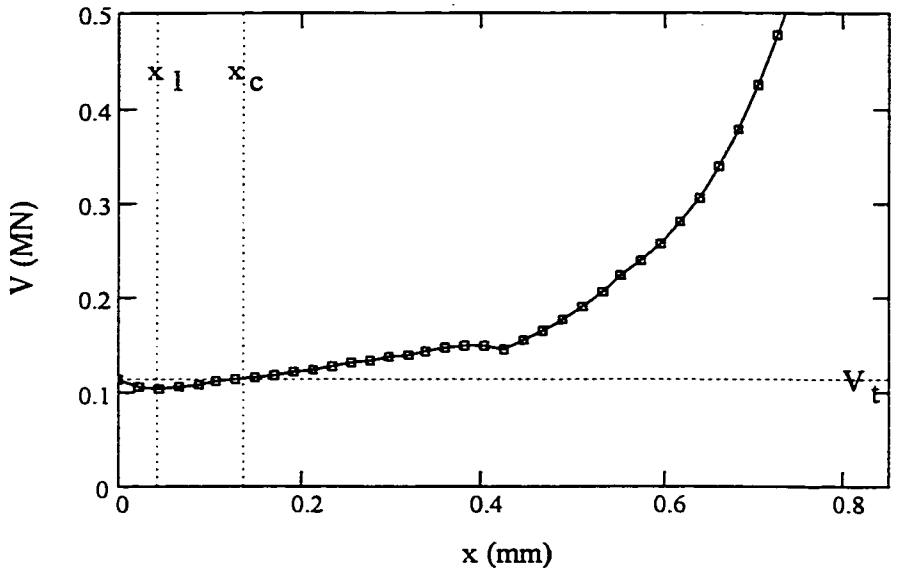

Figure 4.20: Effect of crack location on shear strength for beam B-1

is almost identical with V_t.

For B-7, the distance t is equal to the clear shear span, when $x_c = 0$, because the ψ $(\rho_v f_{vy}/f'_c)$ of B-7 is larger than 0.03 (see Figure 3.13). Consequently, the crack location can be determined only by using the simplified equation (3.9). Interestingly, the shear capacities calculated by equation (3.9) are almost identical at the three planes which started beside stirrups shown in Figure 4.21. These three planes exactly match the locations of three actual shear cracks as seen in Figure 4.6.

In Figure 4.22 and 4.23 the dashed lines are the locations of the critical shear crack predicted by equation (3.32). They are quite close to the actual one.

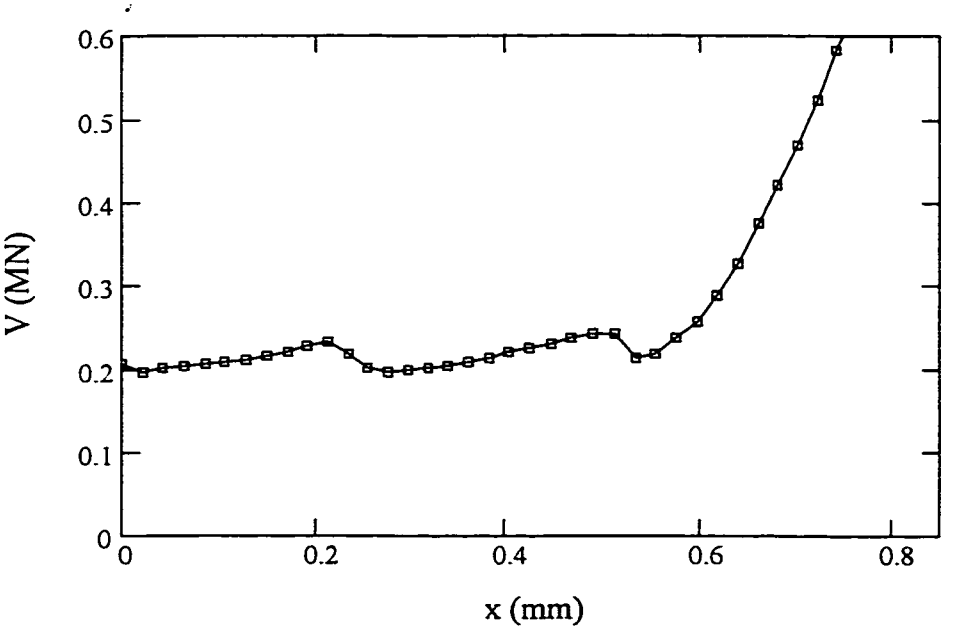

Figure 4.21: Effect of crack loation on shear strength for beam B-7

4.4.4 Effect of Amount of Shear Reinforcement on Shear Strength

In this test program, the web reinforcement index, $\rho_v f_{vy}$, was increased from 0.301 to 1.308 MPa by decreasing spacing of stirrups and changing the diameter. It can be seen, from Table 4.3, that an increase in the web reinforcement index resulted in an increase in the shear capacity.

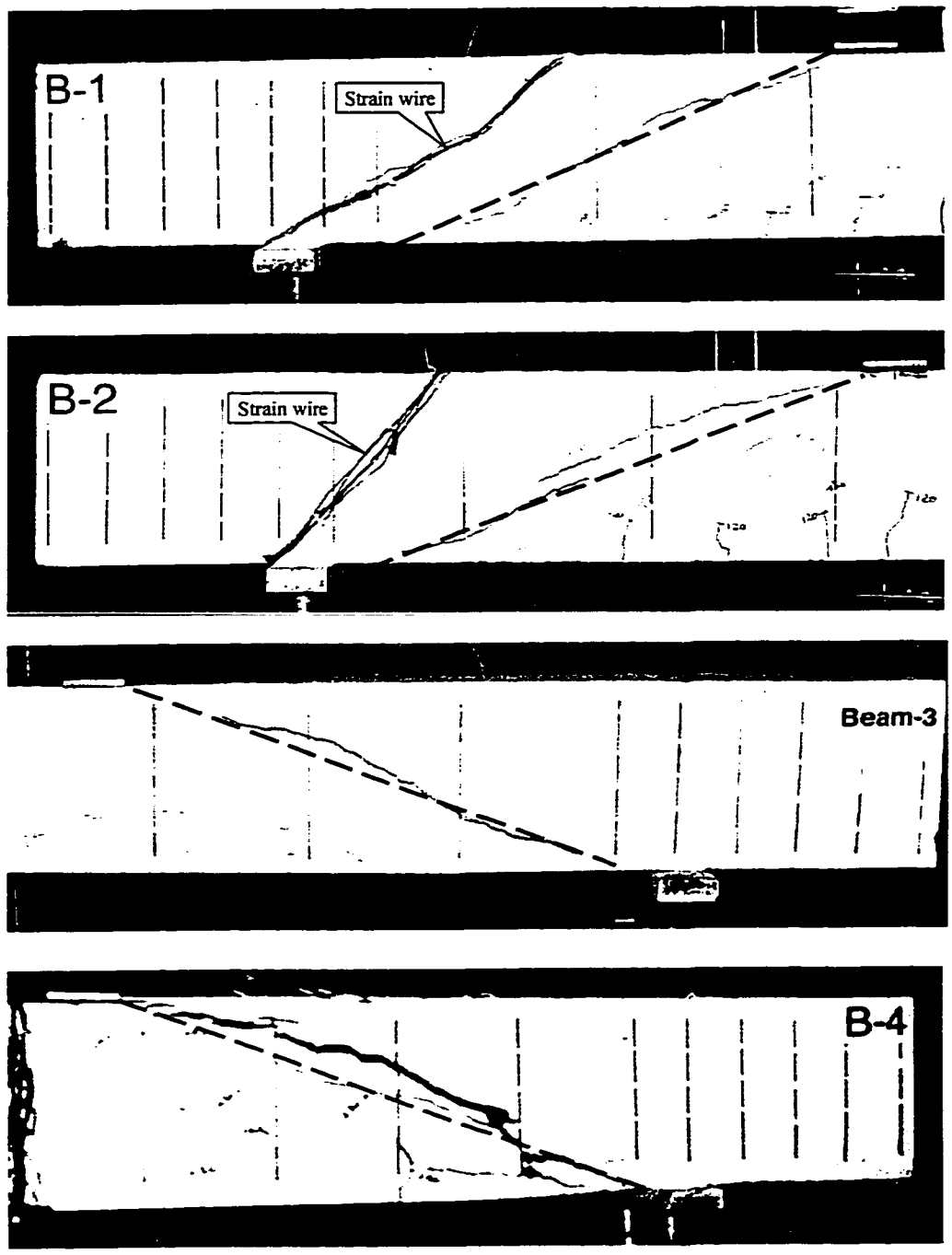

Figure 4.22: Comparison of crack locations (B-1 - B-4)

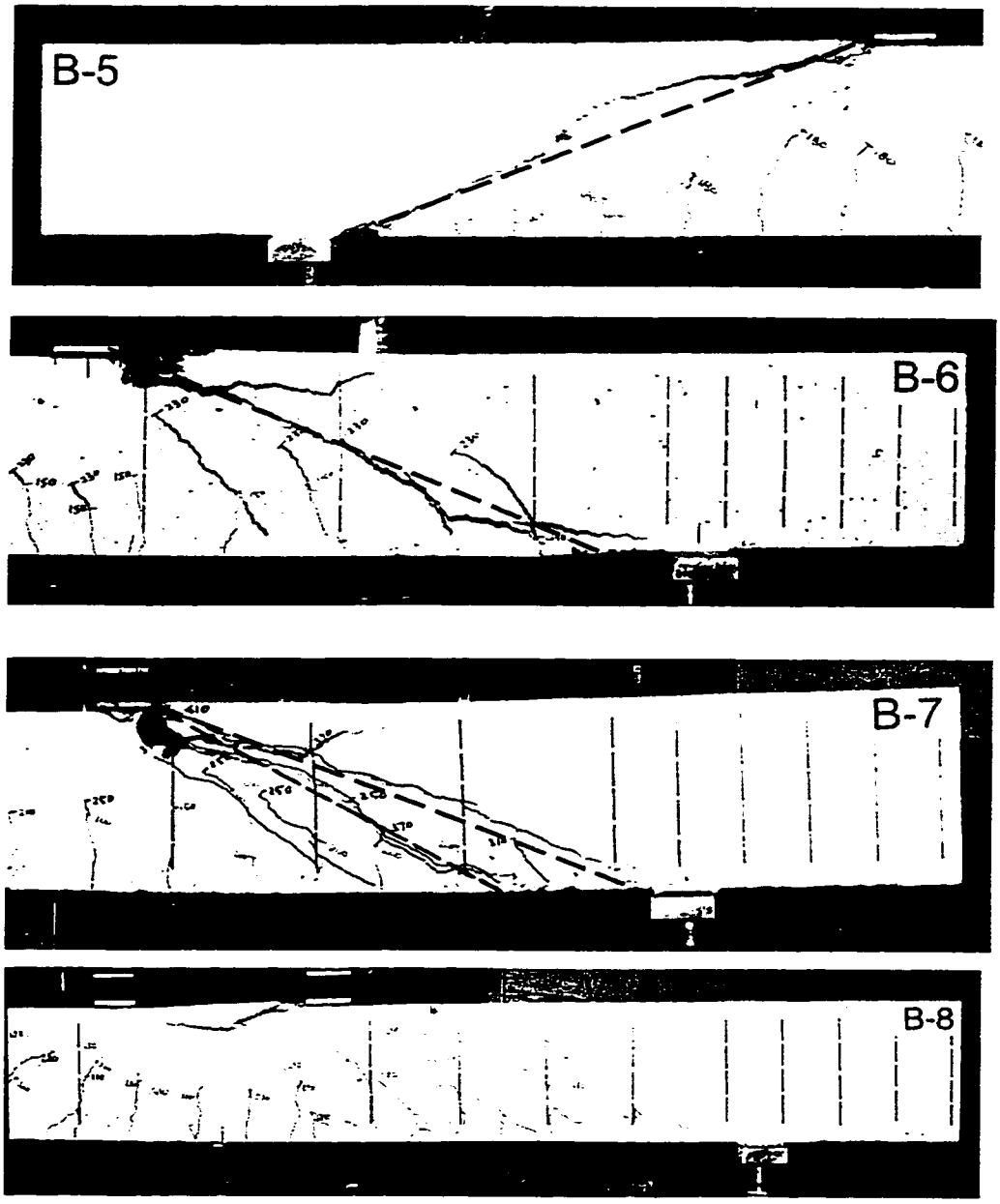

Figure 4.23: Comparison of crack locations (B-5 - B-8)

Chapter 5

Comparison of Different Methods with Test Results in Literature

5.1 Introduction

As shown before, the shear-friction method is a physically meaningful rational approach. In addition, it has a clear concept and simple expression, but more investigation to this method needs to be done. For instance, the effects of concrete strength, shear span ratio, amount of longitudinal reinforcement, amount of shear reinforcement and so on need to be studied. In this chapter, the shear-friction method as well as the design provisions of several current codes, CSA-A23.3-94, ACI 318M-95 and CEB-FIP MC90, were compared with existing test results. Note that all comparisons are made using only the shear equations for all methods. The limitations for spacing, V_c, V_s and so on, are not accounted for.

5.2 Reinforced Concrete Beams without stirrups

5.2.1 Review of Equations of Various Methods

The provisions of the recent design codes, CSA-A23.3-94, ACI 318M-95 and CEB-FIP MC90, have been reviewed in Chapter 2, and the design equation (3.35) for the shear-friction method was derived in Chapter 3. Only the equations, therefore, will be mentioned in this section for the purpose of comparison. The factors λ, ϕ_c and

ϕ_s in the code equations will be taken as 1.

Shear-Friction Method

Combining the simplified equation (3.9) and the projection of the crack equation (3.34) gives the design equation (3.35) for reinforced concrete beams without stirrups.

$$V_{sf} = 0.25k^2 f'_c b_w h \sqrt{\frac{h}{a_{cie}}} \tag{3.35}$$

$$k = 1.93 f'^{-0.39}_c \tag{3.37}$$

If the above two equations are combined , the design equation is:

$$V_{sf} = 0.93(f'_c)^{-0.22} b_w h \sqrt{\frac{h}{a_{cie}}} \tag{5.1}$$

CSA-A23.3-94

The Canadian code provides two alternative methods for the shear design of beams. The first one is a simplified method, which is based on the 45 degree truss model. The shear strength of a beams without stirrups is assumed to be equal to the strength corresponding to diagonal cracking. For sections having an effective depth, d, less than or equal to 300 mm, the shear strength should be calculated from:

$$V_c = 0.835\,(0.2)\,\sqrt{f'_c} b_w d \tag{5.2}$$

in which the 0.835 is obtained from N.11.3.5 of the Canadian code.

For sections having an effective depth, d, greater than 300 mm, the shear strength

is:

$$V_c = 0.835 \left(\frac{260}{1000 + d} \right) \sqrt{f'_c} b_w d \tag{5.3}$$

An alternative approach, the general method, is based on the variable angle truss model. The shear strength of the beams without stirrups is calculated as:

$$V_{cg} = \beta \sqrt{f'_c} b_w d_v \tag{5.4}$$

where β is a factor which varies with longitudinal strain and the spacing between crack control reinforcement. For comparison with test results, the factor 1.3 in equation (2.37) is taken out based on N.11.4.3.1 of the Canadian code.

ACI 318M–95

The American Concrete Institute gives two expressions for calculating the shear strength, V_c, of reinforced concrete members subjected to shear and flexure only:

$$V_c = \sqrt{f'_c} b_w d/6 \tag{2.20}$$

or more accurately:

$$V_c = \left[\left(\sqrt{f'_c} + 120 \rho_w \frac{V_u d}{M_u} \right) /7 \right] b_w d \tag{2.21}$$

in which M_u and V_u are the moment and shear force at the section with factored loads, and ρ_w is the longitudinal steel ratio (A_s/b_{wd}).

CEB-FIP MC90

In the CEB-FIP code, the shear resistance for reinforced concrete beams without shear reinforcement also corresponds to diagonal cracking. The design resistance to shear cracking at sections already cracked in flexure is given as:

$$\begin{aligned} V_{RD} &= 0.15\left(3\frac{d}{a}\right)^{\frac{1}{3}}\xi\left(\frac{100A_s}{b_w d}f'_c\right)^{\frac{1}{3}}b_w d \\ \xi &= 1+\sqrt{200/d} \end{aligned} \tag{2.45}$$

Note that:

- The powers of f'_c are 0.50 for the CSA and ACI codes, 0.33 for the CEB code and 0.22 for the shear-friction method. The power of f'_c describes how much the shear strength can be enhanced by increasing concrete strength.
- The shear strength is proportional to the effective depth, d, or internal lever due to flexure, d_v, in all the above equations except for the shear-friction equation. Obviously, using h directly to calculate shear strength is more convenient than calculating d or d_v.
- Only the CEB code equation, CSA general method (by β) and the more complex equation in ACI code account for the influence of the ratio of longitudinal reinforcement
- Only the CSA simplified method, CSA general method and the CEB code account for the size effect.
- The shear-friction method, CEB equation and the more complex equation in the ACI code account for the effect of the shear span ratio.

5.2.2 Summary of Test Beams

Most test beams without stirrups in the literature are simply supported and loaded by one or two concentrated loads. Their sections are rectangular. In order to investigate the influence of the ratio of clear shear span to overall depth, a_{cle}/h, concrete strength, f'_c, and the ratio of longitudinal reinforcement, ρ, on shear resistance a series of tests from the literature were reviewed. 104 reinforced concrete beams without stirrups were selected with ratios of a_{cle}/h from 0.5 to 5.6, concrete strengths from 20 MPa to 105 MPa and ratios of ρ from 1.63% to 6.64% (ρf_y from 5 MPa to 28 MPa). All beams failed by shear. The details of these beams are listed in Table 5.1. The beams which failed by bond and flexure failure were not included.

The test results of these beams were compared to the shear capacity predicted by the design equation (3.35) of the shear-friction method and the equations in CSA, ACI and CEB codes. The details for each beam and the ratios of the shear measured to the shear calculated, V_t/V_{cal}, by different methods for each beam are listed in Appendix C and D. The mean values of the ratios based on the three codes were greater than 1. To obtain a fair comparison, the coefficient of variation was used. In Table 5.2 the standard deviation and average value of the ratios, V_t/V_{cal} , for each series of test and the coefficient of variation of the ratios, V_t/V_{cal} , for all tests, are listed.

It can be seen that the shear-friction method gives a better prediction for these test beams than other code equations, especially, in the range of $a_{cle}/h \leq 2$. The reason for getting this superior prediction is because the shear-friction method considers the effect of concrete strength and the clear shear span ratio properly.

Table 5.1: Detail of test series without stirrups

Test Series	Type	Section	f '$_c$ (MPa)	a_{cle}/h	ρ (%)
Kani et al			24.5 - 30.3	0.68 - 5.58	1.88, 2.8
Leonhardt & Walther	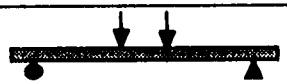		34.8, 36.5	0.48 - 4.56	4.64
Moody et al*	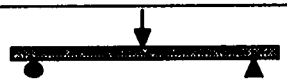		21.1 - 36.7	2.22 - 2.50	1.62 -2.37
Van Den Berg			24.5 - 58.6	2.18 - 4.00	4.30
Mphonde & Frantz**			22.6 - 101.8	2.70	3.36
Ahmad et al			65.4 - 72	1.93 - 3.06	1.77 - 6.64
Bresler & Scordelis	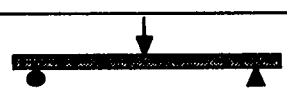		22.6 - 37.6	2.85 - 5.30	1.88 - 2.74
Xie et al	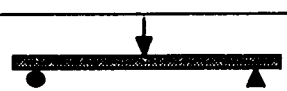		39.7, 104.2	2.15	2.07
Yoon et al	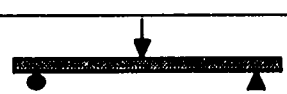		36 - 87	2.66	2.80

* Four beams in Moody series had two point load.

** One beam in Mphonde series had ρ of 2.32%.

Table 5.2: Comparison of predictions for test series without stirrups

Test Series	No.	SF-d		SF-g		CSA-s		CSA-g		ACI		CEB	
		s	*x*	*s*	*x*	*s*	*x*	*s*	*x*	*s*	*x*	*s*	*x*
Kani et al	22	0.367	1.149	0.371	1.359	1.329	1.957	2.177	2.901	1.055	2.000	1.522	2.308
Leonhardt & Walther	8	0.505	1.124	0.427	1.100	1.983	2.246	1.929	1.958	1.314	1.914	1.969	2.233
Moody et al	10	0.060	0.824	0.101	0.973	0.104	1.236	0.151	1.721	0.094	1.410	0.114	1.582
Van Den Berg	30	0.116	1.013	0.128	1.121	0.115	1.294	0.157	1.430	0.101	1.289	0.128	1.336
Mphonde & Frantz	9	0.094	1.128	0.109	1.232	0.171	1.232	0.202	1.736	0.153	1.272	0.099	1.495
Ahmad et al	18	0.197	0.929	0.416	1.187	0.275	1.046	0.541	1.783	0.390	1.613	0.354	1.285
Bresler & Scordelis	3	0.175	0.952	0.182	1.067	0.120	1.373	0.052	2.225	0.086	1.384	0.157	1.630
Xie et al	2	0.050	0.771	0.116	0.665	0.177	0.951	0.263	1.269	0.172	1.092	0.098	1.338
Yoon et al	3	0.135	0.704	0.204	0.602	0.366	1.014	0.319	1.109	0.299	0.894	0.335	1.179
Total, *s*	105	0.287		0.321		0.896		1.257		1.082		0.524	
(a_{cle}/h = 0.5 - 5.6), *x*		1.063		1.152		1.440		1.904		1.584		1.287	
V		0.270		0.279		0.622		0.660		0.560		0.407	
Total, *s*	95	0.173		0.269		0.216		0.367		0.241		0.247	
(a_{cle}/h = 2 - 6.5), *x*		1.036		1.094		1.202		1.597		1.384		1.154	
V		0.167		0.246		0.180		0.230		0.174		0.214	

5.2.3 Effect of Clear Shear Span Ratio a_{cle}/h

Traditionally, the shear span ratio, a/d, has been used as one of the critical parameters for shear strength, but in the shear-friction method, the clear shear span ratio a_{cle}/h is used instead of a/d. It is clear that the shear capacity of a beam with shear span a, and a wide bearing is higher than that of a beam with the same shear span but a narrow bearing. This is more obvious for a short span beam than a slender beam, so using the term a_{cle}/h would be more reasonable than a/d.

As we know, shear strength increases with a decrease of the a_{cle}/h ratio in the range of $a_{cle}/h \leq 2$. For beams with $a_{cle}/h > 2$, increasing a_{cle}/h has a smaller effect on the shear strength. The ratios of V_t/V_{cal} against a_{cle}/h are plotted in Figures 5.1-5.6. It can be seen that all test beams in the range of $a_{cle}/h \leq 2$ exhibited shear strengths much higher than predicted. The differences between the maximum ratios and the average ratios are respectively:

SF-d	SF-g	CSA-s	CSA-g	ACI	CEB
1.15	0.99	4.98	6.95	3.06	2.17

In literature, it is assumed that the high shear strengths of beams with $a_{cle}/h \leq 2$ may be attributed to arch action. The smaller the clear shear span ratio (the steeper the line of thrust), the more efficient the arch action is. In fact, the angle of the failure plane has the dominant influence on the concrete contribution to shear strength for beams with $a_{cle}/h \leq 2$. The h/a_{cle} is equal to $tan\theta$. As we know, the rate of increase of $tan\theta$ increases with θ. For this reason, the shear strength of beams with $a_{cle}/h < 1$ increases extremely quickly.

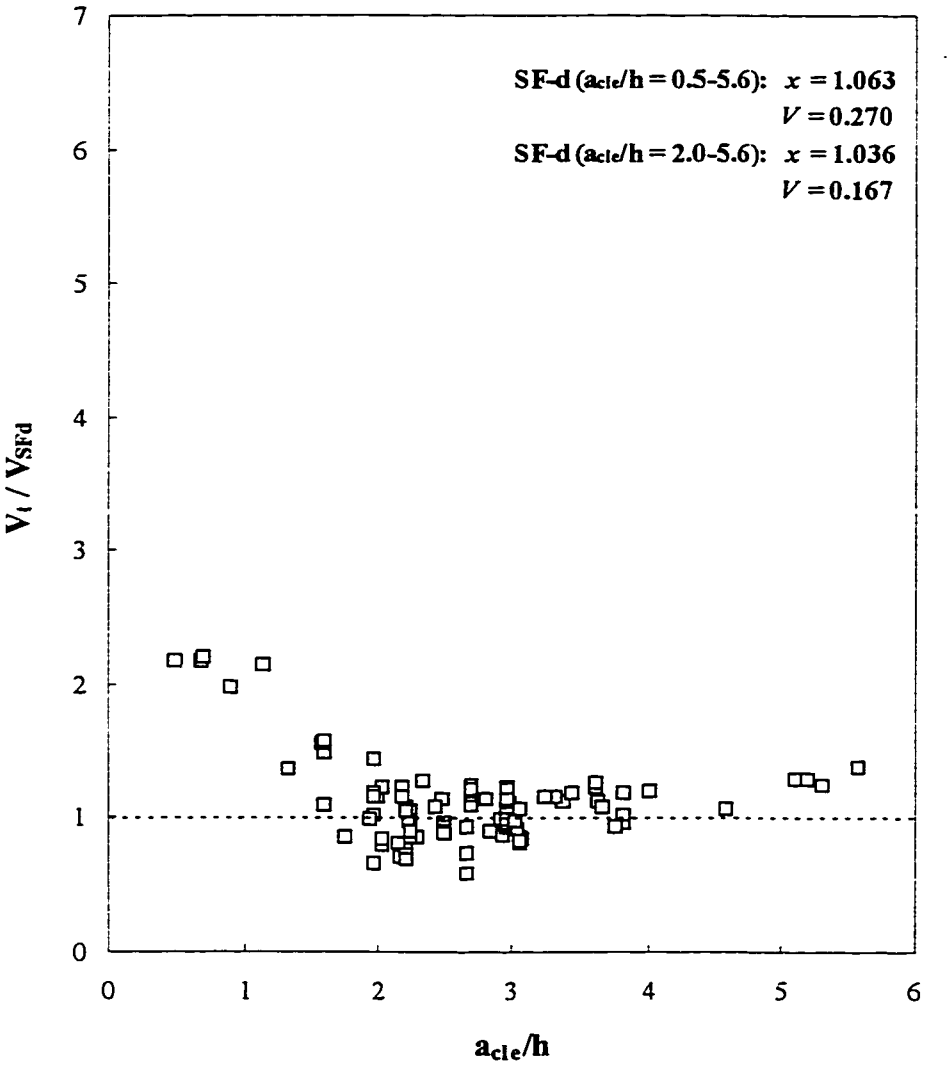

Figure 5.1: Effect of a_{cle}/h on beams without stirrups by SF design Equ.

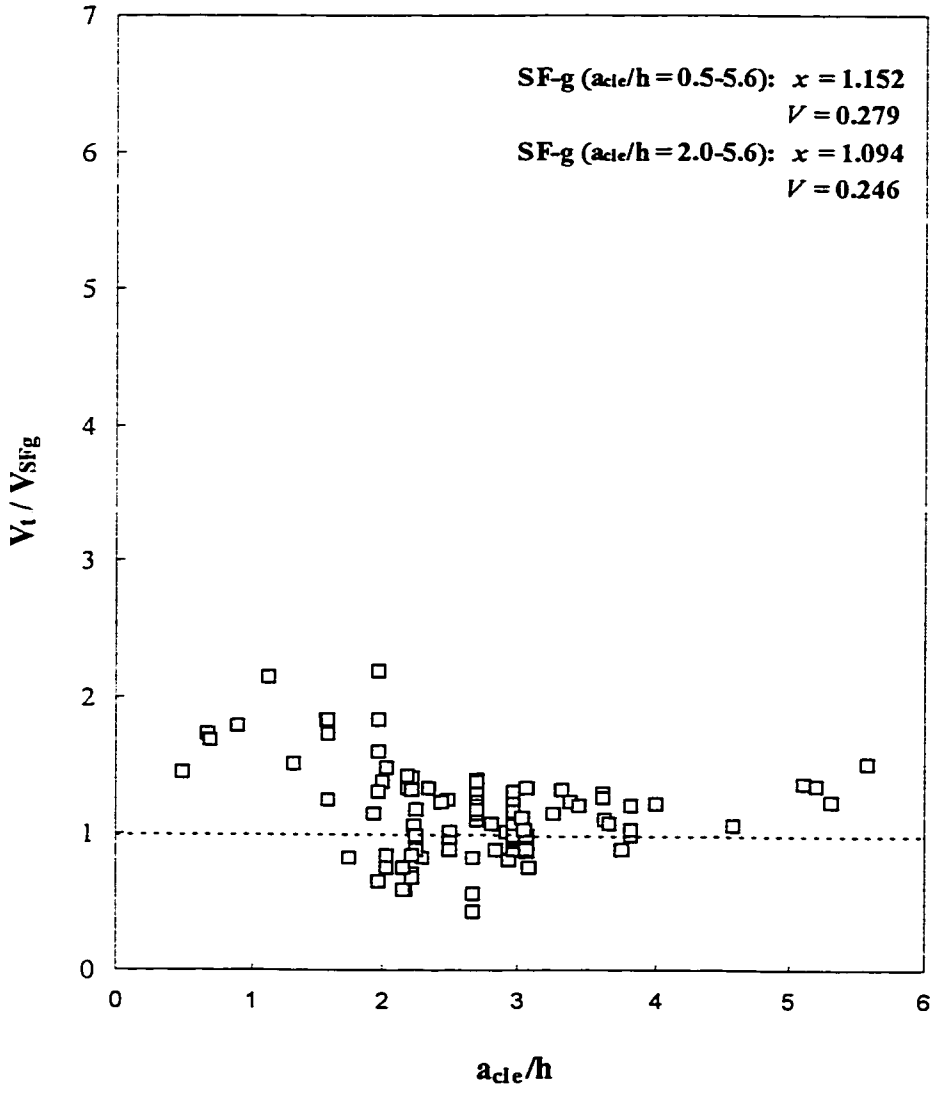

Figure 5.2: Effect of a_{cle}/h on beams without stirrups by SF general Equ.

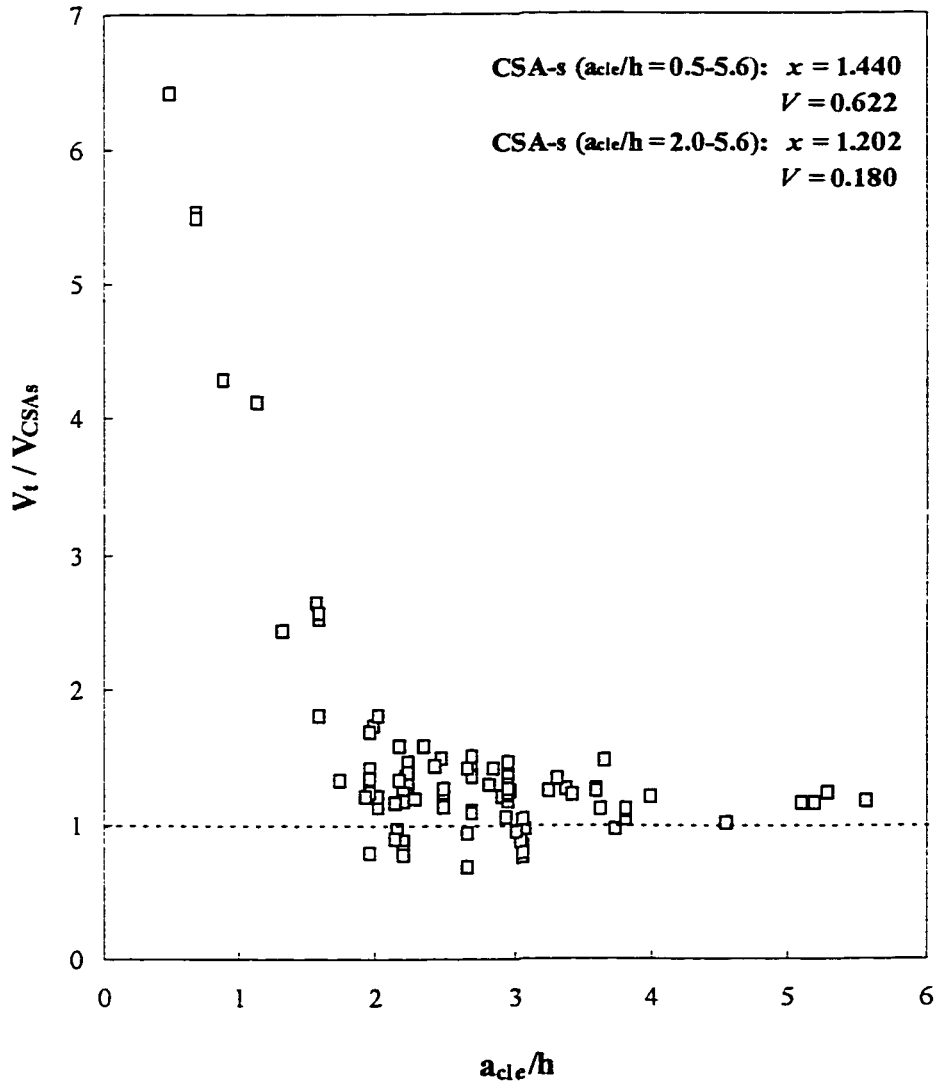

Figure 5.3: Effect of a_{cle}/h on beams without stirrups by CSA simplified method

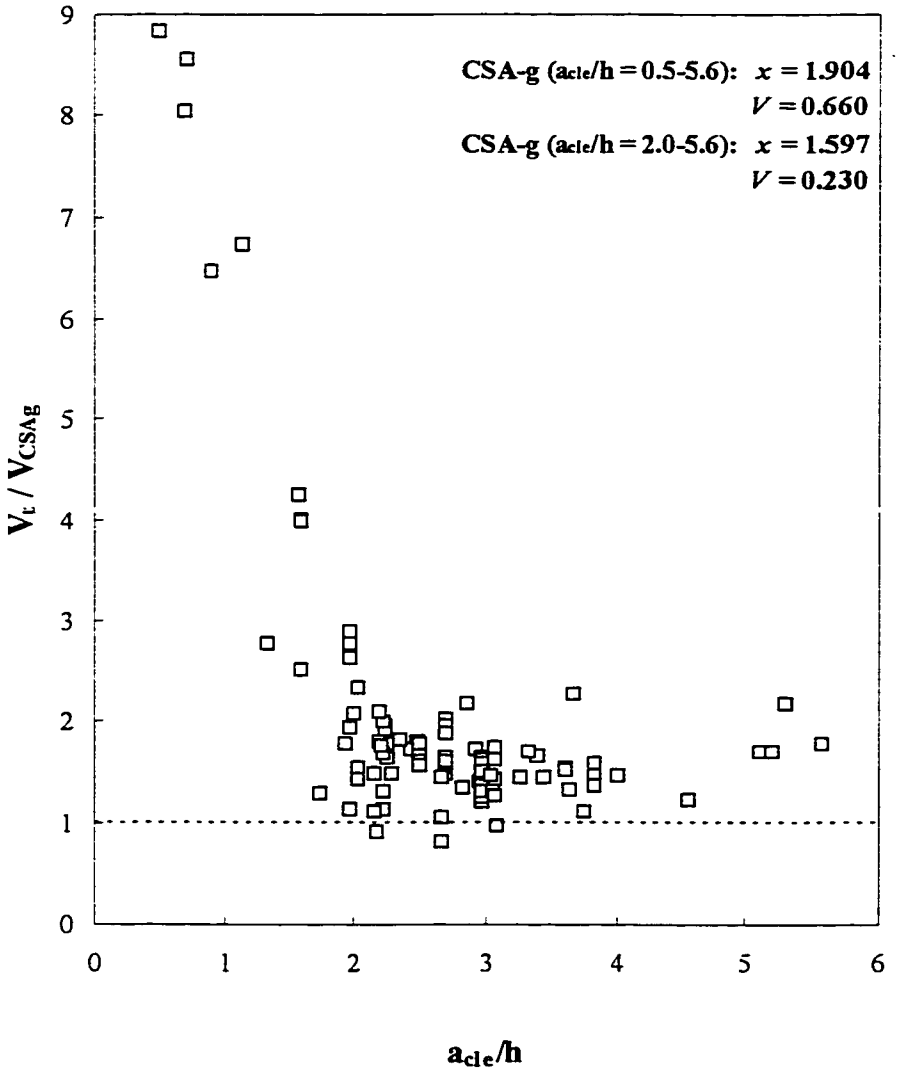

Figure 5.4: Effect of a_{cle}/h on beam without stirrups by CSA general method

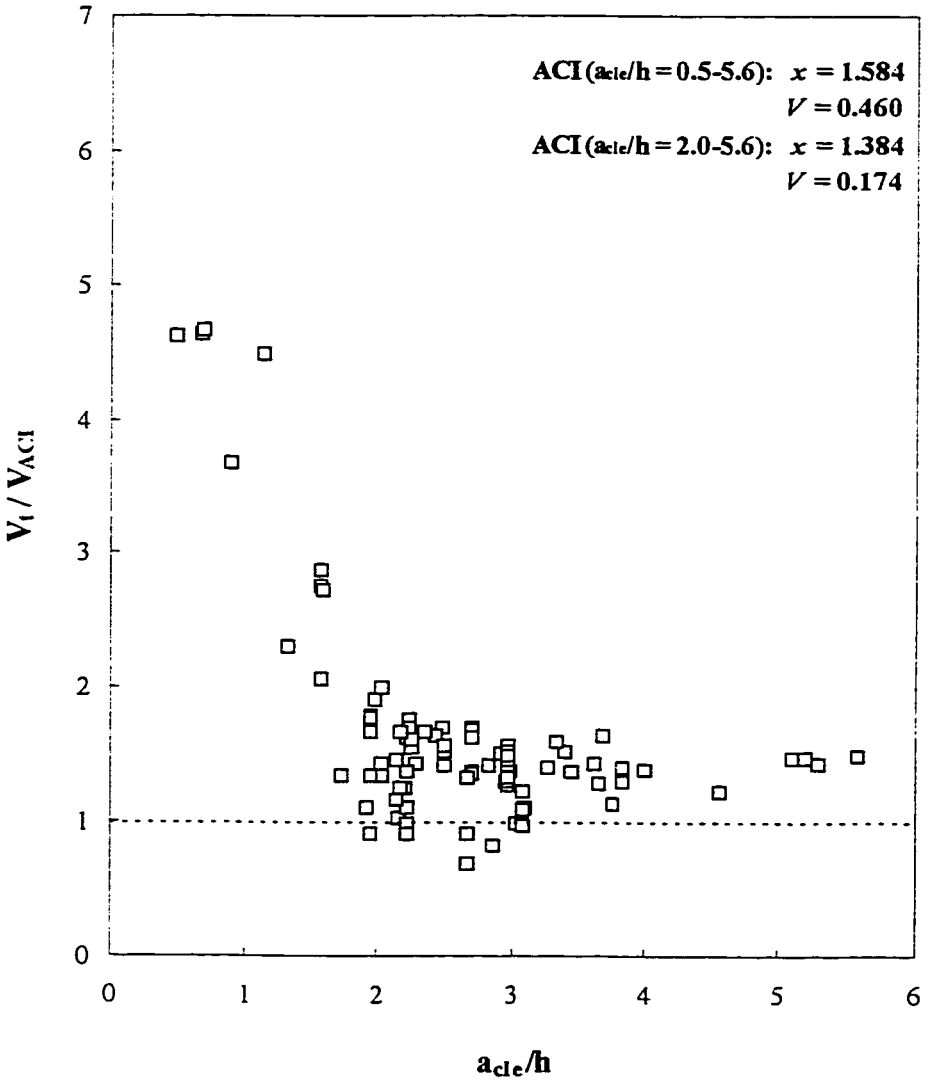

Figure 5.5: Effect of a_{cle}/h on beam without stirrups by ACI method (Eq. 2.21)

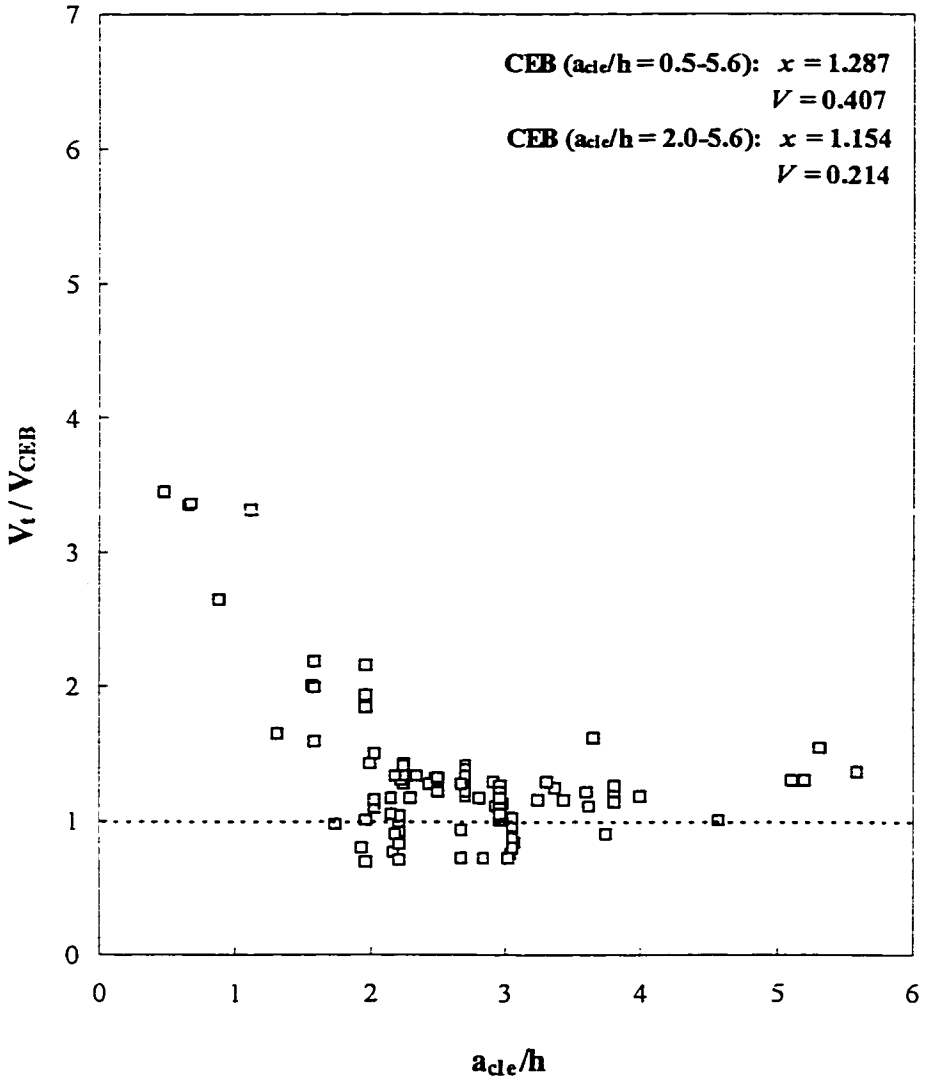

Figure 5.6: Effect of a_{cle}/h on beams without stirrups by CEB method

It can be seen that from Figures 5.1-5.6, the code equations do not apply for deep beams as mentioned in the three codes. For this reason, the coefficient of variations are respectively calculated for all the range of a_{cle}/h and for slender beams.

In the shear-friction method, the influence of angle θ (t/h) is considered. In the range of $a_{cle}/h \leq 2$, the design equation for the shear friction-method gives a much lower coefficient of variation than others. This has been shown in Table 5.2 and Figure 5.1-5.6. The design equation for the shear-friction method, therefore, can be considered for design purposes due to its simplicity and much closer correlation with test results in all a_{cle}/h ranges.

5.2.4 Effect of Concrete Strength

The shear strength increases with an increase in concrete compressive strength. This conclusion can be easily found in the literature. How much enhancement of shear strength can be provided by increasing concrete strength, for instance from 25 MPa to 100 MPa? The different code provisions give different results.

For a reinforced concrete beam without stirrups and with $b = 280$ mm, $h = 320$ mm, $d = 300$ mm, $a_{cle}/h = 3.5$, and $\rho = 2.8\%$, the shear strength versus concrete compressive strength is plotted in Figure 5.7 using the various methods. The ACI and CSA equations predict the highest enhancement of shear strength. Some researchers pointed out that the ratio of measured to calculated capacity using ACI equations (11-30) and (11-6) decreases with an increase of concrete strength. The ACI code equations therefore overestimate the shear strength of beams with high-strength concrete.

Elzanaty, Nilson and Slate explained this in their paper. Increasing concrete

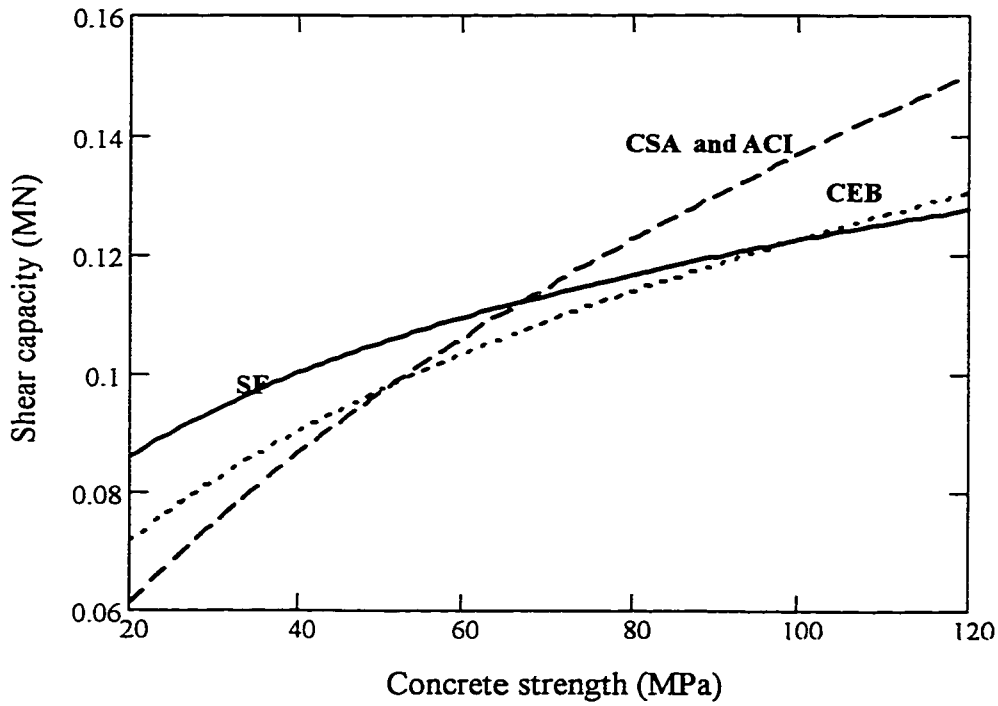

Figure 5.7: Enhancements of shear strength with increased f'_c using different methods

strength increases the flexure cracking load. Up to the cracking load, shear is resisted mostly by shear stresses in the concrete. After cracking, shear is resisted by aggregate interlock, dowel action of the main reinforcing bars, and the resistance of the still uncracked concrete at the top of the beam (ACI-ASCE, 1973). The percentage of shear force carried by aggregate interlock depends strongly on the surface roughness at the crack. Examination of the failure surfaces of the beams in this investigation confirmed that, for higher concrete strengths, the crack surfaces were distinctly smoother, indicating that the shear force carried by aggregate interlock can be expected to decrease with an increase in concrete strength (Elzanaty et al,

1986).

It can be seen that the ACI and CSA equations have not accounted for the effect of the roughness change on the failure surface for the beams with higher concrete strengths. By contrast, the shear-friction method includes this influence by varying the factor k:

$$k = 1.93 f_c'^{-0.39}$$

This equation for k was obtained using the statistical regression analysis mentioned in Chapter 3. The factor k decreases with an increase of f_c'.

With regard to the other aspects, increasing concrete strength will increase shear strength in the compression zone, and increasing the longitudinal reinforcement ratio, ρ, will increase dowel force. These shear transfer mechanisms are interdependent and not easy to separate (Elzanaty, Nilson, and Slate, 1986). It seems that the aggregate interlock is a critical term for most cases when concrete strength increases, since the compression zone becomes smaller for a high-strength concrete member and the dowel force can not be large compared to the aggregate interlock influence.

In order to investigate the effect of f_c' on shear strength, one series of test data (Mphonde and Frantz, 1984) was chosen because its parameters remained relatively constant, except for f_c' which varied from 22.6 MPa to 108.1 MPa. The ratios of measured to calculated capacity against concrete strength for all methods are plotted in Figure 5.8-5.12. The ratios of measured/calculated capacity show a decrease with an increase of f_c' except when using the equation for the shear-friction method.

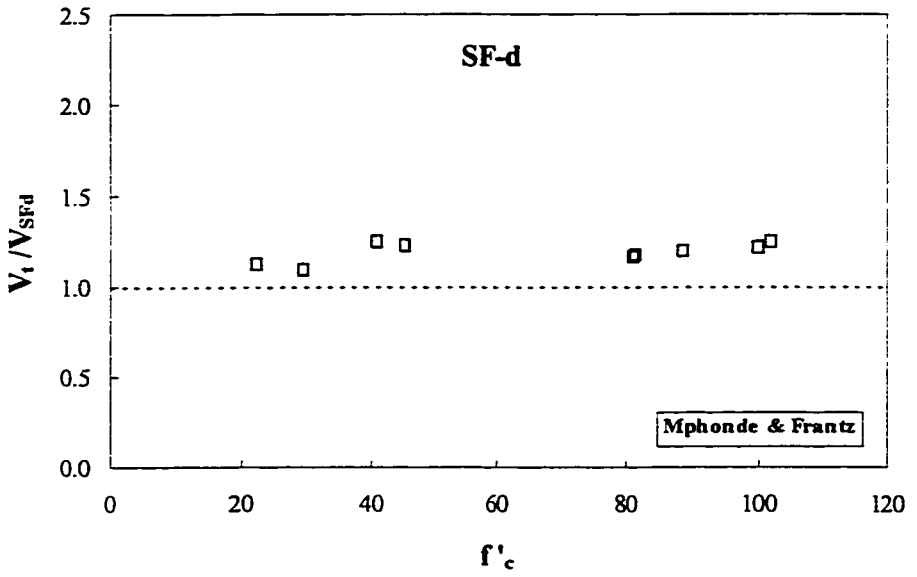

Figure 5.8: Effect of f'_c on beams without stirrups by SF design Eq.

5.2.5 Effect of Longitudinal reinforcement Ratio

Many earlier researchers found that increasing the longitudinal steel ratio increases the shear strength of concrete beams without stirrups no matter what the concrete strength. There are two reasons for this enhancement.

One is that increasing the amount of longitudinal reinforcement will enhance the dowel capacity of the beam. As mentioned, after cracking, the shearing slip along diagonal crack is partly resisted by the dowel force in the longitudinal reinforcement.

Another reason is that increasing ρ also affects the aggregate interlock capacity. Beams with low ρ will have wide, long cracks in contrast to the shorter, narrower cracks found in beams with high ρ. Since the aggregate interlock mechanism depends on the crack width, an increase in the aggregate interlock force is to be expected with

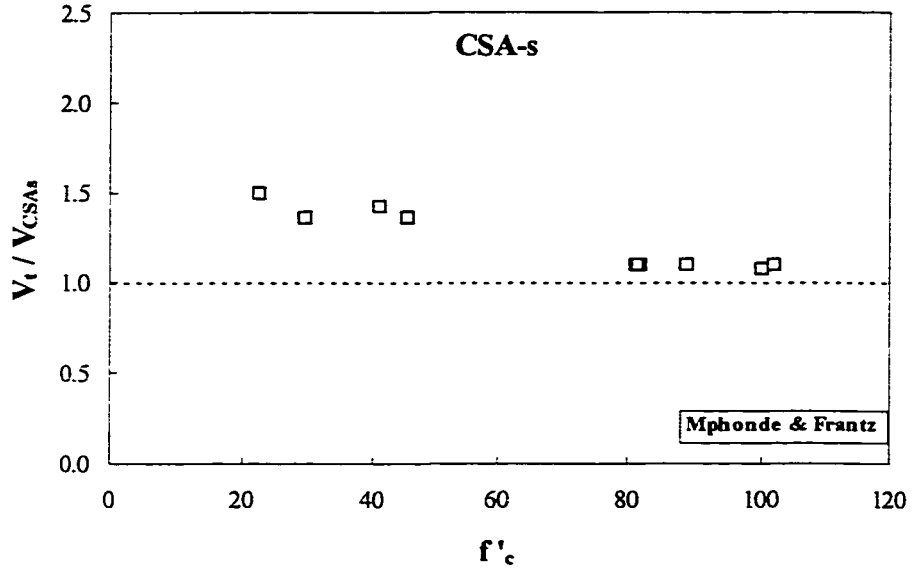

Figure 5.9: Effect of f'_c on beams without stirrups by CSA simplified method

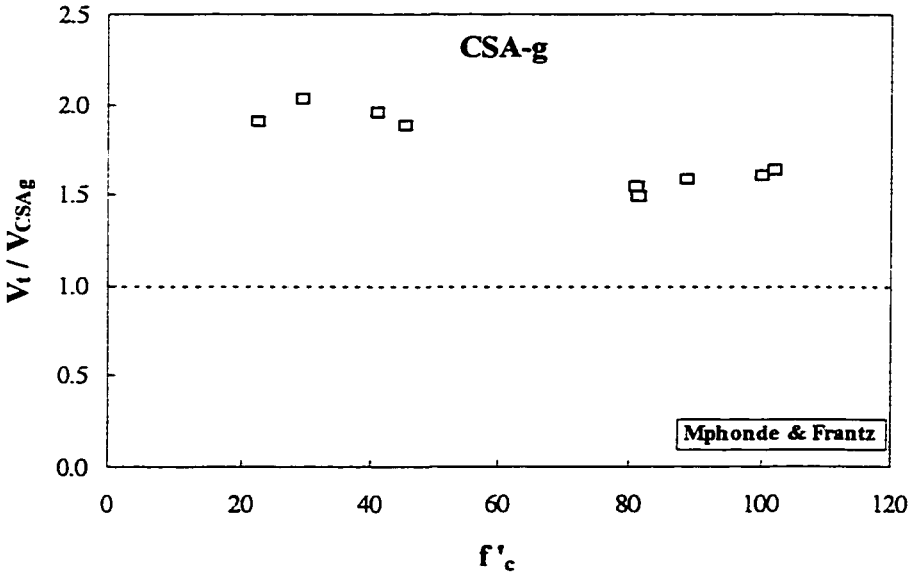

Figure 5.10: Effect of f'_c on beams without stirrups by CSA general method

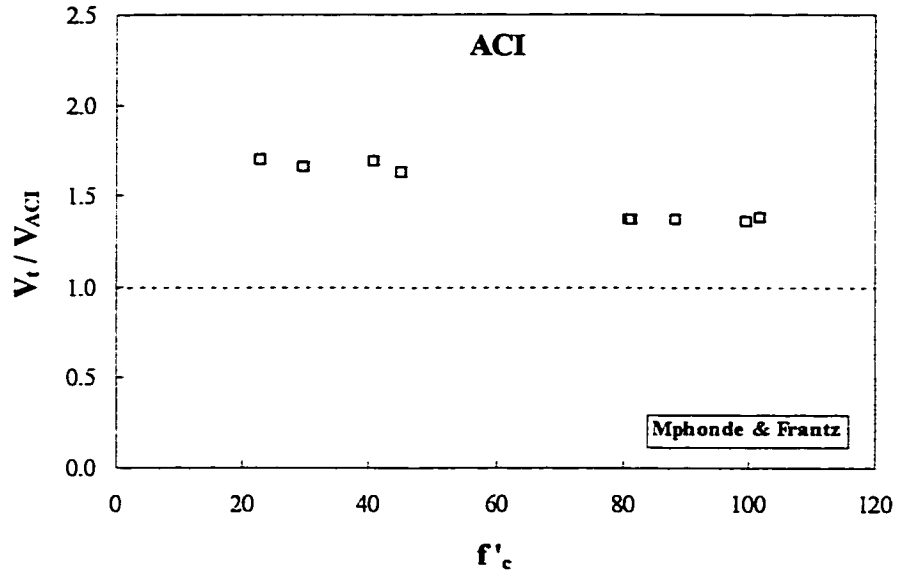

Figure 5.11: Effect of f'_c on beams without stirrups by ACI method (Eq. 2.21)

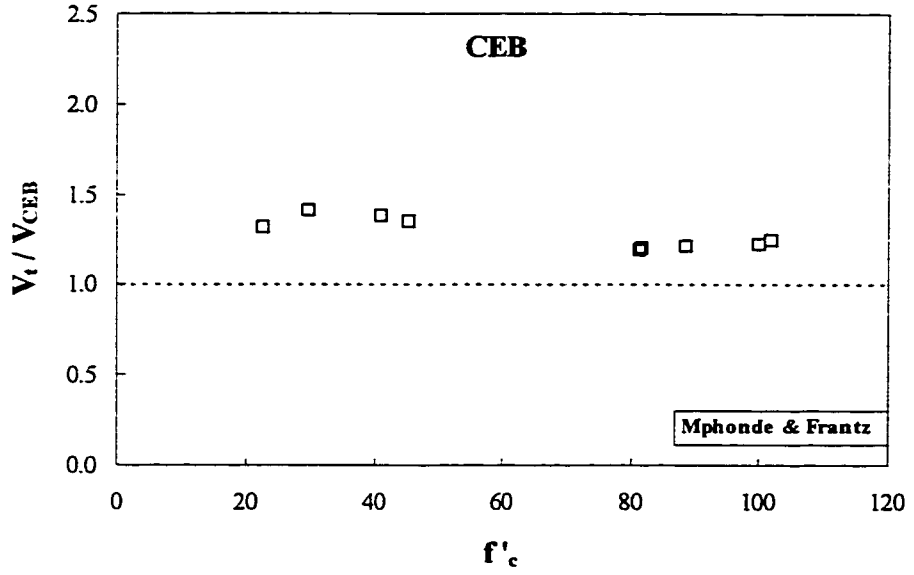

Figure 5.12: Effect of f'_c on beams without stirrups using CEB method

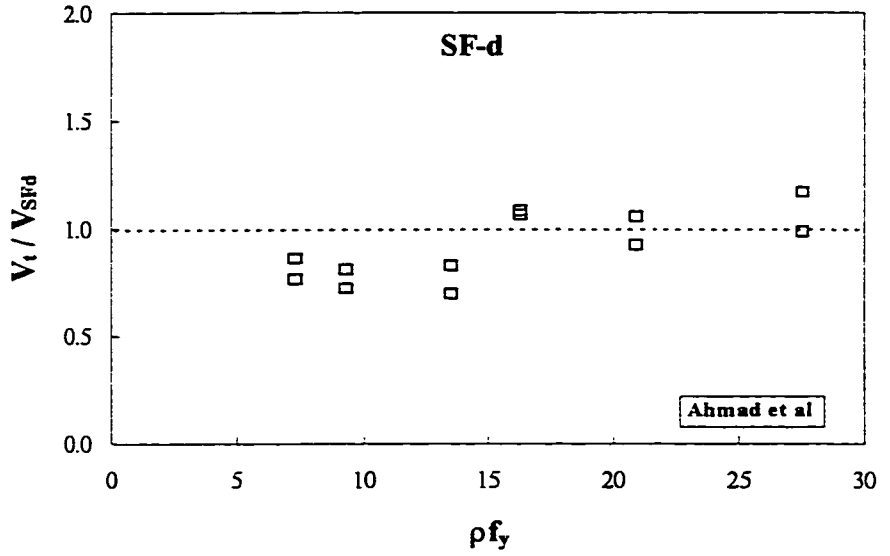

Figure 5.13: Effect of ρf_y on beams without stirrups by SF design Equ.

an increase in ρ (Elzanaty, Nilson, and Slate, 1986).

In the shear-friction equation, the longitudinal force is approximated by T_{opt}, which is not directly related to the amount of reinforcement. Also, in the equation $k = 1.93 f_c'^{-0.39}$, only the effect of concrete strength on aggregate interlock is taken into account, but the effect of ρ on aggregate interlock is ignored. This could make the ratios of measured to predicted increase with an increase of ρ. One series of tests (Ahmad, Khaloo, and Poveda, 1986) was chosen here. Its ρ changed from 1.77% to 6.44% and f_c' from 65 MPa to 72 MPa. Only beams with $a_{cle}/h > 2$ are chosen. In Figure 5.13-5.17 the ratios of measured/calculated are plotted for all methods. The shear ratios predicted by the shear-friction, ACI and CSA simplified methods slightly increase with an increase of ρ. The CEB code equation seems to slightly

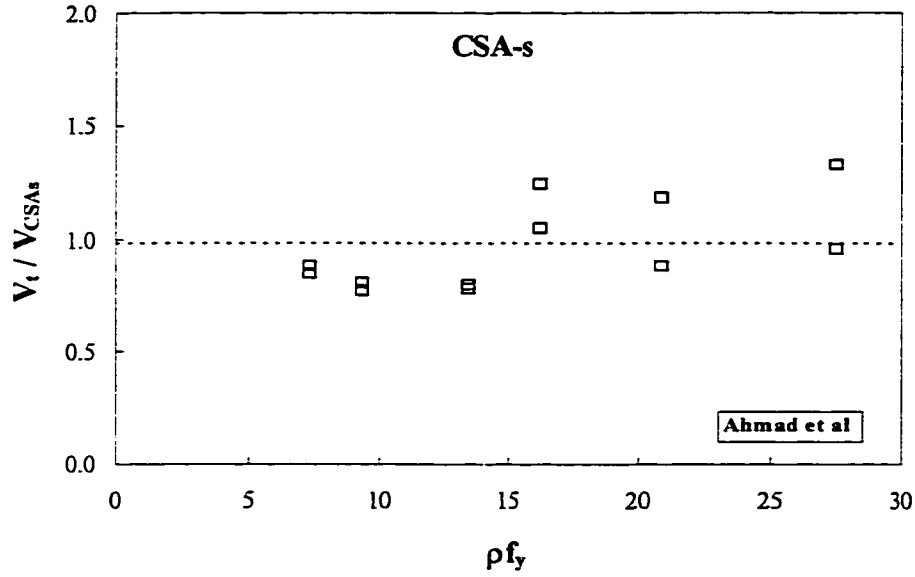

Figure 5.14: Effect of ρf_y on beams without stirrups by CSA simplified method

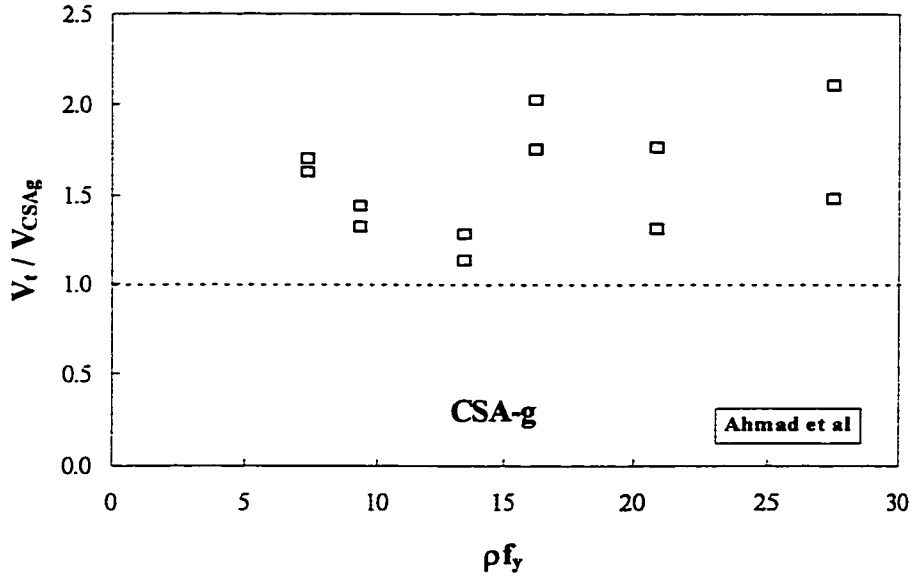

Figure 5.15: Effect of ρf_y on beams without stirrups by CSA general method

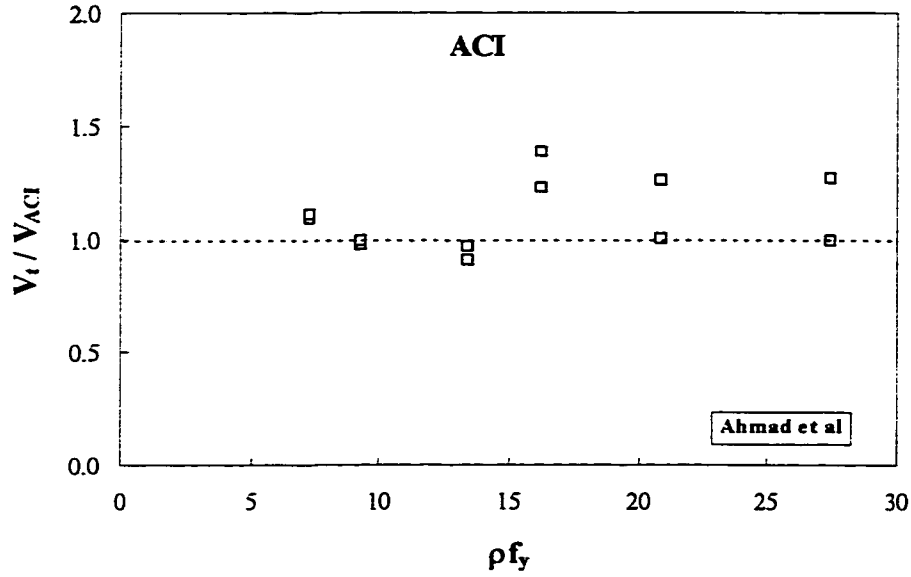

Figure 5.16: Effect of ρf_y on beams without stirrups by ACI method (Eq. 2.21)

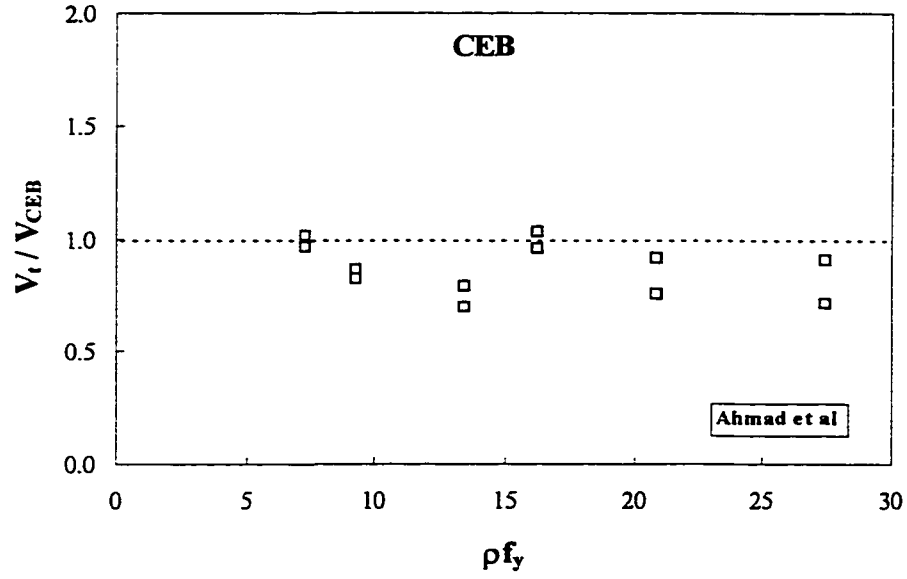

Figure 5.17: Effect of ρf_y on beams without stirrups by CEB method

overcompensate for the effect of ρ. The CSA general method shows a wide scatter but a slight upward trend. It is difficult to see a tendency. It can be seen from Figure 5.13-5.17 the shear ratios have not varied much with an increase of ρ using all methods. This means the ratio is not sensitive to an increase in ρ in this range.

5.2.6 Summary for Reinforced Concrete Beam without Stirrups

The equations for beam shear in the CSA, ACI and CEB codes are not appropriate for determining shear strength when the clear shear span ratio is less than or equal to 2, so the strut-tie model is required to predict the shear strength of a deep beam. However, the equation for the shear-friction method can be used to calculate the shear strength in all span ranges.

The effect of concrete strength on shear strength due to a reduction of aggregate interlock capacity is not accounted for in the three code equations, but is included in the shear-friction equation.

The influence of the ratio of longitudinal reinforcement in the range of 1.77% to 6.44% on shear strength is not large.

The shear-friction equation is simple and gives a better prediction of shear strength for beams without stirrups compared with the other codes mentioned above.

5.3 Reinforced Concrete Beam with Stirrups

5.3.1 Review of Equation of Various Methods

Shear-friction Method

The design equation (3.13) for shear-friction is also very simple. It can be expressed as:

$$V_{sf} = k\sqrt{f'_c b_w h T_v \frac{d_s}{s}} - T_v \tag{3.13}$$

$$k = 1.93 f'^{-0.39}_c \tag{3.37}$$

$$T_v = A_v f_{vy}$$

The factor k is the same as for beams without stirrups.

CSA Simplified Method and ACI 318M-95

The simplified method in the Canadian code uses the same approach as the method in ACI 318M-95 for shear design. It is based on the 45 degree truss model and on the assumption of stirrup and concrete contributions to the total shear strength.

$$V_r = V_c + V_s$$

The concrete contribution is equal to the diagonal cracking strength.

$$V_c = 0.835\,(0.2)\,\sqrt{f'_c} b_w d \tag{5.2}$$

$$V_s = \frac{A_v f_{vy} d}{s} \tag{2.30}$$

CSA General Method

The general method in the Canadian code is based on a variable angle truss model. The shear strength of a beam is determined by:

$$V_{rg} = V_{cg} + V_{sg}$$

in which

$$V_{cg} = \beta\sqrt{f'_c}b_w d_v \tag{5.4}$$

$$V_{sg} = \frac{A_v f_{vy} d_v \cot\theta}{s} \tag{2.38}$$

where β is a factor accounting for the shear resistance of cracked concrete and θ is the angle of inclination of the diagonal compressive stresses to the longitudinal axis of the member.

CEB-FIP MC90

The CEB-FIP MC90 code for shear design is also based on a variable angle truss model. It uses a similar approach to the general method in the Canadian code. For design purposes, it can be assumed that the stirrups will yield and the web concrete will reach its limiting compression if the shear resistance of a beam is controlled by the stirrups and web concrete alone. The shear resistance is

$$V_{RD} = \frac{A_{sw} f_{yd}(z\cot\theta)}{s} \tag{2.48}$$

$$V_{RD} = f_{cd2} b_w z \frac{\cot\theta}{\sqrt{1+\cot 2\theta}} \tag{2.49}$$

Combining these two equations gives:

$$\cot\theta = \sqrt{\frac{f_{cd2}}{\rho_w f_{yd}} - 1} \tag{2.45}$$

and

$$1 \leq \cot\theta \leq 3 \tag{2.46}$$

where A_{sw} is the same as A_v, f_{yd} is the same as f_{vy}, z is the same as d_v and f_{cd2} is the same as f'_c.

5.3.2 Summary of Test Beams

In order to compare test results in the literature to the different methods mentioned above, 144 reinforced concrete beams with stirrups were selected. The majority of the test beams selected were simply supported rectangular beams subjected to a symmetrical single or two point load. Thirty eight beams had T or I section. Twelve beams had a ratio of clear shear span to effective depth less than 2. Only one series of test beams was two-span continuous. All beams which failed by bond and flexure were taken out from the test series. The general information for these beams is provided in Table 5.3. The concrete strength ranged from 20 MPa to 125 MPa, the web reinforcement index ranged from 0.32 MPa to 8.3 MPa and the s/d ratios ranged from 0.11 to 1.3.

Table 5.3: Details of test series with stirrups

Test Series	Type	Section	f'_c (MPa)	a_{cle}/h	ρ (%)	$\rho_v f_{vy}$ (MPa)
Rodrigues et al	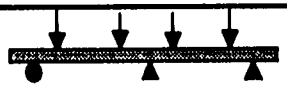		21 - 28.8	2.04 - 3.25	1.6, 2.66	1.32 - 3.60
Hsiug and Frantz			43	2.53	1.82	0.64 - 0.96
Debaiky & Elniema			20.2 - 31.4	1.83 - 2.5	1.92, 2.89	0.63 - 1.62
Mphonde	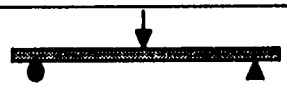		22.1 - 83	2.79	3.36	0.37 - 1.14
Elzanaty et al			20 - 62.7	3.17	2.5, 3.3	0.73
Anderson & Ramirez	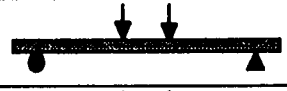		29.2 - 32.3	2.00	2.30	2.22
Johnson & Ramirez	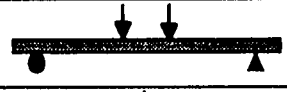		36.4 - 72.3	2.47	2.50	0.37 - 0.75
Roller & Russell			72.4 - 125.3	1.71 - 1.99	1.24 - 6.08	0.35 - 8.35
Bresler & Scordelis			21.1 - 29.6	2.85 - 3.68	1.80 - 3.66	0.32 - 0.65
Xie et al	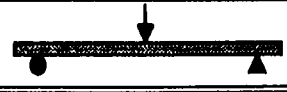		42.9 - 104.0	2.14	3.2, 4.54	1.65 - 2.65

Table 5.3 (continued): Details of test series with stirrups

Test Series	Type	Section	f '$_c$ (MPa)	a_{cle}/h	ρ (%)	$\rho_v f_{vy}$ (MPa)
Yoon et al			36 - 87	2.66	2.80	0.35 - 1.02
Kriski	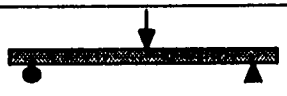		28.9 - 77.8	1.88, 2.26	2.01	0.56
Peng			29.3 - 33.0	2.66	2.7	0.30 – 1.31
Clark			23.4 - 29.0	0.8 - 2.32	1.63 - 3.10	1.19 - 1.58
Taylor			25.6 - 28.5	2.59 - 3.34	1.6, 2.66	1.09, 1.46
Haddadin et el			24.1 - 44.9	1.76 - 4.6	3.81	0.69 - 4.94
Sorensen			23.2 - 34.2	2.68	3.84	0.76 - 1.48
Lyngberg			25.7, 26.6	2.25	1.94	3.46, 3.57
Bach et al			20.1 - 36.7	2.32	2.86	0.43 - 2.82

Table 5.4: Comparison of predictions for test series with stirrups

Test Series	No.	SF-d		SF-g		ACI & CSA-s		CSA-g		CEB	
		s	*x*	*s*	*x*	*s*	*x*	*s*	*x*	*s*	*x*
Rodrigues et al	9	0.093	1.114	0.074	0.972	0.239	1.033	0.309	1.051	0.090	0.556
Hsiug & Frantz	4	0.145	0.830	0.047	0.753	0.040	0.820	0.066	0.925	0.056	0.891
Debaiky & Elniema	8	0.150	0.967	0.112	0.864	0.199	1.096	0.213	1.164	0.268	0.824
Mphonde	12	0.134	1.096	0.115	1.085	0.121	1.126	0.146	1.234	0.462	1.361
Elzanaty et al	3	0.283	1.062	0.281	1.055	0.209	1.233	0.315	1.411	0.333	1.078
Anderson & Ramirez	3	0.119	0.975	0.227	0.961	0.325	1.152	0.367	1.174	0.048	0.541
Johnson & Ramirez	6	0.095	0.852	0.072	0.805	0.073	1.050	0.172	1.171	0.278	1.244
Roller & Russell	10	0.195	0.966	0.303	0.905	0.303	1.064	0.321	1.209	0.385	0.999
Bresler & Scordelis	6	0.041	1.000	0.051	0.980	0.092	1.180	0.105	1.344	0.274	1.473
Xie et al	5	0.040	0.972	0.032	0.982	0.041	0.977	0.036	1.076	0.075	0.699
Yoon et al	9	0.076	0.994	0.099	1.004	0.163	1.201	0.225	1.336	0.202	1.444

Table 5.4 (continued): Comparison of predictions for test series with stirrups

Test Series	No.	SF-d		SF-g		ACI &CSA-s		CSA-g		CEB	
		s	*x*	*s*	*x*	*s*	*x*	*s*	*x*	*s*	*x*
Kriski	8	0.242	1.119	0.239	1.069	0.381	1.596	0.521	1.967	0.334	1.476
Peng	7	0.127	1.072	0.114	0.998	0.085	1.224	0.167	1.320	0.374	1.099
Clark	16	0.156	1.191	0.137	1.168	0.204	1.588	0.251	1.631	0.128	0.858
Taylor	3	0.098	0.912	0.097	0.923	0.109	1.094	0.095	1.102	0.071	0.795
Haddadin et al	17	0.146	1.001	0.143	1.020	0.279	1.181	0.303	1.165	0.254	0.823
Sorensen	10	0.083	1.203	0.095	1.348	0.257	1.661	0.349	1.772	0.217	1.143
Lyngberg	2	0.011	1.114	0.014	1.110	0.012	1.422	0.012	1.152	0.001	0.754
Bach et al	6	0.174	1.052	0.104	1.253	0.249	1.156	0.250	1.167	0.718	1.502
Total, *s*	144	0.174		0.196		0.307		0.365		0.410	
x		1.062		1.035		1.238		1.331		1.047	
V		0.164		0.190		0.248		0.275		0.391	

These test results are compared to the shear capacity predicted by the shear-friction method, ACI 318M-95, CSA-A23.3-94 and CEB-FIP MC90. The average values and standard deviations of measured/calculated ratios for each series test and the coefficient of variations of measured/calculated ratios for all tests by using different methods are listed in Table 5.4. An adjustment of section effect for T-beams and I-beam is made for the prediction by the shear-friction method. The details of each beam and the measured/calculated ratios for each beam are listed in Appendix E and F.

It can be seen that the shear-friction method has a much closer correlation to test results than the three codes.

5.3.3 Effect of clear shear span ratio, a_{cle}/h

In Figure 5.18 - 5.22, the ratios of V_t/V_{cal} predicted by the code equations have not shown as much difference from the ones predicted by the shear-friction equation as the beams without stirrups. Adequate stirrups force the critical shear plane to be steeper so that the influence of a_{cle}/h is no longer as pronounced.

There are larger scatters of the measured/calculated ratio from the predictions by the ACI 318M-95, CSA-A23.3-94 and CEB-FIP MC90 equations than the scatter predicted by the shear-friction equation, even though a large improvement is seen in the range of $a_{cle}/h \leq 2$. This has been shown in Table 5.4 and Figure 5.18-5.22. The shear ratios calculated by the CEB code equations have a very wide scatter. This is because most value of $cot\theta$ calculated by equation (2.48) are more than 3. Based on (2.49) $\cot\theta$ is taken as 3. In addition the CEB code equations does not have a separate term for the concrete contribution as does the CSA general method.

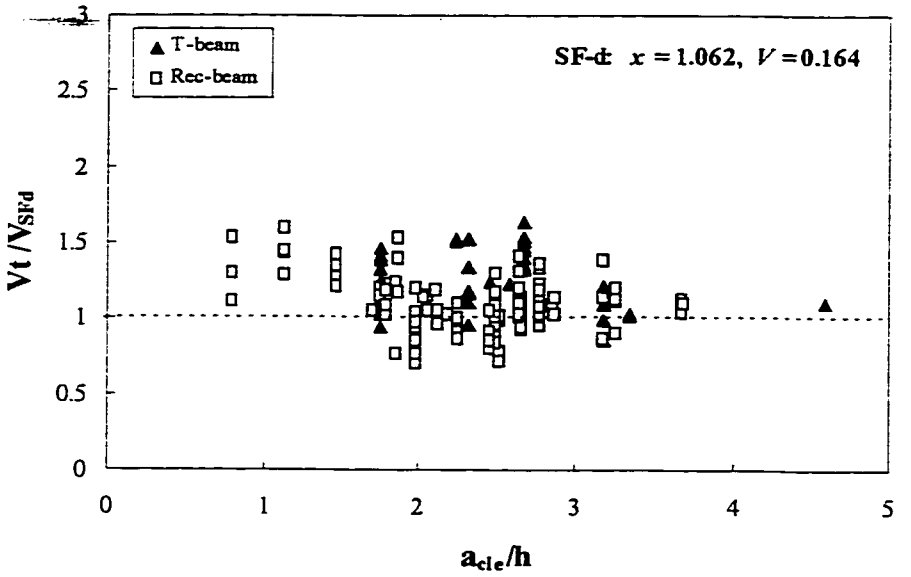

Figure 5.18: Effect of a_{cle}/h on beams with stirrups by SF design Eq.

Note that the shear-friction equation uses d_s instead of d for calculating the number of stirrups. Using d_s/s to determine the number of stirrups is more accurate than using d/s. However, using d is more convenient and familiar than d_s. There is not much difference between using d_s and d. The coefficient of variation increase from 0.164 to 0.172 if d is used.

5.3.4 Effect of Amount of Shear Reinforcement

An increase in the web reinforcement index $\rho_v f_{vy}$ results in an increase in shear strength, which has been shown in many tests from the literature. It is necessary to evaluate whether the current code provisions and the shear-friction method consider this effect properly.

Two series of tests are selected here. One series (Mphonde and Frantz, 1984) has

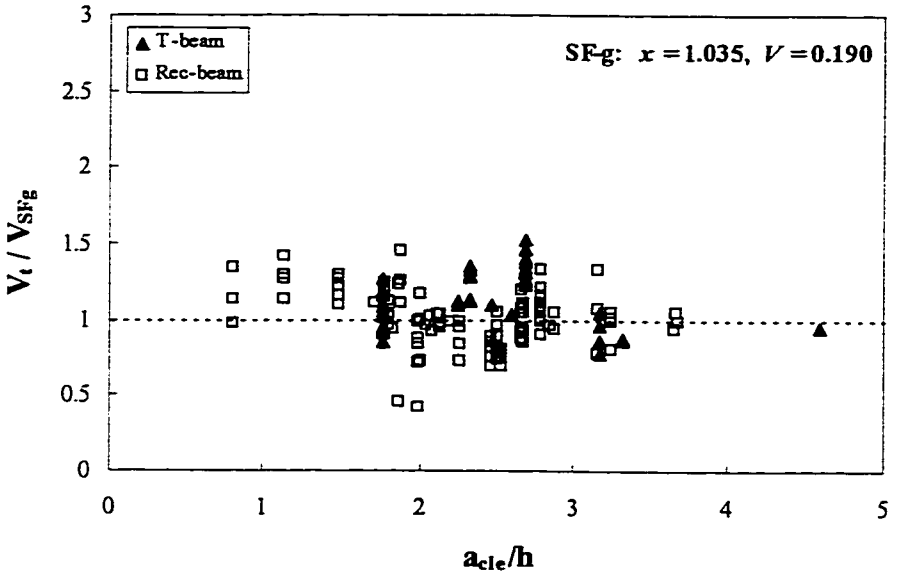

Figure 5.19: Effect of a_{cle}/h on beams with stirrups by SF general Eq.

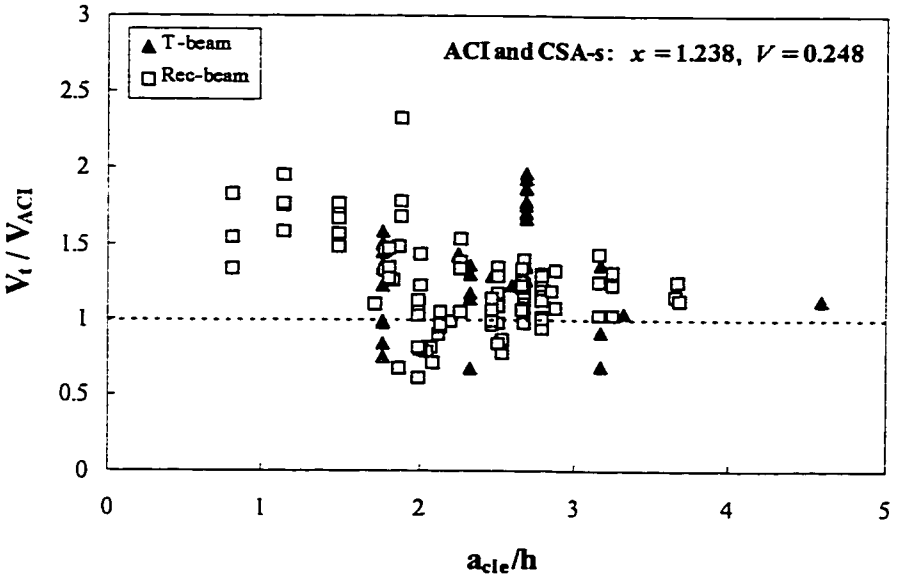

Figure 5.20: Effect of a_{cle}/h on beams with stirrups by ACI & CSA-s method

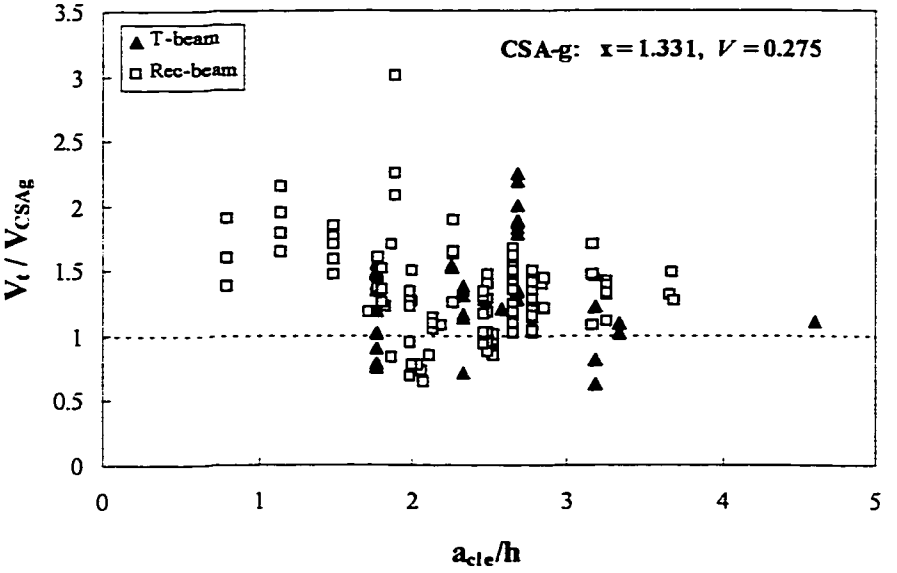

Figure 5.21: Effect of a_{cle}/h on beams with stirrups by CSA general method

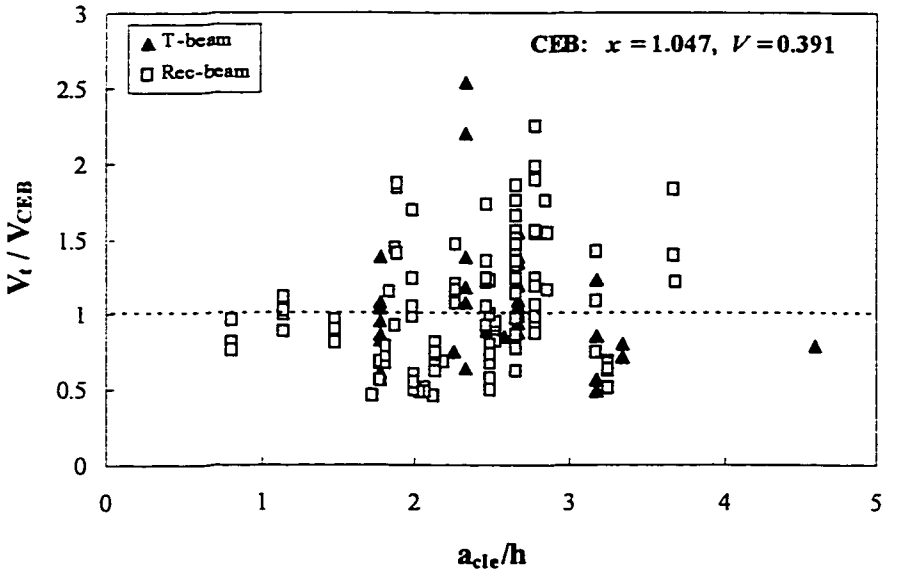

Figure 5.22: Effect of a_{cle}/h on beams with stirrups by CEB method

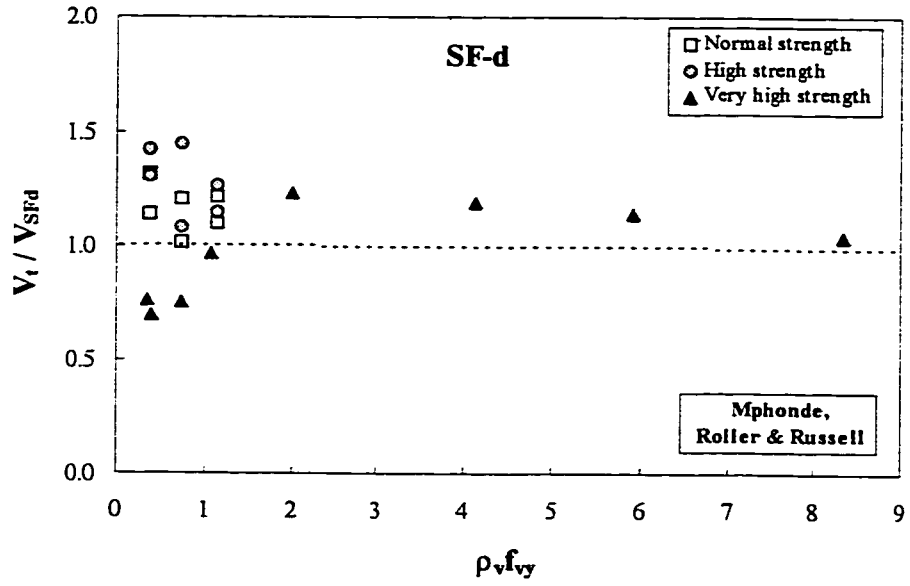

Figure 5.23: Effect of $\rho_v f_{vy}$ on beams with stirrups by SF design Eq.

$\rho_v f_{vy}$ of 0.37, 0.73 and 1.14 MPa and f'_c from 22 MPa to 83 MPa. The other series has $\rho_v f_{vy}$ from 0.35 to 8.35 MPa and f'_c of 120 and 125 MPa. The measured/calculated ratios for shear versus $\rho_v f_{vy}$ for these two series of tests by different methods are plotted in Figure 5.23-5.26.

In Figure 5.23, the shear-friction equation shows no obvious trend in the shear ratios with an increase of $\rho_v f_{vy}$. A few beams with f'_c of 120 and 125 MPa in the minimum shear reinforcement range have lower shear ratios than the average by up to 34%. This could be due to the fact that the decrease in aggregate interlock capacity has not been sufficiently accounted for in a very high strength concrete. This result, however, is obtained from only one test series. More investigation needs to be done on very high strength concretes.

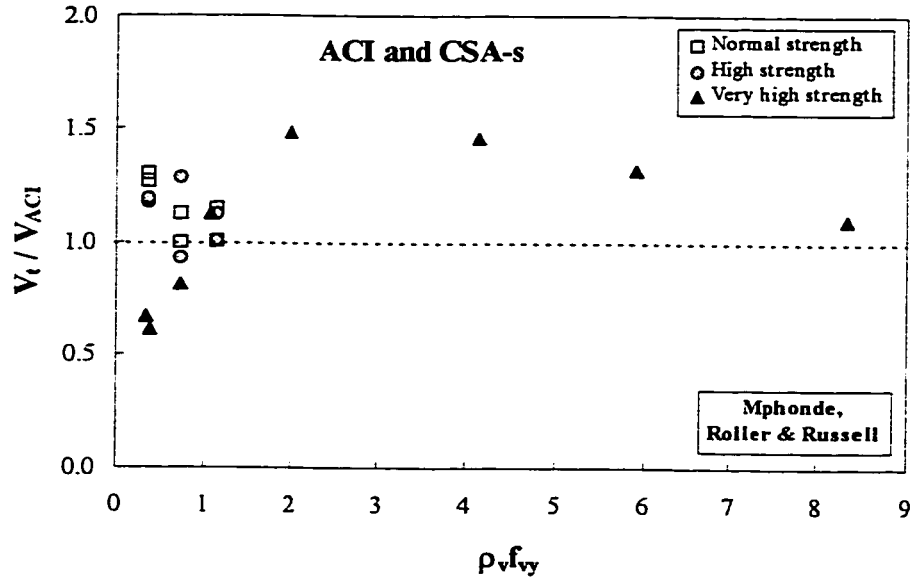

Figure 5.24: Effect of $\rho_v f_{vy}$ on beams with stirrups by ACI & CSA-s method

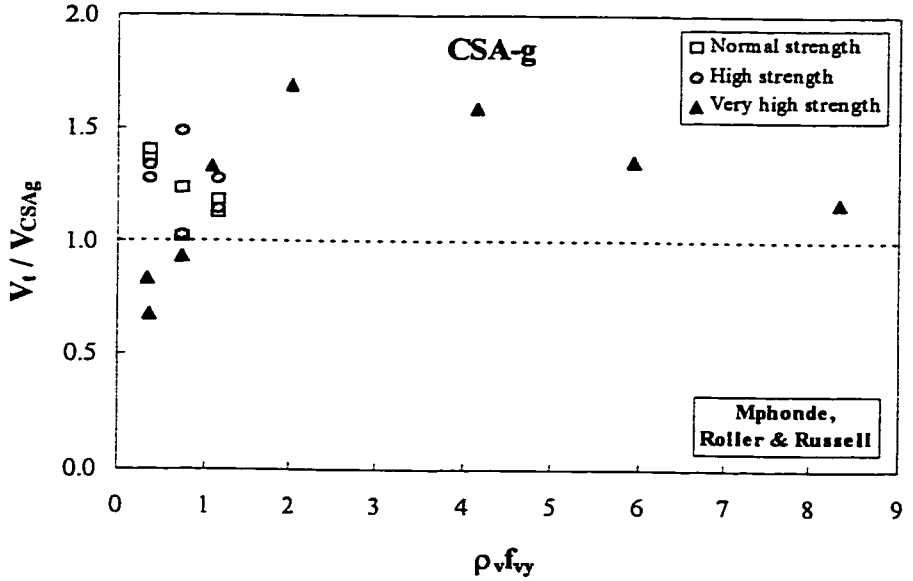

Figure 5.25: Effect of $\rho_v f_{vy}$ on beams with stirrups by CSA general method

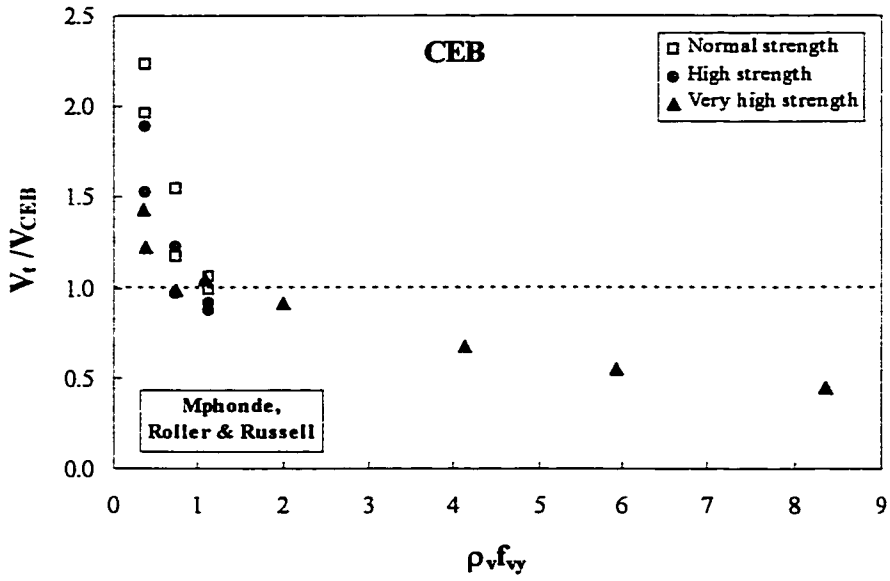

Figure 5.26: Effect of $\rho_v f_{vy}$ on beams with stirrups by CEB method

In Figure 5.24 and 5.25, the shear ratios show more variation with an increase of $\rho_v f_{vy}$ for very high strength concrete beams. These code provisions possibly over-account for the effect of increasing $\rho_v f_{vy}$. Also, in the minimum shear reinforcement range, the beams with f'_c of 125 MPa have lower shear ratios than the average value of the 144 test beams by up to 52% while a few of them have a shear ratio more than the average ratio. The requirement for minimum shear reinforcement, therefore, need to increase with increasing concrete strength for these codes. As noted in the last section, the shear ratios by the CEB code show a wide scatter.

It is clear that the shear-friction equation accounts for the effect of the amount of shear reinforcement more accurately than these recent code provisions.

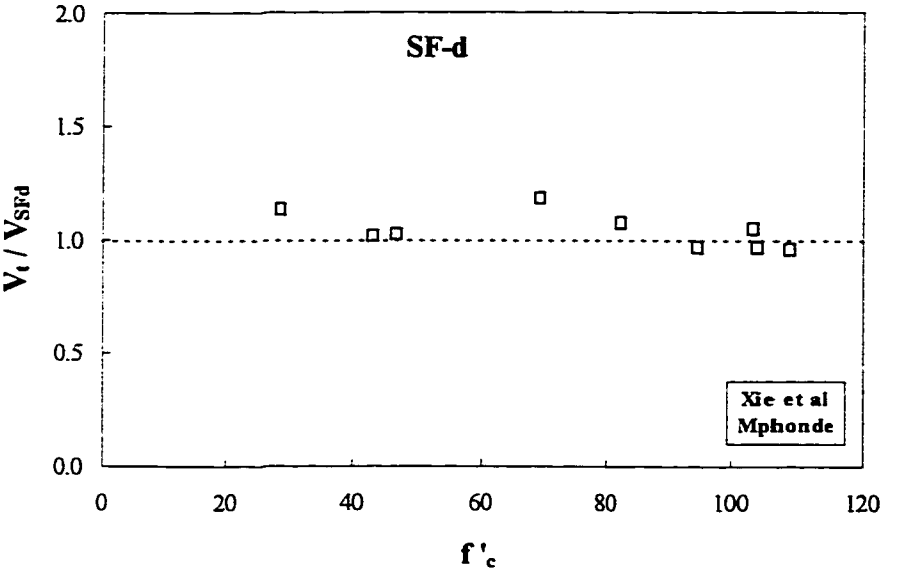

Figure 5.27: Effect of f'_c on beams with stirrups by SF design Eq.

5.3.5 Effect of Concrete Strength

The shear capacity of a member is contributed by both web reinforcement and concrete strength. The contribution of the concrete depends on three aspects: shear stress in the uncracked concrete, aggregate interlock along the diagonal crack and dowel action. The web reinforcement can improve the contribution of the dowel action because a stirrup can provide some support to a longitudinal bar that is being crossed by a flexure shear crack close to the stirrup. It also can limit the opening of diagonal cracks within the elastic range, thus enhancing and preserving shear transfer by aggregate interlock (Park and Paulay, 1975).

The shear strength will increase with an increase of concrete strength, nevertheless, some researchers found, by using ACI codes, that the shear ratio (V_t/V_{ACI}) of

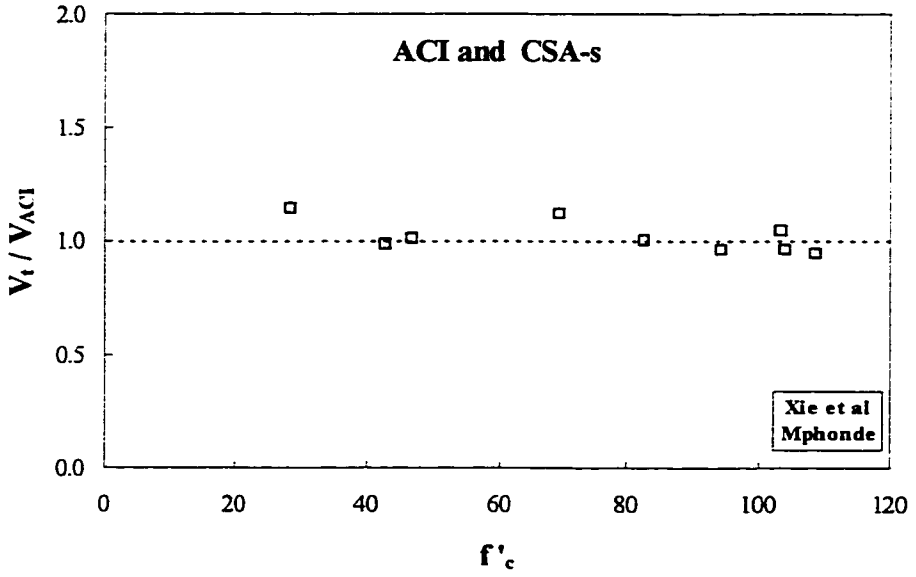

Figure 5.28: Effect of f'_c on beams with stirrups by ACI & CSA -s method

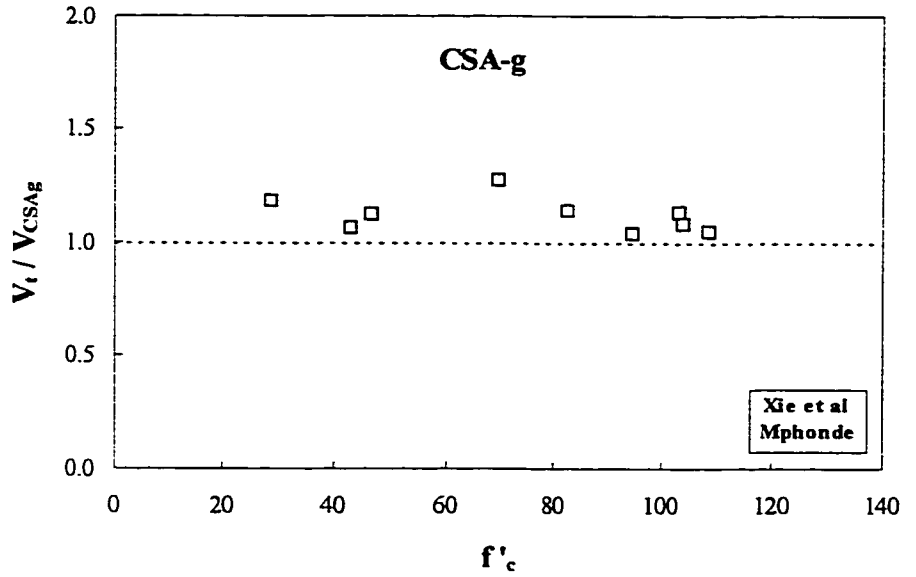

Figure 5.29: Effect of f'_c on beams with stirrups by CSA general method

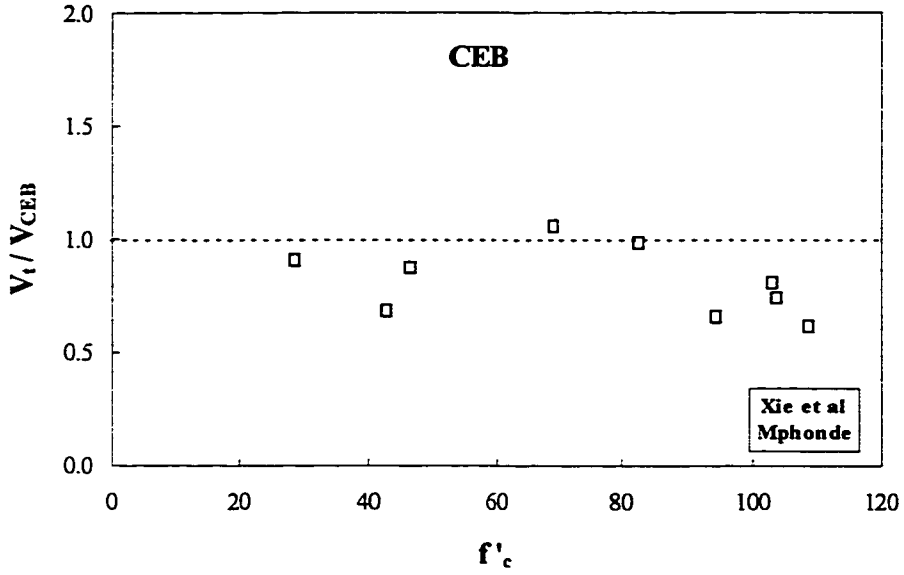

Figure 5.30: Effect of f'_c on beams with stirrups by CEB method

a beam with a low $\rho_v f_{vy}$ (i.e. minimum shear reinforcement) could decrease with an increase of concrete strength due to small increases in aggregate interlock (smoother surface). The shear ratio of a beam with a high $\rho_v f_{vy}$ could increase with an increase of concrete strength due to the greater contribution of web reinforcement.

It is difficult to find test series that have constant ρf_y and $\rho_v f_{vy}$, as well as a wide range of concrete strength. Two test series (Mphonde, 1990 and Xie et al,1994) were chosen. In order to have nearly constant $\rho_v f_{vy}$, only four beams with $\rho_v f_{vy}$ of 1.14 were selected from Mphonde's tests. The shear ratios from the all methods tend to decrease slightly with an increase in concrete strength (Figure 5.27-5.30). This may be due to the fact that the smoother failure surfaces for high-strength concrete beams have not been accounted for enough.

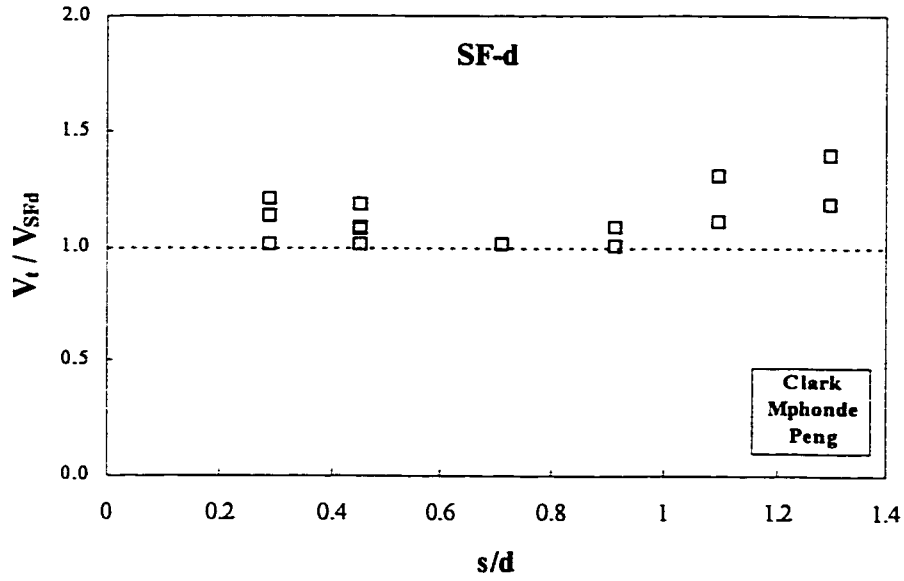

Figure 5.31: Effect of s/d on beams with stirrups by SF design Eq.

5.3.6 Effect of s/d ratio

It is difficult to find reinforced concrete beam tests in the literature with s/d ratios higher than 0.7. Traditionally, it has been thought that the s/d ratios needed to remain less than 0.7 (CSA) or 0.5 (ACI).

When s/d ratios are higher than 0.9, the shear ratios show an increase with increasing s/d ratios for all method (see Figure 5.31-5.34). Therefore, it is not necessary based on strength requirements, to have a maximum stirrup spacing limit for all procedures. Also based on observation of experiments mentioned in Chapter 4, shear cracks have not yet formed at the service load stage except for one beam (B-6). Of course, more experiments need to be performed with wide stirrup spacings.

When s/d ratios are less than 0.7, the shear ratios predicted by the code equations

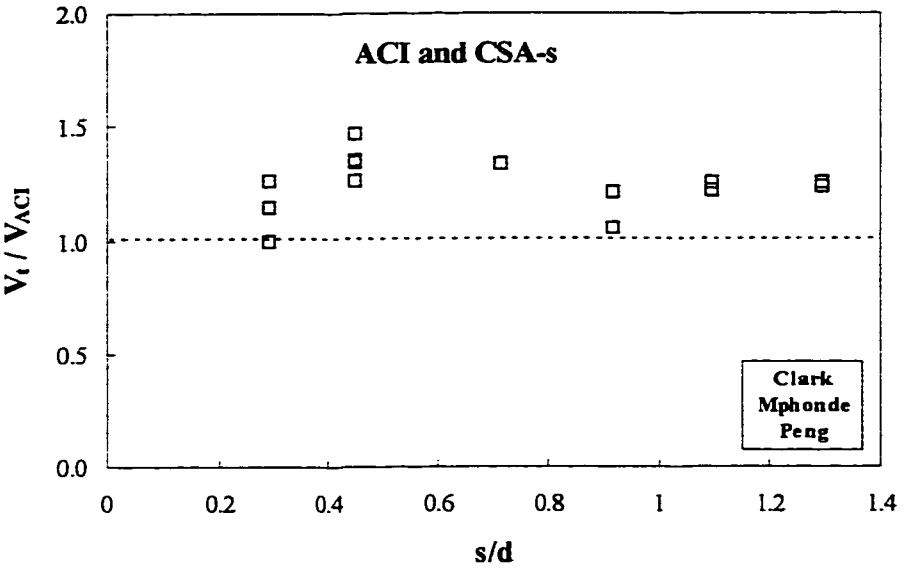

Figure 5.32: Effect of s/d on beams with stirrups using ACI & CSA-s method

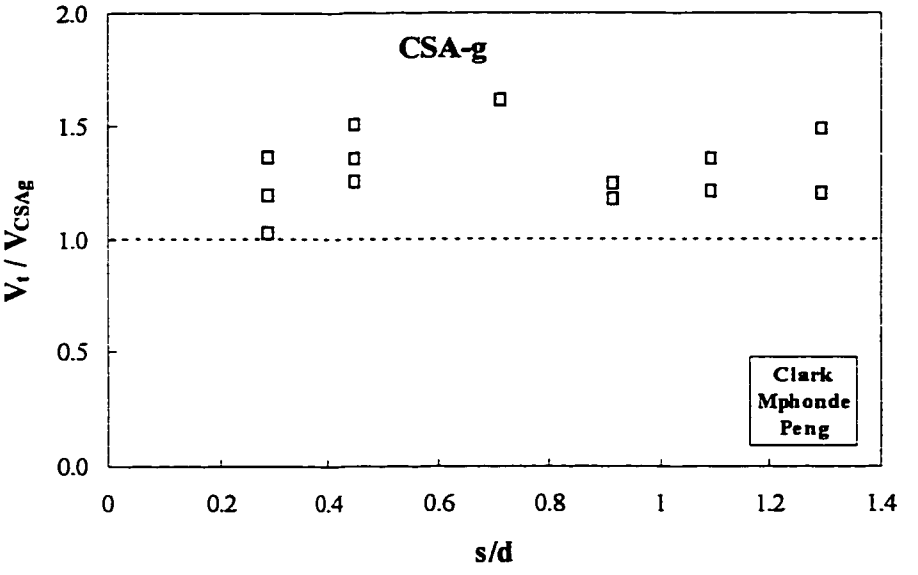

Figure 5.33: Effect of s/d on beams with stirrups by CSA general method

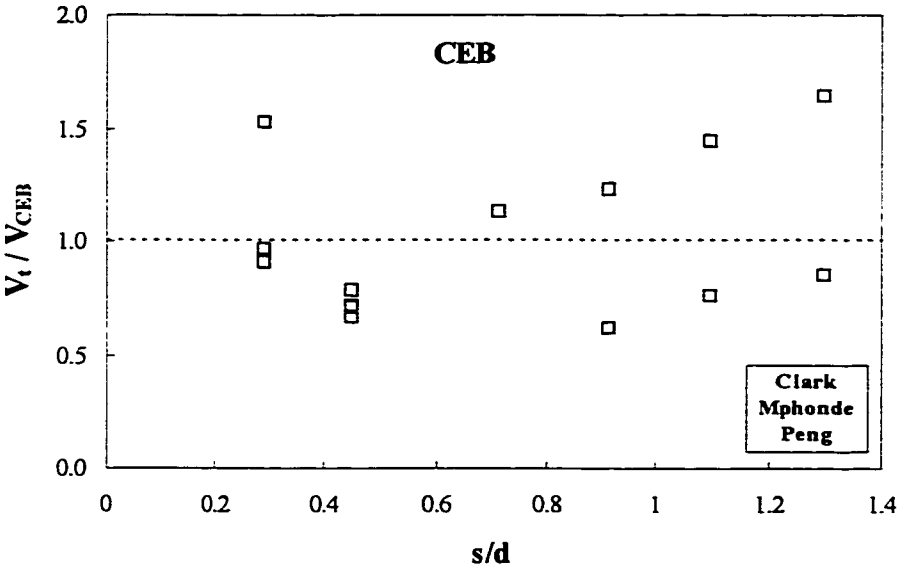

Figure 5.34: Effect of s/d on beams with stirrups by CEB method

show more scatter than by the shear-friction equation. This can be seen from Figures 5.18-5.21 (All beams have $s/d < 0.8$). One of the reasons probably is from the equations for calculating the contribution of shear reinforcement V_s.

$$V_s = A_v f_{vy} \frac{d}{s}$$
$$V_s = A_v f_{vy} \frac{d_v \cot\theta}{s}$$

If the critical shear crack starts between stirrups (see Figure 5.35a), the number of stirrups crossing the crack is equal to d/s or $d_v cot\theta/s$ (actually we should use d_s). If the critical shear crack starts beside a stirrup (see Figure 5.35b), the number of stirrups crossing the crack is equal to $(d/s - 1)$ or $(d_v cot\theta/s - 1)$. This situation happens more frequently than another one, because the shear capacity will have

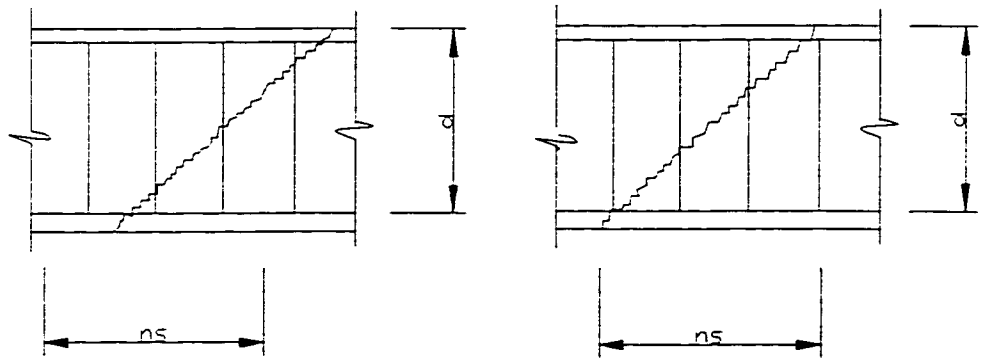

Figure 5.35: Number of stirrups crossing shear crack

a large increment immediately after intercepting a stirrup. Therefore, the code equation for V_s, sometimes overestimates the contribution of shear reinforcement.

5.3.7 Effect of Section Shape

Many researches have shown that a T-beam will provide a higher shear strength than a rectangular beam with the same depth and web width. Normally, the shear strength of the T-beam is conservatively calculated to be the same as a rectangular beam with the same depth and web width. Generally, this is too conservative (i.e. T-beams with a deep flange).

The section effect is derived here by using a statistical regression method applied to 38 T-beams (and a few I beams) based on the shear-friction equation.

The shear-friction equation

$$V_{sf} = k\sqrt{f'_c b_w h T_v \frac{d_s}{s}} - T_v \tag{3.13}$$

can be rewritten using A_c instead of $b_w h$ as:

$$A_c = \left(\frac{V_{sf} + \rho_v f_{vy}}{k}\right)^2 \frac{s}{f'_c \rho_v f_{vy} d_s} \tag{5.5}$$

in which A_c is the effective section which contributes to the shear strength of the beam. If b_f is assumed as a additional effective width on each side of the flange, seen in Figure 5.36, the above equation can be further rewritten as:

$$\cot\alpha = \frac{b_f}{h_f} = \left(\frac{V_{sf} + \rho_v f_{vy}}{k}\right)^2 \cdot \frac{s}{f'_c h_f^2 \rho_v f_{vy} d_s} - \frac{b_w h}{h_f^2} \tag{5.6}$$

Substituting the shear capacity measured from tests for V_{sf} in the above equation for 38 beams gives the average of $cot\alpha$ which correspond to about $\alpha = 40^0$. Thus A_c can be calculated as:

$$\begin{aligned} A_c &= b_w h + \cot 40^0 h_f^2 \\ &= b_w h + 1.2 h_f^2 \end{aligned} \tag{5.7}$$

Substituting this A_c for $b_w h$ in the design equation gives the shear capacity for T sections. Applying this A_c to these 38 test beams, the standard deviation for the shear ratios decreases from 0.202 to 0.169. If the A_c had not been applied in Figure 5.18, the coefficient of variation for shear ratios would increase to 0.179 from 0.164.

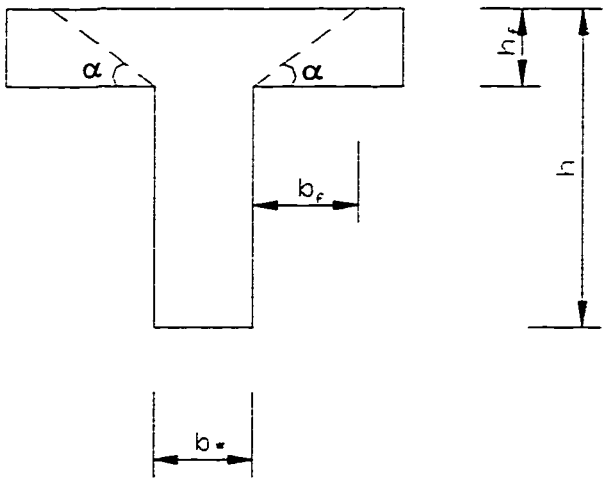

Figure 5.36: Effect of section

The equation (5.7) is only based on the test results of 38 beams. More test data are need to investigate the T-section effect.

5.3.8 Summary for Reinforced Concrete Beams with Stirrups

By comparing the coefficient of variation, it is clear that the shear-friction method provides a better prediction, for reinforced concrete beams with stirrups, than the CSA-A23.3-94, ACI 318M-95 and CEB-FIP MC90 code provisions.

The shear-friction equation accounts for the effect of the amount of shear reinforcement more accurately than the code equations.

It does not seem necessary to set a maximum stirrup spacing limit with the shear-friction method and the current code procedures.

The CSA-A23.3-94 and ACI 318M-95 code equations seem to overestimate the shear strength of reinforced concrete beams, with high and very high strength concrete, in low shear reinforcement ranges.

The CSA-A23.3-94 and ACI 318M-95 code equations might not properly account for the effect of the amount of shear reinforcement, especially for very high strength concrete beams.

Chapter 6

Conclusions and Recommendations

6.1 Conclusions

The following conclusions were made based on the results of the eight beams tested and a review of the results of 242 beams from the literature.

6.1.1 Equations developed

1. It is suitable to use the parabolic stress equation,

$$v = k\sqrt{\sigma f_c'} \tag{2.10}$$

to derive the shear strength of reinforced concrete beams due to the fact that for rectangular beams the normal stress on the inclined shear crack can not be more than $0.34f_c'$. The equation gives suitable results over this range of normal stress. This is confirmed by the test results of 249 beams from the literature.

2. For reinforced concrete beams without stirrups, the approximate equation

$$t \approx h\sqrt{\frac{a_{cle}}{h}}$$

can be used to determine the location of the critical inclined crack.

For reinforced concrete beams with stirrups, the approximate equation

$$t \approx h\left(\frac{a_{cle}}{h}\right)^{(0.5+\psi/0.3)} \tag{3.34}$$

can be used to determine the range where the critical shear crack can occur.

3. The effect of concrete strength is properly accounted for by equation.

$$k = 1.93 f_c'^{-0.39} \tag{3.37}$$

4. The parabolic crack failure model gives a better prediction than the straight crack failure model for beams with a curved failure plane.

5. The shear-friction design equations for reinforced concrete rectangular beams without shear reinforcement

$$V_{sf} = 0.25 k^2 f_c' b_w h \sqrt{\frac{h}{a_{cle}}} \tag{3.35}$$

and for reinforced concrete beams with shear reinforcement

$$V_{sf} = k\sqrt{f_c' b_w h A_v f_{vy} \frac{d_s}{s}} - A_v f_{vy} \tag{3.13}$$

are simple and, based on the analysis of 249 test beams from the literature, give better predictions than three current codes.

6.1.2 Reinforced Concrete Beams without Stirrups

1. The effect of concrete strength on shear capacity due to a reduction of aggregate interlock with an increase of concrete strength is properly accounted for in the shear-

friction equation by the modification to k.

Although the shear strength of beams increases with an increase in concrete strength, the shear ratio (measured/calculated) decreases with an increase in concrete strength when calculated using three codes (CSA, ACI and CEB), indicating that these code equations become less conservative with increased concrete strength. This seems to result from the smoother failure surfaces (low interlock of aggregate) produced by higher concrete strengths. This effect has not been considered in CSA and ACI code equations.

2. For short concrete beams ($a_{cle}/h < 2$) without stirrups, these code equation are so conservative that another method, the strut-and-tie model, should be used. The shear capacities predicted by the shear-friction equation are conservative but sufficiently close to the shear capacities measured from tests.

For more slender beams ($a_{cle}/h > 2$), the coefficient of variation of the shear ratio for 95 beams using the shear-friction equation (0.167) is lower than the ones using the code equations (0.174 to 0.230).

3. The shear strength is not sensitive to an increase of ρ. The shear-friction equation and ACI and CSA code equations predict the shear capacity of beams with the ratio of longitudinal reinforcement in the range of ρ = 1.8% to 6.4% slightly increasing with an increase of ρ. The CEB code equation slightly overcompensates the effect of high ρ.

6.1.3 Reinforced Concrete Beams with Stirrups

1. For short concrete beams ($a_{cle}/h < 2$) with stirrups, even though a large improvement occurs due to the contribution of shear reinforcement, there is a larger scatter

for the shear ratio predicted by the code equations than the scatter predicted by the shear-friction equation,

For the 144 beams with stirrups, the coefficient of variation for the shear ratio calculated using the shear-friction equation (0.164) is lower than the ones calculated using the code equations (0.248 to 0.391).

2. The shear-friction equation properly accounts for the effect of the amount of shear reinforcement, regardless of concrete strength. The code equations become unconservative with an increase of the web reinforcement index $\rho_v f_{vy}$, especially for high and very high strength concrete beams.

3. It does not seem necessary to set a maximum stirrup spacing limit for any shear design method based on the test results of the 8 beams.

4. It is conservative to use only the web area of T-beams or I-beams to calculate shear strength. The contribution of the flanges of T-beams could be accounted for by using A_c instead of $b_w h$ in equation (3.13).

$$A_c = b_w h + 1.2 h_f^2$$

From all the above conclusions, it is clear that the simple rational shear-friction method provides a better prediction for reinforced concrete beams, with or without shear reinforcement, than the CSA-A23.3-94, ACI 318-94 and CEB-FIP MC90 provisions.

6.2 Recommendations for Future Work

1. The load type on all beams analyzed in this thesis is symmetrical two or one point loading, so investigations need to be done for beams with uniform load.

2. The beam type of all beams analyzed in this thesis is a simply supported beam, so investigations need to be done for continuous beams.

Bibliography

[1] ACI 318-M95, 1995, *Building Code requirements for Reinforced Concrete, American Concrete Institute*, Detroit Michigan.

[2] Ahmad, S.H., A.R. Khaloo & A. Poveda, *Shear Capacity of reinforced High-Strength Concrete Beams*, ACI Journal, Proceedings V. 83, No. 2, March-April 1986, pp. 297-305.

[3] Anderson, N.S. & J.A. Ramirez, *Detailing of Stirrup Reinforcement*, ACI Structural Journal, V. 86, No. 5, Sept.-Oct. 1989, pp. 507-515.

[4] Bach, F., M.P. Nielsen & M.W. Braestrup, *Shear Tests on Reinforced Concrete T-beams Series V, U, X, B and S*, Structural Research Laboratory Report R120, Technical University of Denmark, 1980, 86 pp.

[5] Birkeland, H.W. 1976, Reader's Comments on, *Shear Transfer in Reinforced Concrete with Moment or Tension Across the Shear Plane*, By A.H. Mattock , L. Johal & H.C. Chow, PCI Journal May-June 1976, pp. 112-113.

[6] Birkeland, P.W. & H.W. Birkeland, 1966, *Connections in Precast Concrete Construction*, ACI Journal, Proceedings V. 63, No. 3,March 1966, pp. 345-367.

[7] Bresler, B. & A.C. Scordelis, *Shear Strength of Reinforced Concrete Beams*, ACI Journal, Proceedings V. 60, No. 1, Jan. 1963, pp.51-74.

[8] CEB-FIP Model Code, 1990, *Model code for Concrete Structure*, Secretariat Permanent, case Postale 88, CH-1015 Lausanne, Switzerland.

[9] Clark, A.P., *Diagonal Tension in Reinforced Concrete Beams*, ACI Journal, Proceedings V. 48, No. 10, October 1951, pp. 145-156.

[10] CSA Standard A23.3-94, 1994, *Design of Concrete Structures for Buildings*, Canadian Standards Association, Rexdale , Ontario.

[11] Debaiky, S.Y. & E.I. Elniema, *Behavior and Strength of Reinforced Concrete Haunched Beams in Shear*, ACI Journal, Proceedings V. 79, No. 3, May-June 1982, pp. 184-194.

[12] Elzanaty, A.H., A.H. Nilson & F.O. Slate, *Shear Capacity of Reinforced Concrete Beams Using High Strength Concrete*, ACI Journal, Proceedings V. 83, No. 2, March-April 1986, pp. 290-296.

[13] Haddadin, M.J., S.T. Hong & A. H. Mattock, *Stirrup Effectiveness in Reinforced Concrete Beams with Axial Force*, Proceedings, ASCE, V. 97, ST9, Sep. 1971, pp. 2277-2297.

[14] Hermansen, B.R. & J. Cowan, 1974, *Modified Shear-Friction Theory for Bracket Design*, ACI Journal, Proceedings V. 71, No. 2, Feb. 1974, pp. 55-60.

[15] Hofbeck, J.A., I.O. Ibrahim & A.H. Mattock, 1969, *Shear Transfer in Reinforced Concrete*, ACI Journal, Proceedings V. 66, No. 2, Feb. 1969, pp. 119-128.

[16] Hsiung, W. & G.C. Frantz, *Transverse Stirrup Spacing in R/C Beams, ASCE Journal of Structural Engineering*, ASCE, V. 111, No. 2, Feb. 1985, pp. 353-362.

[17] Johnson, M.K., J.A. Ramirez, *Minimum Shear Reinforcement in Beams with Higher Strength Concrete*, ACI Structural Journal, V. 86, No. 4 July-Aug. 1989,

pp. 376-382.

[18] Kani, W.M., M.W. Huggins & R.R. Wittkopp, *Kani on Shear in Reinforced Concrete*, Department of Civil Engineering University of Toronto, 1979, pp. 174, 176.

[19] Kriski, W., 1996, *Shear Strength of Reinforced Concrete Beams*, M.Sc. Thesis, Department of Civil Engineering University of Calgary, Calgary, Alberta.

[20] Leonhardt, F. & R. Walther, *Contributions to the Treatment of the problems of Shear in Reinforced Concrete Construction*, A translation of the articles that appeared in Beton- und Stahlbetonbau. Vol. 56, No. 12. 1961. Vol. 57, Nos. 2,3,6,7,and 8. 1962.

[21] Loov, R.E., 1998, *Review of A23.3-94 Simplified Method of Shear Design and Comparison with Results Using Shear Friction*, Can. J. Eng. 25: 437-450, pp. 437-449.

[22] Loov, R.E., 1997, *The Direct Computation of Stirrup Spacing Based on Shear-Friction*, Symposium on Advanced Design Concrete Structures, Chalmers, University of Technology, Goteborg, June 12-14.

[23] Loov, R.E., 1994, *Horizontal Shear Strength of Composite Concrete Beams with a Rough Interface*, PCI Journal Jan.-Feb. 1994, pp. 48-66.

[24] Loov, R.E., 1978, *Design of Precast Connections*, Paper presented at a seminar organized by Compa International Pte, Ltd., Sep. 25-27, 1978, Singapore 8 pages.

[25] Lyngberg, B.S., *Ultimate Shear Resistance of Partially Prestressed Reinforced Concrete I-beams*, ACI Journal, Proceedings V. 73, No. 5, April 1976, pp. 214-222.

[26] MacGregor, J.G., *Reinforced Concrete Mechanics & Design*, Prentice Hall, 1992, 1988.

[27] Mast, R.F., 1968, *Auxiliary Reinforcement in Concrete Connections*, ASCE Journal, June 1968,pp. 1485-1501.

[28] Mattock, A.H., 1988, Readers' Comments on *Influence of Concrete Strength and Load History on the Shear Friction Capacity of Concrete members*, by J. Walraven, J. Frenay & A. Pruijssers, PCI Journal, Jan.-Feb. 1988, pp. 165-166.

[29] Mattock, A.H., L. Johal & H.C. Chow, 1976, Author' Closure of *Shear Transfer in Reinforced Concrete with Moment or Tension Across the Shear Plane*, PCI Journal May-June 1976, pp. 113-114.

[30] Mattock, A.H., L. Johal & H.C. Chow, 1975, *Shear Transfer in Reinforced Concrete with Moment or Tension Across the Shear Plane*, PCI Journal July-Aug. 1975, pp. 76-93.

[31] Mattock, A.H., 1974, *Shear Transfer in Concrete Having Reinforcement at an Angle to the Shear Plane*, in ACI Special Publication SP-42: Shear in Reinforced Concrete, Vol 1, American Concrete Institute, Detroit, pp. 17-42.

[32] Mattock, A.H., N.M. Hawkin, 1972, *Shear Transfer in Reinforced Concrete - Recent Research*, PCI Journal March-April 1972, pp. 55-75.

[33] Mau, S.T. & T.C. Hsu, 1988, Reader Comments on *Influences Concrete Strength and Load History on the Shear Friction Capacity of Concrete Members* by J. Walraven, J. Frenay & A. Pruijssers, PCI Journal, Jan.-Feb. 1988, pp. 166-168.

[34] Morsch, E, *Der Eisinbeton Seine Theorie und Anwendung*, Wittwer, Stuttgart, 1908.

[35] Mphonde, A.G. & G.C. Frantz, *Shear Tests of High- and Low-Strength Concrete Beams Without Stirrups*, ACI Journal, Proceedings V. 81, No. 4, July-August,1984, pp. 350-357.

[36] Mphonde, A.G., *Use of Stirrup Effectiveness in Shear Design of Concrete Beams*, ACI Structrual Journal, V. 86, No. 5, Sep.-Oct. 1989, pp. 541-545.

[37] Moody, K.G., I.M. Viest, R.C. Elstner & E. Hognestad, *Shear Strength of Reinforced Concrete Beams Part 1 - Tests of Simple Beams*, ACI Journal, Proceedings V. 51, No. 12, Dec. 1954, pp. 317-332.

[38] Olesen, S.E., M.A. Sozen & C.P. Siess, *Investigation of Prestressd Reinforced Concrete for Highway Bridges - part IV: Strength in Shear of beams with Web Reinforcement*, Structural Research Series No. 295, University of Illinois, August 1965.

[39] Park, R. & T. Paulay, *Reinforced Concrete Structures*, John Wiley & Sons, 1975.

[40] Raths, C.H. 1977, Reader Comments on *Design Proposals for Reinforced Concrete Corbels* by A.H. Mattock, PCI Journal March-April 1977, pp. 93-98.

[41] Rodriguez, J.J., A.C. Bianchini, I.M. Viest & C.E. Kesler, *Shear Strength of Two-span Continuous Reinforced Concrete Beams*, ACI Journal, Proceedings V. 56, No. 4, April 1959, pp. 1089-1130.

[42] Roller, J.J. and H.G. Russell, *Shear Strength of High-Strength Concrete Beams with Web Reinforcement*, ACI Structural Journal, V. 87, No. 2, March-April 1990, pp. 191-198.

[43] Shaikh, A.F., 1978, *Proposed Revisions to Shear-Friction Provisions*, PCI Journal March-April 1978, pp. 12-21.

[44] Sorensen, H.C., *Shear Tests on 12 Reinforced Concrete T-beams*, Translation - Structural Research Laboratory Report R60, Technical University of Denmark. 1974, 51 pp.

[45] Taylor, R., *Some Shear Tests on Reinforced Concrete T-beams with stirrups,* Magazine of Concrete Research, V. 18, No. 57, Dec. 1966, pp. 221-230.

[46] Tsoukantas, S.G. & T.P. Tassios, 1989, *Shear Resistance of Connections Between Reinforced Concrete Linear Precast Elements*, ACI structural Journal, May-June, 1989, pp. 242-249.

[47] Van Den Berg, F.J., *Shear Strength of Reinforced Concrete Beams without Web Reinforcement Part 2 - Factors Affecting Load at diagonal Cracking*, ACI Journal, Proceedings V. 59, No. 11, Nov. 1962, pp.1587-1599.

[48] Walraven, J, J. Frenay & A. Pruijssers, 1987, *Influence of Concrete Strength and Load History on the Shear Friction Capacity of Concrete Members*, PCI

Journal, Jan.-Feb. 1987, pp. 66-84.

[49] Yoon, Y.S., W.D. Cook & D. Mitchell, *Minimum Shear Reinforcement in Normal, Medium, and High-Strength Concrete Beams*, ACI Structural Journal, V. 93, No. 5, Sep.-Oct. 1996, pp. 576-584.

[50] Xie, Y., S.H. Ahmad, T. Yu, S. Hion & W. Chung, *Shear Ductility of Reinforced Concrete Beams of Normal and High-Strength Concrete*, ACI Structural Journal, V. 91, No. 2, March-April 1994, pp. 140-149.

[51] Zhang, J.P., 1997, *Diagonal Cracking and Shear Strength of Reinforced Concrete Beams*, Magazine of Concrete Research March 1997, pp. 55-65.

Apendix A

Review Values of b Table 11-1 of CSA (by Loov)

$$\beta_{40_{k,j}} = \frac{\alpha 1 \alpha 2 \cdot 0.33 \cdot \cot(\theta a_{k,j})}{1 + \sqrt{500 \cdot \varepsilon 1 a_{k,j}}}$$

$$\beta = \begin{bmatrix} 0.405 & 0.290 & 0.208 & 0.197 & 0.185 & 0.162 & 0.143 \\ 0.405 & 0.250 & 0.205 & 0.194 & 0.179 & 0.158 & 0.137 \\ 0.271 & 0.211 & 0.200 & 0.189 & 0.174 & 0.143 & 0.120 \\ 0.216 & 0.208 & 0.197 & 0.181 & 0.167 & 0.133 & 0.112 \\ 0.212 & 0.203 & 0.189 & 0.171 & 0.160 & 0.125 & 0.103 \\ 0.203 & 0.194 & 0.174 & 0.151 & 0.131 & 0.100 & 0.083 \\ 0.191 & 0.167 & 0.136 & 0.126 & 0.116 & 0.108 & 0.104 \end{bmatrix}$$

$$\beta_{41_{k,j}} = \frac{0.18}{0.3 + \frac{24 \cdot \varepsilon 1 a_{k,j} \cdot s}{a + 16} m\theta}$$

$$\beta_{40} = \begin{bmatrix} 0.443 & 0.324 & 0.277 & 0.231 & 0.201 & 0.161 & 0.142 \\ 0.409 & 0.318 & 0.265 & 0.225 & 0.198 & 0.163 & 0.144 \\ 0.394 & 0.308 & 0.255 & 0.218 & 0.196 & 0.169 & 0.152 \\ 0.357 & 0.289 & 0.244 & 0.214 & 0.193 & 0.170 & 0.153 \\ 0.330 & 0.274 & 0.236 & 0.210 & 0.189 & 0.169 & 0.154 \\ 0.288 & 0.249 & 0.220 & 0.200 & 0.185 & 0.164 & 0.146 \\ 0.255 & 0.224 & 0.199 & 0.180 & 0.168 & 0.148 & 0.132 \end{bmatrix}$$

$$\beta_{41} = \begin{bmatrix} 0.463 & 0.289 & 0.212 & 0.200 & 0.187 & 0.168 & 0.146 \\ 0.406 & 0.252 & 0.209 & 0.195 & 0.181 & 0.160 & 0.139 \\ 0.273 & 0.212 & 0.201 & 0.191 & 0.175 & 0.144 & 0.122 \\ 0.218 & 0.213 & 0.199 & 0.182 & 0.168 & 0.134 & 0.114 \\ 0.213 & 0.207 & 0.191 & 0.173 & 0.161 & 0.126 & 0.104 \\ 0.199 & 0.198 & 0.176 & 0.153 & 0.132 & 0.101 & 0.085 \\ 0.190 & 0.168 & 0.137 & 0.121 & 0.117 & 0.111 & 0.106 \end{bmatrix}$$

Compare Tabulated Values with above limits

$$r_{\beta_{k,j}} = \frac{\beta_{k,j}}{\beta_{40_{k,j}}}$$

$$r_{\beta} = \begin{bmatrix} 0.914 & 0.896 & 0.750 & 0.853 & 0.920 & 1.006 & 1.008 \\ 0.991 & 0.787 & 0.775 & 0.864 & 0.902 & 0.968 & 0.951 \\ 0.688 & 0.684 & 0.784 & 0.866 & 0.890 & 0.849 & 0.789 \\ 0.604 & 0.719 & 0.807 & 0.845 & 0.867 & 0.784 & 0.730 \\ 0.642 & 0.740 & 0.802 & 0.815 & 0.844 & 0.741 & 0.670 \\ 0.706 & 0.780 & 0.793 & 0.756 & 0.708 & 0.611 & 0.567 \\ 0.750 & 0.745 & 0.684 & 0.700 & 0.690 & 0.730 & 0.789 \end{bmatrix}$$

Values at 1,6 and 1,7 exceed the limit for β_{40}

$$r_{\beta_{k,j}} = \frac{\beta_{k,j}}{\beta_{41_{k,j}}}$$

$$r_{\beta} = \begin{bmatrix} 0.876 & 1.002 & 0.980 & 0.985 & 0.989 & 0.962 & 0.979 \\ 0.997 & 0.992 & 0.982 & 0.993 & 0.989 & 0.991 & 0.985 \\ 0.992 & 0.995 & 0.997 & 0.990 & 0.996 & 0.991 & 0.984 \\ 0.992 & 0.978 & 0.992 & 0.993 & 0.992 & 0.993 & 0.986 \\ 0.995 & 0.982 & 0.989 & 0.988 & 0.991 & 0.993 & 0.986 \\ 1.021 & 0.981 & 0.988 & 0.988 & 0.990 & 0.986 & 0.981 \\ 1.004 & 0.992 & 0.991 & 1.041 & 0.992 & 0.977 & 0.980 \end{bmatrix}$$

The values at 1,2 6,1 7,1 and 7,4 exceed the limit for β_{41}

Conclusion: Values of β which exceed the smaller of β_{40} or β_{41} should be reduced

Reduce β for 1,2 1,6 1,7 6,1 7,1 7,4 and 7,5

$$\beta_{ra} = \begin{bmatrix} 0.405 & 0.288 & 0.208 & 0.197 & 0.185 & 0.161 & 0.141 \\ 0.405 & 0.250 & 0.205 & 0.194 & 0.179 & 0.158 & 0.137 \\ 0.271 & 0.211 & 0.200 & 0.189 & 0.174 & 0.143 & 0.120 \\ 0.216 & 0.208 & 0.197 & 0.181 & 0.167 & 0.133 & 0.112 \\ 0.212 & 0.203 & 0.189 & 0.171 & 0.160 & 0.125 & 0.103 \\ 0.198 & 0.194 & 0.174 & 0.151 & 0.131 & 0.100 & 0.083 \\ 0.190 & 0.167 & 0.136 & 0.121 & 0.115 & 0.108 & 0.104 \end{bmatrix}$$

Recheck revised values of β

Recheck β with respect to β_{40}

$$r_{\beta_{k,j}} = \frac{\beta_{ra_{k,j}}}{\beta_{40_{k,j}}}$$

$$r_{\beta} = \begin{bmatrix} 0.914 & 0.890 & 0.750 & 0.853 & 0.920 & 1.000 & 0.994 \\ 0.991 & 0.787 & 0.775 & 0.864 & 0.902 & 0.968 & 0.951 \\ 0.688 & 0.684 & 0.784 & 0.866 & 0.890 & 0.849 & 0.789 \\ 0.604 & 0.719 & 0.807 & 0.845 & 0.867 & 0.784 & 0.730 \\ 0.642 & 0.740 & 0.802 & 0.815 & 0.844 & 0.741 & 0.670 \\ 0.688 & 0.780 & 0.793 & 0.756 & 0.708 & 0.611 & 0.567 \\ 0.746 & 0.745 & 0.684 & 0.672 & 0.684 & 0.730 & 0.789 \end{bmatrix}$$

Recheck β with respect to β_{45}

$$r_{\beta_{k,j}} = \frac{\beta_{ra_{k,j}}}{\beta_{41_{k,j}}}$$

$$r_{\beta} = \begin{bmatrix} 0.876 & 0.995 & 0.980 & 0.985 & 0.989 & 0.956 & 0.965 \\ 0.997 & 0.992 & 0.982 & 0.993 & 0.989 & 0.991 & 0.985 \\ 0.992 & 0.995 & 0.997 & 0.990 & 0.996 & 0.991 & 0.984 \\ 0.992 & 0.978 & 0.992 & 0.993 & 0.992 & 0.993 & 0.986 \\ 0.995 & 0.982 & 0.989 & 0.988 & 0.991 & 0.993 & 0.986 \\ 0.996 & 0.981 & 0.988 & 0.988 & 0.990 & 0.986 & 0.981 \\ 0.999 & 0.992 & 0.991 & 1.000 & 0.984 & 0.977 & 0.980 \end{bmatrix}$$

The revised values of β are now within specified limits

$$\Delta\theta_{k,j} = \theta da_{k,j} - \theta d_{k,j}$$

$$\Delta\theta = \begin{bmatrix} 0 & 0 & 0 & 0 & 0 & 0 & 0 \\ 0 & 0 & 0 & 0 & 0 & 0 & 0 \\ 0 & 0 & 0 & 0 & 0 & 0 & 0 \\ 0 & 0 & 0 & 0 & 0 & 0 & 0 \\ 0 & 0 & 0 & 0 & 0 & 0 & 0 \\ 0 & 0 & 0 & 0 & 0 & 0 & 0.1 \\ 0 & 0 & 0 & 0.3 & 0.3 & 0.2 & 0 \end{bmatrix}$$

$$\Delta\beta_{k,j} = \beta ra_{k,j} - \beta_{k,j}$$

$$\Delta\beta = \begin{bmatrix} 0 & -2\cdot10^{-3} & 0 & 0 & 0 & -1\cdot10^{-3} & -2\cdot10^{-3} \\ 0 & 0 & 0 & 0 & 0 & 0 & 0 \\ 0 & 0 & 0 & 0 & 0 & 0 & 0 \\ 0 & 0 & 0 & 0 & 0 & 0 & 0 \\ 0 & 0 & 0 & 0 & 0 & 0 & 0 \\ -5\cdot10^{-3} & 0 & 0 & 0 & 0 & 0 & 0 \\ -1\cdot10^{-3} & 0 & 0 & -5\cdot10^{-3} & -1\cdot10^{-3} & 0 & 0 \end{bmatrix}$$

Compare β_{40} with β_{41} using the adjusted values for θ

$$r\beta_{k,j} = \frac{\beta 41_{k,j}}{\beta 40_{k,j}}$$

$$r\beta = \begin{bmatrix} 1.044 & 0.894 & 0.765 & 0.865 & 0.931 & 1.046 & 1.030 \\ 0.995 & 0.793 & 0.789 & 0.870 & 0.913 & 0.977 & 0.965 \\ 0.694 & 0.688 & 0.786 & 0.875 & 0.894 & 0.856 & 0.802 \\ 0.609 & 0.735 & 0.813 & 0.850 & 0.874 & 0.789 & 0.741 \\ 0.645 & 0.753 & 0.811 & 0.825 & 0.852 & 0.747 & 0.679 \\ 0.691 & 0.795 & 0.803 & 0.765 & 0.715 & 0.620 & 0.578 \\ 0.747 & 0.752 & 0.691 & 0.672 & 0.696 & 0.747 & 0.805 \end{bmatrix}$$

Conclusion: All values of β with the exception of 1,1 1,6 and 1,7 are based on β_{41}

Appendix B

Example of Calculation Using Shear-Friction

General Procedure for shear friction analysis (B-7)

$b_w = 0.28$ $\quad h = 0.32$ $\quad w_t = 0.1$ $\quad c_t = 0.02$

$d_b = 0.0299$ $\quad d_{bv} = 0.0113$ $\quad w_b = 0.1$ $\quad c_b = 0.02$

$d = h - c_b - 0.5 \cdot d_b - d_{bv}$ $\quad d = 0.274$ $\quad a = 0.95$ $\quad \frac{a}{d} = 3.47$

$d_s = h - c_t - c_b - d_{bv}$ $\quad d_s = 0.269$ $\quad L = 2 \cdot a + 0.5$

$a_{cle} = a - 0.5 \cdot (w_b + w_t)$ $\quad a_{cle} = 0.85$ $\quad L = 2.4$ $\quad \frac{a_{cle}}{d} = 3.105$

$f_y = 477.7$ $\quad f_{vy} = 456.4$ $\quad f_c = 32.15$ $\quad s = 0.25$

$A_s = \left(\frac{\pi}{4} \cdot d_b^2\right) \cdot 3$ $\quad A_v = 2 \cdot \left(\frac{\pi}{4} \cdot d_{bv}^2\right)$ $\quad C = f_c \cdot b_w \cdot h$ $\quad \frac{s}{d} = 0.913$

$A_s = 2.106 \cdot 10^{-3}$ $\quad A_v = 2.006 \cdot 10^{-4}$ $\quad C_d = f_c \cdot b_w \cdot d$ $\quad \rho_v = \frac{A_v}{b_w \cdot s}$

$\rho = \frac{A_s}{b_w \cdot d}$ $\quad T_{vy} = A_v \cdot f_{vy}$ $\quad T_y = A_s \cdot f_y$ $\quad \rho_v \cdot f_{vy} = 1.308$

$\rho = 0.027$ $\quad T_{vy} = 0.092$ $\quad T_y = 1.006$

Other Calculations

$\frac{T_{vy}}{C} = 0.032$ $\quad \frac{T_{vy}}{C_d} = 0.037$ $\quad N = 40$

$x = 0.11$

$L_{overhange} = 0.42$

Indices

$j = 0 .. N$

$i = 0 .. N$

$q = 0 .. 1$

Calculte Self-weight

$w = 0.024 \cdot b_w \cdot h \cdot 0$

Number and Location of Stirrups

$ns = 4$ $\quad st = 1 .. ns$

$xs_{st} =$

0.11
0.36
0.61
0.86

Limiting Angles of Shear Plane

$\Delta x = \frac{a_{cle}}{N}$

$t_{i,j} = \Delta x \cdot (N - (i + j)) \cdot (N > (i + j))$

$\theta_{i,j} = \text{angle}\left(t_{i,j}, h\right)$

Development and Force in Stirrups

ys = available development length

T_v = force in stirrup

T_{vt} = total stirrup force

$$L_{dv1} = \left(\frac{0.019\cdot 10^6 \cdot A_v \cdot f_{vy}}{\sqrt{f_c}}\right)\cdot 0.001$$

$$L_{dv2} = d_{bv}\cdot 0.058\cdot f_{vy}$$

$$L_{dv} = \text{if}(L_{dv1} < L_{dv2}, L_{dv2}, L_{dv1})$$

$$B = \frac{T_{vy}}{L_{dv}} \qquad H = \frac{2}{3}\cdot T_{vy}$$

$$y(\theta, xs, j) = \tan(\theta)\cdot\left[0.5\cdot w_b + \Delta x\cdot(N - j) - xs\right] - \left(c_t + 0.5\cdot d_{bv}\right)$$

$$ys(\theta, xs, j) = \text{if}\left(d_s - y(\theta, xs, j) < y(\theta, xs, j), d_s - y(\theta, xs, j), y(\theta, xs, j)\right)$$

$$Tv(\theta, xs, j) = \text{if}\left[ys(\theta, xs, j) < 0, 0, \text{if}\left[ys(\theta, xs, j) < 2.5\cdot d_{bv}, \frac{ys(\theta, xs, j)\cdot H}{2.5\cdot d_{bv}}, H + \left(ys(\theta, xs, j) - 2.5\cdot d_{bv}\right)\cdot B\right]\right]$$

$$Tva(\theta, xs, j) = \text{if}\left(Tv(\theta, xs, j) > T_{vy}, T_{vy}, Tv(\theta, xs, j)\right)$$

$$x_{vo_j} = 0.5\cdot w_b + \Delta x\cdot(N - j)$$

$$Tvt_{i,j} = \sum_{st}(N > i + j)\cdot\left(xs_{st} > \Delta x\cdot i + 0.5\cdot w_b\right)\cdot\left(xs_{st} < x_{vo_j}\right)\cdot Tva\left(\theta_{i,j}, xs_{st}, j\right) \qquad f_r = 4.41$$

$$V_t = 0.187 \qquad x_t = 0.1$$

$$xx_{test} = \text{root}\left[\frac{b_w\cdot f_r\cdot\left[\left(a_{cle} - x_t\right)^2 + h^2\right]}{6\cdot\left(x_t + 0.5\cdot w_b\right) + 4\cdot\left(a_{cle} - x_t\right)} - V_t, x_t\right]$$

$$ff_r = 1.4\cdot\left(\frac{f_c}{10}\right)^{\frac{2}{3}}\cdot\frac{1 + 1.5\cdot\left(\frac{h}{0.1}\right)^{0.7}}{1.5\cdot\left(\frac{h}{0.1}\right)^{0.7}}$$

$$x_{test} = \text{if}\left(a_{cle} \le 2\cdot d, 0, xx_{test}\right) \qquad x_{test} = 0.14$$

$$f_c = 32.15$$

$$ff_r = 3.95$$

$$k_{opt_{i,j}} = \sqrt{\frac{V_t - Tvt_{i,j}}{0.25\cdot f_c\cdot b_w\cdot h}}\cdot\cot\left(\theta_{i,j}\right)$$

$$kk = 0.1$$

$$k_{yy_{i,j}} = \text{if}\left[i + j \ge N, 0, \text{root}\left[\left[0.5\cdot kk^2\cdot f_c\cdot b_w\cdot h\cdot\left[\sqrt{\frac{2\cdot T_y}{0.5\cdot kk^2\cdot f_c\cdot b_w\cdot h} + \left(\cot\left(\theta_{i,j}\right)\right)^2} - \left(\cot\left(\theta_{i,j}\right)\right)\right]\right]\cdot\left[1 + \left(\cot\left(\theta_{i,j}\right)\right)^2\right] - T_y\cdot\left(\cot\left(\theta_{i,j}\right)\right)\right.\right.$$

$$k_{o_i} = \max\left[\left(k_{opt}^{T}\right)^{<i>}\right] \qquad k_{y_i} = \max\left[\left(k_{yy}^{T}\right)^{<i>}\right]$$

$$T_{oopt_{i,j}} = \left[0.25\cdot\left(k_{opt_{i,j}}\right)^2\cdot f_c\cdot b_w\cdot h\right]\cdot\left[1 + \left(\sec\left(\theta_{i,j}\right)\right)^2\right] \qquad T_{oo_i} = \min\left[\left(T_{oopt}^{T}\right)^{<i>}\right]$$

$$k_i = \text{if}\left[\left(T_{oo_i}\right) > T_y, k_{y_i}, k_{o_i}\right]\cdot\left(\Delta x\cdot i \ge x_{test} - 0.5\cdot\Delta x\right)$$

$$k_{test} = \max(k) \qquad k_{test} = 0.488 \qquad t_d = 0.665$$

$X_t = 0.1$

$$XX_{cal} = root\left[\frac{b_w \cdot f_r \cdot \left[(a_{cle} - X_t)^2 + h^2\right]}{6 \cdot (X_t + 0.5 \cdot w_b) + 4 \cdot (a_{cle} - X_t)} - 0.25 \cdot k_{test}^2 \cdot f_c \cdot b_w \cdot \frac{h^2}{(a_{cle} - X_t)} - \rho_v \cdot f_y \cdot b_w \cdot (a_{cle} - X_t), X_t\right]$$

$X_{cal} = if(XX_{cal} < 0.0, XX_{cal})$ $\quad X_{cal} = 0$

$$kd = if\left(s = 0., \frac{V_t - T_{vy}}{\sqrt{f_c \cdot b_w \cdot h \cdot T_{vy} \cdot \frac{d_s}{s}}}, .0\right)$$

$k_{ssf_i} = if\left[(T_{oo_i}) > T_y, k_{y_i}, k_{o_i}\right] \cdot (\Delta x \cdot i \geq X_{cal} - 0.5 \cdot \Delta x)$

$kk_{sf} = \max(k)$ $\quad kk_{sf} = 0.488$ $\quad k_{sf} = 2.16 \cdot f_c^{-0.42}$ $\quad kd = 0.523$

$T_c = 0$ $\quad \lambda = 1$ $\quad \phi_c = 1$ $\quad BB = 0.5$

$K = 0.5 \cdot k_{sf}^2 \cdot \lambda \cdot \phi_c \cdot f_c \cdot b_w \cdot h$

$T_{opt_{i,j}} = if\left[i + j \geq N, T_y, BB \cdot K \cdot \left(1 + \sec(\theta_{i,j})^2\right)\right]$ $\quad T_{o_i} = \min\left[\left(T_{opt}^T\right)^{<i>}\right]$

$T_{i,j} = if\left[(T_{opt_{i,j}}) > T_y, T_y, T_{opt_{i,j}}\right]$

Shear Equation

$V_v = \sqrt{2 \cdot K \cdot T_y}$

$$V_{i,j} = if\left[(N > i + j), K \cdot \left[\sqrt{\frac{2 \cdot (T_{i,j} + T_c)}{K}} + \cot(\theta_{i,j})^2 - \cot(\theta_{i,j})\right] \cdot \left(1 + \cot(\theta_{i,j})^2\right) - T_{i,j} \cdot \cot(\theta_{i,j}) + Tvt_{i,j}, V_v\right]$$

$VV_{i,j} = if\left[(\Delta x \cdot i \geq X_{cal} - 0.5 \cdot \Delta x), V_{i,j}, 10000\right]$ $\quad V_{SF_i} = \min\left[\left(V^T\right)^{<i>}\right]$

$V_{sf} = \min(VV)$

$$V_{cr_i} = \frac{b_w \cdot f_r \cdot \left[(a_{cle} - \Delta x \cdot i)^2 + h^2\right]}{6 \cdot (\Delta x \cdot i - 0.5 \cdot w_b) + 4 \cdot (a_{cle} - \Delta x \cdot i)}$$ $\quad V_{C_i} = \min\left[\left(V_{cr}^T\right)^{<i>}\right]$

Moment Calculations

$\alpha_1 = (0.85 - 0.0015 \cdot f_c) \cdot \frac{1}{0.9}$ $\quad \alpha_1 = 0.891$

$VV = 0.2$

$$V_m = \frac{T_y}{a} \cdot \left(d - \frac{T_y}{2 \cdot \alpha_1 \cdot f_c \cdot b_w}\right)$$

Tv = Force in stirrup
T_{ij} = Longitudinal force
V_{Mj} = Shear force governed by moment

Shear is also limited by flexure on vertical sections between loads

$iv_{i,j} := if(V_{sf} = V_{i,j}, i, 100)$

$jv_{i,j} := if(V_{sf} = V_{i,j}, j, 100)$

$V_{min} := if(V_{sf} < V_m, V_{sf}, V_m)$

$k_d := 1.93 \cdot f_c^{-0.39}$

$V_{sfd} := k_d \cdot \sqrt{f_c \cdot b_w \cdot h \cdot T_{vy} \cdot \frac{d_s}{s}} - T_{vy}$

$V_{sfd} = 0.174$

$q := 0..1$

GRAPH OF V_{sf} vs LENGTH TO THE INTERCEPT WITH TOP OF BEAM

$V_{min} := floor(V_{min} \cdot 10000 + 0.5) \cdot 0.0001$

$y_q =$ $ys_q =$

0	$c_b + 0.5 \cdot d_{bv}$
h	$h - (c_t + 0.5 \cdot d_{bv})$

$T_y = 1.006$

$V_m = 0.2235$

$V_t = 0.1870$

$V_{sf} = 0.1931$

$T_{vy} = 0.092$

$\frac{V_t}{V_{sf}} = 0.968$

$V_{min} = 0.1931$

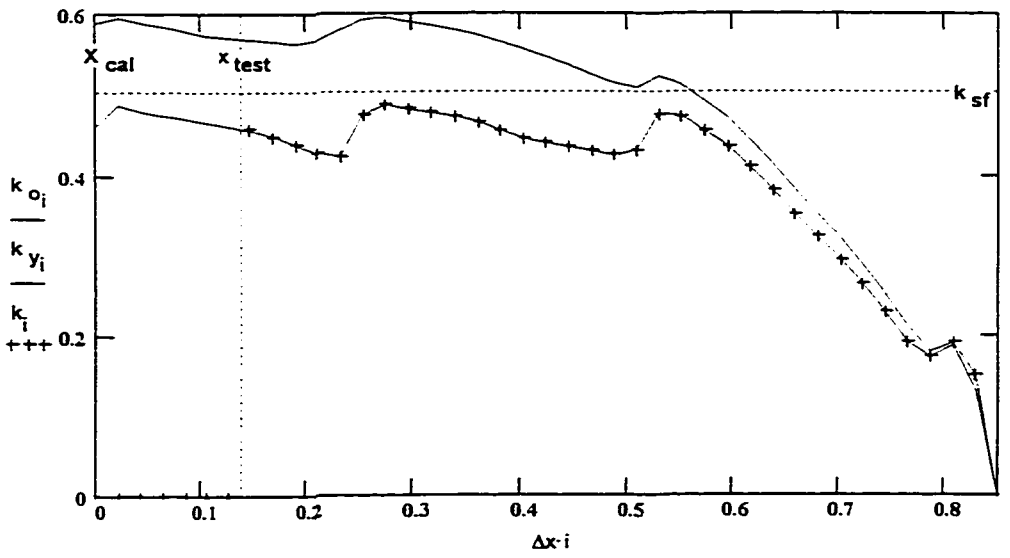

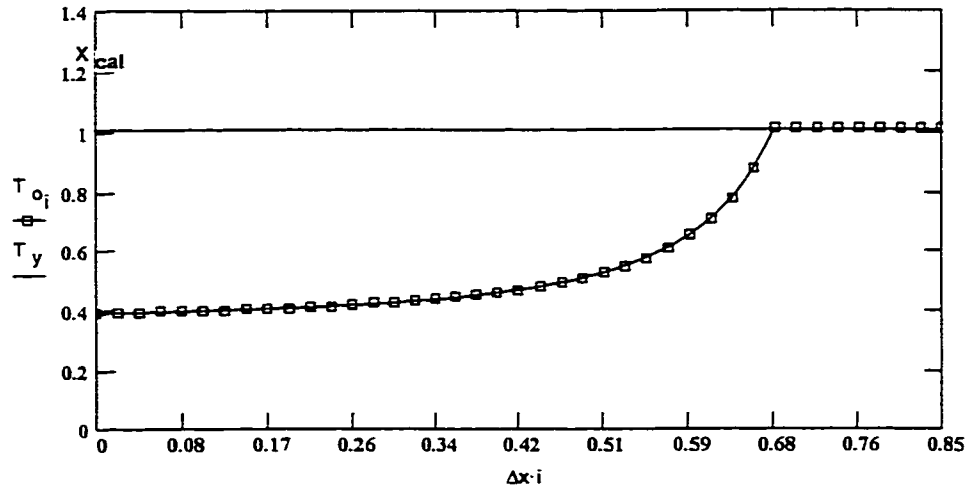
1.4
X cal
1.2
1
T o_i
0.8
T y
0.6
0.4
0.2
0
0
0.08
0.17
0.26
0.34
0.42
0.51
0.59
0.68
0.76
0.85
Δx·i

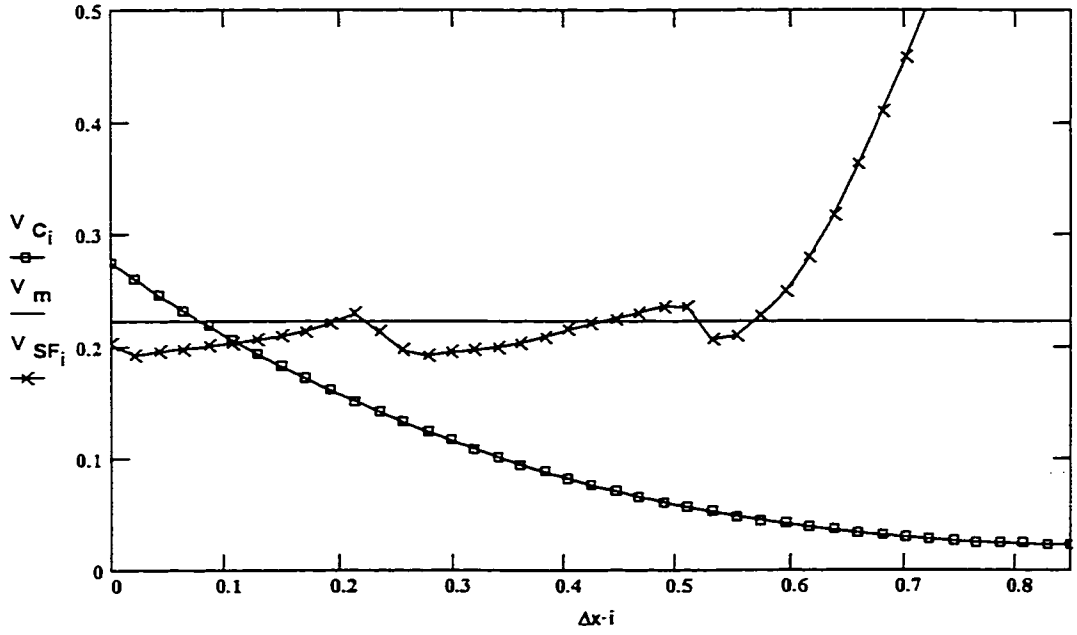
0.5
0.4
V c_i
0.3
V m
V SF_i
0.2
0.1
0
0
0.1
0.2
0.3
0.4
0.5
0.6
0.7
0.8
Δx·i

Appendix C

Details of Beams without Stirrups

	Beam	b_w (mm)	d (mm)	a (mm)	h (mm)	a_{cle} (mm)	a_{cle}/h	f'_c (MPa)	ρ (%)	f_y (MPa)	t/h	x_c (mm)	V_t (MN)
Kani et al	24	153	273	407	305	346.7	1.14	27.9	2	395.8	1.07	22	0.1819
	25	153	273	543	305	483.2	1.58	24.5	1.88	395.8	1.26	99	0.1041
	26	153	273	543	305	483.2	1.58	27.1	1.88	395.8	1.26	99	0.0781
	85	153	273	271	305	207.5	0.68	25.5	2.80	380.6	0.82	0	0.2335
	87	153	273	272	305	210.2	0.69	27.2	2.80	366.1	0.83	0	0.2395
	94	153	273	544	305	480.5	1.58	25.3	2.80	351.6	1.26	98	0.1105
	100	153	273	545	305	485.9	1.59	27.2	2.80	366.1	1.26	101	0.1119
	27	153	273	678	305	619.7	2.03	29.8	1.88	395.8	1.43	185	0.0514
	28	153	273	678	305	619.7	2.03	29.2	1.88	395.8	1.43	185	0.0543
	29	153	273	1221	305	1165.7	3.82	24.5	1.88	350.3	1.95	569	0.0429
	30	153	273	1213	305	1165.7	3.82	25.2	1.88	350.3	1.95	569	0.0463
	35	153	273	950	305	898.2	2.94	26.1	1.88	490.9	1.72	375	0.0449
	36	153	273	964	305	890.0	2.92	26.1	1.88	490.9	1.71	369	0.0516
	81	153	273	1629	305	1558.8	5.11	27.5	2.80	343.4	2.26	869	0.0512
	83	153	273	814	305	756.2	2.48	27.4	2.80	342.7	1.57	276	0.0649
	84	153	273	1087	305	1031.9	3.38	27.4	2.80	342.0	1.84	471	0.0554
	91	153	273	1626	305	1586.1	5.20	27.4	2.80	364.0	2.28	891	0.0510
	93	153	273	1762	305	1700.8	5.58	30.3	2.80	372.3	2.36	981	0.0538
	95	153	273	677	305	608.8	2.00	25.3	2.80	337.8	1.41	178	0.0727
	96	153	273	1084	305	1012.8	3.32	25.3	2.80	335.1	1.82	457	0.0563
	97	153	273	815	305	742.6	2.43	27.2	2.80	366.1	1.56	267	0.0625
	99	153	273	679	305	619.7	2.03	26.2	2.80	366.1	1.43	185	0.0772
Leondardt & Walther	1	190	270	270	320	153.9	0.48	34.8	4.64	343.3	0.69	0	0.3884
	2	190	270	400	320	286.2	0.89	34.8	4.64	343.3	0.95	0	0.2600
	3	190	270	540	320	423.9	1.32	34.8	4.64	343.3	1.15	56	0.1470
	4	190	270	670	320	556.2	1.74	34.8	4.64	343.3	1.32	134	0.0804
	5	190	270	810	320	693.9	2.17	34.8	4.64	343.3	1.47	223	0.0589
	6	190	270	1100	320	985.5	3.08	34.8	4.64	343.3	1.75	424	0.0589
	7	190	270	1350	320	1198.8	3.75	36.5	4.64	343.3	1.94	579	0.0598

	Beam	b_w (mm)	d (mm)	a (mm)	h (mm)	a_{cle} (mm)	a_{cle}/h	f'_c (MPa)	ρ (%)	f_y (MPa)	t/h	x_c (mm)	V_l (MN)
Leondardt & Walther	8	190	270	1620	320	1460.7	4.56	36.5	4.64	343.3	2.14	777	0.0628
Moody et al	A1-A	178	262	800	305	699.5	2.29	30.3	2.17	302.0	1.51	238	0.0610
	A2-A	178	262	800	305	686.4	2.25	31.0	2.15	315.1	1.50	229	0.0667
	A3-A	178	262	800	305	683.8	2.24	31.0	2.22	315.1	1.50	227	0.0756
	A4-A	178	262	800	305	678.6	2.22	31.5	2.37	303.4	1.49	224	0.0712
	B1-A	178	262	800	305	686.4	2.25	21.1	1.62	303.4	1.50	229	0.0563
	B2-A	178	262	800	305	683.8	2.24	21.6	1.63	303.4	1.50	227	0.0601
	B1-B	152	268	914	305	761.1	2.50	36.7	1.89	310.3	1.58	279	0.0578
	B3-B	152	268	914	305	761.1	2.50	25.8	1.89	310.3	1.58	279	0.0523
	B5-B	152	268	914	305	761.1	2.50	30.7	1.89	310.3	1.58	279	0.0520
	B7-B	152	268	914	305	761.1	2.50	30.9	1.89	310.3	1.58	279	0.0512
Berg	A4-1	229	359	991	419	983.7	2.35	51.3	4.30	310.3	1.53	342	0.1779
	A4-2	229	359	1372	419	1364.2	3.26	45.8	4.30	310.3	1.80	608	0.1334
	A4-3	229	359	1448	419	1439.6	3.44	49.2	4.30	310.3	1.85	663	0.1343
	A4-4	229	359	1524	419	1511.4	3.61	45.8	4.30	310.3	1.90	716	0.1350
	A4-5	229	359	1257	419	1249.3	2.98	46.5	4.30	310.3	1.73	526	0.1334
	A4-6	229	359	1524	419	1511.4	3.61	52.8	4.30	310.3	1.90	716	0.1423
	A4-7	229	359	1257	419	1181.1	2.82	49.2	4.30	310.3	1.68	478	0.1423
	A4-8	229	359	1600	419	1522.2	3.63	50.3	4.30	310.3	1.91	724	0.1246
	A4-9	229	359	1676	419	1601.1	3.82	56.0	4.30	310.3	1.95	782	0.1312
	A4-10	229	359	1753	419	1676.5	4.00	41.7	4.30	310.3	2.00	838	0.1223
	A4-12	229	359	991	419	915.5	2.18	51.7	4.30	310.3	1.48	296	0.1779
	D-1	229	359	1257	419	1242.1	2.96	58.6	4.30	310.3	1.72	521	0.1512
	D-2	229	359	1257	419	1242.1	2.96	50.5	4.30	310.3	1.72	521	0.1312
	D-3	229	359	1257	419	1242.1	2.96	42.5	4.30	310.3	1.72	521	0.1290
	D-4	229	359	1257	419	1242.1	2.96	41.8	4.30	310.3	1.72	521	0.1446
	D-5	229	359	1257	419	1242.1	2.96	50.5	4.30	310.3	1.72	521	0.1312
	D-6	229	359	1257	419	1242.1	2.96	48.6	4.30	310.3	1.72	521	0.1401
	D-7	229	359	1257	419	1242.1	2.96	37.9	4.30	310.3	1.72	521	0.1401
	D-8	229	359	1257	419	1242.1	2.96	30.0	4.30	310.3	1.72	521	0.1179
	D-10	229	359	1257	419	1242.1	2.96	31.4	4.30	310.3	1.72	521	0.1268
	D-11	229	359	1257	419	1242.1	2.96	22.5	4.30	310.3	1.72	521	0.1090
	D-12	229	359	1257	419	1242.1	2.96	27.4	4.30	310.3	1.72	521	0.1001
	D-13	229	359	1257	419	1242.1	2.96	24.5	4.30	310.3	1.72	521	0.0992

	Beam	b_w (mm)	d (mm)	a (mm)	h (mm)	a_{cle} (mm)	a_{cle}/h	f'_c (MPa)	ρ (%)	f_y (MPa)	t/h	x_c (mm)	V_t (MN)
Berg	D-14	229	359	1257	419	1242.1	2.96	28.1	4.30	310.3	1.72	521	0.1068
	D-15	229	359	1257	419	1242.1	2.96	26.3	4.30	310.3	1.72	521	0.1023
	D-16	229	359	1257	419	1242.1	2.96	30.5	4.30	310.3	1.72	521	0.1112
	D-17	229	359	1257	419	1242.1	2.96	26.1	4.30	310.3	1.72	521	0.1045
	D-18	229	359	1257	419	1242.1	2.96	28.7	4.30	310.3	1.72	521	0.1045
	D-19	229	359	1257	419	1242.1	2.96	32.3	4.30	310.3	1.72	521	0.1157
	D-20	229	359	1257	419	1242.1	2.96	28.5	4.30	310.3	1.72	521	0.1068
Mphonde & Frantz	AO-33b	152	298	1074	337	908.9	2.70	22.6	3.36	448.2	1.64	355	0.0646
	AO-33c	152	298	1074	337	908.9	2.70	29.5	2.32	448.2	1.64	355	0.0668
	AO-73a	152	298	1074	337	908.9	2.70	40.9	3.36	448.2	1.64	355	0.0822
	AO-73b	152	298	1074	337	908.9	2.70	45.2	3.36	448.2	1.64	355	0.0828
	AO-113a	152	298	1074	337	908.9	2.70	81.4	3.36	448.2	1.64	355	0.0897
	AO-113b	152	298	1074	337	908.9	2.70	81.1	3.36	448.2	1.64	355	0.0894
	AO-153a	152	298	1074	337	908.9	2.70	88.4	3.36	448.2	1.64	355	0.0935
	AO-153b	152	298	1074	337	908.9	2.70	101.8	3.36	448.2	1.64	355	0.1000
	AO-153c	152	298	1074	337	908.9	2.70	99.8	3.36	448.2	1.64	355	0.0978
Ahmad et al	A1	127	270	813	320	980.1	3.06	65.4	3.93	413.7	1.75	420	0.0578
	A2	127	270	610	320	710.1	2.22	65.4	3.93	413.7	1.49	233	0.0689
	A3	127	270	549	320	629.1	1.97	65.4	3.93	413.7	1.40	180	0.0689
	A7	127	270	832	320	980.1	3.06	65.4	1.77	413.7	1.75	420	0.0467
	A8	127	270	624	320	710.1	2.22	65.4	1.77	413.7	1.49	233	0.0489
	A9	127	270	562	320	629.1	1.97	65.4	1.77	413.7	1.40	180	0.0801
	B1	127	270	807	320	977.4	3.05	72.0	5.04	413.7	1.75	418	0.0512
	B2	127	270	605	320	707.4	2.21	72.0	5.04	413.7	1.49	232	0.0689
	B3	127	270	545	320	626.4	1.96	72.0	5.04	413.7	1.40	179	0.1000
	B7	127	270	831	320	980.1	3.06	72.0	2.25	413.7	1.75	420	0.0446
	B8	127	270	624	320	710.1	2.22	72.0	2.25	413.7	1.49	233	0.0467
	B9	127	270	562	320	626.4	1.96	72.0	2.25	413.7	1.40	179	0.0801
	C1	127	270	737	320	969.3	3.03	69.2	6.64	413.7	1.74	412	0.0543
	C2	127	270	552	320	699.3	2.19	69.2	6.64	413.7	1.48	226	0.0756
	C3	127	270	497	320	618.3	1.93	69.2	6.64	413.7	1.39	173	0.0689
	C7	127	270	826	320	980.1	3.06	69.2	3.26	413.7	1.75	420	0.0454
	C8	127	270	620	320	710.1	2.22	69.2	3.26	413.7	1.49	233	0.0445
	C9	127	270	558	320	629.1	1.97	69.2	3.26	413.7	1.40	180	0.0454

	Beam	b_w (mm)	d (mm)	a (mm)	h (mm)	a_{cle} (mm)	a_{cle}/h	f'_c (MPa)	ρ (%)	f_y (MPa)	t/h	x_c (mm)	V_i (MN)
Bresler & Scordelis	OA-1	305	457	183	555	1581.2	2.85	22.6	1.81	555.0	1.69	644	0.1668
	OA-2	305	457	2284	555	2033.7	3.66	23.7	2.27	555.0	1.91	971	0.1780
	OA-3	305	457	3202	555	2943.1	5.30	37.6	2.74	555.0	2.30	1665	0.1890
Xie et al	NNN-3	127	198	648	254	546.5	2.15	39.7	2.07	421.0	1.47	174	0.0370
	NHN-3	127	198	645	254	546.5	2.15	104.2	2.07	421.0	1.47	174	0.0460
Yoon et al	N1S	375	655	2150	750	1997.8	2.66	36.0	2.80	400.0	1.63	774	0.3270
	M1S	375	655	2150	750	1997.8	2.66	67.0	2.80	400.0	1.63	774	0.2960
	H1S	375	655	2150	750	1997.8	2.66	87.0	2.80	400.0	1.63	774	0.2490

Appendix D

Predictions for Beams without Stirrups

	Beam	ρf_y (Mpa)	V_{SFg} (MN)	V_t/V_{SFg}	V_{SFd} (MN)	V_t/V_{SFd}	V_{CSAs} (MN)	V_t/V_{CSAs}	V_{CSAg} (MN)	V_t/V_{CSAg}	V_{CEB} (MN)	V_t/V_{CEB}	V_{CEB} (MN)	Vt/V_{ACI}
Kani et al	24	0.27	0.0848	2.145	0.0956	1.903	0.0451	4.037	0.0270	6.737	0.0550	3.310	0.0430	4.230
	25	0.30	0.0597	1.744	0.0796	1.308	0.0422	2.465	0.0260	4.004	0.0478	2.178	0.0390	2.669
	26	0.27	0.0626	1.248	0.0806	0.968	0.0444	1.759	0.0310	2.519	0.0494	1.580	0.0410	1.905
	85	0.42	0.1340	1.743	0.1221	1.912	0.0431	5.420	0.0290	8.052	0.0697	3.348	0.0540	4.324
	87	0.38	0.1410	1.699	0.1223	1.958	0.0445	5.383	0.0280	8.554	0.0712	3.365	0.0530	4.519
	94	0.39	0.0601	1.839	0.0801	1.379	0.0429	2.575	0.0260	4.250	0.0551	2.004	0.0430	2.570
	100	0.38	0.0606	1.847	0.0805	1.391	0.0445	2.515	0.0280	3.996	0.0565	1.982	0.0440	2.543
	27	0.25	0.0683	0.753	0.0721	0.713	0.0466	1.104	0.0360	1.428	0.0474	1.085	0.0410	1.254
	28	0.25	0.0650	0.835	0.0719	0.755	0.0461	1.178	0.0350	1.551	0.0471	1.154	0.0410	1.324
	29	0.27	0.0436	0.984	0.0512	0.837	0.0422	1.016	0.0290	1.479	0.0365	1.176	0.0350	1.226
	30	0.26	0.0449	1.031	0.0514	0.900	0.0428	1.081	0.0290	1.597	0.0369	1.254	0.0360	1.286
	35	0.35	0.0551	0.815	0.0589	0.763	0.0436	1.030	0.0320	1.403	0.0405	1.108	0.0370	1.214
	36	0.35	0.0507	1.018	0.0591	0.873	0.0436	1.184	0.0300	1.720	0.0403	1.280	0.0370	1.395
	81	0.35	0.0373	1.373	0.0450	1.138	0.0447	1.144	0.0300	1.707	0.0393	1.302	0.0380	1.347
	83	0.35	0.0517	1.255	0.0646	1.005	0.0447	1.453	0.0360	1.803	0.0495	1.311	0.0420	1.545
	84	0.35	0.0445	1.245	0.0553	1.002	0.0447	1.241	0.0330	1.679	0.0450	1.232	0.0390	1.421
	91	0.37	0.0377	1.353	0.0446	1.144	0.0447	1.142	0.0300	1.700	0.0393	1.297	0.0380	1.342
	93	0.34	0.0353	1.524	0.0436	1.233	0.0470	1.146	0.0300	1.793	0.0396	1.359	0.0400	1.345
	95	0.37	0.0524	1.387	0.0712	1.021	0.0429	1.694	0.0350	2.077	0.0513	1.418	0.0420	1.731
	96	0.37	0.0424	1.328	0.0552	1.020	0.0429	1.312	0.0330	1.706	0.0438	1.285	0.0390	1.444
	97	0.38	0.0504	1.240	0.0651	0.960	0.0445	1.405	0.0360	1.736	0.0494	1.266	0.0410	1.524
	99	0.39	0.0521	1.482	0.0709	1.089	0.0437	1.768	0.0330	2.339	0.0518	1.490	0.0410	1.883
				0.371		0.367		1.329		2.177		0.738		1.055
				1.359		1.149		1.957		2.901		1.672		2.002
				0.273		0.319		0.679		0.750		0.442		0.527
Leondardt	1	0.46	0.2666	1.457	0.1971	1.971	0.0620	6.269	0.4390	0.885	0.1124	3.454	0.0888	4.374
& Walther	2	0.46	0.1450	1.793	0.1445	1.799	0.0620	4.197	0.0401	6.484	0.0986	2.636	0.0755	3.444
	3	0.46	0.0972	1.512	0.1187	1.238	0.0620	2.373	0.0530	2.774	0.0892	1.647	0.0683	2.152
	4	0.46	0.0971	0.828	0.1037	0.776	0.0620	1.298	0.0627	1.282	0.0831	0.968	0.0643	1.250
	5	0.46	0.0991	0.594	0.0928	0.635	0.0620	0.951	0.0640	0.920	0.0780	0.755	0.0614	0.959

	Beam	ρf_y (Mpa)	V_{SFg} (MN)	V_t/V_{SFg}	V_{SFd} (MN)	V_t/V_{SFd}	V_{CSAs} (MN)	V_t/V_{CSAs}	V_{CSAg} (MN)	V_t/V_{CSAg}	V_{CEB} (MN)	V_t/V_{CEB}	V_{CEB} (MN)	Vt/V_{ACI}
Leondardt	6	0.46	0.0787	0.748	0.0779	0.756	0.0620	0.951	0.0600	0.982	0.0704	0.837	0.0578	1.019
& Walther	7	0.44	0.0674	0.887	0.0711	0.842	0.0635	0.942	0.0537	1.114	0.0668	0.895	0.0588	1.017
	8	0.44	0.0593	1.059	0.0644	0.976	0.0635	0.990	0.0512	1.227	0.0629	0.999	0.0574	1.094
				0.427		0.505		1.983		1.929		1.001		1.314
				1.110		1.124		2.246		1.958		1.524		1.914
				0.385		0.449		0.883		0.985		0.657		0.686
Moody et al	A1-A	0.22	0.0739	0.825	0.0791	0.771	0.0529	1.153	0.0408	1.495	0.0526	1.160	0.0461	1.323
	A2-A	0.22	0.0706	0.945	0.0801	0.832	0.0535	1.247	0.0404	1.651	0.0528	1.263	0.0475	1.404
	A3-A	0.23	0.0644	1.174	0.0803	0.942	0.0535	1.413	0.0385	1.964	0.0534	1.416	0.0480	1.575
	A4-A	0.23	0.0675	1.055	0.0808	0.882	0.0539	1.320	0.0417	1.707	0.0549	1.298	0.0491	1.450
	B1-A	0.23	0.0634	0.888	0.0762	0.739	0.0441	1.278	0.0316	1.782	0.0423	1.331	0.0388	1.451
	B2-A	0.23	0.0610	0.985	0.0766	0.785	0.0447	1.348	0.0311	1.932	0.0427	1.407	0.0394	1.525
	B1-B	0.16	0.0568	1.018	0.0664	0.870	0.0506	1.142	0.0339	1.705	0.0448	1.289	0.0430	1.344
	B3-B	0.23	0.0515	1.016	0.0634	0.825	0.0424	1.233	0.0291	1.797	0.0399	1.312	0.0367	1.425
	B5-B	0.19	0.0554	0.939	0.0649	0.801	0.0463	1.124	0.0324	1.605	0.0422	1.231	0.0396	1.313
	B7-B	0.19	0.0582	0.880	0.0649	0.788	0.0464	1.103	0.0325	1.575	0.0423	1.209	0.0397	1.290
				0.100		0.060		0.104		0.151		0.081		0.094
				0.973		0.824		1.238		1.721		1.292		1.410
				0.103		0.073		0.085		0.087		0.063		0.067
Van Den	A4-1	0.26	0.1324	1.344	0.1481	1.201	0.1127	1.579	0.0970	1.834	0.1338	1.330	0.1150	1.547
Berg	A4-2	0.29	0.1165	1.145	0.1239	1.076	0.1064	1.253	0.0920	1.450	0.1156	1.154	0.1040	1.283
	A4-3	0.27	0.1110	1.210	0.1218	1.103	0.1103	1.217	0.0930	1.444	0.1163	1.155	0.1060	1.267
	A4-4	0.29	0.1040	1.298	0.1177	1.147	0.1064	1.268	0.0870	1.552	0.1116	1.210	0.1020	1.324
	A4-5	0.29	0.1215	1.098	0.1298	1.028	0.1073	1.244	0.0950	1.404	0.1196	1.115	0.1060	1.258
	A4-6	0.25	0.1124	1.266	0.1200	1.186	0.1143	1.245	0.0930	1.530	0.1170	1.216	0.1090	1.306
	A4-7	0.27	0.1328	1.072	0.1344	1.058	0.1103	1.290	0.1050	1.355	0.1219	1.168	0.1170	1.216
	A4-8	0.27	0.1126	1.107	0.1188	1.049	0.1115	1.117	0.0940	1.326	0.1133	1.100	0.1060	1.175
	A4-9	0.24	0.1088	1.206	0.1175	1.117	0.1177	1.115	0.0960	1.367	0.1156	1.135	0.1100	1.193
	A4-10	0.32	0.0994	1.230	0.1104	1.108	0.1016	1.204	0.0830	1.473	0.1032	1.185	0.0960	1.274
	A4-12	0.26	0.1325	1.343	0.1537	1.157	0.1131	1.573	0.0980	1.815	0.1341	1.326	0.1150	1.547
	D-1	0.23	0.1326	1.140	0.1342	1.127	0.1204	1.258	0.1010	1.497	0.1292	1.170	0.1170	1.292
	D-2	0.26	0.1298	1.011	0.1316	0.997	0.1118	1.174	0.1020	1.286	0.1229	1.067	0.1100	1.193
	D-3	0.31	0.1199	1.076	0.1286	1.003	0.1025	1.258	0.0930	1.387	0.1161	1.111	0.1020	1.265
	D-4	0.32	0.1137	1.272	0.1283	1.127	0.1017	1.422	0.0880	1.643	0.1154	1.253	0.1010	1.432
	D-5	0.26	0.1298	1.011	0.1316	0.997	0.1118	1.174	0.1020	1.286	0.1229	1.067	0.1100	1.193
	D-6	0.27	0.1223	1.146	0.1309	1.070	0.1096	1.278	0.0970	1.444	0.1214	1.154	0.1080	1.297
	D-7	0.35	0.1067	1.313	0.1267	1.106	0.0968	1.447	0.0860	1.629	0.1117	1.254	0.0970	1.444

	Beam	ρf_y (Mpa)	V_{SFg} (MN)	V_t/V_{SFg}	V_{SFd} (MN)	V_t/V_{SFd}	V_{CSAs} (MN)	V_t/V_{CSAs}	V_{CSAg} (MN)	V_t/V_{CSAg}	V_{CEB} (MN)	V_t/V_{CEB}	V_{CEB} (MN)	Vt/V_{ACI}
Van Den	D-8	0.44	0.1032	1.142	0.1229	0.960	0.0861	1.369	0.0810	1.456	0.1034	1.141	0.0880	1.340
Berg	D-10	0.42	0.1038	1.222	0.1236	1.026	0.0881	1.439	0.0800	1.585	0.1049	1.208	0.0900	1.409
	D-11	0.59	0.0940	1.160	0.1183	0.921	0.0746	1.461	0.0720	1.514	0.0939	1.161	0.0790	1.380
	D-12	0.49	0.1125	0.890	0.1214	0.825	0.0823	1.216	0.0830	1.206	0.1003	0.998	0.0850	1.178
	D-13	0.54	0.1052	0.943	0.1196	0.829	0.0779	1.274	0.0780	1.272	0.0966	1.027	0.0820	1.210
	D-14	0.47	0.1073	0.995	0.1218	0.877	0.0834	1.281	0.0810	1.319	0.1011	1.056	0.0860	1.242
	D-15	0.51	0.1063	0.962	0.1207	0.847	0.0807	1.268	0.0790	1.295	0.0989	1.034	0.0840	1.218
	D-16	0.44	0.1086	1.024	0.1231	0.903	0.0869	1.280	0.0870	1.278	0.1039	1.070	0.0890	1.249
	D-17	0.51	0.1061	0.985	0.1206	0.866	0.0804	1.301	0.0790	1.323	0.0987	1.059	0.0840	1.244
	D-18	0.46	0.1076	0.971	0.1221	0.856	0.0843	1.240	0.0830	1.259	0.1018	1.026	0.0870	1.201
	D-19	0.41	0.1095	1.057	0.1241	0.933	0.0894	1.294	0.0850	1.361	0.1059	1.092	0.0910	1.271
	D-20	0.47	0.1075	0.993	0.1220	0.875	0.0840	1.272	0.0810	1.319	0.1016	1.051	0.0870	1.228
				0.128		0.116		0.115		0.157		0.086		0.101
				1.121		1.013		1.294		1.430		1.136		1.289
				0.115		0.114		0.089		0.110		0.076		0.078
Mphonde	AO-33b	0.67	0.0494	1.308	0.0662	0.975	0.0431	1.498	0.0340	1.900	0.0492	1.312	0.0410	1.576
& Frantz	AO-33c	0.35	0.0537	1.244	0.0686	0.974	0.0493	1.358	0.0330	2.024	0.0476	1.405	0.0440	1.518
	AO-73a	0.37	0.0590	1.393	0.0716	1.148	0.0580	1.417	0.0420	1.957	0.0600	1.370	0.0530	1.551
	AO-73b	0.33	0.0598	1.385	0.0726	1.141	0.0610	1.357	0.0440	1.882	0.0620	1.335	0.0560	1.479
	AO-113a	0.19	0.0805	1.114	0.0784	1.144	0.0819	1.096	0.0600	1.495	0.0755	1.188	0.0720	1.246
	AO-113b	0.19	0.0804	1.112	0.0784	1.141	0.0817	1.094	0.0580	1.541	0.0754	1.186	0.0720	1.242
	AO-153a	0.17	0.0815	1.147	0.0793	1.180	0.0853	1.098	0.0590	1.585	0.0776	1.205	0.0750	1.247
	AO-153b	0.15	0.0831	1.203	0.0807	1.239	0.0915	1.092	0.0610	1.639	0.0813	1.230	0.0800	1.250
	AO-153c	0.15	0.0829	1.180	0.0805	1.214	0.0906	1.079	0.0610	1.603	0.0808	1.211	0.0790	1.238
				0.109		0.094		0.171		0.202		0.084		0.153
				1.232		1.128		1.232		1.736		1.271		1.372
				0.088		0.083		0.139		0.116		0.066		0.112
Ahmad et al	A1	0.25	0.0431	1.341	0.0567	1.019	0.0568	1.018	0.0331	1.746	0.0608	0.951	0.0361	1.601
	A2	0.25	0.0488	1.412	0.0666	1.034	0.0568	1.214	0.0342	2.015	0.0669	1.030	0.0376	1.832
	A3	0.25	0.0527	1.307	0.0708	0.973	0.0568	1.214	0.0353	1.952	0.0693	0.995	0.0382	1.804
	A7	0.11	0.0473	0.987	0.0567	0.823	0.0568	0.823	0.0288	1.622	0.0462	1.010	0.0345	1.354
	A8	0.11	0.0580	0.843	0.0666	0.734	0.0568	0.861	0.0288	1.698	0.0509	0.961	0.0352	1.389
	A9	0.11	0.0436	1.837	0.0708	1.132	0.0568	1.411	0.0288	2.781	0.0527	2.147	0.0355	2.256
	B1	0.29	0.0496	1.032	0.0575	0.890	0.0596	0.860	0.0391	1.309	0.0683	0.749	0.0386	1.326
	B2	0.29	0.0522	1.320	0.0676	1.019	0.0596	1.157	0.0391	1.762	0.0752	0.916	0.0405	1.701
	B3	0.29	0.0456	2.193	0.0718	1.392	0.0596	1.678	0.0344	2.907	0.0779	1.831	0.0413	2.421
	B7	0.13	0.0512	0.871	0.0574	0.777	0.0596	0.749	0.0311	1.434	0.0517	0.862	0.0367	1.215

	Beam	ρf_y (Mpa)	V_{SFg} (MN)	V_t/V_{SFg}	V_{SFd} (MN)	V_t/V_{SFd}	V_{CSAs} (MN)	V_t/V_{CSAs}	V_{CSAg} (MN)	V_t/V_{CSAg}	V_{CEB} (MN)	V_t/V_{CEB}	V_{CEB} (MN)	Vt/V_{ACI}
Ahmad et al	B8	0.13	0.0662	0.705	0.0675	0.692	0.0596	0.784	0.0355	1.315	0.0569	0.821	0.0375	1.245
	B9	0.13	0.0498	1.608	0.0718	1.115	0.0596	1.345	0.0303	2.644	0.0589	1.919	0.0379	2.113
	C1	0.40	0.0485	1.120	0.0575	0.945	0.0584	0.930	0.0368	1.476	0.0762	0.713	0.0363	1.496
	C2	0.40	0.0527	1.435	0.0676	1.118	0.0584	1.295	0.0359	2.106	0.0839	0.901	0.0385	1.964
	C3	0.40	0.0596	1.156	0.0719	0.958	0.0584	1.180	0.0385	1.790	0.0869	0.793	0.0395	1.744
	C7	0.19	0.0513	0.885	0.0571	0.795	0.0584	0.777	0.0357	1.272	0.0579	0.784	0.0369	1.230
	C8	0.19	0.0663	0.671	0.0671	0.663	0.0584	0.762	0.0393	1.132	0.0637	0.699	0.0380	1.171
	C9	0.19	0.0705	0.644	0.0713	0.637	0.0584	0.777	0.0398	1.141	0.0660	0.688	0.0386	1.176
				0.417		0.197		0.275		0.541		0.442		0.390
				1.187		0.929		1.046		1.783		1.043		1.613
				0.351		0.212		0.263		0.303		0.423		0.242
Bresler & Scordelis	OA-1	0.44	0.1895	0.880	0.2130	0.783	0.1182	1.411	0.0760	2.195	0.2342	0.712	0.1182	1.411
	OA-2	0.53	0.1650	1.079	0.1890	0.942	0.1211	1.470	0.0779	2.285	0.1106	1.609	0.1225	1.453
	OA-3	0.40	0.1520	1.243	0.1669	1.132	0.1525	1.239	0.0861	2.195	0.1227	1.540	0.1468	1.287
				0.182		0.175		0.120		0.052		0.499		0.086
				1.067		0.952		1.373		2.225		1.287		1.384
				0.170		0.183		0.087		0.023		0.388		0.062
Xie et al	NNN-3	0.22	0.0495	0.747	0.0503	0.736	0.0344	1.076	0.0249	1.486	0.0319	1.158	0.0305	1.213
	NHN-3	0.08	0.0789	0.583	0.0571	0.806	0.0557	0.826	0.0413	1.114	0.0441	1.042	0.0474	0.970
				0.116		0.049		0.177		0.263		0.082		0.172
				0.665		0.771		0.951		1.300		1.100		1.092
				0.174		0.064		0.186		0.202		0.075		0.157
Yoon et al	N1S	0.31	0.3973	0.823	0.3891	0.840	0.2315	1.412	0.2250	1.453	0.2583	1.266	0.2686	1.217
	M1S	0.17	0.5280	0.561	0.4222	0.701	0.3159	0.937	0.2810	1.053	0.3178	0.931	0.3530	0.839
	H1S	0.13	0.5900	0.422	0.4370	0.570	0.3599	0.692	0.3030	0.822	0.3467	0.718	0.3980	0.626
				0.204		0.135		0.366		0.319		0.276		0.299
				0.602		0.704		1.014		1.109		0.972		0.894
				0.338		0.192		0.361		0.288		0.284		0.335

Appendix E

Details of Beams with stirrups

	Beam	b_w (mm)	d (mm)	d_s (mm)	h (mm)	h_f (mm)	a_{cle}/h	s (mm)	f'_c (MPa)	ρ (%)	f_y (MPa)	A_v (mm^2)	f_{vy} (MPa)	T_{vy} (MN)	V_t (MN)
Rodriguez et al	E2A1	152	318	305	368		3.25	245	25.2	1.60	320.0	143	346.1	0.0493	0.1300
	E2A2	152	318	305	368		3.25	245	19.3	1.60	325.4	143	346.8	0.0494	0.1190
	E2A3	152	318	305	368		3.25	245	20.0	1.60	323.3	143	350.9	0.0500	0.1290
	C2A1	152	318	305	368		3.25	245	22.6	1.60	317.8	143	353.7	0.0504	0.0995
	C2A2	152	318	305	368		3.25	245	22.1	1.60	324.1	143	348.9	0.0497	0.1224
	E3H1	152	318	305	368		2.07	147	24.8	2.66	405.4	253	330.9	0.0839	0.2140
	E3H2	152	318	305	368		2.12	184	28.8	2.66	397.1	253	317.8	0.0805	0.1896
	C3H1	152	318	305	368		2.07	147	22.6	2.66	413.7	253	317.8	0.0805	0.1896
	C3H2	152	318	305	368		2.04	184	22.8	2.66	412.3	253	317.8	0.0805	0.1742
Hsiung & Frantz	A	152	419	402	457		2.53	103	43.0	1.82	448.2	36	282.7	0.0101	0.1103
	B	305	419	402	457		2.53	110	43.0	1.82	448.2	71	303.4	0.0216	0.2002
	C	305	419	402	457		2.53	103	43.0	1.82	448.2	107	283.7	0.0303	0.3389
	D	305	419	402	457		2.53	103	43.0	1.82	448.2	107	283.7	0.0303	0.3478
Debaiky & Elniema	A1	120	260	245	300		2.50	200	24.5	2.89	452.2	48	318.3	0.0151	0.0721
	B1	120	260	245	300		1.83	200	24.5	2.89	452.2	48	318.3	0.0151	0.0675
	C1	120	260	245	300		2.50	200	28.1	2.89	452.2	48	387.3	0.0184	0.0711
	D1	120	260	245	300		2.50	100	29.8	2.89	452.2	48	387.3	0.0184	0.0819
	D2	120	260	245	300		2.50	200	30.6	2.89	452.2	101	387.3	0.0389	0.0736
	E3	120	260	245	300		2.50	150	31.4	1.92	452.2	57	313.9	0.0178	0.0613
	F5	120	260	245	300		2.50	200	20.2	1.92	452.2	57	381.6	0.0216	0.0662
	F6	120	260	245	300		2.50	200	20.5	1.92	452.2	57	381.6	0.0216	0.0613
Mphonde	B50-3-3	150	298	283	337		2.79	86	22.1	3.36	448.2	16	302.7	0.0048	0.0761
	B50-7-3	150	298	283	337		2.79	86	39.8	3.36	448.2	16	302.7	0.0048	0.0939
	B50-11-3	150	298	283	337		2.79	86	59.7	3.36	448.2	16	302.7	0.0048	0.0979
	B50-15-3	150	298	283	337		2.79	86	83.0	3.36	448.2	16	302.7	0.0048	0.1112
	B100-3-3	150	298	283	337		2.79	86	27.9	3.36	448.2	36	265.8	0.0095	0.0952
	B100-7-3	150	298	283	337		2.79	86	47.1	3.36	448.2	36	265.8	0.0095	0.1205

	Beam	b_w (mm)	d (mm)	d_s (mm)	h (mm)	h_f (mm)	a_{cle}/h	s (mm)	f'_c (MPa)	ρ (%)	f_y (MPa)	A_v (mm^2)	f_{vy} (MPa)	T_{vy} (MN)	V_t (MN)
Mphonde	B100-11-3	150	298	283	337		2.79	86	68.6	3.36	448.2	36	265.8	0.0095	0.1517
	B100-15-3	150	298	283	337		2.79	86	81.9	3.36	448.2	36	265.8	0.0095	0.1156
	B150-3-3	150	298	283	337		2.79	86	28.7	3.36	448.2	52	284.2	0.0147	0.1390
	B150-7-3	150	298	283	337		2.79	86	46.6	3.36	448.2	52	284.2	0.0147	0.1334
	B150-11-3	150	298	283	337		2.79	86	69.5	3.36	448.2	52	284.2	0.0147	0.1615
	B150-15-3	150	298	283	337		2.79	86	82.7	3.36	448.2	52	284.2	0.0147	0.1500
Elzanaty et al	G4	178	267	260	305		3.17	184	62.7	3.30	434.4	63	379.2	0.0240	0.1472
	G5	178	267	260	305		3.17	184	40.0	2.50	434.4	63	379.2	0.0240	0.1132
	G6	178	267	260	305		3.17	184	20.0	2.50	434.4	63	379.2	0.0240	0.0776
Anderson & Ramirez	W1	406	345	320	406		2.00	172	29.2	2.30	434.4	285	544.0	0.1550	0.4600
	W2	406	345	320	406		2.00	172	32.2	2.30	434.4	285	544.0	0.1550	0.5490
	W3	406	345	320	406		2.00	86	32.3	2.30	434.4	143	544.0	0.0775	0.5040
Johnson & Ramirez	No.1	305	539	552	610		2.47	133	36.4	2.50	524.7	63	479.20	0.0304	0.3385
	No.2	305	539	552	610		2.47	267	36.4	2.50	524.7	63	479.20	0.0304	0.2224
	No.4	305	539	552	610		2.47	267	72.3	2.50	524.7	63	479.20	0.0304	0.3158
	No.5	305	539	552	610		2.47	133	55.8	2.50	524.7	63	479.20	0.0304	0.3825
	No.7	305	539	552	610		2.47	267	51.3	2.50	524.7	63	544.00	0.0345	0.2808
	No.8	305	539	552	610		2.47	267	51.3	2.50	524.7	63	544.00	0.0345	0.2580
Roller & Ressell	1	356	559	545	680		1.87	208	120.1	1.24	472.3	63	406.7	0.0258	0.2970
	2	356	559	545	680		1.87	159	120.1	3.04	430.9	253	448.2	0.1136	1.0970
	3	356	559	618	718		1.77	123	120.1	4.56	430.9	396	457.8	0.1812	1.6650
	4	356	559	618	718		1.77	86	120.1	6.08	430.9	396	457.8	0.1812	1.9400
	5	356	559	644	743		1.71	61	120.1	6.97	462.0	396	457.8	0.1812	2.2350
	6	457	762	777	870		1.99	368	72.4	1.73	464.0	143	445.1	0.0634	0.6650
	7	457	762	777	870		1.99	190	72.4	1.88	483.2	143	445.1	0.0634	0.7880
	8	457	762	777	870		1.99	368	125.3	1.88	483.2	143	445.1	0.0634	0.4830
	9	457	762	777	870		1.99	190	125.3	2.35	483.2	143	445.1	0.0634	0.7490
	10	457	762	777	870		1.99	129	125.3	2.89	464.1	143	445.1	0.0634	1.1720
Bresler & Scordelis	A-1	305	457	465	555		2.85	210	21.1	1.80	555.0	63	325.4	0.0206	0.2340
	A-2	305	457	465	555		3.67	210	24.3	2.28	555.0	63	325.4	0.0206	0.2450
	B-1	229	457	465	555		2.87	195	24.8	2.43	555.0	63	325.4	0.0206	0.2220
	B-2	229	457	465	555		3.66	195	23.2	2.43	555.0	63	325.4	0.0206	0.2000

	Beam	b_w (mm)	d (mm)	d_s (mm)	h (mm)	h_f (mm)	a_{cle}/h	s (mm)	f'_c (MPa)	ρ (%)	f_y (MPa)	A_v (mm^2)	f_{vy} (MPa)	T_{vy} (MN)	V_t (MN)
Bresler Scordelis	C-1	152	457	465	555		2.87	210	29.6	1.80	555.0	63	325.4	0.0206	0.1560
	C-2	152	457	465	555		3.68	210	23.8	3.66	555.0	63	325.4	0.0206	0.1620
Xie et al	NNW-3	127	203	197	254		2.19	98	42.9	3.20	421.0	63	324.1	0.0205	0.0870
	NHW-3	127	198	197	254		2.14	96	103.4	4.54	421.0	63	324.1	0.0205	0.1024
	NHW-3a	127	198	197	254		2.14	74	94.7	4.54	421.0	63	324.1	0.0205	0.1082
	NHW-3b	127	198	197	254		2.14	61	108.7	4.54	421.0	63	324.1	0.0205	0.1225
	NHW-4	127	198	197	254		2.14	96	104.0	4.54	421.0	63	324.1	0.0205	0.0937
Yoon et al	N1N	375	655	661	750		2.66	325	36.0	2.80	400.0	101	430.0	0.0432	0.4570
	N2S	375	655	661	750		2.66	465	36.0	2.80	400.0	142	430.0	0.0610	0.3630
	N2N	375	655	661	750		2.66	325	36.0	2.80	400.0	142	430.0	0.0610	0.4830
	M1N	375	655	661	750		2.66	325	67.0	2.80	400.0	101	430.0	0.0432	0.4050
	M2S	375	655	661	750		2.66	325	67.0	2.80	400.0	142	430.0	0.0610	0.5520
	M2N	375	655	661	750		2.66	230	67.0	2.80	400.0	142	430.0	0.0610	0.6890
	H1N	375	655	661	750		2.66	325	87.0	2.80	400.0	101	430.0	0.0432	0.4830
	H2S	375	655	661	750		2.66	270	87.0	2.80	400.0	142	430.0	0.0610	0.5980
	H2N	375	655	661	750		2.66	160	87.0	2.80	400.0	142	430.0	0.0610	0.7210
Kriski	1	360	345	344	400		2.26	150	28.9	2.01	433.0	51	600.0	0.0304	0.2490
	2	360	345	344	400		1.88	150	30.2	2.01	433.0	51	600.0	0.0304	0.3835
	3	360	345	344	400		2.26	150	28.9	2.01	433.0	51	600.0	0.0304	0.2245
	5	360	345	344	400		1.88	150	30.1	2.01	433.0	51	600.0	0.0304	0.2930
	7	360	345	344	400		2.26	150	74.3	2.01	433.0	51	600.0	0.0304	0.3045
	8	360	345	344	400		1.88	150	77.8	2.01	433.0	51	600.0	0.0304	0.3910
	9	360	345	344	400		2.26	150	77.0	2.01	433.0	51	600.0	0.0304	0.2420
	10	360	345	344	400		1.88	150	76.3	2.01	433.0	51	600.0	0.0304	0.3905
Peng	B-1	280	274	264	320		2.65	355	31.3	2.70	477.7	51	586.70	0.0299	0.1140
	B-2	280	274	264	320		2.65	300	31.8	2.70	477.7	51	586.70	0.0299	0.1190
	B-3	280	274	264	320		2.65	250	32.7	2.70	477.7	51	586.70	0.0299	0.1210
	B-4	280	274	264	320		2.65	195	33.0	2.70	477.7	51	586.70	0.0299	0.1430
	B-5	280	274	264	320		2.65	355	32.4	2.70	477.7	201	456.40	0.0916	0.1810
	B-6	280	274	264	320		2.65	300	29.3	2.70	477.7	201	456.40	0.0916	0.1910
	B-7	280	274	264	320		2.65	250	32.2	2.70	477.7	201	456.40	0.0916	0.1870
Talor	ST1-B	114	248	248	305	76	3.33	110	25.9	2.83	441.3	63	289.6	0.0183	0.0892

	Beam	b_w (mm)	d (mm)	d_s (mm)	h (mm)	h_f (mm)	a_{clv}/h	s (mm)	f'_c (MPa)	ρ (%)	f_y (MPa)	A_v (mm^2)	f_{vy} (MPa)	T_{vy} (MN)	V_t (MN)
Talor	ST4-B	114	248	248	305	76	3.33	147	28.5	2.83	441.3	63	289.6	0.0183	0.0747
	ST2-C	114	248	248	305	76	2.59	110	27.1	2.83	441.3	63	289.6	0.0183	0.1066
Haddadin et al	A2	178	381	413	470	102	1.76	184	29.2	3.81	517.1	63	358.5	0.0227	0.1943
	A3	178	381	413	470	102	1.76	184	30.1	3.81	517.1	143	344.7	0.0491	0.2915
	A4	178	381	413	470	102	1.76	98	28.6	3.81	517.1	143	344.7	0.0491	0.3427
	A5	178	381	413	470	102	1.76	61	26.3	3.81	517.1	143	344.7	0.0491	0.3872
	B3	178	381	413	470	102	2.46	184	27.7	3.81	517.1	143	344.7	0.0491	0.2714
	C2	178	381	413	470	102	3.18	184	27.8	3.81	517.1	63	358.5	0.0227	0.1733
	C3	178	381	413	470	102	3.18	184	24.1	3.81	517.1	143	344.7	0.0491	0.2602
	C4	178	381	413	470	102	3.18	98	25.7	3.81	517.1	143	344.7	0.0491	0.3106
	C5	178	381	413	470	102	3.18	61	30.4	3.81	517.1	143	344.7	0.0491	0.3583
	D3	178	381	413	470	102	4.60	184	29.3	3.81	517.1	143	344.7	0.0491	0.2410
	F3	178	381	413	470	102	1.76	184	44.9	3.81	517.1	143	344.7	0.0491	0.3298
	G3	178	381	413	470	102	1.76	184	26.2	3.81	517.1	143	456.4	0.0650	0.3326
	G4	178	381	413	470	102	1.76	123	26.8	3.81	517.1	143	456.4	0.0650	0.3835
	G5	178	381	413	470	102	1.76	74	26.1	3.81	517.1	143	456.4	0.0650	0.4278
	H2	178	381	413	470	102	1.76	184	28.2	3.81	517.1	143	344.7	0.0491	0.3185
	J3	178	381	413	470	102	1.76	184	30.4	3.81	517.1	143	344.7	0.0491	0.2630
	J5	178	381	413	470	102	1.76	61	32.5	3.81	517.1	143	344.7	0.0491	0.4334
Sorensen	T21	110	298	295	355	80	2.68	175	32.5	3.84	421.8	101	268.8	0.0270	0.1295
	T22	110	298	295	355	80	2.68	210	31.3	3.84	421.8	77	445.4	0.0343	0.1275
	T23	110	298	295	355	80	2.68	150	34.2	3.84	421.8	57	346.3	0.0196	0.1393
	T3a	110	298	295	355	80	2.68	105	24.6	3.84	421.8	57	259.0	0.0146	0.1275
	T4a	110	298	295	355	80	2.68	105	25.2	3.84	421.8	39	397.3	0.0156	0.1324
	T1b	110	298	295	355	80	2.68	117	23.2	3.84	421.8	57	259.0	0.0146	0.1177
	T2b	110	298	295	355	80	2.68	117	24.9	3.84	421.8	39	397.3	0.0156	0.1295
	T3b	110	298	295	355	80	2.68	175	24.6	3.84	421.8	57	259.0	0.0146	0.1158
	T4b	110	298	295	355	80	2.68	175	24.7	3.84	421.8	39	397.3	0.0156	0.1069
	T5	110	298	295	355	80	2.68	175	25.5	3.84	421.8	39	397.3	0.0156	0.1099
Lyngberg	5A0	120	540	540	600	100	2.25	158	25.7	1.94	725.0	101	674.0	0.0677	0.4350
	5B0	120	540	540	600	100	2.25	158	26.6	1.94	733.0	101	647.0	0.0650	0.4350
Bach et al	V6002	200	343	540	400	90	2.32	210	36.7	2.86	650.0	113	319.4	0.0361	0.2450
	V6004	200	343	540	400	90	2.32	131	36.4	2.86	650.0	113	319.4	0.0361	0.3060

	Beam	b_w (mm)	d (mm)	d_s (mm)	h (mm)	h_f (mm)	a_{cle}/h	s (mm)	f'_c (MPa)	ρ (%)	f_y (MPa)	A_v (mm^2)	f_{vy} (MPa)	T_{vy} (MN)	V_f (MN)
Bach et al	U6002	200	343	540	400	90	2.32	210	20.0	2.86	650.0	57	319.4	0.0181	0.1940
	U6004	200	343	540	400	90	2.32	210	21.1	2.86	650.0	57	319.4	0.0181	0.2240
	U6017	200	343	540	400	90	2.32	175	20.1	2.86	650.0	314	314.5	0.0988	0.3060
	U5604p	200	343	540	400	90	2.32	210	23.4	2.86	716.5	113	389.1	0.0440	0.2550
Clark	A1-1	203	390	346	457		1.80	176	24.6	3.1	320.6	143	331.1	0.0472	0.225
	A1-2	203	390	346	457		1.80	176	23.6	3.1	320.6	143	331.1	0.0472	0.2091
	A1-3	203	390	346	457		1.80	176	23.4	3.1	320.6	143	331.1	0.0472	0.2225
	A1-4	203	390	346	457		1.80	176	24.6	3.1	320.6	143	331.1	0.0472	0.2454
	B1-1	203	390	346	457		1.48	184	23.4	3.1	320.6	143	331.1	0.0472	0.2788
	B1-2	203	390	346	457		1.48	184	25.4	3.1	320.6	143	331.1	0.0472	0.2566
	B1-3	203	390	346	457		1.48	184	23.7	3.1	320.6	143	331.1	0.0472	0.2848
	B1-4	203	390	346	457		1.48	184	23.3	3.1	320.6	143	331.1	0.0472	0.2681
	B1-5	203	390	346	457		1.48	184	24.6	3.1	320.6	143	331.1	0.0472	0.2415
	C1-1	203	390	346	457		1.14	196	25.6	2.1	320.6	143	331.1	0.0472	0.2777
	C1-2	203	390	346	457		1.14	196	26.3	2.1	320.6	143	331.1	0.0472	0.3111
	C1-3	203	390	346	457		1.14	196	23.9	2.1	320.6	143	331.1	0.0472	0.2459
	C1-4	203	390	346	457		1.14	196	29	2.1	320.6	143	331.1	0.0472	0.2859
	D1-1	203	390	346	457		0.80	147	26.2	1.63	335.3	143	331.1	0.0472	0.3011
	D1-2	203	390	346	457		0.80	147	26.1	1.63	335.3	143	331.1	0.0472	0.3567
	D1-3	203	390	346	457		0.80	147	24.5	1.63	335.3	143	331.1	0.0472	0.2566

Appendix F

Predictions for Beams with Stirrups

	Beam	ρf_y (MPa)	$\rho_v f_{vy}$ (MPa)	s/d	V_{SFg} (MN)	V_t/V_{SFg}	V_{SFd} (MN)	V_t/V_{SFd}	V_{ACI} (MN)	V_t/V_{ACI}	V_{ACI} (MN)	V_t/V_{CSAg}	V_{CEB} (MN)	V_t/V_{CEB}
Rodriguez	E2A1	5.12	1.324	0.770	0.1240	1.048	0.1006	1.292	0.0999	1.301	0.0924	1.407	0.1920	0.677
et al	E2A2	5.21	1.327	0.770	0.1216	0.979	0.0963	1.235	0.0966	1.232	0.0919	1.295	0.1924	0.618
	E2A3	5.17	1.343	0.770	0.1277	1.010	0.0972	1.327	0.0986	1.309	0.0940	1.372	0.1947	0.663
	C2A1	5.08	1.353	0.770	0.1239	0.803	0.0994	1.001	0.0971	1.025	0.0910	1.093	0.1963	0.507
	C2A2	5.19	1.335	0.770	0.1252	0.978	0.0987	1.240	0.1000	1.224	0.0926	1.322	0.1936	0.632
	E3H1	10.78	3.753	0.462	0.2104	1.017	0.1681	1.273	0.2627	0.815	0.2935	0.729	0.4295	0.498
	E3H2	10.56	2.879	0.579	0.1844	1.028	0.1438	1.318	0.2130	0.890	0.2272	0.835	0.4175	0.454
	C3H1	11.00	3.604	0.462	0.2054	0.923	0.1639	1.157	0.2652	0.715	0.2981	0.636	0.4000	0.474
	C3H2	10.97	2.879	0.579	0.1817	0.959	0.1381	1.261	0.2226	0.783	0.2254	0.773	0.3660	0.476
					s =	0.074		0.101		0.239		0.309		0.090
					x =	0.972		1.234		1.033		1.051		0.555
					V =	0.076		0.082		0.231		0.294		0.162
Hsiung	A	8.16	0.643	0.246	0.1460	0.755	0.1425	0.774	0.1350	0.817	0.1201	0.918	0.1229	0.897
& Frantz	B	8.16	0.644	0.263	0.2917	0.686	0.2847	0.703	0.2613	0.766	0.2394	0.836	0.2471	0.810
	C	8.16	0.965	0.246	0.4379	0.774	0.3446	0.983	0.4049	0.837	0.3569	0.950	0.3701	0.916
	D	8.16	0.965	0.246	0.4379	0.794	0.3446	1.009	0.4049	0.859	0.3500	0.994	0.3701	0.940
					s =	0.047		0.152		0.040		0.066		0.056
					x =	0.752		0.868		0.820		0.924		0.891
					V =	0.062		0.175		0.048		0.072		0.063
Debaiky &	A1	13.07	0.630	0.769	0.0689	1.046	0.0557	1.293	0.0537	1.343	0.0495	1.457	0.0590	1.222
Elniema	B1	13.07	0.630	0.769	0.0725	0.931	0.0557	1.211	0.0537	1.257	0.0554	1.218	0.0590	1.144
	C1	13.07	0.767	0.769	0.0739	0.962	0.0610	1.166	0.0555	1.281	0.0510	1.394	0.0718	0.991
	D1	13.07	1.534	0.385	0.1110	0.738	0.0946	0.866	0.0843	0.972	0.0809	1.012	0.1436	0.571
	D2	13.07	1.622	0.769	0.0937	0.785	0.0776	0.949	0.0879	0.837	0.0849	0.867	0.1518	0.485
	E3	8.68	0.986	0.577	0.0831	0.738	0.0733	0.836	0.0735	0.834	0.0657	0.933	0.0923	0.664
	F5	8.68	0.899	0.769	0.0745	0.889	0.0613	1.080	0.0567	1.168	0.0523	1.266	0.0842	0.787
	F6	8.68	0.899	0.769	0.0746	0.822	0.0614	0.998	0.0568	1.079	0.0526	1.165	0.0842	0.728
					s =	0.112		0.166		0.199		0.213		0.268
					x =	0.864		1.050		1.096		1.164		0.824
					V =	0.130		0.158		0.182		0.183		0.326

	Beam	ρf_y (MPa)	$\rho_v f_{vy}$ (MPa)	s/d	V_{SFg} (MN)	V_t/V_{SFg}	V_{SFd} (MN)	V_t/V_{SFd}	V_{ACI} (MN)	V_t/V_{ACI}	V_{ACI} (MN)	V_t/V_{CSAg}	V_{CEB} (MN)	V_t/V_{CEB}
Mphonde	B50-3-3	15.06	0.371	0.289	0.0771	0.987	0.0718	1.060	0.0604	1.260	0.0561	1.357	0.0498	1.528
	B50-7-3	15.06	0.371	0.289	0.0813	1.155	0.0769	1.221	0.0726	1.293	0.0670	1.401	0.0498	1.885
	B50-11-3	15.06	0.371	0.289	0.0885	1.106	0.0806	1.214	0.0834	1.174	0.0768	1.275	0.0498	1.965
	B50-15-3	15.06	0.371	0.289	0.0927	1.200	0.0838	1.327	0.0939	1.184	0.0833	1.335	0.0498	2.232
	B100-3-3	15.06	0.734	0.289	0.1065	0.894	0.1010	0.943	0.0957	0.995	0.0936	1.017	0.0984	0.967
	B100-7-3	15.06	0.734	0.289	0.1109	1.087	0.1076	1.120	0.1077	1.119	0.0977	1.233	0.0984	1.224
	B100-11-3	15.06	0.734	0.289	0.1144	1.326	0.1125	1.348	0.1185	1.280	0.1021	1.486	0.0984	1.541
	B100-15-3	15.06	0.734	0.289	0.1163	0.994	0.1149	1.006	0.1243	0.930	0.1127	1.026	0.0984	1.174
	B150-3-3	15.06	1.140	0.289	0.1300	1.069	0.1234	1.126	0.1214	1.145	0.1173	1.185	0.1529	0.909
	B150-7-3	15.06	1.140	0.289	0.1351	0.987	0.1310	1.019	0.1326	1.006	0.1187	1.124	0.1529	0.872
	B150-11-3	15.06	1.140	0.289	0.1397	1.156	0.1375	1.174	0.1441	1.121	0.1269	1.273	0.1529	1.056
	B150-15-3	15.06	1.140	0.289	0.1418	1.058	0.1405	1.068	0.1498	1.001	0.1312	1.143	0.1529	0.981
					s =	0.115		0.128		0.121		0.145		0.462
					x =	*1.085*		*1.136*		*1.126*		*1.238*		*1.361*
					V =	0.106		0.111		0.108		0.118		0.339
Elzanaty et al	G4	14.34	0.733	0.689	0.1106	1.331	0.1066	1.381	0.1027	1.433	0.0868	1.696	0.1046	1.408
	G5	10.86	0.733	0.689	0.1062	1.066	0.1003	1.129	0.0905	1.251	0.0774	1.463	0.1046	1.083
	G6	10.86	0.733	0.689	0.1009	0.769	0.0912	0.851	0.0763	1.017	0.0723	1.073	0.1046	0.742
					s =	0.281		0.265		0.209		0.315		0.333
					x =	1.055		1.120		1.234		1.411		1.078
					V =	0.266		0.237		0.169		0.223		0.309
Anderson & Ramirez	W1	9.99	2.220	0.499	0.4627	0.994	0.4549	1.011	0.3760	1.223	0.3637	1.265	0.9329	0.493
	W2	9.99	2.220	0.499	0.4693	1.170	0.4615	1.190	0.3824	1.436	0.3692	1.487	0.9329	0.588
	W3	9.99	2.220	0.249	0.6997	0.720	0.5393	0.935	0.6321	0.797	0.6550	0.769	0.9329	0.540
					s =	0.227		0.131		0.325		0.367		0.048
					x =	0.961		1.045		1.152		1.174		0.541
					V =	0.236		0.125		0.282		0.313		0.088
Johnson & Ramirez	No.1	13.12	0.748	0.247	0.4189	0.808	0.4084	0.829	0.3000	1.128	0.2570	1.317	0.3690	0.917
	No.2	13.12	0.373	0.495	0.3209	0.693	0.2793	0.796	0.2330	0.955	0.1920	1.158	0.1838	1.210
	No.4	13.12	0.373	0.495	0.3717	0.850	0.3036	1.040	0.3000	1.053	0.2450	1.289	0.1838	1.718
	No.5	13.12	0.748	0.247	0.4324	0.885	0.4295	0.891	0.3390	1.128	0.2880	1.328	0.3690	1.037
	No.7	13.12	0.423	0.495	0.3326	0.844	0.3082	0.911	0.2640	1.064	0.2790	1.006	0.2087	1.346
	No.8	13.12	0.423	0.495	0.3447	0.748	0.3082	0.837	0.2640	0.977	0.2790	0.925	0.2087	1.236
					s =	0.072		0.087		0.073		0.172		0.278
					x =	0.805		0.884		1.051		1.171		1.244
					V =	0.089		0.099		0.070		0.147		0.223

	Beam	ρf_y (MPa)	$\rho_v f_{vy}$ (MPa)	s/d	V_{SFg} (MN)	V_t/V_{SFg}	V_{SFd} (MN)	V_t/V_{SFd}	V_{ACI} (MN)	V_t/V_{ACI}	V_{ACI} (MN)	V_t/V_{CSAg}	V_{CEB} (MN)	V_t/V_{CEB}
Roller & Ressell	1	5.86	0.348	0.372	0.6607	0.450	0.3920	0.758	0.4439	0.669	0.3577	0.830	0.2077	1.430
	2	13.10	2.006	0.284	0.8911	1.231	0.8897	1.233	0.7408	1.481	0.6500	1.688	1.1979	0.916
	3	19.65	4.139	0.220	1.3474	1.236	1.3955	1.193	1.1418	1.458	1.0463	1.591	2.4711	0.674
	4	26.20	5.920	0.154	1.6247	1.194	1.7044	1.138	1.4753	1.315	1.4324	1.354	3.5342	0.549
	5	32.20	8.346	0.109	2.0300	1.101	2.1438	1.043	2.0320	1.100	1.9028	1.175	4.9827	0.449
	6	8.03	0.377	0.483	0.7581	0.877	0.6499	1.023	0.6321	1.052	0.5138	1.294	0.3940	1.688
	7	9.08	0.730	0.249	0.9440	0.835	0.9293	0.848	0.7714	1.022	0.6482	1.216	0.7631	1.033
	8	9.08	0.377	0.483	1.1402	0.424	0.6942	0.698	0.7940	0.608	0.7164	0.674	0.3940	1.226
	9	11.36	0.730	0.249	1.0450	0.717	0.9910	0.758	0.9275	0.808	0.8028	0.933	0.7631	0.981
	10	13.41	1.076	0.169	1.1855	0.989	1.2163	0.964	1.0430	1.124	0.8800	1.332	1.1240	1.043
					s =	0.303		0.193		0.303		0.321		0.385
					x =	0.905		0.965		1.064		1.209		0.999
					V =	0.334		0.200		0.285		0.265		0.385
Bresler & Scordelis	A-1	9.99	0.322	0.460	0.2450	0.955	0.2166	1.080	0.1984	1.179	0.1677	1.395	0.1346	1.739
	A-2	12.65	0.322	0.460	0.2353	1.041	0.2203	1.112	0.1971	1.243	0.1662	1.474	0.1346	1.821
	B-1	13.49	0.462	0.427	0.2134	1.040	0.1965	1.130	0.1676	1.325	0.1553	1.429	0.1449	1.532
	B-2	13.49	0.462	0.427	0.2145	0.932	0.1950	1.026	0.1746	1.145	0.1533	1.305	0.1449	1.380
	C-1	9.99	0.646	0.460	0.1677	0.930	0.1532	1.018	0.1459	1.069	0.1293	1.206	0.1346	1.159
	C-2	20.31	0.646	0.460	0.1653	0.980	0.1491	1.087	0.1450	1.117	0.1290	1.256	0.1346	1.204
					s =	0.050		0.045		0.092		0.105		0.274
					x =	0.980		1.075		1.180		1.344		1.473
					V =	0.052		0.042		0.078		0.078		0.186
Xie et al	NNW-3	13.47	1.649	0.483	0.0885	0.983	0.0859	1.012	0.0887	0.981	0.0813	1.070	0.1276	0.682
	NHW-3	19.11	1.684	0.485	0.0989	1.035	0.0980	1.045	0.0980	1.045	0.0903	1.134	0.1270	0.806
	NHW-3a	19.11	2.184	0.374	0.1137	0.952	0.1132	0.956	0.1127	0.960	0.1036	1.044	0.1648	0.657
	NHW-3b	19.11	2.650	0.308	0.1256	0.975	0.1290	0.950	0.1300	0.942	0.1169	1.048	0.1999	0.613
	NHW-4	19.11	1.684	0.485	0.0973	0.963	0.0981	0.956	0.0981	0.955	0.0863	1.086	0.1270	0.738
					s =	0.032		0.043		0.041		0.036		0.075
					x =	0.982		0.984		0.977		1.076		0.699
					V =	0.033		0.043		0.042		0.034		0.107
Yoon et al	N1N	11.20	0.355	0.496	0.4111	1.112	0.4068	1.123	0.3272	1.397	0.3010	1.518	0.2613	1.749
	N2S	11.20	0.350	0.710	0.3954	0.918	0.3860	0.941	0.3260	1.113	0.3341	1.087	0.2577	1.409
	N2N	11.20	0.500	0.496	0.4643	1.040	0.4736	1.020	0.3604	1.340	0.3331	1.450	0.3687	1.310
	M1N	11.20	0.355	0.496	0.4790	0.846	0.4387	0.923	0.4168	0.972	0.3995	1.014	0.2613	1.550
	M2S	11.20	0.500	0.496	0.5145	1.073	0.5114	1.079	0.4500	1.227	0.3937	1.402	0.3687	1.497
	M2N	11.20	0.707	0.351	0.6328	1.089	0.6195	1.112	0.4927	1.398	0.4146	1.662	0.5209	1.323
	H1N	11.20	0.355	0.496	0.5129	0.942	0.4527	1.067	0.4636	1.042	0.4179	1.156	0.2613	1.849

	Beam	ρf_y (MPa)	$\rho_v f_{vy}$ (MPa)	s/d	V_{SFg} (MN)	V_t/V_{SFg}	V_{SFd} (MN)	V_t/V_{SFd}	V_{ACI} (MN)	V_t/V_{ACI}	V_{ACI} (MN)	V_t/V_{CSAg}	V_{CEB} (MN)	V_t/V_{CEB}
	H2S	11.20	0.602	0.412	0.5484	1.090	0.5853	1.022	0.5202	1.150	0.4458	1.341	0.4438	1.348
	H2N	11.20	1.016	0.244	0.7765	0.929	0.7786	0.926	0.6147	1.173	0.5189	1.389	0.7488	0.963
					s =	0.099		0.074		0.163		0.225		0.202
					x =	1.004		1.024		1.201		1.335		1.444
					V =	0.098		0.073		0.135		0.169		0.140
Kriski	1	8.70	0.563	0.435	0.2625	0.949	0.2496	0.998	0.1620	1.537	0.1328	1.875	0.2098	1.187
	2	8.70	0.563	0.435	0.2647	1.449	0.2510	1.528	0.1645	2.331	0.1284	2.987	0.2098	1.828
	3	8.70	0.563	0.435	0.2668	0.841	0.2496	0.899	0.1620	1.386	0.1391	1.614	0.2098	1.070
	5	8.70	0.563	0.435	0.2646	1.107	0.2509	1.168	0.1643	1.783	0.1305	2.245	0.2098	1.396
	7	8.70	0.563	0.435	0.3109	0.979	0.2802	1.087	0.2293	1.328	0.1865	1.633	0.2098	1.451
	8	8.70	0.563	0.435	0.3131	1.249	0.2818	1.387	0.2334	1.675	0.1897	2.061	0.2098	1.864
	9	8.70	0.563	0.435	0.3313	0.730	0.2815	0.860	0.2325	1.041	0.1936	1.250	0.2098	1.153
	10	8.70	0.563	0.435	0.3124	1.250	0.2812	1.389	0.2316	1.686	0.1883	2.074	0.2098	1.861
					s =	0.239		0.248		0.381		0.521		0.334
					x =	1.069		1.164		1.596		1.967		1.476
					V =	0.223		0.213		0.239		0.265		0.226
Peng	B-1	12.90	0.301	1.296	0.1107	1.030	0.0960	1.188	0.0910	1.253	0.0950	1.200	0.0693	1.644
	B-2	12.90	0.356	1.095	0.1134	1.049	0.1073	1.109	0.0950	1.253	0.0990	1.202	0.0820	1.450
	B-3	12.90	0.428	0.912	0.1338	0.904	0.1208	1.001	0.1001	1.209	0.0980	1.235	0.0985	1.229
	B-4	12.90	0.548	0.712	0.1516	0.943	0.1409	1.015	0.1070	1.336	0.0890	1.607	0.1262	1.133
	B-5	12.90	0.921	1.296	0.1511	1.198	0.1294	1.398	0.1460	1.240	0.1220	1.484	0.2120	0.854
	B-6	12.90	1.090	1.095	0.1786	1.069	0.1462	1.306	0.1567	1.219	0.1420	1.345	0.2509	0.761
	B-7	12.90	1.308	0.912	0.1931	0.968	0.1716	1.090	0.1770	1.056	0.1600	1.169	0.3010	0.621
					s =	0.097		0.149		0.085		0.167		0.374
					x =	1.023		1.158		1.224		1.320		1.099
					V =	0.095		0.128		0.069		0.127		0.341
Talor	ST1-B	12.49	1.462	0.444	0.1024	0.871	0.0963	0.926	0.0868	1.028	0.0879	1.015	0.1240	0.719
	ST4-B	12.49	1.094	0.593	0.0865	0.864	0.0819	0.913	0.0723	1.033	0.0686	1.089	0.0928	0.805
	ST2-C	12.49	1.462	0.444	0.1030	1.035	0.0969	1.101	0.0874	1.220	0.0886	1.203	0.1240	0.860
					s =	0.097		0.105		0.109		0.095		0.071
					x =	0.923		0.980		1.094		1.102		0.795
					V =	0.105		0.107		0.100		0.086		0.089
Haddadin et al	A2	19.70	0.693	0.483	0.1893	1.026	0.1731	1.122	0.1290	1.506	0.1327	1.464	0.1411	1.377
	A3	19.70	1.500	0.483	0.2520	1.157	0.2399	1.215	0.2148	1.357	0.2169	1.344	0.3051	0.955
	A4	19.70	2.816	0.257	0.3605	0.951	0.3446	0.994	0.3470	0.988	0.3820	0.897	0.5729	0.598
	A5	19.70	4.524	0.160	0.4571	0.847	0.4454	0.869	0.5164	0.750	0.5160	0.750	0.6731	0.575
	B3	19.70	1.500	0.483	0.2481	1.094	0.2372	1.144	0.2123	1.278	0.2143	1.266	0.3051	0.889

	Beam	ρf_y (MPa)	$\rho_v f_{vy}$ (MPa)	s/d	V_{SFg} (MN)	V_t/V_{SFg}	V_{SFd} (MN)	V_t/V_{SFd}	V_{ACI} (MN)	V_t/V_{ACI}	V_{ACI} (MN)	V_t/V_{CSAg}	V_{CEB} (MN)	V_t/V_{CEB}
	C2	19.70	0.693	0.483	0.1818	0.953	0.1721	1.007	0.1275	1.359	0.1181	1.467	0.1411	1.229
	C3	19.70	1.500	0.483	0.2504	1.039	0.2329	1.117	0.2084	1.249	0.2137	1.218	0.3051	0.853
	C4	19.70	2.816	0.257	0.3598	0.863	0.3400	0.913	0.3439	0.903	0.3806	0.816	0.5444	0.570
	C5	19.70	4.524	0.160	0.4629	0.774	0.4533	0.790	0.5208	0.688	0.5821	0.616	0.7339	0.488
	D3	19.70	1.500	0.483	0.2557	0.943	0.2390	1.008	0.2140	1.126	0.2193	1.099	0.3051	0.790
	F3	19.70	1.500	0.483	0.2609	1.264	0.2528	1.304	0.2286	1.443	0.2212	1.491	0.3051	1.081
	G3	19.70	1.986	0.483	0.2819	1.180	0.2624	1.267	0.2107	1.579	0.2152	1.546	0.4040	0.823
	G4	19.70	2.971	0.323	0.3534	1.085	0.3365	1.140	0.2877	1.333	0.2775	1.382	0.5705	0.672
	G5	19.70	4.938	0.194	0.4680	0.914	0.4511	0.948	0.4398	0.973	0.4210	1.016	0.6931	0.617
	H2	19.70	1.500	0.483	0.2507	1.270	0.2378	1.339	0.2129	1.496	0.2157	1.477	0.3051	1.044
	J3	19.70	1.500	0.483	0.2523	1.042	0.2402	1.095	0.2152	1.222	0.2225	1.182	0.3051	0.862
	J5	19.70	4.524	0.160	0.4640	0.934	0.4570	0.948	0.5229	0.829	0.5561	0.779	0.7630	0.568
					s =	0.143		0.156		0.279		0.303		0.254
					x =	1.020		1.072		1.181		1.165		0.823
					V =	0.140		0.146		0.236		0.260		0.308
Sorensen	T21	16.20	1.403	0.587	0.0980	1.321	0.1036	1.251	0.1034	1.252	0.1023	1.266	0.1380	0.938
	T22	16.20	1.484	0.705	0.0954	1.336	0.0994	1.282	0.0766	1.664	0.0718	1.776	0.1459	0.874
	T23	16.20	1.187	0.503	0.0954	1.460	0.1012	1.377	0.0794	1.754	0.0742	1.877	0.1167	1.193
	T3a	16.20	1.268	0.352	0.1011	1.261	0.1057	1.206	0.0949	1.344	0.0960	1.328	0.1247	1.022
	T4a	16.20	1.351	0.352	0.1055	1.255	0.1090	1.215	0.0745	1.777	0.0710	1.865	0.1328	0.997
	T1b	16.20	1.138	0.393	0.0956	1.231	0.0987	1.193	0.0871	1.351	0.0871	1.351	0.1119	1.052
	T2b	16.20	1.212	0.393	0.0990	1.308	0.1023	1.266	0.0695	1.863	0.0650	1.992	0.1192	1.086
	T3b	16.20	0.761	0.587	0.0759	1.526	0.0786	1.473	0.0678	1.708	0.0634	1.826	0.0748	1.548
	T4b	16.20	0.810	0.587	0.0779	1.372	0.0807	1.325	0.0554	1.930	0.0488	2.191	0.0797	1.341
	T5	16.20	0.810	0.587	0.0781	1.407	0.0810	1.357	0.0559	1.966	0.0490	2.243	0.0797	1.379
					s =	0.095		0.089		0.257		0.349		0.217
					x =	1.348		1.294		1.661		1.772		1.143
					V =	0.070		0.069		0.155		0.197		0.190
Lyngberg	5A0	14.07	3.573	0.293	0.3954	1.100	0.3650	1.192	0.3040	1.431	0.2842	1.531	0.5762	0.755
	5B0	14.22	3.430	0.293	0.3882	1.121	0.3606	1.206	0.3077	1.414	0.2875	1.513	0.5776	0.753
					s =	0.014		0.010		0.012		0.012		0.001
					x =	1.110		1.199		1.422		1.522		0.754
					V =	0.013		0.009		0.009		0.008		0.002
Bach et al	V6002	18.59	0.859	0.612	0.1804	1.358	0.2257	1.086	0.1885	1.300	0.1785	1.373	0.1769	1.385
	V6004	18.59	1.378	0.382	0.2384	1.284	0.2950	1.037	0.2616	1.170	0.2656	1.152	0.2835	1.079
	U6002	18.59	0.430	0.612	0.1721	1.127	0.1551	1.250	0.1713	1.133	0.1721	1.127	0.0885	2.192
	U6004	18.59	0.430	0.612	0.1728	1.296	0.1562	1.434	0.1727	1.297	0.1724	1.299	0.0885	2.531

	Beam	ρf_y (MPa)	$\rho_v f_{vy}$ (MPa)	s/d	V_{SFg} (MN)	V_t/V_{SFg}	V_{SFd} (MN)	V_t/V_{SFd}	V_{ACI} (MN)	V_t/V_{ACI}	V_{ACI} (MN)	V_t/V_{CSAg}	V_{CEB} (MN)	V_t/V_{CEB}
	U6017	18.59	2.823	0.510	0.2735	1.119	0.3452	0.886	0.4516	0.678	0.4359	0.702	0.4792	0.639
	U5604p	20.49	1.047	0.612	0.1912	1.334	0.2310	1.104	0.1878	1.358	0.1888	1.351	0.2154	1.184
					s =	0.104		0.189		0.249		0.250		0.718
					x =	1.253		1.133		1.156		1.167		1.502
					V =	0.083		0.166		0.216		0.214		0.478
Clark	A1-1	9.94	1.321	0.451	0.2191	1.027	0.2075	1.085	0.1668	1.349	0.1675	1.343	0.3137	0.717
	A1-2	9.94	1.321	0.451	0.2184	0.957	0.2063	1.014	0.1654	1.264	0.1674	1.249	0.3137	0.667
	A1-3	9.94	1.321	0.451	0.2182	1.020	0.2061	1.080	0.1651	1.348	0.1656	1.344	0.3137	0.709
	A1-4	9.94	1.321	0.451	0.2192	1.120	0.2075	1.183	0.1669	1.470	0.1639	1.497	0.3137	0.782
	B1-1	9.94	1.263	0.472	0.2209	1.262	0.2005	1.391	0.1610	1.732	0.1587	1.757	0.3000	0.929
	B1-2	9.94	1.263	0.472	0.2224	1.154	0.2027	1.266	0.1637	1.568	0.1632	1.572	0.3000	0.855
	B1-3	9.94	1.263	0.472	0.2211	1.288	0.2008	1.418	0.1614	1.765	0.1550	1.837	0.3000	0.949
	B1-4	9.94	1.263	0.472	0.2208	1.214	0.2004	1.338	0.1609	1.666	0.1585	1.691	0.3000	0.894
	B1-5	9.94	1.263	0.472	0.2218	1.089	0.2019	1.196	0.1627	1.484	0.1661	1.454	0.3000	0.805
	C1-1	6.73	1.186	0.503	0.2186	1.270	0.1952	1.423	0.1580	1.758	0.1558	1.782	0.2816	0.986
	C1-2	6.73	1.186	0.503	0.2193	1.419	0.1959	1.588	0.1589	1.958	0.1449	2.147	0.2816	1.105
	C1-3	6.73	1.186	0.503	0.2170	1.133	0.1934	1.272	0.1557	1.579	0.1509	1.630	0.2816	0.873
	C1-4	6.73	1.186	0.503	0.2217	1.290	0.1985	1.440	0.1623	1.762	0.1480	1.932	0.2816	1.015
	D1-1	5.47	1.581	0.377	0.2661	1.132	0.2334	1.290	0.1946	1.547	0.1887	1.596	0.3755	0.802
	D1-2	5.47	1.581	0.377	0.2661	1.340	0.2333	1.529	0.1954	1.825	0.1877	1.900	0.3755	0.950
	D1-3	5.47	1.581	0.377	0.2647	0.969	0.2313	1.109	0.1924	1.334	0.1874	1.369	0.3755	0.683
					s =	0.137		0.170		0.204		0.251		0.128
					x =	1.168		1.269		1.588		1.631		0.858
					V =	0.117		0.132		0.128		0.154		0.149